

**1,3-Disubstituted-tetrahydro- β -carbolines: A New Method for Stereochemical
Assignment and Synthesis of Potential Antimalarial Agents**

Kristýna Cagašová

Dissertation submitted to the faculty of the Virginia Polytechnic Institute and State
University in partial fulfillment of the requirements for the degree of

Doctor of Philosophy

In

Chemistry

Paul R. Carlier, Chair

Felicia Etzkorn

Webster Santos

James Tanko

May 11th, 2021

Blacksburg, Virginia

Keywords: (malaria, tetrahydro- β -carboline, IspD, MEP pathway, MMV008138, Pictet-Spengler reaction, γ -gauche effect, NMR, ^1H - ^1H coupling, bioisostere synthesis, tetrazole, phosphonic acid)

Copyright 2021, Kristyna Cagasova

1,3-Disubstituted-tetrahydro- β -carbolines: A New Method for Stereochemical Assignment and Synthesis of Potential Antimalarial Agents

Kristýna Cagašová

ABSTRACT

Malaria is a serious mosquito-borne disease affecting the majority of Earth's southern hemisphere. While consistent efforts to curb malaria spread throughout 20th and early 21st century were largely successful, the recent rise in resistance to antimalarial treatments resulted in an increasing incidence rate and stalling mortality rate. This trend clearly signifies the need for the development of novel antimalarial agents able to circumvent current drug-resistance mechanisms.

In 2014, in collaboration with Prof. Maria Belen Cassera from the University of Georgia, our group found that compound **1a** (1*R*,3*S*-MMV008138), discovered from the publicly available Malaria Box, targets an essential biosynthetic pathway (MEP pathway) of malaria-causing parasite *Plasmodium falciparum*. Analogs of **1a** synthesized in our laboratory were found effective against multi-resistant Dd2 strain of *P. falciparum* which, together with an absence of MEP pathway in humans, suggests that potent analogs of **1a** may be safe and efficient antimalarial drug candidates.

The initial bioassay studies determined that only one of four possible MMV008138 stereoisomers satisfactorily inhibits the target *Pf*IspD enzyme. Thus, a secure determination of stereochemistry in **1a** analogs was of utmost importance to the structure-activity relationship studies performed in our group. The second chapter of this work discusses the validation of the previously known empirical stereoassignment method based on analysis of relative shift of ¹³C NMR resonances between *cis* and *trans* diastereomers and compares it to a new method based

on $^3J_{\text{HH}}$ coupling constants developed in our laboratory. We demonstrate that the new method relying on the analysis of ^1H - ^1H coupling is reliable over large samples of experimental data and suitable even when only a single diastereomer is produced in the synthetic process. Importantly, the origin of $^3J_{\text{HH}}$ coupling constants is well understood, unlike the source of relative differences in ^{13}C NMR shifts observed in the older method. The empirical observations for both stereoassignment methods are supported by extensive density-functional theory calculations, which validate the new ^1H - ^1H coupling-based assignment but do not provide a conclusive explanation for the origin of the ^{13}C NMR-based method.

In the third chapter, we discuss the replacement of the carboxylic acid moiety in **1a** by alternative functional groups promising improved toxicity and bioavailability profile. The total synthesis of tetrazole (*trans*-**23a**) and phosphonic acid ((±)-**62a**) derivatives of **1a** is discussed in detail. The tetrazole analog **23a** was previously synthesized in the Carlier group as a diastereomeric mixture of *cis* and *trans* isomers (dr = 3:7), and it was tested for growth inhibition of multi-resistant *P. falciparum* with promising results. Later, the synthesis was revisited to obtain a stereochemically pure sample of *trans*-**23a**, which was expected to show improved potency compared to the original sample. Furthermore, the synthesis of pure *trans*-**23a** confirmed the accuracy of the previous assignment of *cis* and *trans* diastereomers in the mixture. Unfortunately, neither analog showed an improvement in potency relative to **1a**.

1,3-Disubstituted-tetrahydro- β -carbolines: A New Method for Stereochemical Assignment and Synthesis of Potential Antimalarial Agents

Kristýna Cagašová

GENERAL AUDIENCE ABSTRACT

The most severe form of malaria disease is caused by the parasite, *Plasmodium falciparum*, which gives rise to over 200 million infections and more than 400 thousand deaths every year, the majority of which affect young children. In recent years, the effectiveness of clinically used antimalarial medicines decreased due to an increase in drug-resistant strains of *P. falciparum*. Therefore, there is an urgent need for new antimalarial agents that could bypass the emerging resistance.

A promising candidate for a new antimalarial drug is a molecule named MMV008138. This molecule exists in four distinct forms called stereoisomers. Stereoisomers are molecules with the same chemical formula, but the atoms in each molecule are positioned differently. Only one of MMV008138's four stereoisomers (**1a**) was effective in killing the *P. falciparum*. The second chapter of this work discusses a new method for identifying stereoisomers in molecules like MMV008138. We demonstrate that the new method is both reliable and simpler than the previously used procedures.

The third chapter of this dissertation discusses the preparation of two new compounds based on the structure of **1a** that contain modifications promising improved biological activity. Unfortunately, neither of these two molecules was able to kill the *P. falciparum* efficiently.

*To my husband Petr and my parents Petra and Vladimir for their love and support
without whom none of this would be possible*

Acknowledgements

First and foremost, I would like to thank my advisor, Prof. Paul Carlier, for his kindness, support, guidance, and patience. Throughout the years of his mentorship, I have learned many invaluable lessons not only in synthetic chemistry and chemical biology but also in life in general. He encouraged me to step out of my comfort zone, which made me a better scientist and led to unexpected results, like my publishing of a paper primarily based on numerical simulations.

Further, my gratitude goes to my committee members, who provided helpful feedback and suggestions to my research throughout my years in graduate school. Namely, I thank Prof. Felicia Etzkorn for her support and advice in matters of research and professional life and her inspiring passion for green chemistry, Prof. Webster Santos for encouraging me to deepen my understanding of chemistry and explore new approaches to various research problems, and Prof. James Tanko for his unwavering optimism, support in my research, and the trust he put in my feedback to the course development of CHEM 2555 and 2556.

Additionally, I would like to thank all my colleagues with whom I interacted in the research laboratories. Namely Kiaya Vincent and Alexander Hawes for mentoring me through my first year and teaching me how to become a capable synthetic chemist, Dr. Zhong-Ke Yao from whom I learned helpful tips and tricks, which saved me a lot of time during my synthetic work, Dr. José A. Rodríguez-Corrales for becoming my scientist role-model and also wonderful friend who constantly challenged my ideas, encouraged me to go above and beyond in all aspects of my work, and was a great mentor in the fields of biology and laboratory safety, Dr. Maryam Ghavami and Lixuan Liu for being great lab partners and for all the work they accomplished in the bioisostere project before I joined in, Dr. Sha Ding and Jeremy Cunningham for our long and fruitful

conversations about research and compound characterization, Hanan AlMolhim for not only being a fantastic teammate, but also becoming a cherished friend, Scot Barry for sharing his synthetic experience, and Jopaul Mathew for his insights on work with aliphatic Pictet-Spengler adducts and synthesis of compounds **4an/5an** included in this work.

Furthermore, I would like to extend my appreciation to Dr. Maria Belen Cassera and her students for the biological evaluation of the synthesized compounds in this work, Dr. Murthy Shanaiah for his helpful advice regarding NMR measurements and interpretation, Dr. Mehdi Ashraf-Khorassani for analyzing my compounds by HRMS, Dr. Carla Slebodnick for measurement and interpretation of X-ray crystal structures of compounds **48a/49a**, Dr. Shamindri Arachchige for allowing me to participate in chemistry outreach programs under her guidance, Negin Nazem for all the help and support during my work as teaching and lab prep assistant, and Joli Huynh without whom all the graduate students would be lost.

I would also like to express my gratitude to my dear friends who were always here for me during both the challenging and exciting times of my PhD journey. With this, I would like to thank Ashley and Loren Brown, who became amazing friends and neighbors, Erin Shibley and Chirag Rathod, for being wonderful friends and board game partners and who shared our social bubble with me and my husband Petr throughout the majority of 2020, José Rodríguez-Corrales who taught me invaluable life lessons and became my trusted confidant, and Kiaya and Matt Vincent, who gave me not only lots of support and advice in my early years in the graduate school but also brought my furry son, cat Binky, into my life for which I will be forever thankful to them.

And last but not least, I am giving my greatest thanks to my family, who always showed me love and support even when I felt that I did not deserve it. I want to thank my parents Petra and Vladimír, who not only made sure that I grew up into a strong, independent, and forever curious

person but also allowed me to make the enormous life decision of moving across the ocean to the United States. I am also thankful to my little sister Kateřina, who motivates me to be the best version of myself. I am also grateful to my cat Binky for being the most amazing pet in the whole world and for not accidentally deleting this entire document when constantly walking over my keyboard.

My final thanks belong to my beloved husband and soulmate Petr, who brought up the idea of moving to America. Even though not obvious at first, I am very happy that we made this decision together. Thanks to Petr, I achieved things I never dared to dream of before, and I would certainly not be where I am now without him. He was at my side throughout the most joyful and most awful moments of the past 12 years, and I cannot imagine anyone better than him to go through this challenging period of my life with.

Table of Contents

1	Overview of <i>P. falciparum</i> 's biology and methods to fight malaria	1
1.1	Epidemiology of falciparum malaria	2
1.2	Clinical outcomes of falciparum malaria	2
1.3	Transmission and life cycle	3
1.3.1	Mosquito phase and transmission to human host	3
1.3.2	Asymptomatic liver phase (pre-erythrocytic phase)	5
1.3.3	Symptomatic blood stage	6
1.3.4	Sexual development and transmission to mosquito	8
1.4	Prevention of falciparum malaria	10
1.4.1	Malaria vaccine	11
1.4.2	Vector control	11
1.5	Treatment of falciparum malaria	13
1.5.1	Quinoline-type antimalarials	15
1.5.2	Antifolates, mitochondrial inhibitors, and antibiotics	16
1.5.3	Artemisinin-based antimalarials	17
1.5.4	Resistance to antimalarial drugs	18
1.6	The search for a new target	19
1.7	MMV008138 and its analogs	21
2	Stereoassignment of 1,3-disubstituted-tetrahydro- β -carboline using ^1H - ^1H coupling constants	31
2.1	Methods for stereoassignment in tetrahydro- β -carboline	32
2.2	Gamma effect in ^{13}C NMR and its use for stereochemistry assignment	34
2.3	Development of ^1H NMR method for analysis of 1,3-disubstituted tetrahydro- β -carboline	37

2.4	Density functional theory conformational analysis	47
2.4.1	Energetic distribution of calculated conformers	49
2.4.2	Calculation of $^3J_{\text{HH}}$ coupling constants	53
2.4.3	Calculation of ^{13}C NMR chemical shifts	54
2.4.4	Computational evaluation of the role of steric compression in the ^{13}C chemical shifts of C1 and C3 in 4a and 4b	57
2.4.5	Conclusions	59
3	Tetrazole and phosphonate analogs of MMV008138	66
3.1	Structure-activity relationship of MMV008138 and carboxylic acid derivatives	67
3.2	The usefulness of carboxylic isosteres and their possible application to MMV008138	74
3.3	Synthesis of the enantiopure <i>trans</i> -tetrazole analog	82
3.3.1	Approaches to the tetrazole analog by previous group members	83
3.3.2	Attempt of stereoselective synthesis using N-allyl substitution	88
3.3.3	Stereoselective synthesis of tetrazole derivative via nitrile intermediate	92
3.4	Synthesis of the racemic phosphonic acid derivative	105
3.4.1	Synthesis of diethylphosphonate analog of tryptophan	106
3.4.2	Synthesis of phosphonic acid derivative of MMV008138	110
4	Experimental	123
4.1	General	123
4.2	Chapter 1 – Synthesis of D-ring variants of 1a	126
4.3	Chapter 2 – Synthesis of aliphatic Pictet-Spengler adducts	134
4.4	Chapter 3 – Synthesis of tetrazole and phosphonate bioisosteres of 1a	140
5	Supporting information for Chapter 2	170
5.1	Tabulated NMR data for analyzed compounds	170
5.1.1	Conformational distribution in compound 4a/4b and 5a/5b	174

5.1.2 ^1H - ^1H coupling constants for conformers of 4a/4b and 5a/5b	185
5.1.3 Calculated ^{13}C NMR chemical shifts and shielding tensors of 4a/4b and 5a/5b	187
5.1.4 B3LYP/6-31G(d) Cartesian coordinates for all conformers of 4a , 4b , 5a , and 5b	201

List of Figures

Figure 1.1 Malaria incidence and mortality globally and in Africa in years 2000-2019	1
Figure 1.2 Status of global malaria incidence rates in 2018	2
Figure 1.3 Mosquito stage of <i>P. falciparum</i> life cycle	4
Figure 1.4 Pre-erythrocytic stage of <i>P. falciparum</i> life cycle	6
Figure 1.5 Asexual replication of <i>P. falciparum</i> during the blood stage of its life cycle	6
Figure 1.6 Sexual development of <i>P. falciparum</i>	10
Figure 1.7 Examples of clinically used antimalarial agents	14
Figure 1.8 Prevalence of delayed clearance phenotype	19
Figure 1.9 Comparison of the full-length amino acid sequence of <i>PfIsD</i> and <i>AtIsD</i>	22
Figure 2.1 Example of Cook's empirical rule as applied to one of the MMV001838 analog precursors	33
Figure 2.2 Graphical representation of γ -gauche effect in methylcyclohexane	34
Figure 2.3 Examples of γ -gauche effect observed in various substituted cyclohexanes	36
Figure 2.4 First-principle analysis of possible conformers adopted by aromatic <i>trans</i> (4a-ah) and <i>cis</i> (5a-ah) analogs	41
Figure 2.5 Assignment of H4 α and H4 β in compounds 4a and 5a via 1D NOE	44
Figure 2.6 Five-bond coupling of H1 to H4 α and H4 β in 4b and 5b	46
Figure 2.7 Representative calculated (B3LYP/6-31G(d)) structures of 4a illustrating the orientation of the CO ₂ Me, NH, and 2'-Cl groups	48
Figure 2.8 The lowest ΔG (298 K) $\psi_{\text{eq-}}$ and $\psi_{\text{ax-}}$ conformers of 4a and the global minimum of 5a	51
Figure 2.9 Weighted (mPW1PW91/6-311+G(2d,p) (PCM,CHCl ₃)/B3LYP/6-31G(d)) ¹³ C NMR chemical shifts for C1 & C3 of 4a and 4b in the $\psi_{\text{eq-}}$ and $\psi_{\text{ax-CO}_2\text{Me}}$ tetrahydropyridine conformational ensembles B and C	58

Figure 3.1 Tetrahydro- β -carbolines included in Malaria Box compound library	66
Figure 3.2 Effect of various substituents on pK _a of amines	69
Figure 3.3 Structural comparison of C3-substituents in analogs 8a and 4a with potent 1a and 9a	71
Figure 3.4 Structural comparison of C3-substituents in analogs 16a and 17a with potent 9a	74
Figure 3.5 Examples of improved pharmacokinetic properties of selected carboxylic acid bioisosteres	77
Figure 3.6 Comparison of physical properties and structural alignment of the carboxylic acid group (present in our lead compound 1a) and tetrazole ring, present in proposed analog 23a	79
Figure 3.7 Metabolic products of tetrazolic acid glucuronidation	80
Figure 3.8 Comparison of physical properties and structural alignment of the carboxylic acid group (present in our lead compound 1a) and phosphonic acid	81
Figure 3.9 Steps of MEP pathway catalyzed by IspC (reductoisomerase) and IspD (cytidyltransferase)	82
Figure 3.10 Anisotropic displacement ellipsoid drawing of X-ray structures of compounds 48a and 49a	99
Figure 3.11 Growth inhibition of <i>P. falciparum</i> (Dd2 strain) induced by pure diastereomer <i>trans</i> - 23a	105
Figure 3.12 Synthesis of acetyl chloride 59	108
Figure 3.13 Synthesis of oxime 61 from 58	109
Figure 3.14 Monitoring of reaction between (\pm)- 56a and TMSBr in CDCl ₃	113
Figure 3.15 Solvent related stereochemical preference seen in the hydrolysis of (\pm)- 56a and (\pm)- 57a	115
Figure 5.1 The lowest ΔG (298 K) ψ_{eq} - and ψ_{ax} - conformers of 4a and the global minimum of 5a	174

Figure 5.2 The lowest ΔG (298 K) ψ_{eq} - and ψ_{ax} - conformers of **4b** and the global minimum of **5b**

175

List of Schemes

Scheme 1.1 MEP pathway	21
Scheme 1.2 Synthetic pathway to D-ring variants of MMV008138	23
Scheme 3.1 Phase II metabolism of carboxylic acids	76
Scheme 3.2 Racemization of α -amino nitriles	83
Scheme 3.3 First attempts of tetrazole bioisostere synthesis	84
Scheme 3.4 Synthesis of cyanoethyl-tetrazole analog 34a with use of modified Mitsunobu reaction	86
Scheme 3.5 Attempted synthesis of <i>trans</i> - 23a directly from 21a	86
Scheme 3.6 Removal of Boc protecting group from 32 and formation of by-product 33-2	88
Scheme 3.7 Mechanism of acid-catalyzed TH β C epimerization	89
Scheme 3.8 Selective synthesis of <i>trans</i> diastereomer using N-allyl protection	91
Scheme 3.9 Attempt of <i>trans</i> -selective synthesis of <i>N</i> 2-allyl protected 40a	92
Scheme 3.10 Synthesis of <i>N</i> -allyl protected 36a and an attempt to convert 36a to its primary amide analog 41a	93
Scheme 3.11 Installation of tetrazole group on an <i>N</i> -Cbz protected TH β C as presented by Saiga et al	94
Scheme 3.12 Synthesis of <i>N</i> -Bn protected analogs 47a and 50a , and <i>N</i> -Cbz protected esters 48a and 49a	96
Scheme 3.13 Proposed mechanism for the formation of 47a from 8a	97
Scheme 3.14 Hydrodehalogenation as a side reaction of 54a with H ₂ over Pd/C	103
Scheme 3.15 Diethyl phosphonate TH β Cs synthesized from (\pm)- 55 by Viveros-Ceballos et al.	106
Scheme 3.16 Literature pathway to diethyl phosphonate analog of tryptophan (\pm)- 55	107

Scheme 3.17 Preparation of diethylphosphonate TH β Cs from (\pm)-**55** via Pictet-Spengler reaction

110

List of Tables

Table 1.1 Overview of biological activity of MMV008138 D-ring variants synthesized in Carrier lab	24
Table 2.1 C1-substitution of <i>trans</i> (4) and <i>cis</i> (5) Pictet-Spengler adducts studied in Chapter 2	37
Table 2.2 ¹³ C NMR resonances used to determine the stereochemistry of compounds shown in Table 2.1	39
Table 2.3 Average ¹³ C NMR resonances expected to show the γ -gauche effect in compound 4a-ar and 5a-ar	42
Table 2.4 Selected average ¹ H chemical shifts and coupling constants (CDCl ₃) for compounds shown in Table 2.1	45
Table 2.5 The number of B3LYP/6-31G(d) potential energy minima found for 4a/5a , 4b/5b within each conformational ensemble	47
Table 2.6 Boltzmann distribution of conformational ensembles in 4a/b and 5a/b	53
Table 2.7 Calculated (B3LYP/6-31(d,p)u+1s//B3LYP/6-31G(d)) ^a vs experimental (CDCl ₃) ¹ H- ¹ H coupling constants	54
Table 2.8 All-carbon ^a mean absolute deviation (MAD) in calculated ¹³ C NMR resonances	56
Table 2.9 Calculated vs. observed ¹³ C NMR chemical shifts	57
Table 3.1 Growth inhibition activity of MMV008138 modified on position C3	67
Table 3.2 Bioisosteres synthesized from 1a by Dr. Ghavami and Ms. Liu	72
Table 3.3 <i>P. falciparum</i> growth inhibition of compounds 16a-22a	73
Table 3.4 Attempt to protect secondary amine in 8a with Cbz group	95
Table 3.5 Optimization of Cbz-protection reaction for 4a and 5a	98
Table 3.6 Optimization of primary amide 51a synthesis	101

Table 3.7 Optimization of tetrazole 54a synthesis	102
Table 3.8 Optimization of Cbz-deprotection in the formation of 23a	104
Table 3.9 Reduction of oxime 61 to tryptophan analog (\pm)- 55	110
Table 3.10 Attempts of (\pm)- 57a hydrolysis under acidic conditions monitored by TLC	111
Table 3.11 Hydrolysis of (\pm)- 56a /(\pm)- 57a with TMSBr monitored by ^1H and ^{31}P NMR	112
Table 5.1 ^{13}C NMR chemical shifts (CDCl_3) of C-1 and C-3 for 4a-ar and 5a-ar	170
Table 5.2 ^{13}C NMR chemical shifts (CDCl_3) of C=O and C1' for 4a-ar and 5a-ar	171
Table 5.3 ^1H NMR chemical shifts (CDCl_3) of H-3, H-4 α , and H-4 β for 4a-ar and 5a-ar	172
Table 5.4 J_{HH} [Hz] values (CDCl_3) for H-3, H-4 α , and H-4 β for 4a-ar and 5a-ar	173
Table 5.5 Selected 1D NOE correlations observed in 4a/5a	174
Table 5.6 Calculated energies of 4a at MMFF94 and B3LYP/6-31G(d) levels of theory	176
Table 5.7 Calculated energies of 4a at B3LYP/6-311+G(2d,p)// B3LYP/6-31G(d) (Method 1), mPW1PW91/6-311+G(2d,p)// B3LYP/6-31G(d) (Method 2), and M06-2X/def2-TZVP//B3LYP/6-31G(d) (Method 3), all with SCRF=(PCM, solvent=chloroform)	177
Table 5.8 Calculated energies of 4b at MMFF94 and B3LYP/6-31G(d) levels of theory	178
Table 5.9 Calculated energies of 4b at B3LYP/6-311+G(2d,p)// B3LYP/6-31G(d) (Method 1), mPW1PW91/6-311+G(2d,p)// B3LYP/6-31G(d) (Method 2), and M06-2X/def2-TZVP//B3LYP/6-31G(d) (Method 3), all with SCRF=(PCM, solvent=chloroform)	179
Table 5.10 Calculated energies of 5a at MMFF94 and B3LYP/6-31G(d) levels of theory	180
Table 5.11 Calculated energies of 5a at B3LYP/6-311+G(2d,p)// B3LYP/6-31G(d) (Method 1), mPW1PW91/6-311+G(2d,p)// B3LYP/6-31G(d) (Method 2), and M06-2X/def2-TZVP//B3LYP/6-31G(d) (Method 3), all with SCRF=(PCM, solvent=chloroform)	181
Table 5.12 Calculated energies of 5b at MMFF94 and B3LYP/6-31G(d) levels of theory	182

Table 5.13 Calculated energies of 5b at B3LYP/6-311+G(2d,p)// B3LYP/6-31G(d) (Method 1), mPW1PW91/6-311+G(2d,p)// B3LYP/6-31G(d) (Method 2), and M06-2X/def2-TZVP//B3LYP/6-31G(d) (Method 3), all with SCRF=(PCM, solvent=chloroform)	183
Table 5.14 Boltzmann distribution of conformer ensembles of 4a , 5a , 4b , 5b [%]	184
Table 5.15 Calculated (B3LYP/6-31G(d,p)u+1s//B3LYP/6-31G(d)) ¹ H- ¹ H coupling constants for all conformers	185
Table 5.16 Observed and calculated Boltzmann weighted average ¹ H- ¹ H coupling constants for 4a , 5a , 4b , 5b	186
Table 5.17 Calculated Boltzmann weighted average ¹³ C NMR compared to experimentally obtained chemical shifts in compound 4a	187
Table 5.18 4a Shielding tensors B3LYP/6-311+G(2d,p)//B3LYP/6-31G(d) SCRF = (PCM, CHCl ₃)	188
Table 5.19 4a Shielding tensors mPW1PW91/6-311+G(2d,p)//B3LYP/6-31G(d) SCRF = (PCM, CHCl ₃)	189
Table 5.20 Calculated Boltzmann weighted average ¹³ C NMR compared to experimentally obtained chemical shifts in compound 4b	190
Table 5.21 4b Shielding tensors B3LYP/6-311+G(2d,p)//B3LYP/6-31G(d) SCRF = (PCM, CHCl ₃)	191
Table 5.22 4b Shielding tensors mPW1PW91/6-311+G(2d,p)//B3LYP/6-31G(d) SCRF = (PCM, CHCl ₃)	192
Table 5.23 Calculated Boltzmann weighted average ¹³ C NMR compared to experimentally obtained chemical shifts in compound 5a	193
Table 5.24 5b Shielding tensors B3LYP/6-311+G(2d,p)//B3LYP/6-31G(d) SCRF = (PCM, CHCl ₃)	194
Table 5.25 5b Shielding tensors mPW1PW91/6-311+G(2d,p)//B3LYP/6-31G(d) SCRF = (PCM, CHCl ₃)	195

Table 5.26 Calculated Boltzmann weighted average ^{13}C NMR compared to experimentally obtained chemical shifts in compound 5b	196
Table 5.27 5b Shielding tensors B3LYP/6-311+G(2d,p)//B3LYP/6-31G(d) SCRF = (PCM, CHCl_3)	197
Table 5.28 5b Shielding tensors mPW1PW91/6-311+G(2d,p)//B3LYP/6-31G(d) SCRF = (PCM, CHCl_3)	198
Table 5.29 Predicted ^{13}C NMR shifts in C-1 and C-3 for conformers of compound 4a	199
Table 5.30 Predicted ^{13}C NMR shifts in C-1 and C-3 for calculated conformers of compound 4b	200

1 Overview of *P. falciparum*'s biology and methods to fight malaria

Malaria is a mosquito-borne disease caused in humans by one of five species of *Plasmodium* parasite. The most prevalent species in Africa is *Plasmodium falciparum*, which is also associated with the most severe disease outcomes. Although the incidence of malaria cases was steadily declining until 2014, since then, a slow increase in new cases has been observed every year (Figure 1.1). In 2019, there have been an estimated 229 million new cases, 94% of which were diagnosed in Africa. In the same year, 409 thousand deaths were reported, 67% of which were among children under the age of five. Since 2016, the previously steady decrease in mortality began to stall. Moreover, emerging resistance to antimalarial drugs and insecticides used for mosquito control has resulted in a renewed increase in malaria incidence in past years.¹ Consequently, there is currently a dire need to explore novel treatment and control methods to eradicate malaria.

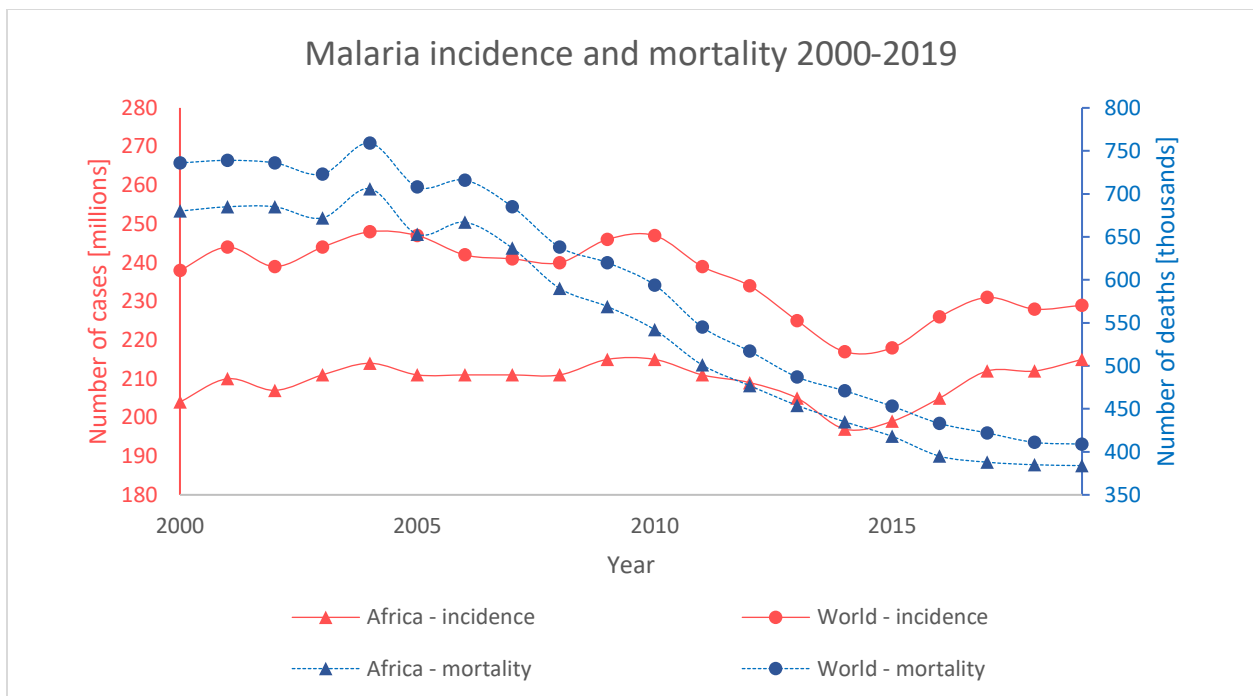


Figure 1.1 Malaria incidence and mortality globally and in Africa in years 2000-2019. Graph was produced with data from World Malaria Report 2020 (License: CC BY-NC-SA 3.0 IGO).¹

1.1 Epidemiology of falciparum malaria

The pathogen causing the most severe form of malaria – *P. falciparum* is most widely spread in Africa, where it is responsible for up to 99.7% of local malaria cases, but is also endemic to South-East Asia (50%), Eastern Mediterranean (71%), and the Western Pacific Region (65%, Figure 1.2).² The worldwide incidence of malaria infection decreased from 7.1 to 5.7% among the population at risk between 2010 and 2014. Unfortunately, since 2014, the rise of resistance to the current prophylactic and therapeutic methods caused a significant slowdown in malaria eradication efforts.²

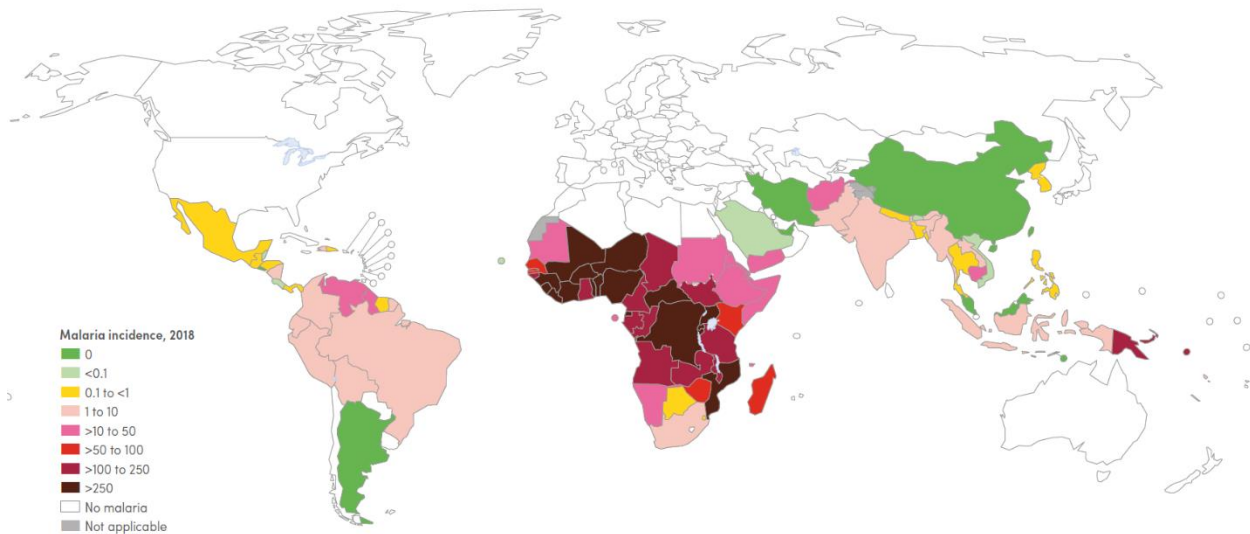


Figure 1.2 Status of global malaria incidence rates in 2018. The incidence is reported as a number of cases per 1000 people at risk. Reproduced from World Malaria Report 2019 (License: CC BY-NC-SA 3.0 IGO).²

1.2 Clinical outcomes of falciparum malaria

The demographic most at risk in areas with stable transmission of *P. falciparum* includes young children and pregnant women. Initial infection by *P. falciparum* presents itself with non-specific symptoms, including fever, headaches, nausea, and muscle pain, but may also be connected to severe outcomes with clearly differentiated clinical symptoms among various age groups. Severe

falciparum malaria in children often results in coma (also called cerebral malaria), respiratory distress leading to tissue hypoxia, and severe anemia. Among adults, severe malaria usually presents itself with hepatic and renal dysfunctions and pulmonary edema. The risk of developing severe malaria declines rapidly with age in areas endemic to *P. falciparum* due to naturally acquired immunity, however, the susceptibility to infection persists.³

1.3 Transmission and life cycle

The members of *Plasmodium spp.* spend their complex lifecycle alternating between two hosts – mosquitos of the *Anopheles* genus and a vertebrate host, such as humans. *P. falciparum* is transmitted into a human host by a bite from an infected female *Anopheles* mosquito. Shortly after, they infect hepatocytes and begin a brief, asymptomatic liver stage, followed by a blood stage responsible for the aforementioned clinical symptoms of malaria. During the blood stage, most parasites reproduce asexually, while a small portion of the parasites turns to sexual reproduction and form gametocytes, the transmissible form of the parasite that can be ingested by another mosquito during a blood meal. The single cycle of *P. falciparum*'s sexual reproduction occurs within the mosquito host, producing sporozoites that are ready to infect another human host.^{3, 4} Thus, the *P. falciparum*'s life cycle can be divided into four major phases – mosquito, liver, blood, and transmission phase.

1.3.1 Mosquito phase and transmission to the human host

The mosquito phase of *P. falciparum*'s life cycle starts with the ingestion of gametocytes by a female *Anopheles* mosquito during a blood meal from an infected host (Figure 1.3). Xanthurenic acid present in a mosquito's gastrointestinal tract, together with a drop in temperature and increase in the environment's pH, initializes gametogenesis. Both male and female gametocytes lose the erythrocyte membrane and differentiate into spherical gametes. Male gametes then undergo

exflagellation – a set of three DNA replication cycles to produce and release up to eight motile microgametes.^{4,5} Fertilization of a female gamete leads to the formation of a zygote, which then undergoes meiosis and transforms into an ookinete. Unlike spherical zygotes, elongated ookinetes are capable of motility, tissue traversal, and invasion. Shortly after their formation, ookinetes permeate the peritrophic matrix surrounding the blood meal and continue across epithelial cells. The migration is over when an ookinete exits the basal end of the epithelium, attaches to the midgut wall, and transforms into an oocyst. The oocyst maturation takes 10-12 days, during which many mitotic cycles occur, forming sporozoites. Mature oocyst then erupts to release thousands of sporozoites into the mosquito's hemolymph, which then carries them to all mosquito's tissues, including salivary glands. The sporozoites adhere to salivary glands and invade the salivary ducts, where they further mature and become infectious to mammalian hosts.⁴

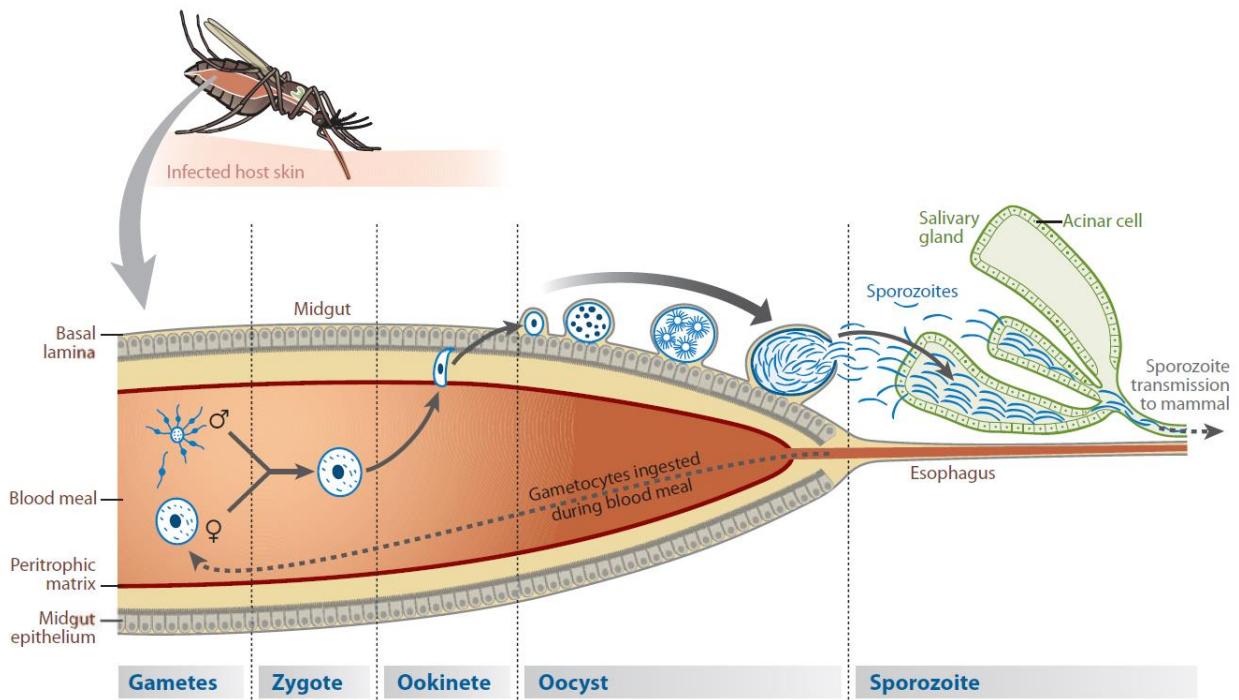


Figure 1.3 Mosquito stage of *P. falciparum* life cycle. ⁴ Republished with permission of Annual Reviews, Inc., from Malaria parasite development in the mosquito and infection of the mammalian host, Aly *et al. Annu. Rev. Microbiol.* **2009**, *68*, 195-221; permission conveyed through Copyright Clearance Center, Inc.

1.3.2 Asymptomatic liver phase (pre-erythrocytic phase)

When an infected *Anopheles* mosquito takes a blood meal, *P. falciparum* sporozoites are injected into the host's dermis and initiate the migration part of the pre-erythrocytic phase of their life cycle (Figure 1.4). During the first 1-3 hours after the bite, sporozoites rely solely on their gliding motility to reach the bloodstream. When they find and penetrate a blood vessel, the sporozoites travel through the cardiovascular system to the liver where they find and invade suitable hepatocytes.^{3,4} The sporozoites then form parasitophorous vacuole membrane (PVM) inside of the hepatocyte and undergo schizogony to form up to forty thousand merozoites per infected hepatocyte. This stage of development takes about ten days and culminates in a release of merozoites, vesicular structures which transport thousands of merozoites into the bloodstream where they are released.³

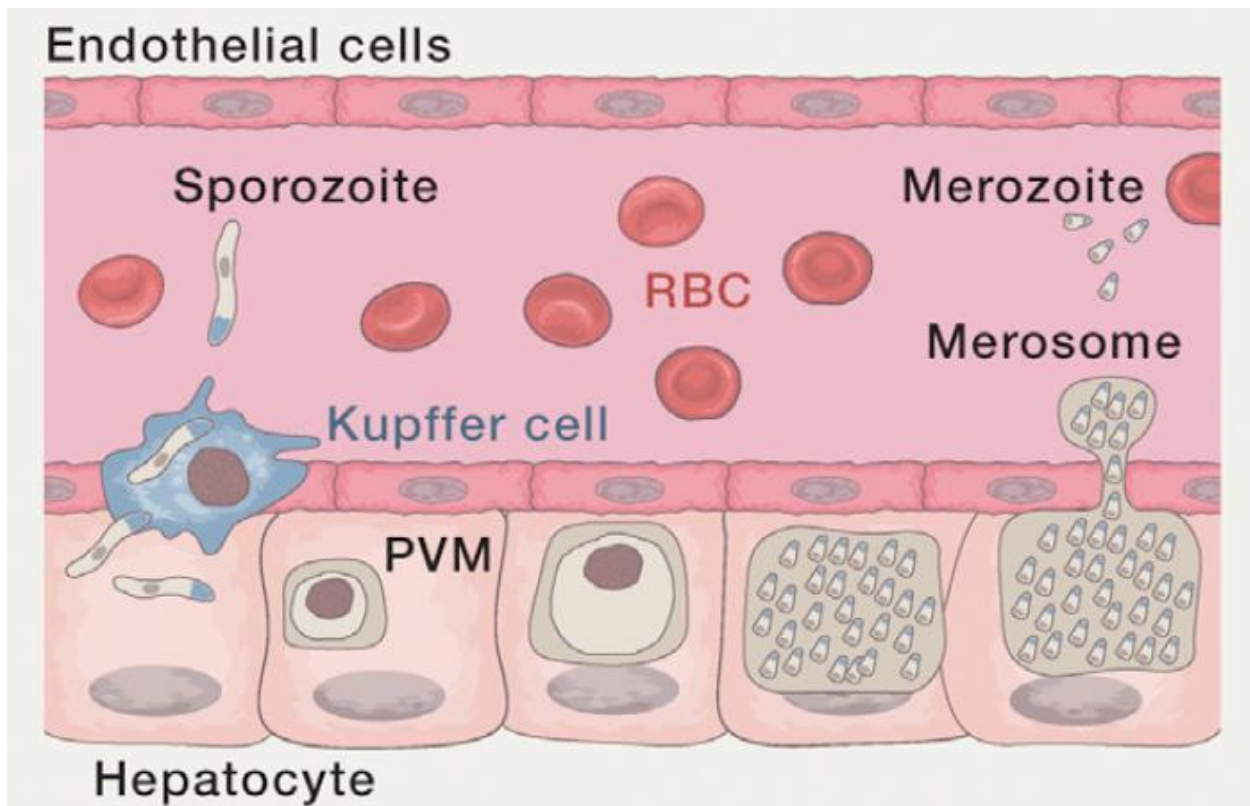


Figure 1.4 Pre-erythrocytic stage of *P. falciparum* life cycle.³ Adapted from *Cell*, vol. 167, Cowman *et al.*, Malaria: biology and disease, p. 610-524, 2016, with permission from Elsevier.

1.3.3 Symptomatic blood stage

The merozoites released into a blood vessel rapidly attack and invade available red blood cells (Figure 1.5).⁶ The merozoite invasion into an erythrocyte takes only about two minutes. Upon entry, merozoite forms a new PVM, which is sealed when merozoite is fully incorporated along with the erythrocyte plasma membrane. Subsequent schizogony takes about two days and results in an explosive release of 16-32 merozoites which infect other erythrocytes.³

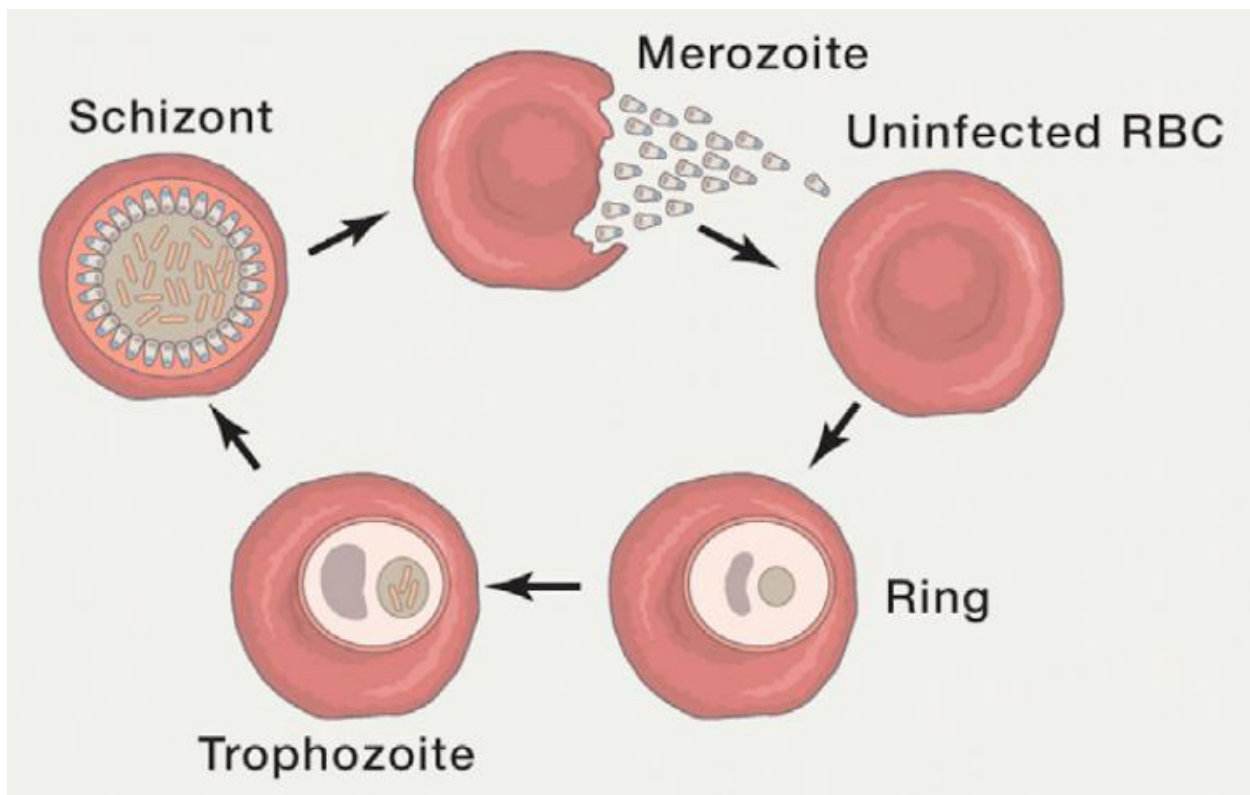


Figure 1.5 Asexual replication of *P. falciparum* during the blood stage of its life cycle.³ Adapted from *Cell*, vol. 167, Cowman *et al.*, Malaria: biology and disease, p. 610-524, 2016, with permission from Elsevier.

1.3.3.1 Ring stage of asexual development

The ring stage follows directly after the incorporation of merozoite into the erythrocyte and is characterized by extensive remodeling of the infected red blood cell (iRBC). The parasite induces

the formation of Maurer's clefts – vesicular structures used for trafficking of proteins from the parasite to the iRBC surface, and most of the parasite's activity within the iRBC is focused on the expression and export of *Plasmodium* proteins. Notably, the ring stage is also the only stage of asexual reproduction in which the iRBCs are mobile and found in blood samples of infected patients.⁶

1.3.3.2 Trophozoite stage of asexual development

Approximately 24 hours after infection, the iRBC is transformed into an immobilized, hemoglobin-consuming trophozoite stage. This phase of the cycle is characterized by a rapid increase in hemoglobin metabolism and the parasite's growth.⁶ The trophozoite stage expresses the *P. falciparum* erythrocyte membrane protein 1 (*PfEMP1*), allowing it to adhere to the cell wall of a blood capillary and to avoid splenic clearance.^{3, 6} The high diversity of *PfEMP1*'s tissue-specific binding receptors allows the parasite to infect a wide variety of tissues, sequester in peripheral capillaries, and even avoid destruction by the immune system through switching between antigenically distinct isoforms of *PfEMP1*.⁷

1.3.3.3 Schizont stage of asexual development

The transition from trophozoite to schizont stage is not accompanied by any significant morphological changes of the iRBC. The parasite steadily grows, and its food vacuole moves towards the center of the parasite (10-15 hours before rupture). About 3-4 hours before rupture, the parasite occupies most of the iRBC, invagination of the parasitological plasma membrane is detectable, and Maurer's clefts are disassembled. About 2 hours before the iRBC ruptures, cell division is initiated to form up to 32 merozoites. Subsequently, the host cell with mature merozoites ruptures, and the released merozoites re-infect healthy erythrocytes.⁶

1.3.4 Sexual development and transmission to the mosquito

The commitment of an asexual schizont to differentiate into non-dividing male or female gametocytes relies on the DNA-binding protein *PfAP2-G*, which activates early gametocyte gene transcription.⁸ The exact molecular basis of the merozoite's commitment to sexual development is unknown; however, some environmental stimuli (e.g., high parasitemia or exposure to antimalarial drugs) have been shown to cause this developmental switch.³ The decision to undergo gametocytogenesis is made in the last preceding asexual replication cycle when all merozoites formed in the schizont commit to becoming either male or female gametocyte. The factors that determine gametocyte sex are not well understood, but the ratio seems to be female-biased.⁵ The sexual development of *P. falciparum* is a complex process lasting 10-14 days and consisting of five morphologically distinctive stages depicted in Figure 1.6.⁹ To avoid clearance by the immune system or spleen during the long gametocytogenesis, the immature gametocytes of *P. falciparum* are sequestered in parenchyma – the extravascular compartment of bone marrow in which erythropoiesis happens.¹⁰

The sexual merozoites and young gametocytes are either formed in parenchyma from committed asexual schizonts already sequestered in bone marrow, or they find their way to the parenchyma from the vascular system.⁹ While the early gametocyte stages (I and II) express a number of membrane proteins, including *PfEMP1*, that allow them to adhere to bone marrow cells,⁵ later stages of gametocyte development no longer have these membrane proteins, and their sequestration inside parenchyma relies on a different mechanism.¹⁰ The exact mechanism of later-stage gametocyte sequestration is not known; however, increased rigidity of gametocytes in stages II-IV of the development may play a role by mechanically trapping the gametocytes within the parenchyma. The increase in rigidity of stage II-IV gametocytes is at least partially caused by the

development of an extensive microtubule cytoskeleton, which is also responsible for the elongated shape of the gametocytes.¹¹ The protein synthesis and hemoglobin digestion of gametocytes cease by the end of stage III, and further nucleic acid synthesis is restricted to the synthesis of RNA in preparation for exflagellation and rapid nuclear division upon transmission to the *Anopheles* host. In stage IV, the parasite occupies most of the host cell, and the sex of the gametocyte can be distinguished under a microscope.⁵ After reaching the maturation in stage V, the cytoskeleton is disassembled, and a highly deformable mature gametocyte can re-enter the bloodstream. High deformability of the crescent shape gametocyte enables it to transit through interendothelial slits inside the spleen and thus allows it to survive in circulation.¹¹ Even though the maximum survival time of a mature gametocyte is estimated to be three weeks, the mean circulation time is only about six days.^{5, 10}

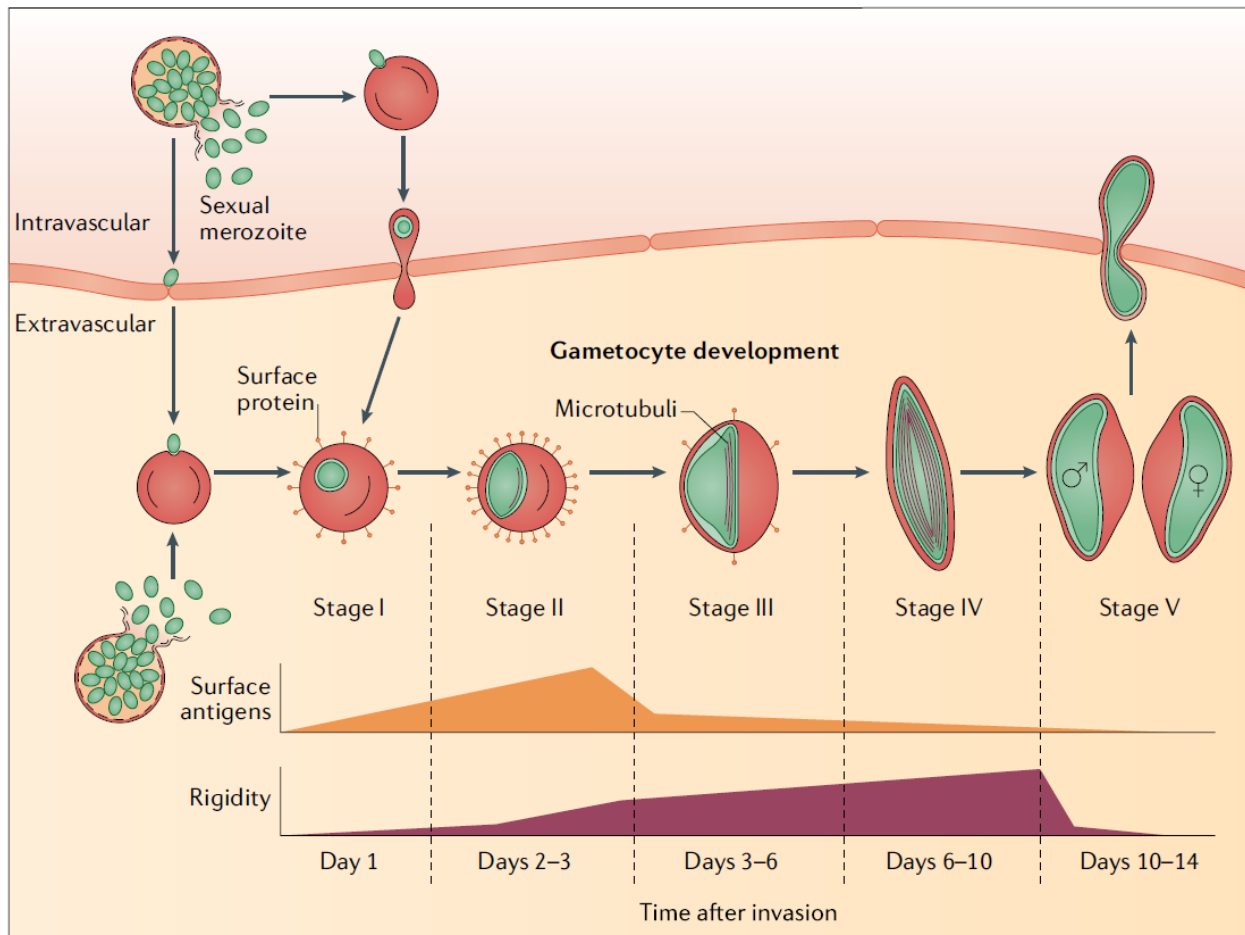


Figure 1.6 Sexual development of *P. falciparum*. Adapted by permission from Springer Nature Customer Service Centre GmbH: Springer Nature, *Nat. Rev. Microbiol.*, Plasmodium asexual growth and sexual development in the haematopoietic niche of the host, Venugopal *et al.* 2020.

1.4 Prevention of falciparum malaria

Prevention of malaria infection is nowadays focused primarily on vector control via distribution of insecticide-treated nets (ITNs) and application of indoor residual spraying (IRS). On an individual scale, the use of topical repellents or insecticide-treated clothing is also common. Methods directly targeting the *Plasmodium spp.* include vaccine development, which unfortunately has not reached commercial availability yet, and the use of antimalarial medicines for chemoprevention. The prophylactic use of antimalarials is usually recommended to travelers

and pregnant women in areas endemic to *P. falciparum*. Prophylactic antimalarial drugs are discussed in Subchapter 1.5.¹²

1.4.1 Malaria vaccine

The high complexity of the parasite's biology and life cycle discussed in the previous section poses great challenges for the development of a vaccine against malaria. Currently, there is no commercially available vaccine; however, over 20 vaccine candidates are now being evaluated in clinical trials. The most advanced vaccine candidate – RTS, S/AS01 recently succeeded in the Phase 3 clinical trial.¹³ The protection offered by this first-generation vaccine targeting sporozoite infection is likely to be partial and temporary, and, in order to obtain a genuinely efficient vaccine for malaria eradication, the development of further vaccine generations will be necessary. The landmarks set for a positive evaluation of the first-generation vaccine are more than 50% efficacy over at least one year. New landmarks set for next generations already call for at least 75% efficacy over a two-year period.¹⁴

1.4.2 Vector control

An *Anopheles* mosquito, as the only natural source of malaria transmission, presents itself as an ideal target for vector control. The majority of vector control efforts are focused on adult female *Anopheles*, primarily via the application of insecticides. The use of chemical pesticides dates back as early as the 19th century, which has been revolutionized by the discovery of new insecticides during the 20th century.¹⁵ Notable success in malaria control was achieved by the employment of dichlorodiphenyltrichloroethane (DDT). The use of DDT is currently banned in many countries due to its environmental toxicity, persistence, and ability to accumulate in various human tissues.^{12,}

¹⁵ The World Health Organization (WHO) still allows the use of DDT under specific circumstances, when no alternative equally effective insecticide is available, and with strict

adherence to safety guidelines established by the Stockholm Convention on Persistent Organic Pollutants.¹²

Insecticides are usually applied as IRS, used to treat ITNs, or as space spraying in emergency scenarios. The space spraying distributes fine aerosol of fast-acting insecticide or can be applied as spraying with several insecticides within a short time frame. This method, used for the rapid decrease in active mosquitoes' population, is discouraged by current WHO guidelines due to a lack of evidence about its efficiency.¹² IRS and ITNs – including long-lasting ITNs with required efficiency for at least three years, are the method of choice for malaria vector control in sub-Saharan Africa.¹⁵ Both of these indoor methods successfully reduce malaria transmission by more than 90%; however, they have only limited effect on malaria prevalence in the region.¹⁶ Typically, IRS and ITNs are not combined because the added benefit of an additional insecticide method has been shown to be negligible in most scenarios.¹² The ITNs are typically treated with pyrethroid class of insecticides, which is known for minimal mammalian toxicity,¹⁵ and thus the current WHO guidelines recommend that if a combination of ITNs and IRS is required, the IRS must be based on a different class of insecticides. Resistance to the insecticides used for ITNs and IRS is rising moderately and, so far, has not led to a failure of vector control methods. However, as the cautious use of insecticides is the necessary first step, the development of new insecticides is necessary to fight emerging mosquito resistance.^{12, 16}

Apart from widely used ITNs and IRS, other methods of vector control are being developed. Additional chemical control consists of poisoned sugar baits targeting both male and female sugar-feeding mosquitos and the introduction of insecticide-coated membranes inside of house air ventilation ducts. Notable efforts have been made in larval control by introduction of aquatic predators and use of chemical and bacterial larvicides.^{15, 16}

Genetic modification methods to reduce the malaria-transmitting mosquito population have been developed as well. Notable examples of genetically modified mosquitoes are sterile male mosquitoes or mosquitoes artificially infected with *Wolbachia* bacteria, which is symbiotic to *Anopheles* mosquitoes affecting its reproduction cycle. Mosquitoes carrying *Wolbachia* are incompatible with *Wolbachia*-free mosquitoes or mosquitoes infected by a different strain of *Wolbachia*. Progenies resulting from the mating of incompatible mosquitoes are not viable. The recent discovery of CRISPR gene editing techniques allowed for the development of gene drive mosquitoes that can rapidly spread desirable traits by traditional sexual reproduction. An example of a desirable trait in the genetically modified mosquito is the inability to transmit *Plasmodium* pathogen into the human host.¹⁵⁻¹⁷

1.5 Treatment of falciparum malaria

The first historically used antimalarial drug was quinine, a natural product found in the bark of cinchona trees native to South America, which was introduced to western medicine by Spanish monks in the early 17th century who used it in the form of a crude bark extract.¹⁸ Pure quinine was isolated much later, in 1820, by French chemists Pierre Pelletier and Joseph Caventou. However, soon it became the medicine of choice to treat malaria in both Europe and the United States.^{18, 19} Advances in the production of synthetic quinoline-type antimalarials, such as chloroquine and mefloquine, throughout the 20th century played a significant role in eliminating malaria from many parts of the world. Another important antimalarial agent is artemisinin, isolated from the plant *Artemisia annua* in China in 1972. Artemisinin and its derivatives are currently routinely used in malaria treatment.²⁰ Commercially available antimalarials can be classified into several categories based on their structure and mode of action. Representative examples of these drugs are shown in Figure 1.7.²¹ The current guidelines provided by WHO in response to the rise in antimalarial

resistance discourage the use of single drugs and instead promote combinational therapy based on artemisinin and one or more other antimalarials.²²

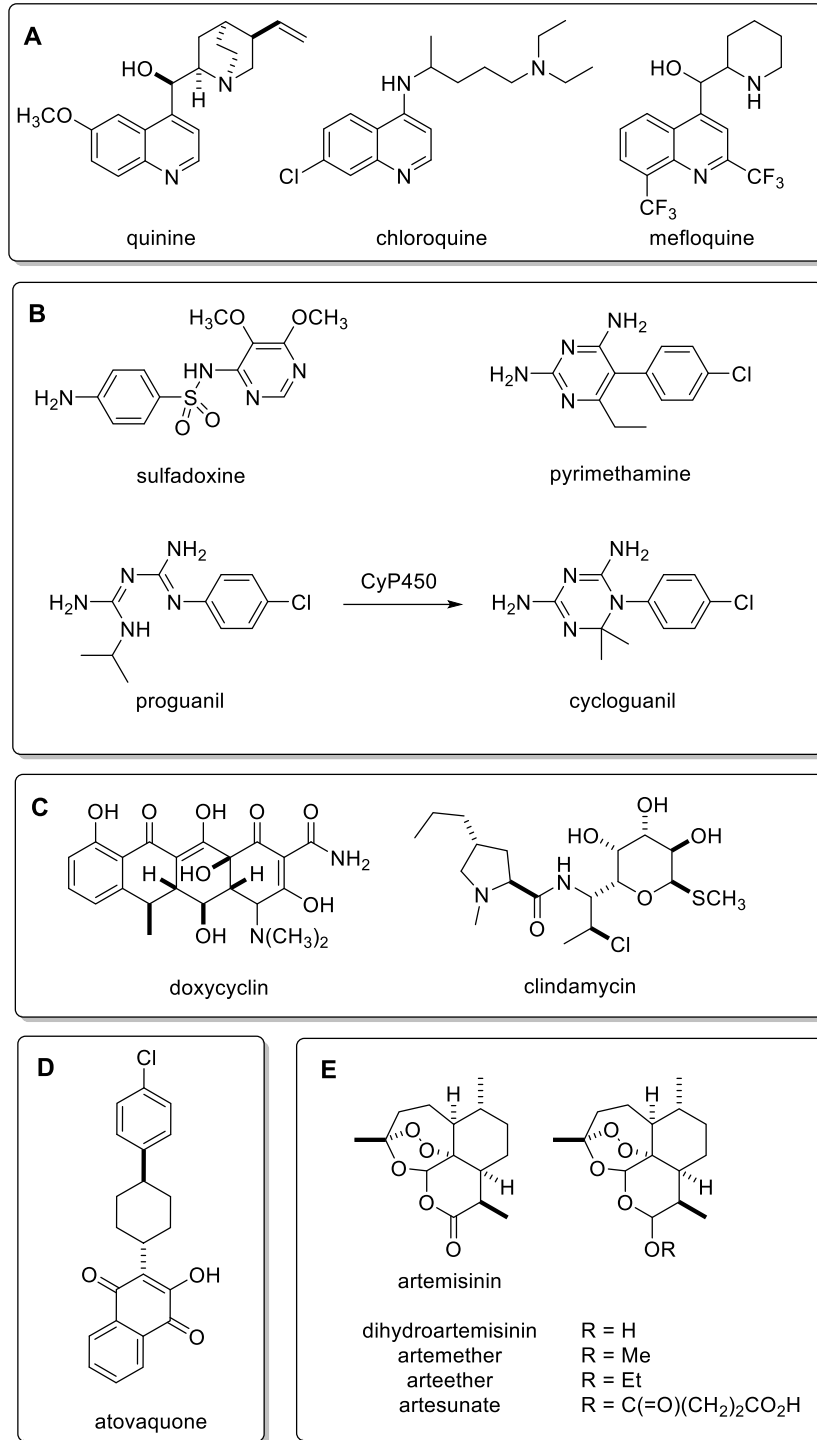


Figure 1.7 Examples of clinically used antimalarial agents

1.5.1 Quinoline-type antimalarials

The original malaria drug quinine is a representative of quinoline-type antimalarials (Figure 1.7A). Due to many side effects related to treatment with quinine, its use is currently limited. Nonetheless, quinine is still valuable for treating uncomplicated multi-drug-resistant malaria and severe malaria when intravenous medication administration is necessary.²⁰ Moreover, quinine is one of the few antimalarials considered safe to use during the first trimester of pregnancy.²²

The first notable quinoline-containing synthetic antimalarial drug was chloroquine, introduced to the market in 1946, which played a significant role in malaria eradication efforts. By the end of the 1950s, large-scale prophylactic use of chloroquine resulted in the development of chloroquine-resistant strains of *P. falciparum* that are now found in most regions with endemic malaria. Nonetheless, chloroquine is still used against sensitive parasites due to its low cost and minimal side effects.²⁰ The mechanism of chloroquine's action stems from targeting the trophozoite stage of asexual reproduction, where it inhibits polymerization of heme into hemozoin which, unlike heme, is non-toxic to the parasite.²¹

Mefloquine was developed after the Vietnam War in response to high levels of chloroquine-resistant malaria infections in the U.S. military.²⁰ The widespread use in Asia resulted in a drastic decrease in the efficiency of mefloquine monotherapy; however, it is still highly effective against most chloroquine-resistant *P. falciparum* strains.²¹ Despite the number of structural similarities with chloroquine, mefloquine inhibits endocytosis and catabolism of hemoglobin rather than hindering the detoxification of hemoglobin metabolites.²³ The use of mefloquine is limited due to its high cost and neuropsychiatric side effects observed in some patients.^{20, 21}

1.5.2 Antifolates, mitochondrial inhibitors, and antibiotics

Antifolate antimalarials are used as a combination of two active compounds, each targeting one enzyme in *P. falciparum*'s folate mechanism and thus depleting the parasite of essential folate cofactors (Figure 1.7B). The two targeted enzymes are dihydropteroate synthase (DHPS) and dihydrofolate reductase (DHFR).^{24, 25} DHPS inhibitors alone show only minimal efficacy against *P. falciparum* and simultaneously exhibit serious toxicity; however, they act synergistically when administered with DHFR inhibitors increasing potency of the latter.^{21, 25} A notable example of antifolate combination therapy is sulfadoxine-pyrimethamine (Fansidar[®]), which became popular for its low cost and efficacy comparable to chloroquine.²¹ Fansidar's use is very limited nowadays, both due to the rapid emergence of resistance and because prolonged use was connected to life-threatening side effects.^{20, 21}

Another DHFR inhibitor used for malaria treatment and prophylaxis is a prodrug proguanil, which converts to the active species cycloguanil in vivo via oxidation by cytochrome P450.^{20, 22} Similarly to sulfadoxine-pyrimethamine treatment, resistance developed soon after cycloguanil's introduction. Consequently, the drug cannot be used as a monotherapy.²¹ Alternative use for the proguanil was found in combination with atovaquone. Atovaquone is a ubiquinone analog that interferes with the cytochrome electron transport system, resulting in the collapse of membrane potential in the parasite's mitochondria. Atovaquone is not used independently because of the high treatment failure rate linked to the rapid development of resistance. The selection for resistant parasites is significantly decreased when atovaquone and proguanil are used together. This therapeutic combination is considered safe and is recommended by WHO for prophylactic use.²²

Several antibiotics are also known to have antimalarial activity (Figure 1.7C). Their mechanism of action is based on inhibition of procaryote-like RNA and protein synthesis inside a

vestigial organelle called the apicoplast, which will be discussed in more detail later.²⁰ The cytotoxic activity of antibiotics exhibits a so-called delayed death phenotype when the affected parasite dies only in the second replication cycle after exposure to the treatment. This delay leads to a clinically significant time gap between drug administration and improvement of malaria symptoms and could be fatal in non-immune patients. Consequently, antibiotics are employed only in combination with faster-acting antimalarial agents.²¹ Antibiotics commonly used in combination therapy include doxycycline and clindamycin.²²

1.5.3 Artemisinin-based antimalarials

The key structural feature responsible for the antimalarial activity of artemisinin and its semi-synthetic derivatives is their endoperoxide moiety (Figure 1.7D). Upon entry of the parasite, the endoperoxide can interact with iron(II) released from hemoglobin metabolites produced by *Plasmodium*. This reaction then forms oxygen free radicals and carbon-centered radicals. The exact mechanism of action of these radicals is not clear, but parasite death resulting from oxidative stress, alkylation of parasite's proteins and heme, or blockade of calcium channels were proposed.²⁶ Artemisinin is potent against all erythrocytic stages of the parasite life cycle, particularly the early ring stages. Unlike most other known antimalarials, artemisinin is also effective against *P. falciparum* gametocytes.²⁷ The clinical use of the parent drug, artemisinin, is limited by its low bioavailability resulting from poor aqueous solubility. This problem was ameliorated by the development of derivatives with increased water solubility. Representative examples are shown in Figure 1.7E.²⁶ Artemisinin derivatives, which can rapidly decrease parasitemia in patient's blood, in combination with other, slow-acting antimalarials (termed artemisinin combination therapies or ACTs), are now recommended by the WHO as the first line of treatment for most malaria cases.²²

1.5.4 Resistance to antimalarial drugs

The development of *P. falciparum*'s resistance to antimalarials represents a major obstacle in malaria eradication efforts. As mentioned in previous sections, practically all antimalarials introduced in the 20th century resulted in the rise of resistant strains. Treatments with artemisinin derivatives, used in broader clinical practice since the early 2000s, initially appeared to avoid the unfortunate fate of their predecessors.^{27, 28} The delayed clearance phenotype, suggesting early stages of resistance, was first observed in 2007 in western Cambodia where patients have prescribed an artemisinin-based monotherapy or ACTs.²⁹

As of 2020, the resistance of *P. falciparum* to multiple ACTs is widely spread throughout the Greater Mekong subregion of South-East Asia (Figure 1.8).³⁰ Even though few sporadic reports of loss of ACTs efficacy in the African region emerged in recent years, ACTs remain highly effective to treat African *P. falciparum* strains and are preferred as the first line of treatment in the region by WHO.³¹ Genetic studies of resistance-related mutations in parasites collected from blood samples of patients in the Greater Mekong subregion show that specific mutations are contained within a localized *Plasmodium* population. Therefore, the risk of resistance spread by the artemisinin-insensitive parasite is deemed to be low. A much greater risk to the wide spread of ACTs resistance is caused by the fact that, unlike more complicated resistance patterns of older drugs, the artemisinin resistance is caused by a single point mutation in the *PfKelch13* gene and may easily emerge within a population of artemisinin-susceptible *Plasmodium* spp.³⁰ The *PfKelch13* gene encodes the parasite's Kelch13 propeller protein responsible for endocytosis of hemoglobin in the early ring stage of asexual development. Inactivation of this protein leads to a lack of available iron(II) inside the early ring stage targeted by artemisinin, and consequently

reduces the iron(II)-mediated opening of the endoperoxide bridge of artemisinin (and derivatives). Inactivation of *PfKelch13* is also consistent with observation of prolonged development of ring stage among artemisinin-resistant parasites.³²

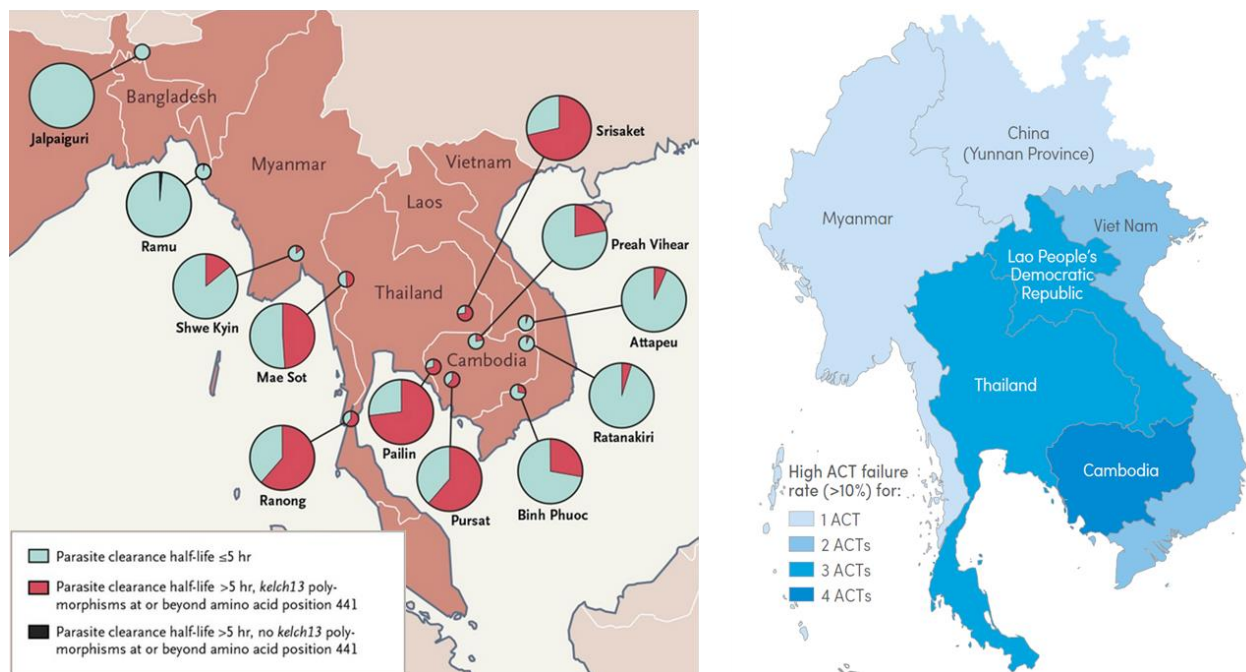
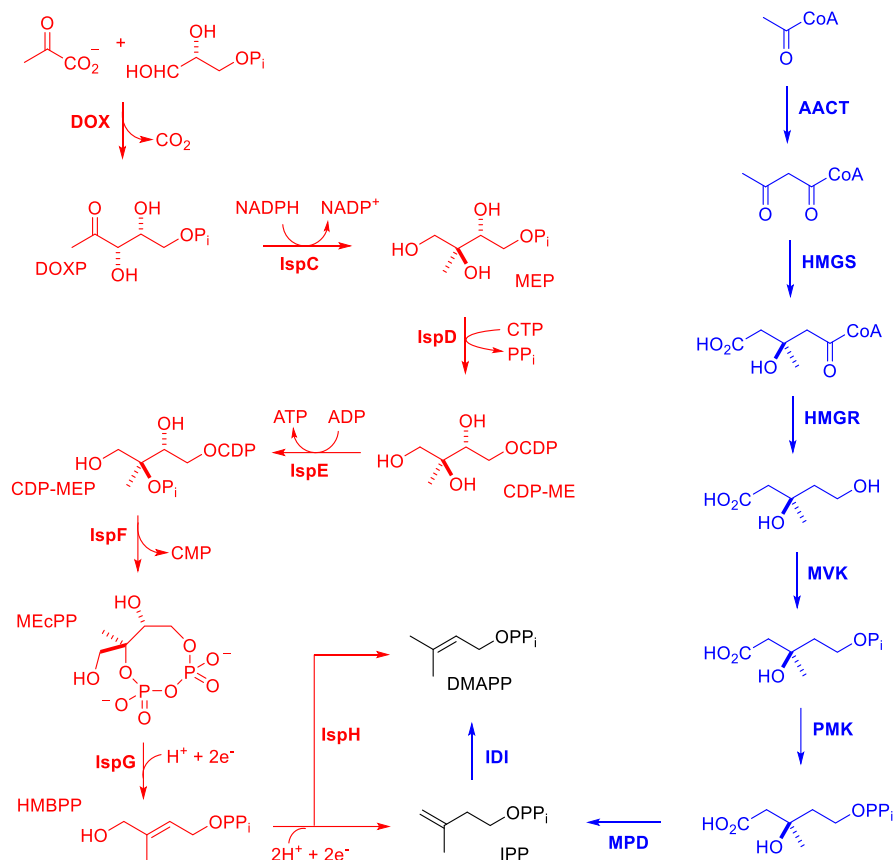


Figure 1.8 Prevalence of delayed clearance phenotype (left) and emerging resistance to multiple ACTs (right) in the Greater Mekong region. The left figure is reproduced with permission from Ashley *et al.* 2014, Copyright Massachusetts Medical Society. Reference Ashley *et al.* 2014. The right figure is reproduced from World Malaria Report 2018, License: CC BY-NC-SA 3.0 IGO.^{33, 34}

1.6 The search for a new target

Like other living organisms, *Plasmodium* parasites rely, among other things, on the biosynthesis of isoprenoid precursors for their survival. These precursors – isopentyl pyrophosphate (IPP) and dimethylallyl pyrophosphate (DMAPP), can be synthesized either via the mevalonate (MVA) pathway or the methylerythritol phosphate (MEP) pathway (Scheme 1.1). The MVA pathway is utilized by animals, fungi, and archaea, while the MEP pathway is found in eubacteria, green algae, and apicomplexan protozoa. Even though higher plants use both aforementioned biosynthetic pathways to produce isoprenoid precursors, the pathways are strictly

compartmentalized within the plant cell. Specifically, the MVA pathway is located in the cytosol and MEP pathway in chloroplasts.^{35, 36} In the *Plasmodium spp.*, the MEP pathway is localized solely within a vestigial plastid organelle called apicoplast. The apicoplast, surrounded by four bounding membranes, has been incorporated into the *Plasmodium*'s cell via secondary endosymbiosis of apicoplast-containing red algae.^{37, 38} The difference between human isoprenoid biosynthesis via MVA pathway and MEP pathway used by *Plasmodium spp.* makes the apicoplast organelle and the MEP pathway enzymes contained within it promising targets for the development of human-safe antimalarials.^{38, 39} Supplementation of IPP can reverse growth inhibition of blood-stage *P. falciparum*, both after treatment with an MEP pathway inhibitor and after a complete loss of the apicoplast.⁴⁰ Consequently, IPP supplementation can be used as a diagnostic tool for the identification of compounds targeting the apicoplast system.⁴⁰



Scheme 1.1 MEP pathway (in red) and mevalonate pathway (in blue).³⁵

1.7 MMV008138 and its analogs

The lead compound investigated in our group – MMV008138, was identified from an open-access compound library, Malaria Box, assembled by Medicine for Malaria Ventures (MMV).⁴¹ The Malaria Box consists of 400 compounds selected based on phenotypic screening of nearly six million compounds from research libraries of GlaxoSmithKline, Novartis, and St. Jude’s Children’s Hospital, against *P. falciparum*.^{41, 42} The MMV008138 was the only compound in the set exhibiting both satisfactory growth inhibition (> 95% at 5 μ M) and rescue of the parasite upon supplementation with IPP (>60% survival with the addition of 200 μ M of IPP) – parameters set by our collaborator Dr. Cassera.⁴³ Further studies revealed that MMV008138 targets the IspD enzyme within the MEP pathway.^{44, 45} Because the stereochemistry of Malaria Box compounds was not

disclosed, Dr. Yao in the Carlier group synthesized all four stereoisomers of the MMV008138, and the growth inhibition assay showed (1*R*,3*S*)-MMV008138 (**1a**) to be the most potent stereoisomer.⁴⁶ The same conclusion was independently reached by other research groups as well.^{44, 45} Several *cis* analogs of the MMV008138 with (1*S*,3*S*)- stereochemistry (**2a**, **2b**, **2e**, **2g**, **2aa**, **2ai**, **2ak**, **2am**) were evaluated, but their growth inhibition potency was low and the focus of the structure-activity relationship (SAR) studies turned solely to the *trans* (1*R*,3*S*)- analogs.^{46, 47}

Unfortunately, a protein crystal structure of the *Pf*IspD has not been obtained to this day. Attempts to model the structure of *Pf*IspD have been made based on homology with known crystal structures of IspD in other species.⁴⁸ However, *in vitro* enzyme inhibition studies showed that **1a** does not inhibit IspD homologs isolated from *Escherichia coli*, *Arabidopsis thaliana*, or *Mycobacterium tuberculosis*. The IspD of *Plasmodium vivax* showed only weak to no inhibition by **1a** in two independent studies.^{44, 45} These results are not entirely surprising, considering the presence of additional domains in the primary amino acid sequence of *Pf*IspD that are absent in homologous IspDs. Moreover, the conserved portions of the *Pf*IspD sequence share $\leq 30\%$ identity with homologous IspDs, including *Pv*IspD. The purpose and tertiary structure of this domain are still to be explored.⁴⁵ Thus, the use of molecular docking calculations to inform SAR design based on homologous structures may not yield reliable results.

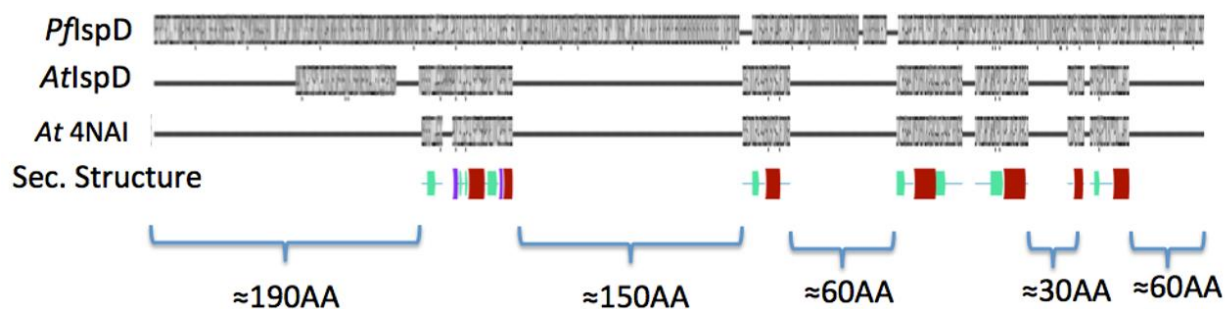
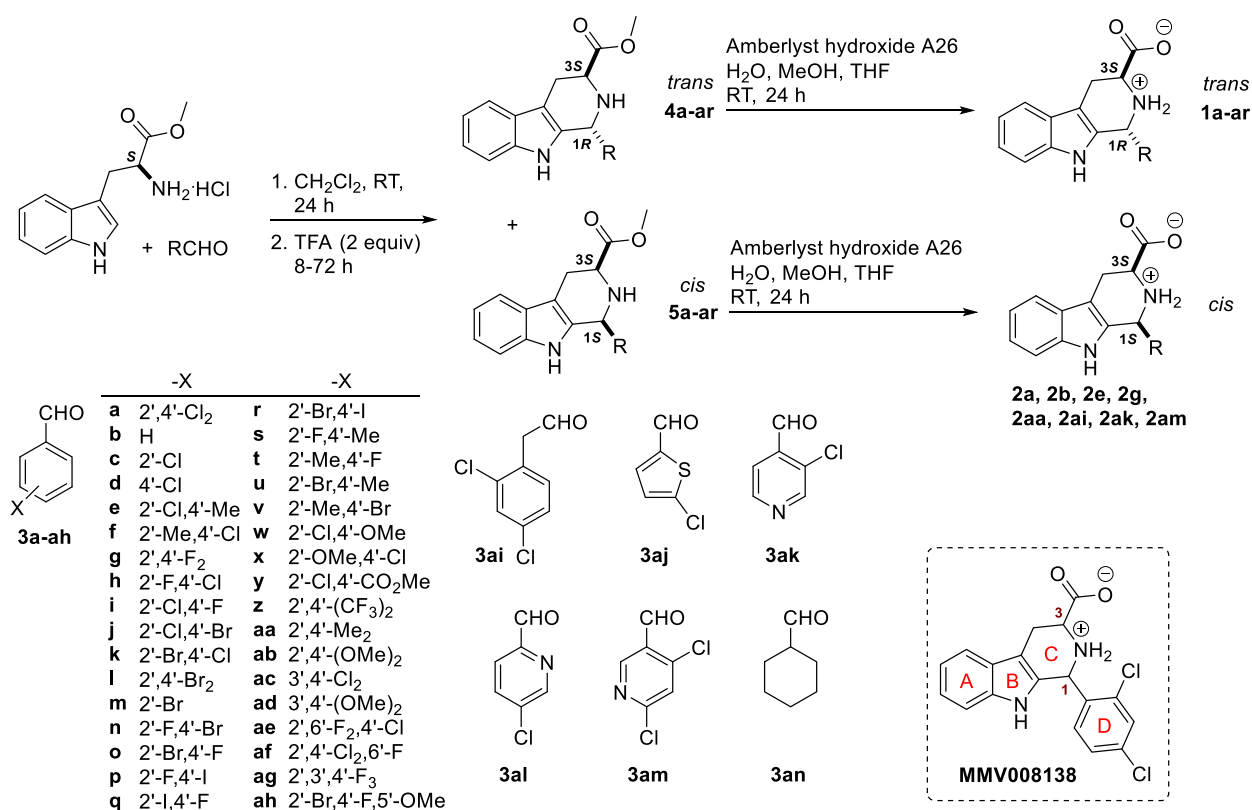


Figure 1.9 Comparison of the full-length amino acid sequence of *Pf*IspD and *At*IspD and sequence of crystallized *At*IspD construct. The figure was produced by our collaborator Dr. Maxim Totrov.

The initial SAR studies performed in the Carrier group focused primarily on the effects of the D-ring substitution (Scheme 1.2, **1a-an**). These D-ring variants were synthesized via Pictet-Spengler reaction from L-tryptophan methyl ester hydrochloride (Trp-OMe·HCl) and the corresponding aldehyde (**3a-an**). The resulting ester diastereomers, **4a-an** and **5a-an**, were separated by column chromatography and individually hydrolyzed using Amberlyst resin (Scheme 1.2).^{46, 47} Stereochemistry of the ester intermediates **4a-an** and **5a-an** was assigned using an empirical method based on ¹³C NMR chemical shifts developed in the early 1980s.⁴⁹ A new method for reliable assignment of these stereoisomers utilizing ¹H NMR was developed in our laboratory and will be discussed in detail in Chapter 2 of this work.



Scheme 1.2 Synthetic pathway to D-ring variants of MMV008138.

The growth inhibition potency of the synthesized compounds against the Dd2 strain of *P. falciparum* was evaluated by SYBR Green assay. SYBR Green is a dye with low intrinsic

fluorescence, which upon interaction with double-stranded DNA (via intercalation and minor-groove binding), dramatically enhances its fluorescent emission.⁵⁰ Because mature red blood cells lack nuclei, and thus DNA, the treatment of *P. falciparum* culture in the presence of potential inhibitor with SYBR Green dye will detect growth inhibition as a function of decreasing fluorescence intensity.⁵¹ Furthermore, MEP was confirmed as a biological target by the IPP rescue assay. As discussed previously, the MEP pathway is solely responsible for the production of essential isoprenoid precursors – IPP and DMAPP, in *P. falciparum*. Consequently, growth inhibition resulting from the lack of isoprenoid precursors can be reverted by IPP supplementation.⁴³ Several synthesized analogs were also tested against recombinant target enzyme – *PflspD*. The results of SAR studies suggest that the 2',4'-substitution pattern and the presence of halogen are necessary for satisfactory growth inhibition and *PflspD* inhibition (Table 1.1).^{46, 47, 52}

Table 1.1 Overview of biological activity of MMV008138 D-ring variants synthesized in Carlier lab. ^aUnpublished work, synthesized by me. ^bSynthesized by Mr. Jopaul Mathew.

	X	<i>P. falciparum</i> Dd2 strain IC ₅₀ (nM)	% Rescue with 200 μM IPP	<i>PflspD</i> IC ₅₀ (nM)	Ref
1a	2', 4'-Cl ₂	250 ± 70	100 @ 2.5 μM	44 ± 15	46, 52
ent-1a	2', 4'-Cl ₂	>10,000	ND	>1000	46
2a	2', 4'-Cl ₂	>10,000	ND	>1000	46
ent-2a	2', 4'-Cl ₂	3000 ± 200	60 @ 10 μM	>1000	46
1b	H	>10,000	ND	>5000	46, 47
2b	H	>10,000	ND	ND	46
1c	2'-Cl	3280 ± 990	60 @ 10 μM	~1000	46, 47
1d	4'-Cl	1170 ± 60	50 @ 10 μM	510 ± 90	46, 47
1e	2'-Cl, 4'-CH ₃	410 ± 40	100 @ 2.5 μM	82 ± 10	46
2e	2'-Cl, 4'-CH ₃	>10,000	ND	ND	46
1f	2'-CH ₃ , 4'-Cl	700 ± 90	100 @ 2.5 μM	260 ± 50	46
1g	2', 4'-F ₂	780 ± 175	100 @ 5 μM	230 ± 10	46
2g	2', 4'-F ₂	>10,000	ND	ND	46
1h	2'-F, 4'-Cl	860 ± 80	100 @ 5 μM	140 ± 30	47
1i	2'-Cl, 4'-F	433 ± 55	100 @ 10 μM	100 ± 10	47
1j	2'-Cl, 4'-Br	320 ± 60	100 @ 5 μM	34 ± 11	47
1k	2'-Br, 4'-Cl	360 ± 40	100 @ 5 μM	31 ± 4	47

1l	2', 4'-Br ₂	590 ± 20	100 @ 10 μM	84 ± 14	47
1m	2'-Br	6000 ± 500	ND	ND	<i>a</i>
1n	2'-F, 4'-Br	1,600 ± 100	90 @ 10 μM	ND	<i>a</i>
1o	2'-Br, 4'-F	784 ± 40	100 @ 2.5 μM	ND	<i>a</i>
1p	2'-I, 4'-F	970 ± 180	100 @ 10	140 ± 70	47
1q	2'-F, 4'-I	3343 ± 496	100 @ 10	130 ± 20	47
1r	2'-Br, 4'-I	1500 ± 200	80 @ 10	ND	47
1s	2'-F, 4'-Me	1909 ± 110	ND	ND	52
1t	2'-Me, 4'-F	2799 ± 258	ND	ND	52
1u	2'-Br, 4'-Me	890 ± 93	100	ND	52
1v	2'-Me, 4'-Br	1444 ± 117	100	ND	52
1w	2'-Cl, 4'-OCH ₃	> 5000	ND	ND	47
1x	2'-OCH ₃ , 4'-Cl	2500 ± 600	ND	ND	47
1y	2'-Cl, 4'-CO ₂ H	NI @ 10 000	ND	ND	47
1z	2', 4'-(CF ₃) ₂	>10,000	ND	> 5000	46, 47
1aa	2', 4'-(CH ₃) ₂	IC ₇₀ ~ 10 μM	ND	~ 1000	46, 47
2aa	2', 4'-(CH ₃) ₂	>10,000	ND	ND	46
1ab	2', 4'-(OCH ₃) ₂	>20,000	ND	> 5000	46, 47
1ac	3', 4'-Cl ₂	>10,000	ND	NI @ 0.5 μM	47
1ad	3', 4'-(OCH ₃) ₂	>20,000	ND	ND	46
1ae	2', 6'-F ₂ , 4'-Cl	1800 ± 150	80 @ 10	ND	47
1af	2', 4'-Cl ₂ , 6'-F	972 ± 110	100	ND	52
1ag	2', 3', 4'-F ₃	~20,000	ND	ND	47
1ah	2'-Br, 4'-F, 5'-OCH ₃	>10,000	ND	ND	47
1ai	2,4-dichlorobenzyl	>10,000	ND	ND	47
2ai	2,4-dichlorobenzyl	>10,000	ND	ND	52
1aj	5-chlorothiophen-2-yl	>10,000	ND	ND	52
1ak	3-chloropyridin-4-yl	>10,000	ND	ND	52
2ak	3-chloropyridin-4-yl	>10,000	ND	ND	52
1al	5-chloropyridin-2-yl	4274 ± 465	ND	ND	52
1am	4,6-dichloropyridin-3-yl	2171 ± 680	ND	ND	52
2am	4,6-dichloropyridin-3-yl	>10,000	ND	ND	52
1an	cyclohexyl	>10,000	ND	ND	53, <i>b</i>

When D-ring modifications did not yield an analog with improved potency to **1a**, further SAR studies followed, with modifications in the A-, B-, and C- rings (Scheme 1.2). Methyl substitution on C1 in the same D-ring variants, as seen in analogs **a**, **b**, **c**, and **d**, resulted in a complete loss of potency.^{47, 54} Methyl substitution of D-ring variant **a** on either C3, N2, or N9 also led to a loss of potency.⁵² Analogs of **1a** bearing fluoro-, chloro-, bromo-, or a methyl- substitution on the A-ring were also prepared, and several of them exhibited good growth inhibition potency of *P. falciparum* (Dd2 strain). However, none of these analogs was equipotent or better than **1a**.⁵²

⁵⁵ Even though **1a** shows the highest growth inhibition potency in the series, it still faces several significant drawbacks, such as poor metabolic stability ($t_{1/2}$ in liver microsomes = 14.5 min) and suboptimal bioavailability (growth inhibition IC_{50} = 250 ± 70 nM, while *PflspD* IC_{50} = 44 ± 15 nM).^{47, 52} We tried to address some of these problems by preparing CO₂H isosteres of **1a**. These analogs will be discussed in detail in Chapter 3. In the following chapter, I describe a new method to assign stereochemistry in 1,3-disubstituted tetrahydro- β -carbolines, such as **4a** and its *cis*-isomer.

References

1. *World Malaria Report 2020: 20 years of global progress and challenges*; 978-92-4-001579-1; World Health Organization: Geneva, 11/30/2020, 2020.
2. *World Malaria Report 2019*; World Health Organization: Geneva, 2019.
3. Cowman, A. F.; Healer, J.; Marapana, D.; Marsh, K., Malaria: biology and disease. *Cell* **2016**, *167* (3), 610-624.
4. Aly, A. S.; Vaughan, A. M.; Kappe, S. H., Malaria parasite development in the mosquito and infection of the mammalian host. *Annu. Rev. Microbiol.* **2009**, *63*, 195-221.
5. Bousema, T.; Drakeley, C., Epidemiology and infectivity of *Plasmodium falciparum* and *Plasmodium vivax* gametocytes in relation to malaria control and elimination. *Clin. Microbiol. Rev.* **2011**, *24* (2), 377-410.
6. Grüning, C.; Heiber, A.; Kruse, F.; Ungefehr, J.; Gilberger, T.-W.; Spielmann, T., Development and host cell modifications of *Plasmodium falciparum* blood stages in four dimensions. *Nat. Commun.* **2011**, *2* (1), 1-11.
7. Hviid, L.; Jensen, A. T. R., Chapter Two - PfEMP1 – A Parasite Protein Family of Key Importance in *Plasmodium falciparum* Malaria Immunity and Pathogenesis. In *Advances in Parasitology*, Rollinson, D.; Stothard, J. R., Eds. Academic Press: 2015; Vol. 88, pp 51-84.
8. Kafsack, B. F. C.; Rovira-Graells, N.; Clark, T. G.; Bancells, C.; Crowley, V. M.; Campino, S. G.; Williams, A. E.; Drought, L. G.; Kwiatkowski, D. P.; Baker, D. A.; Cortés, A.; Llinás, M., A transcriptional switch underlies commitment to sexual development in malaria parasites. *Nature* **2014**, *507* (7491), 248-252.
9. Venugopal, K.; Hentzschel, F.; Valkiūnas, G.; Marti, M., *Plasmodium* asexual growth and sexual development in the haematopoietic niche of the host. *Nat. Rev. Microbiol.* **2020**, 1-13.
10. Joice, R.; Nilsson, S. K.; Montgomery, J.; Dankwa, S.; Egan, E.; Morahan, B.; Seydel, K. B.; Bertuccini, L.; Alano, P.; Williamson, K. C.; Duraisingh, M. T.; Taylor, T. E.; Milner, D. A.; Marti, M., *Plasmodium falciparum* transmission stages accumulate in the human bone marrow. *Sci. Transl. Med.* **2014**, *6* (244), 244re5-244re5.
11. Dearnley, M.; Chu, T.; Zhang, Y.; Looker, O.; Huang, C.; Klonis, N.; Yeoman, J.; Kenny, S.; Arora, M.; Osborne, J. M.; Chandramohanadas, R.; Zhang, S.; Dixon, M. W. A.; Tilley, L., Reversible host cell remodeling underpins deformability changes in malaria parasite sexual blood stages. *Proc. Natl. Acad. Sci.* **2016**, *113* (17), 4800-4805.
12. Choi, L.; Pryce, J.; Richardson, M.; Lutje, V.; Walshe, D.; Garner, P. *Guidelines for malaria vector control*; 2019; pp 1-171.
13. World Health Organization Malaria Vaccines. <https://www.who.int/immunization/research/development/malaria/en/> (accessed 10/20/2020).
14. Draper, S. J.; Sack, B. K.; King, C. R.; Nielsen, C. M.; Rayner, J. C.; Higgins, M. K.; Long, C. A.; Seder, R. A., Malaria Vaccines: Recent Advances and New Horizons. *Cell Host Microbe* **2018**, *24* (1), 43-56.
15. Raghavendra, K.; Barik, T. K.; Reddy, B. N.; Sharma, P.; Dash, A. P., Malaria vector control: from past to future. *Parasitol. Res.* **2011**, *108* (4), 757-779.
16. Benelli, G.; Beier, J. C., Current vector control challenges in the fight against malaria. *Acta Trop.* **2017**, *174*, 91-96.

17. *Ethics and vector-borne diseases: WHO guidance*; 978-92-4-001273-8; World Health Organization: Geneva, 2020.
18. Willcox, M.; Bodeker, G.; Rasoanaivo, P.; Addae-Kyereme, J., *Traditional Medicinal Plants and Malaria*. CRC Press: 2004.
19. Pelletier, P.; Caventou, J., Des Recherches chimiques sur les Quinquinas. *Ann. Chim. Phys.* **1820**, *15*, 337-365.
20. Wiesner, J.; Ortmann, R.; Jomaa, H.; Schlitzer, M., New Antimalarial Drugs. *Angew. Chem., Int. Ed.* **2003**, *42* (43), 5274-5293.
21. Schlitzer, M., Antimalarial drugs—what is in use and what is in the pipeline. *Arch. Pharm. Chem. Life Sci.* **2008**, *341* (3), 149-163.
22. *Guidelines for the treatment of malaria*. World Health Organization: 2015.
23. Ghavami, M.; Dapper, C. H.; Dalal, S.; Holzschneider, K.; Klemba, M.; Carlier, P. R., Parallel inhibition of amino acid efflux and growth of erythrocytic *Plasmodium falciparum* by mefloquine and non-piperidine analogs: Implication for the mechanism of antimalarial action. *Bioorg. Med. Chem. Lett.* **2016**, *26* (19), 4846-4850.
24. Yuthavong, Y., Basis for antifolate action and resistance in malaria. *Microbes Infect.* **2002**, *4* (2), 175-182.
25. Nzila, A., The past, present and future of antifolates in the treatment of *Plasmodium falciparum* infection. *J. Antimicrob. Chemother.* **2006**, *57* (6), 1043-1054.
26. Naß, J.; Efferth, T., Development of artemisinin resistance in malaria therapy. *Pharmacol. Res.* **2019**, *146*, 104275.
27. Heller, L. E.; Roepe, P. D., Artemisinin-based antimalarial drug therapy: Molecular pharmacology and evolving resistance. *Trop. Med. Infect. Dis.* **2019**, *4* (2), 89.
28. Klein, E. Y., Antimalarial drug resistance: a review of the biology and strategies to delay emergence and spread. *Int. J. Antimicrob. Agents* **2013**, *41* (4), 311-317.
29. Imwong, M.; Dhorda, M.; Tun, K. M.; Thu, A. M.; Phyo, A. P.; Proux, S.; Suwannasin, K.; Kunasol, C.; Srisutham, S.; Duanguppama, J., Molecular epidemiology of resistance to antimalarial drugs in the Greater Mekong subregion: an observational study. *The Lancet Infectious Diseases* **2020**.
30. Ménard, D.; Mayor, A., Knowing the enemy: genetics to track antimalarial resistance. *The Lancet Infectious Diseases* **2020**.
31. Conrad, M. D.; Rosenthal, P. J., Antimalarial drug resistance in Africa: the calm before the storm? *Lancet Infect. Dis.* **2019**, *19* (10), e338-e351.
32. Birnbaum, J.; Scharf, S.; Schmidt, S.; Jonscher, E.; Hoeijmakers, W. A. M.; Flemming, S.; Toenhake, C. G.; Schmitt, M.; Sabitzki, R.; Bergmann, B.; Fröhlke, U.; Mesén-Ramírez, P.; Blancke Soares, A.; Herrmann, H.; Bártfai, R.; Spielmann, T., A Kelch13-defined endocytosis pathway mediates artemisinin resistance in malaria parasites. *Science* **2020**, *367* (6473), 51-59.
33. Ashley, E. A.; Dhorda, M.; Fairhurst, R. M.; Amaratunga, C.; Lim, P.; Suon, S.; Sreng, S.; Anderson, J. M.; Mao, S.; Sam, B.; Sopha, C.; Chuor, C. M.; Nguon, C.; Sovannaroeth, S.; Pukrittayakamee, S.; Jittamala, P.; Chotivanich, K.; Chutasmit, K.; Suchatsoonthorn, C.; Runcharoen, R.; Hien, T. T.; Thuy-Nhien, N. T.; Thanh, N. V.; Phu, N. H.; Htut, Y.; Han, K.-T.; Aye, K. H.; Mokuolu, O. A.; Olaosebikan, R. R.; Folaranmi, O. O.; Mayxay, M.; Khanthavong, M.; Hongvanthong, B.; Newton, P. N.; Onyamboko, M. A.; Fanello, C. I.; Tshefu, A. K.; Mishra, N.; Valecha, N.; Phyo, A. P.; Nosten, F.; Yi, P.; Tripura, R.; Borrmann, S.; Bashraheil, M.; Peshu, J.; Faiz, M. A.; Ghose, A.; Hossain, M. A.; Samad, R.; Rahman, M. R.;

- Hasan, M. M.; Islam, A.; Miotto, O.; Amato, R.; MacInnis, B.; Stalker, J.; Kwiatkowski, D. P.; Bozdech, Z.; Jeeyapant, A.; Cheah, P. Y.; Sakulthaew, T.; Chalk, J.; Intharabut, B.; Silamut, K.; Lee, S. J.; Vihokhern, B.; Kunasol, C.; Imwong, M.; Tarning, J.; Taylor, W. J.; Yeung, S.; Woodrow, C. J.; Flegg, J. A.; Das, D.; Smith, J.; Venkatesan, M.; Plowe, C. V.; Stepniewska, K.; Guerin, P. J.; Dondorp, A. M.; Day, N. P.; White, N. J., Spread of Artemisinin Resistance in *Plasmodium falciparum* Malaria. *N. Engl. J. Med.* **2014**, *371* (5), 411-423.
34. *World Malaria Report 2018*. World Health Organization: Geneva, 2018.
35. Zhao, L.; Chang, W.-c.; Xiao, Y.; Liu, H.-w.; Liu, P., Methylerythritol Phosphate Pathway of Isoprenoid Biosynthesis. *Annu. Rev. Biochem.* **2013**, *82* (1), 497-530.
36. Eisenreich, W.; Bacher, A.; Arigoni, D.; Rohdich, F., Biosynthesis of isoprenoids via the non-mevalonate pathway. *Cell. Mol. Life Sci.* **2004**, *61* (12), 1401-1426.
37. McFadden, G. I.; Roos, D. S., Apicomplexan plastids as drug targets. *Trends Microbiol.* **1999**, *7* (8), 328-333.
38. Goodman, C. D.; McFadden, G. I., Targeting apicoplasts in malaria parasites. *Expert Opin. Ther. Targets* **2013**, *17* (2), 167-177.
39. Wiesner, J.; Jomaa, H., Isoprenoid biosynthesis of the apicoplast as drug target. *Curr. Drug Targets* **2007**, *8* (1), 3-13.
40. Yeh, E.; DeRisi, J. L., Chemical Rescue of Malaria Parasites Lacking an Apicoplast Defines Organelle Function in Blood-Stage *Plasmodium falciparum*. *PLoS Biol.* **2011**, *9* (8), e1001138.
41. Spangenberg, T.; Burrows, J. N.; Kowalczyk, P.; McDonald, S.; Wells, T. N.; Willis, P., The open access malaria box: a drug discovery catalyst for neglected diseases. *PLoS One* **2013**, *8* (6), e62906.
42. Guiguemde, W. A.; Shelat, Anang A.; Garcia-Bustos, Jose F.; Diagana, T. T.; Gamo, F.-J.; Guy, R. K., Global Phenotypic Screening for Antimalarials. *Chem. Biol.* **2012**, *19* (1), 116-129.
43. Bowman, J. D.; Merino, E. F.; Brooks, C. F.; Striepen, B.; Carlier, P. R.; Cassera, M. B., Antiapicoplast and Gametocytocidal Screening To Identify the Mechanisms of Action of Compounds within the Malaria Box. *Antimicrob. Agents Chemother.* **2014**, *58* (2), 811-819.
44. Imlay, L. S.; Armstrong, C. M.; Masters, M. C.; Li, T.; Price, K. E.; Edwards, R. L.; Mann, K. M.; Li, L. X.; Stallings, C. L.; Berry, N. G.; O'Neill, P. M.; Odom, A. R., Plasmodium IspD (2-C-Methyl-d-erythritol 4-Phosphate Cytidyltransferase), an Essential and Druggable Antimalarial Target. *ACS Infect. Dis.* **2015**, *1* (4), 157-167.
45. Wu, W.; Herrera, Z.; Ebert, D.; Baska, K.; Cho, S. H.; DeRisi, J. L.; Yeh, E., A chemical rescue screen identifies a *Plasmodium falciparum* apicoplast inhibitor targeting MEP isoprenoid precursor biosynthesis. *Antimicrob. Agents Chemother.* **2015**, *59* (1), 356-364.
46. Yao, Z.-K.; Krai, P. M.; Merino, E. F.; Simpson, M. E.; Slebodnick, C.; Cassera, M. B.; Carlier, P. R., Determination of the active stereoisomer of the MEP pathway-targeting antimalarial agent MMV008138, and initial structure-activity studies. *Bioorg. Med. Chem. Lett.* **2015**, *25* (7), 1515-1519.
47. Ghavami, M.; Merino, E. F.; Yao, Z.-K.; Elahi, R.; Simpson, M. E.; Fernández-Murga, M. L.; Butler, J. H.; Casasanta, M. A.; Krai, P. M.; Totrov, M. M.; Slade, D. J.; Carlier, P. R.; Cassera, M. B., Biological Studies and Target Engagement of the 2-C-Methyl-D-Erythritol 4-Phosphate Cytidyltransferase (IspD)-Targeting Antimalarial Agent (1*R*,3*S*)-MMV008138 and Analogs. *ACS Infect. Dis.* **2018**, *4* (4), 549-559.

48. Chellapandi, P.; Prathiviraj, R.; Prisilla, A., Deciphering structure, function and mechanism of Plasmodium IspD homologs from their evolutionary imprints. *J. Comput.-Aided Mol. Des.* **2019**, *33* (4), 419-436.
49. Ungemach, F.; Soerens, D.; Weber, R.; DiPierro, M.; Campos, O.; Mokry, P.; Cook, J. M.; Silvertson, J. V., General Method for the Assignment of Stereochemistry of 1,3-Disubstituted 1,2,3,4-Tetrahydro- β -carbolines by Carbon-13 Spectroscopy. *J. Am. Chem. Soc.* **1980**, *102* (23), 6976-6984.
50. Dragan, A. I.; Pavlovic, R.; McGivney, J. B.; Casas-Finet, J. R.; Bishop, E. S.; Strouse, R. J.; Schenerman, M. A.; Geddes, C. D., SYBR Green I: Fluorescence Properties and Interaction with DNA. *J. Fluoresc.* **2012**, *22* (4), 1189-1199.
51. Smilkstein, M.; Sriwilaijaroen, N.; Kelly, J. X.; Wilairat, P.; Riscoe, M., Simple and Inexpensive Fluorescence-Based Technique for High-Throughput Antimalarial Drug Screening. *Antimicrob. Agents Chemother.* **2004**, *48* (5), 1803-1806.
52. Ghavami, M. Antimalarial Agents: New Mechanisms of Action for Old and New Drugs. Virginia Polytechnic Institute and State University, Blacksburg, VA, 2018.
53. Cagašová, K.; Ghavami, M.; Yao, Z.-K.; Carlier, P. R., Questioning the γ -gauche effect: stereoassignment of 1,3-disubstituted-tetrahydro- β -carbolines using ^1H - ^1H coupling constants. *Org. Biomol. Chem.* **2019**, *17* (27), 6687-6698.
54. Ding, S.; Ghavami, M.; Butler, J. H.; Merino, E. F.; Slebodnick, C.; Cassera, M. B.; Carlier, P. R., Probing the B- & C-rings of the antimalarial tetrahydro- β -carboline MMV008138 for steric and conformational constraints. *Bioorg. Med. Chem. Lett.* **2020**, *30* (22), 127520.
55. Liu, L. MMV008138 and analogs: potential novel antimalarial agents for *P. falciparum*. Virginia Polytechnic Institute and State University, Blacksburg, VA, 2018.

2 Stereoassignment of 1,3-disubstituted-tetrahydro- β -carbolines using ^1H - ^1H coupling constants

This chapter represents an expanded and slightly revised version of an article we published in 2019.¹ The growth inhibition potency of MMV008138 analogs strongly depends on the absolute stereochemistry of the molecule, as shown in Table 1.1: the (1*R*,3*S*)-configuration is essential. Therefore, in evaluating new analogs, we need to be certain that each possesses that configuration. Since the C3 configuration of MMV008138 analogs is controlled by choice of (*S*)- or (*R*)-tryptophan methyl ester used in the Pictet-Spengler reaction, the challenge is reduced to separating and correctly identifying the desired *trans*- or (1*R*,3*S*)-stereoisomer, from the undesired *cis*- or (1*S*,3*S*)-stereoisomer. X-ray crystallography would, of course, be the gold standard method but getting X-ray quality crystals of every analog is likely not achievable. As shown below, a range of methods to identify the relative configuration of substituted tetrahydro- β -carbolines (TH β C) have been developed over time; however, these methods present inherent problems in either range of applicability, ease of performance, or lack of theoretical support for empirical data. To counter some of these limitations, we have developed a reliable method for assignment of *cis*- and *trans*-stereochemistry in 1,3-disubstituted TH β Cs based on analysis of $^3J_{\text{HH}}$ coupling constants in ^1H NMR. In addition, empirical data based on a selection of diastereomeric pairs of MMV008138 analog precursors were supplemented with density-functional theory calculations that gave us valuable insights into the conformational preference of these molecules and its effect on spectral analysis.

2.1 Methods for stereoassignment in tetrahydro- β -carbolines

A frequently used method for assignment of relative stereochemistry in 1,3-disubstituted TH β Cs compares C1 and C3 ^{13}C NMR shifts between *cis* and *trans* diastereomers.²⁻⁶ The method was formally introduced by the research group of Prof. Cook in 1980. According to the empirical method, both C1 and C3 signals are expected to be shifted upfield in the ^{13}C NMR of the *trans*-diastereomer relative to the *cis*- (Figure 2.1).⁷ The same conclusion was concurrently reached by Prof. Pindur, who examined a series of TH β C acids and esters with aromatic substitution on C1 and who additionally observed a downfield chemical shift in H1 of *trans* diastereomer and H3 of *cis* diastereomer.⁸ It should be noted that the difference between *cis* and *trans* chemical shifts of H1 and H3 tends to be small and, in some cases, inconsistent and thus cannot be used for general stereochemistry assignment.⁷ The rationale for the upfield chemical shift of C1 and C3 provided by both Cook and Pindur is based on the so-called γ -effect resulting from steric interactions within the tetrahydropyridine ring. Further discussion of this phenomenon will be provided in Subsection 2.2.^{7,8}

While the relative C1 and C3 chemical shifts of *cis*- and *trans*-diastereomers are consistent in 1,3-disubstituted TH β Cs, it has been noted that other substitution patterns, for example, 1,1,3-trisubstituted TH β Cs, do not always follow this empirical rule.⁹ A further problem of this widely used method lies in the necessity to obtain ^{13}C NMR spectrum of both diastereomers. This is especially burdensome if the synthetic approach yields selectively only one diastereomer.

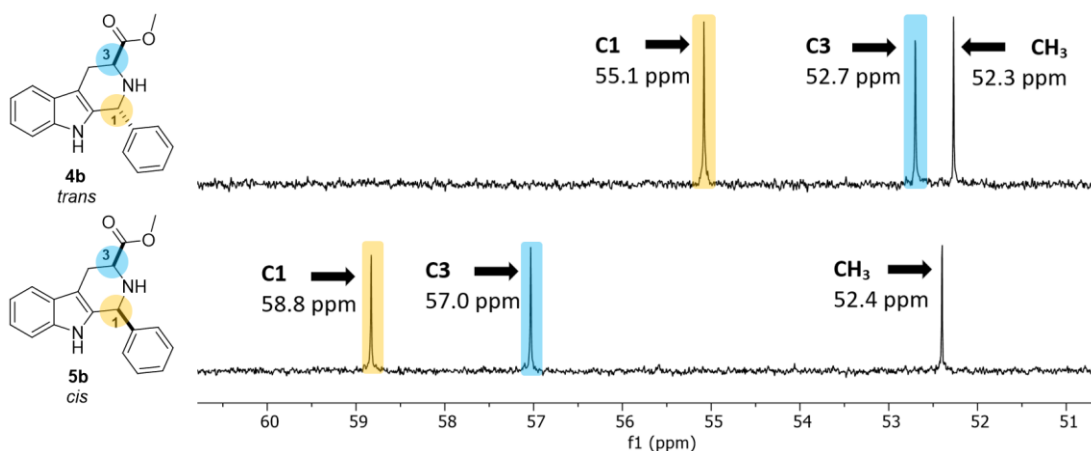


Figure 2.1 Example of Cook's empirical rule as applied to one of the MMV001838 analog precursors synthesized in our laboratory.

The Nuclear Overhauser Effect (NOE) represents another NMR technique used to determine relative stereochemistry in 1,3-disubstituted TH β Cs. Specifically, NOE correlation can be observed between H1 and H3 of the *cis*-diastereomer, whereas the *trans*-diastereomer does not show this correlation due to the *trans*-orientation of these two hydrogens.⁹⁻¹⁴ While using NOE to determine relative stereochemistry in TH β Cs is theoretically sound, the measurement can be quite time-consuming and thus not practical for routine use.

Measuring a change in rotation of polarized light, such as specific optical rotation, optical rotatory dispersion, and circular dichroism, have also been used to determine the stereochemistry of substituted TH β Cs, often in combination with other spectroscopic methods.^{15, 16} The aforementioned stereoassignment methods were in several cases accompanied by selected X-ray structures, which served to support their validity.^{2, 3, 17, 18} Unfortunately, in our experience, the 1,3-disubstituted TH β C esters and acids are rarely crystalline and thus, combined with laboriousness of the X-ray diffraction, render this method impractical for routine stereochemical assessment.

2.2 Gamma effect in ^{13}C NMR and its use for stereochemistry assignment

^{13}C NMR-based stereoassignment presented by both Cook and Pindur relies heavily on analogy to a ^{13}C NMR study of 64 methyl-substituted conformationally-biased cyclohexanes presented by Grant and co-workers.¹⁹⁻²¹ Selective ^{13}C - ^1H decoupling was used to determine methyl substituents from the ring carbons, followed by an extensive analysis of conformationally locked analogs, which led to the determination of parameters allowing assignment of chemical shifts in Me_{ax} - and Me_{eq} - conformers.^{20, 21} The authors attributed the significant upfield chemical shift in γ -gauche carbons (an average of 6 ppm) to steric compression caused by the proximity of attached hydrogens. Specifically, the electron repulsion between proximal hydrogens was proposed to polarize the involved C-H bonds and concentrate electron density towards the carbon resulting in increased shielding and thus an upfield chemical shift (Figure 2.2A).^{19, 22, 23} Because the γ -carbon exhibits a variation in chemical shift only in case of axial substitution on C-1, it can be very valuable for stereochemical assignments (Figure 2.2B).^{20, 21}

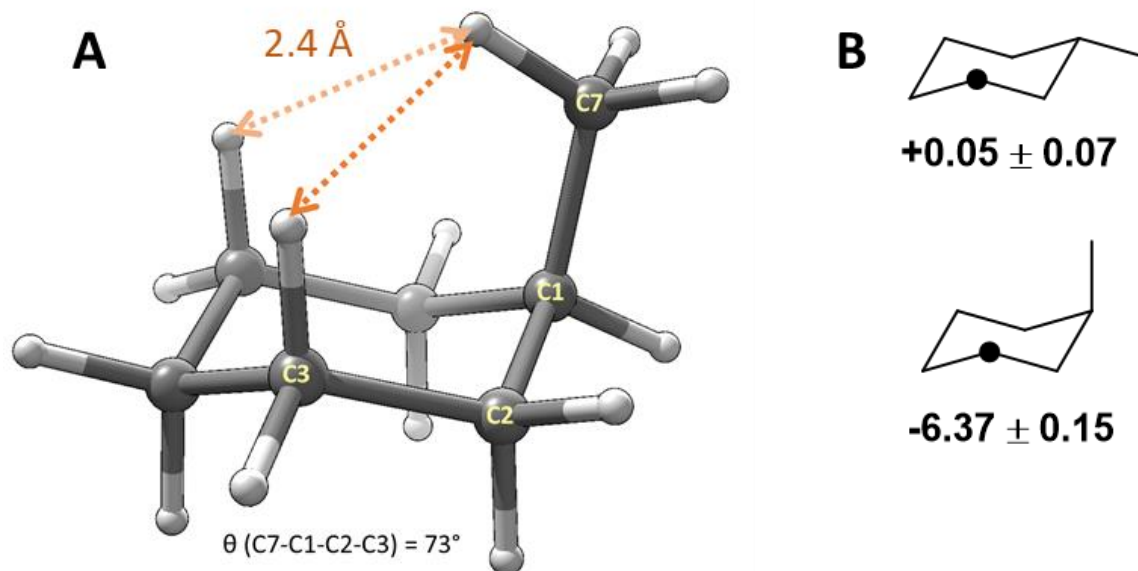


Figure 2.2 Graphical representation of γ -gauche effect in methylcyclohexane. **A)** An illustrative calculated structure of axial methylcyclohexane was calculated at B3LYP/6-31G(d) level of theory and visualized using Chimera. The γ -

gauche interaction of carbons and accompanying steric compression are reflected in H-H non-bonded distances and dihedral angle θ . **B**) Average differences in ^{13}C NMR chemical shifts [ppm] of the indicated carbons (black dot) relative to cyclohexane, as a function of methyl orientation. The average effect of an equatorial methyl substituent is derived from 22 cyclohexane analogs, while the average effect of an axial methyl group is derived from 14 examples.²¹

The γ -gauche effect has also been extensively documented in axial- and equatorial pairs of conformationally-locked cyclohexanes (Figure 2.3).²⁴⁻³¹ For non-carbon substituents (OH, NH₂, SH, Br), the γ -gauche effect resulting from axial substitution causes an upfield shift of 4.6 to 7.0 ppm (cf. **I_{ax}**-**IV_{ax}** and **I_{eq}**-**IV_{eq}** in Figure 2.3). For axial sp³-hybridized carbon substituents CH₃ and CF₃, significant shifts in the γ -carbons of the cyclohexane ring (4.9 and 3.5 ppm, respectively) can be seen relative to their equatorially substituted counterparts (cf. **V_{ax}**-**VI_{ax}** and **V_{eq}**-**VI_{eq}** in Figure 2.3). As expected, a reciprocal upfield shift of the axial methyl group is seen (5.3 ppm), but the CF₃ chemical shift is upfield only by 1.0 ppm. While the γ -gauche effect caused by sp²- and sp-hybridized carbon substituents follows the same trend in an upfield shift of ring γ -carbons (2.5-4.6 ppm), the reciprocal effect of the ring γ -carbons on the axial sp²- (e.g., CO₂Me) and sp-hybridized carbon substituents themselves can be minimal (cf. **V** and **VII** with **VIII-X**, Figure 2.3).^{24-26, 28} In addition, the significant γ -gauche effects seen in structures carrying small (e.g., Br or SH) axial substituents suggests that the initial theory based on steric effects (Figure 2.2A) may not fully explain the origin of the γ -gauche effect. This point is illustrated by comparing the magnitude of the upfield chemical shift with the A-value of the substituent inducing that shift (see Table and Graph in Figure 2.3).

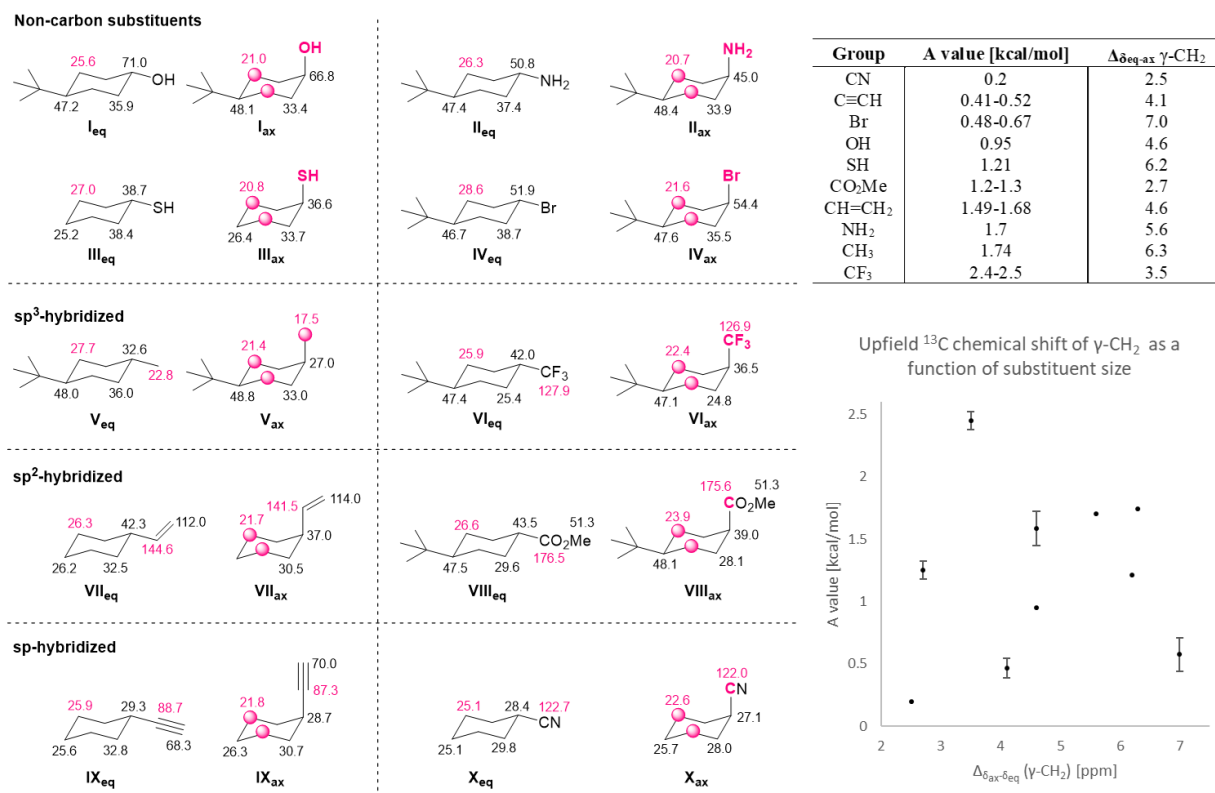


Figure 2.3 Examples of γ -gauche effect observed in various substituted cyclohexanes.^{25, 26, 28, 32} Compounds **I-II**, **IV-VI**, and **VIII** were measured in CDCl₃ at ambient temperature. Compounds **III** and **X** were measured in CFCl₃ at -80 °C, compound **VII** in C₇D₈ at -100 °C, and compound **IX** in CFCl₃ at -93 °C. The table shows conformational energies (A values)³³ of depicted groups and the differences between ¹³C chemical shift of $\gamma\text{-CH}_2$ in equatorially vs. axially substituted species **I-X**. Data from the table are also visually represented in the graph beneath (values reported as range are shown as average with bars signifying the range). As can be seen from the plot, there is no clear correlation between the substituent's size (represented by A value) and the observed upfield shift in γ -carbons.

Despite the incomplete understanding of the physical basis causing the upfield ¹³C NMR chemical shifts of γ -carbons,^{34, 35} the γ -gauche effect is still a widely used method for stereochemistry assignment not only in TH β Cs,³⁶⁻³⁹ but also in steroids and biopolymers.⁴⁰⁻⁴² While the γ -effect observed in saturated hydrocarbons was studied extensively, information pertaining to heterocyclic molecules is limited. Consequently, determination of relative stereochemistry in 1,3-disubstituted TH β Cs based solely on the relative ¹³C chemical shifts of C1 and C3 should be carried out with caution because the initial method was developed in analogy with a model that does not account for either distortion of the tetrahydropyridine ring or the

presence of heteroatoms in near proximity of C1 and C3. If we do not understand the physical basis of this correlation, then we will not know when the empirical method would break down. Any uncertainty in the stereochemical assignment would thus cast doubt on the structure-activity relationships we have developed for MMV008138.

2.3 Development of ^1H NMR method for analysis of 1,3-disubstituted tetrahydro- β -carbolines

Given the uncertainty surrounding the ^{13}C chemical shift method for stereochemical assignment, we sought to develop another method based on three-bond ^1H - ^1H coupling constants since the dependence of $^3J_{\text{HH}}$ on the dihedral angle is firmly established. Coupling our knowledge of this relationship with conformational analysis of THBCs could thus provide a more secure stereochemical assignment method. However, to assess the validity and range of applicability for the new ^1H NMR assignment method, it was first necessary to analyze ^1H and ^{13}C NMR data of a large enough sample of 1,3-disubstituted TH β Cs. For this purpose, we selected 26 pairs of previously published aromatic analogs of **4** and **5** and supplemented them with five additional pairs of Pictet-Spengler adducts derived from aliphatic aldehydes.^{1, 43, 44} In this work, I am also presenting data obtained from three previously unpublished analogs **m-o**, synthesized by me (Table 2.1).

Table 2.1 C1-substitution of *trans* (**4**) and *cis* (**5**) Pictet-Spengler adducts studied in Chapter 2.

	X	Ref		X	Ref
a	2', 4'-Cl ₂	43	r	2'-Br, 4'-I	44
b	H	43	w	2'-Cl, 4'-OCH ₃	44
c	2'-Cl	43	x	2'-OCH ₃ , 4'-Cl	44
d	4'-Cl	43	y	2'-Cl, 4'-CO ₂ CH ₃	44
e	2'-Cl, 4'-CH ₃	43	z	2', 4'-(CF ₃) ₂	43
f	2'-CH ₃ , 4'-Cl	43	aa	2', 4'-(CH ₃) ₂	43
g	2', 4'-F ₂	43	ab	2', 4'-(OCH ₃) ₂	43
h	2'-F, 4'-Cl	44	ac	3', 4'-Cl ₂	44
i	2'-Cl, 4'-F	44	ad	3', 4'-(OCH ₃) ₂	43
j	2'-Cl, 4'-Br	44	ae	2', 6'-F ₂ , 4'-Cl	44

k	2'-Br, 4'-Cl	44	ag	2', 3', 4'-F ₃	44
l	2', 4'-Br ₂	44	ah	2'-Br, 4'-F, 5'-OCH ₃	44
m	2'-Br	—	an	cyclohexyl	1
n	2'-F, 4'-Br	—	ao	<i>n</i> -butyl	1
o	2'-Br, 4'-F	—	ap	<i>i</i> -butyl	1
p	2'-I, 4'-F	44	aq	<i>t</i> -butyl	1
q	2'-F, 4'-I	44	ar	CH(CH ₂ CH ₃) ₂	1

In analogs **a-ah** bearing substituted benzene D ring, the “X” denotes substitution of benzaldehyde used for their synthesis. In analogs **ai-ar**, the “X” denotes the substitution on C1 in the THβC ring. Analogs **a**, **b**, **m-o**, and **ao-ar** were synthesized or re-synthesized by me. Analogs **4an** and **5an** were prepared by Mr. Jopaul Mathew.

All studied analogs were prepared by Pictet-Spengler reaction of (*S*)-Trp-OMe·HCl with a requisite aldehyde (**3a-ar**). Each diastereomeric pair was separated by column chromatography and their relative configuration was assigned using the ¹³C NMR empirical rule (Table 2.2).⁷ Throughout our previous work, we also noted that when the eluent in liquid chromatography comprised a mixture of methylene chloride, hexane, and ethyl acetate, the *cis*-isomer eluted first in each case. Moreover, the assignment of *trans*-configuration to diastereomer **4a** was confirmed by X-ray crystallography of its methyl amide derivative.⁴³

Table 2.2 ¹³C NMR resonances used to determine the stereochemistry of compounds shown in Table 2.1.

		δ C1 [ppm]			δ C3 [ppm]		
		<i>trans</i> (4)	<i>cis</i> (5)	Δ _{δ4-δ5}	<i>trans</i> (4)	<i>cis</i> (5)	Δ _{δ4-δ5}
a	2', 4'-Cl ₂	51.3 ^b	53.9 ^b	-2.6	52.34 ^c	56.7 ^b	-4.3
b	H	55.1 ^b	58.8 ^b	-3.8	52.7 ^b	57.0 ^b	-4.3
c^e	2'-Cl	51.8	54.4	-2.6	52.23	56.8	-4.58
d^e	4'-Cl	54.3	58.1	-3.8	52.5	56.9	-4.4
e^{e,g}	2'-Cl, 4'-CH ₃	51.4	53.9	-2.5	52.0	56.7	-4.7
f^e	2'-CH ₃ , 4'-Cl	51.4	53.5	-2.1	52.6	57.0	-4.4
g^e	2', 4'-F ₂	47.8 ^b	50.6 ^b	-2.8	52.4 ^b	56.8 ^b	-4.4
h^e	2'-F, 4'-Cl	47.9 ^a	50.6 ^a	-2.7	52.6	56.8	-4.3
i	2'-Cl, 4'-F	51.2 ^b	53.8 ^b	-2.6	52.30 ^c	56.7 ^b	-4.4
j^{e,g}	2'-Cl, 4'-Br	51.2	53.9	-2.7	52.2	56.6	-4.4
k	2'-Br, 4'-Cl	53.7 ^b	56.6 ^b	-2.9	52.36 ^c	56.7 ^b	-4.3
l	2', 4'-Br ₂	53.7 ^b	56.57 ^c	-2.8	52.1 ^c	56.57 ^c	-4.5
m	2'-Br	54.2 ^b	57.0 ^d	-2.8	52.2 ^c	56.7 ^d	-4.5
n	2'-F, 4'-Br	47.9 ^b	50.6 ^b	-2.7	52.2 ^b	56.7 ^b	-4.5
o	2'-Br, 4'-F	53.5 ^b	56.4 ^d	-2.9	52.3 ^c	56.7 ^d	-4.4
p	2'-I, 4'-F	58.0 ^b	61.6 ^b	-3.6	52.46 ^c	56.8 ^b	-4.3
q	2'-F, 4'-I	48.0 ^b	50.7 ^b	-2.7	52.5 ^c	56.8 ^b	-4.3
r	2'-Br, 4'-I	53.9 ^b	56.8 ^b	-2.9	52.36 ^c	56.7 ^b	-4.3
w	2'-Cl, 4'-OCH ₃	51.3 ^b	53.9 ^b	-2.6	52.2 ^c	56.9 ^b	-4.7
x	2'-OCH ₃ , 4'-Cl	48.8 ^b	51.3 ^b	-2.5	52.29 ^c	57.0 ^b	-4.7
y	2'-Cl, 4'-CO ₂ CH ₃	51.6 ^b	54.3 ^b	-2.7	52.30 ^c	56.7 ^b	-4.4
z^{e,g}	2', 4'-(CF ₃) ₂	49.8	53.4	-3.6	53.0	56.6	-3.6
aa^{e,g}	2', 4'-(CH ₃) ₂	51.4	53.5	-2.1	52.4	57.0	-4.6
ab^e	2', 4'-(OCH ₃) ₂	49.0	51.5	-2.5	51.9	57.0	-5.1
ac	3', 4'-Cl ₂	53.9 ^b	57.9 ^b	-4.0	52.5 ^c	56.8 ^b	-4.3
ad^e	3', 4'-(OCH ₃) ₂	54.8	58.7	-3.9	53.0	57.1	-4.1
ae	2', 6'-F ₂ , 4'-Cl	44.6 ^b	48.0 ^b	-3.4	53.9 ^b	57.3 ^b	-3.4
ag	2', 3', 4'-F ₃	47.9 ^b	50.5 ^b	-2.6	52.39 ^c	56.7 ^b	-4.3
ah^{e,g}	2'-Br, 4'-F, 5'-OCH ₃	53.5	56.4	-2.9	53.1	56.7	-3.6
an	cyclohexyl	55.4	57.8	-2.4	53.5	56.6	-3.1
ao	<i>n</i> -butyl	50.4	52.9	-2.5	52.7	56.6	-3.9
ap	<i>i</i> -butyl	48.2	50.7	-2.5	52.5	56.6	-4.1
aq	<i>t</i> -butyl	59.4	62.6	-3.2	54.4	56.5	-2.1
ar	CH(CH ₂ CH ₃) ₂	51.0	54.6	-3.6	54.1	56.6	-2.5
Average		51.7	54.6	-2.9	52.6	56.8	-4.2
St. deviation		3.2	3.4	0.5	0.6	0.2	0.6

Signals identified via: ^aJ_{CF}, ^bHSQC, ^c(C)DEPT and HSQC, ^dHMBC and HSQC. ^eSample is unavailable. ^gSample and NMR data unavailable. ^hIf the values are identical, only one of them is shown. ^{e,g}Shifts were assigned based on the pattern seen in proven compounds, unless stated otherwise.

The assignment of the C1 and C3 ¹³C NMR peaks is not always straightforward: the C1 peak may be upfield or downfield of C3, depending on the substitution of the C1-aryl group.

Furthermore, in the *trans*-isomers **4a-ar**, the ^{13}C NMR chemical shifts of C3 and the methoxy carbon are often very close. Thus, the ^{13}C chemical shifts of **4a**, **5a**, and 33 other pairs of diastereomers were confirmed using HSQC, HMBC, and C-DEPT. Taken together, over 34 pairs of diastereomers, the average C3 chemical shift is 52.6 ± 0.6 ppm for *trans*- and 56.8 ± 0.2 ppm for *cis*-, giving an average relative shift of -4.2 ± 0.6 ppm in **4a-ar** relative to **5a-ar**. A large standard deviation in C1 chemical shifts of the *trans*- and *cis*-esters **4a-ar** and **5a-ar** (51.7 ± 3.2 and 54.6 ± 3.4 ppm, respectively) is caused by the significant influence of C1-substituent on the shielding of this carbon. Nevertheless, within a pair of diastereomers, the relative shift of C1 in **4a-ar** relative to **5a-ar** is quite constant ($\Delta\delta_{4.5} = -2.9 \pm 0.5$ ppm). (Table 2.2) With this data in hand, the rationale for sterically caused γ -gauche effect, as proposed by Cook and co-workers,⁷ can be evaluated.

The tetrahydropyridine ring of *cis*-esters **5a-ar** should adopt an all pseudoequatorial conformation **A** because the alternative half-chair conformation (not shown) would feature severe 1,3-diaxial interactions between C1' and CO₂Me (Figure 2.4). In contrast, *trans*-esters **4a-ar** would likely populate two alternative half-chair conformations **B** and **C**, each featuring one pseudoequatorial (ψ_{eq}) and one pseudoaxial (ψ_{ax}) group. Notably, Ungemach et al. did not reach the same conclusion when establishing the ^{13}C NMR empirical method.⁷ Instead, they proposed that the *trans*-configured compounds would adopt an exclusively ψ_{eq} -CO₂Me conformation (conformer **B**, Figure 2.4) to relieve allylic strain between the 1-aryl group and the indole NH. However, as shown in the Newman projections in Figure 2.4 for the *cis*-isomers **5a-ah**, the CO₂Me group on C3 is anti to C1 (view down C3-N2 axis), and C1' of the C1-substituent is anti to C3 (view down N2-C1 axis). However, in conformer **B** (ψ_{eq} -CO₂Me) of **4a-ah**, C1' of the 1-substituent is gauche to C3, while CO₂Me remains anti to C1. Similarly, in conformer **C** (ψ_{ax} -

CO₂Me) of **4a-ah**, the CO₂Me group is gauche to C1, while C1' remains anti to C3. Thus, only if both conformations **B** and **C** of **4a-ar** are populated, both C1 and C3 will experience steric compression relative to those carbons in **5a-ar**, leading to an upfield shift observed in the ¹³C NMR spectrum. Several other researchers reached the same conclusion.^{8, 10, 11}

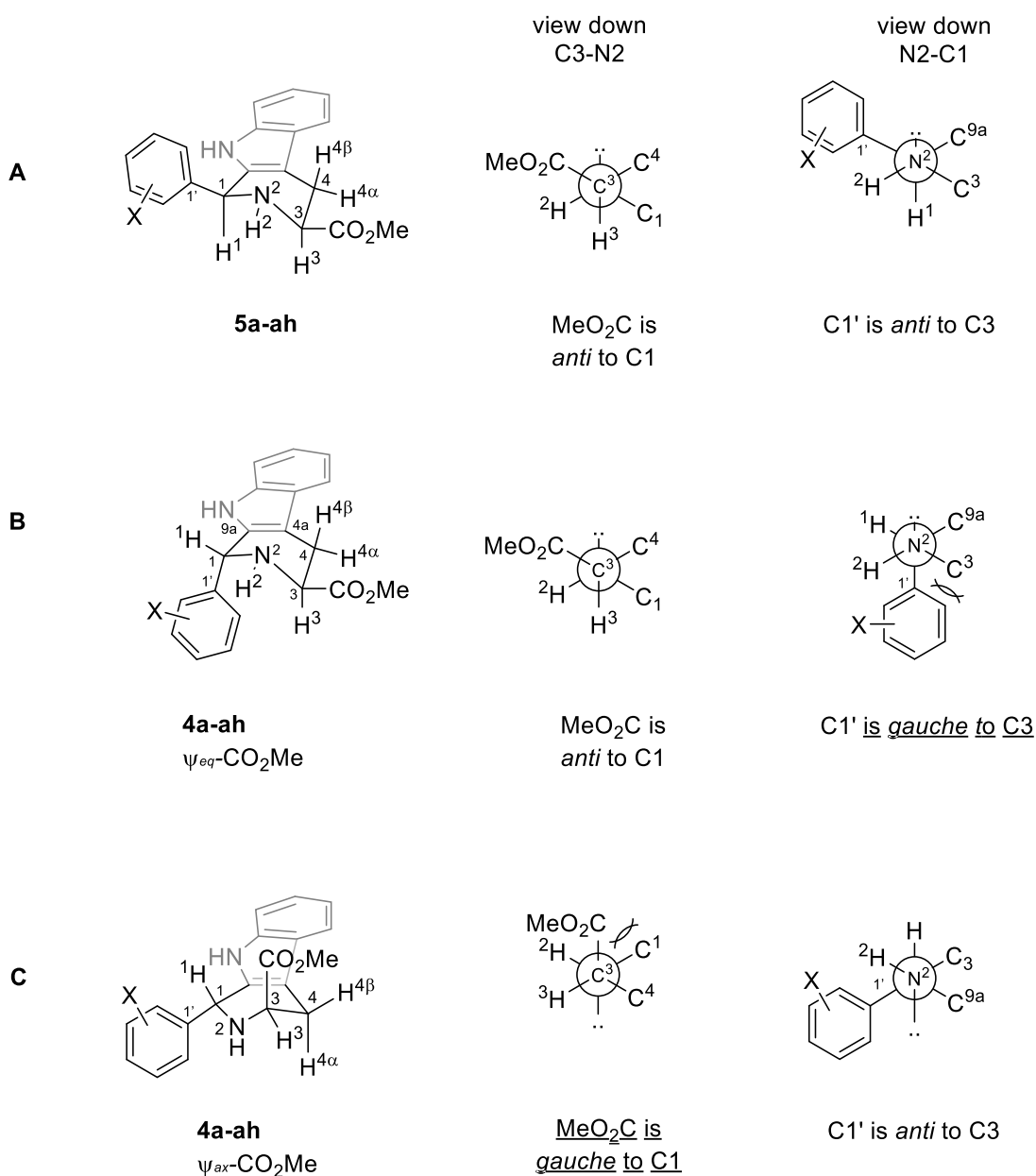


Figure 2.4 First-principle analysis of possible conformers adopted by aromatic *trans* (**4a-ah**) and *cis* (**5a-ah**) analogs. Only pseudo-diequatorial conformer **A** is shown for *cis* isomer because the alternative half-chair conformer would be significantly disfavored due to 1,3-diaxial interaction between the ester and aryl substituent. It is expected that

substituent **ai-ar** will adopt the same geometries as **a-ah**. Cagašová, K.; Ghavami, M.; Yao, Z.-K.; Carlier, P. R., Questioning the γ -gauche effect: stereoassignment of 1,3-disubstituted-tetrahydro- β -carbolines using ^1H - ^1H coupling constants. *Org. Biomol. Chem.* **2019**, *17* (27), 6687-6698. - Reproduced by permission of The Royal Society of Chemistry.

While the reciprocal nature of steric compression might not be pronounced in the case of sp^2 -hybridized ester carbonyl and C1' in aromatic analogs **4a-ah**, it would be expected among the sp^3 -hybridized C1' of aliphatic analogs **4an-ar**. Interestingly, we did not observe this reciprocity. Over 34 diastereomeric pairs, the ^{13}C NMR resonances of **4a-ar** carbonyl are in fact seen slightly downfield of signals in **5a-ar** ($\Delta\delta_{4.5} = +0.8 \pm 0.2$ ppm, Table 2.3, Table 5.2). Similarly, in the 19 cases of 1-aryl Pictet-Spengler adducts where we have unequivocally assigned C1', this resonance is also downfield in the *trans*- relative to the *cis*-isomer ($\Delta\delta_{4.5} = +0.8 \pm 0.5$ ppm, Table 2.3, Table 5.2). To determine if the downfield shift is purely a result of sp^2 -hybridization of carbons in question, we have also analyzed sp^3 hybridized C1' in analogs **an-ar**. However, the sp^3 -hybridized C1' carbons of *trans* isomers are also shifted downfield ($\Delta\delta_{4.5} = +0.7 \pm 0.4$, Table 2.3, Table 5.2). This failure of the gauche-oriented sp^3 -carbons to reciprocally exert upfield shifts on each other (relative to anti-oriented carbon in *cis* isomer) thus clearly undermines the proposal that “steric compression” determines C1 and C3 chemical shifts in TH β Cs.

Table 2.3 Average ^{13}C NMR resonances expected to show the γ -gauche effect in compound **4a-ar** and **5a-ar**.

	<i>trans</i> (4)	<i>cis</i> (5)	$\Delta\delta_{4.5}$
C1	51.7 ± 3.2 ppm	54.6 ± 3.4 ppm	-2.9 ± 0.5 ppm
C3	52.6 ± 0.6 ppm	56.8 ± 0.2 ppm	-4.2 ± 0.6 ppm
C=O	174.0 ± 0.3 ppm	173.3 ± 0.3 ppm	0.8 ± 0.2 ppm
C1' (sp^2)	134.4 ± 7.5 ppm	133.6 ± 7.8 ppm	0.8 ± 0.5 ppm
C1' (sp^3)	41.4 ± 4.9 ppm	40.7 ± 5.2 ppm	0.7 ± 0.4 ppm

With the rationale for the ^{13}C NMR chemical shift assignment method now even more uncertain, we looked for another method to reliably assign relative configuration. As mentioned earlier, NOESY/ROESY has been used periodically to confirm *cis*-configuration (correlation of

H1 and H3),¹⁰⁻¹⁴ but we favored a method of greater operational simplicity. Two previous studies used the magnitude of vicinal coupling constants as a means of assigning *cis*- or *trans*-configuration in 1,3-disubstituted TH β Cs, albeit for a single pair of diastereomers each.^{10, 11} We sought to validate this method with the 34 pairs of diastereomers depicted in Table 2.1. Inspection of conformer **A** for *cis*-esters **5a-ar** suggests that the three-bond coupling constants $^3J_{4\alpha-3}$ and $^3J_{4\beta-3}$ should be well differentiated: H4 α is approximately gauche to H3, and H4 β is approximately anti to H3 (Figure 2.4). In contrast, if the *trans*-diastereomers **4a-ae** populate both tetrahydropyridine conformations **B** and **C** as predicted, then $^3J_{4\beta-3}$ values will not be as well-differentiated from the corresponding $^3J_{4\alpha-3}$ values, since H4 β is approximately anti to H3 in conformer **B**, but is approximately gauche to H3 in conformer **C**. For **5a**, HSQC identified H4 resonances at 3.25 and 3.02 ppm. Individual irradiation of these two resonances resulted in 6.0% and ~0% NOE enhancement of H3 (3.99 ppm), allowing assignment of H4 α to the peak at 3.25 ppm, and H4 β to the peak at 3.02 ppm. Based on these assignments, we measured $^3J_{4\alpha-3}$ and $^3J_{4\beta-3}$ as 4.1 and 11.0 Hz, respectively. Thus, a significant difference is seen in these coupling constants for **5a**, as expected. Similarly, we used 1D NOE experiments to assign H4 β and H4 α in *trans*-ester **4a**. In this case, the values of $^3J_{4\alpha-3}$ and $^3J_{4\beta-3}$ were much more similar (5.0 and 7.8 Hz, respectively). These findings are summarized in Figure 2.5 and Table 5.5.

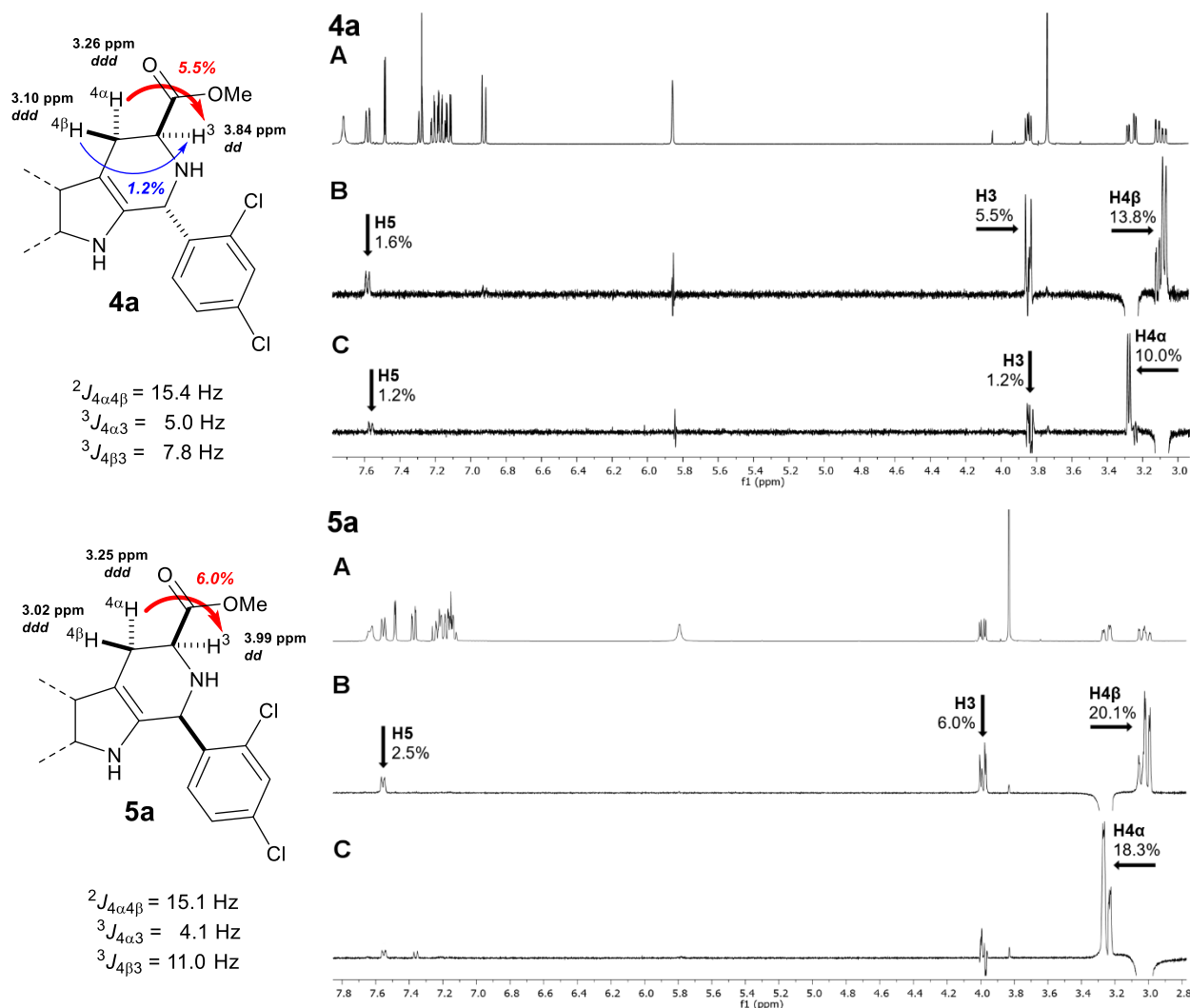


Figure 2.5 Assignment of H4 α and H4 β in compounds **4a** and **5a** via 1D NOE. **A**) The original ^1H NMR spectrum, **B**) 1D NOE ^1H NMR spectrum resulting from irradiation of H4 α , **C**) 1D NOE ^1H NMR spectrum resulting from irradiation of H4 β .

Based on the ^1H chemical shifts and 3J values of **4a** and **5a**, H4 α and H4 β were assigned in the other 33 pairs of diastereomers, and the individual coupling constants were determined (Table 5.3 and Table 5.4). Average ^1H chemical shifts and coupling constants are shown in Table 2.4. As expected from their distance from the C1-substituent, the ^1H chemical shifts of H3, H4 α , and H4 β in **4a-ar** and **5a-ar** fall within very narrow ranges (Table 2.4, entries 1-3). As can be seen, the average value of $^3J_{4\beta-3}$ in *cis*-esters **5a-ar** is $11.1 \pm 0.1 \text{ Hz}$, suggesting an approximately

antiperiplanar arrangement of H4 β and H3. In contrast, the average value of $^3J_{4\beta-3}$ in *trans*-esters **4a-ar** is consistently lower (7.3 ± 0.9 Hz), as expected if both conformers **B** and **C** were populated (Table 2.4, Entry 4). Nakamura et al. performed a similar analysis to assign relative stereochemistry in several products of dihydro- β -carboline reduction.⁴⁵

Table 2.4 Selected average ^1H chemical shifts and coupling constants (CDCl_3) for compounds shown in Table 2.1.

Entry		<i>trans</i> (4)	<i>cis</i> (5)
1	δ H3 [ppm]	3.91 ± 0.08	3.95 ± 0.09
2	δ H4 α [ppm]	3.23 ± 0.05	3.22 ± 0.04
3	δ H4 β [ppm]	3.10 ± 0.05	2.98 ± 0.08
4	$^3J_{4\beta-3}$ (Hz)	7.3 ± 0.9	11.1 ± 0.1
5	$^3J_{4\alpha-3}$ (Hz)	5.1 ± 0.2	4.1 ± 0.1
6	$^2J_{4\alpha-4\beta}$ (Hz)	15.3 ± 0.1	15.1 ± 0.1
7	$^5J_{4\beta-1}$ (Hz)	1.5 ± 0.1	2.5 ± 0.1
8	$^5J_{4\alpha-1}$ (Hz)	1.2 ± 0.2	1.8 ± 0.1

The well-differentiated average values of $^3J_{4\beta-3}$ for *cis*- and *trans*-diastereomers are very similar to those reported for the two pairs of diastereomers noted previously.^{10, 11} Note that the average values of $^3J_{4\alpha-3}$ (Table 2.4, entry 5) are similar for both **4a-ar** and **5a-ar**, which is consistent with a near gauche orientation of H4 α and H3 in all three conformers **A-C**.

One noteworthy feature of the ^1H NMR spectra of **4a-ar** and **5a-ar** is the visible 5-bond coupling between H1 and H4 α , and between H1 and H4 β , as shown for **4b** and **5b** in Figure 2.6 (Table 2.4, entries 7-8). Note that for *trans*-1-aryl derivatives **4a-ah**, H1 appears as a broad singlet, as shown for **4b** in Figure 2.6A. The fine splitting observed in H4 α and H4 β was possible to attribute to a 5-bond coupling H1 and H4 α /H4 β by a single-frequency decoupling in ^1H NMR (Figure 2.6B). For *cis*-1-aryl derivatives **5a-ah**, the 5-bond coupling is occasionally seen at H1, as shown for **5b** in Figure 5C. Although 5-bond ^1H - ^1H coupling is rare, it is particularly common in cyclohexenes,^{46, 47} which resemble the tetrahydropyridine ring of **4a-ar** and **5a-ar**, and has been noted at least once previously in Pictet-Spengler adducts.¹⁰

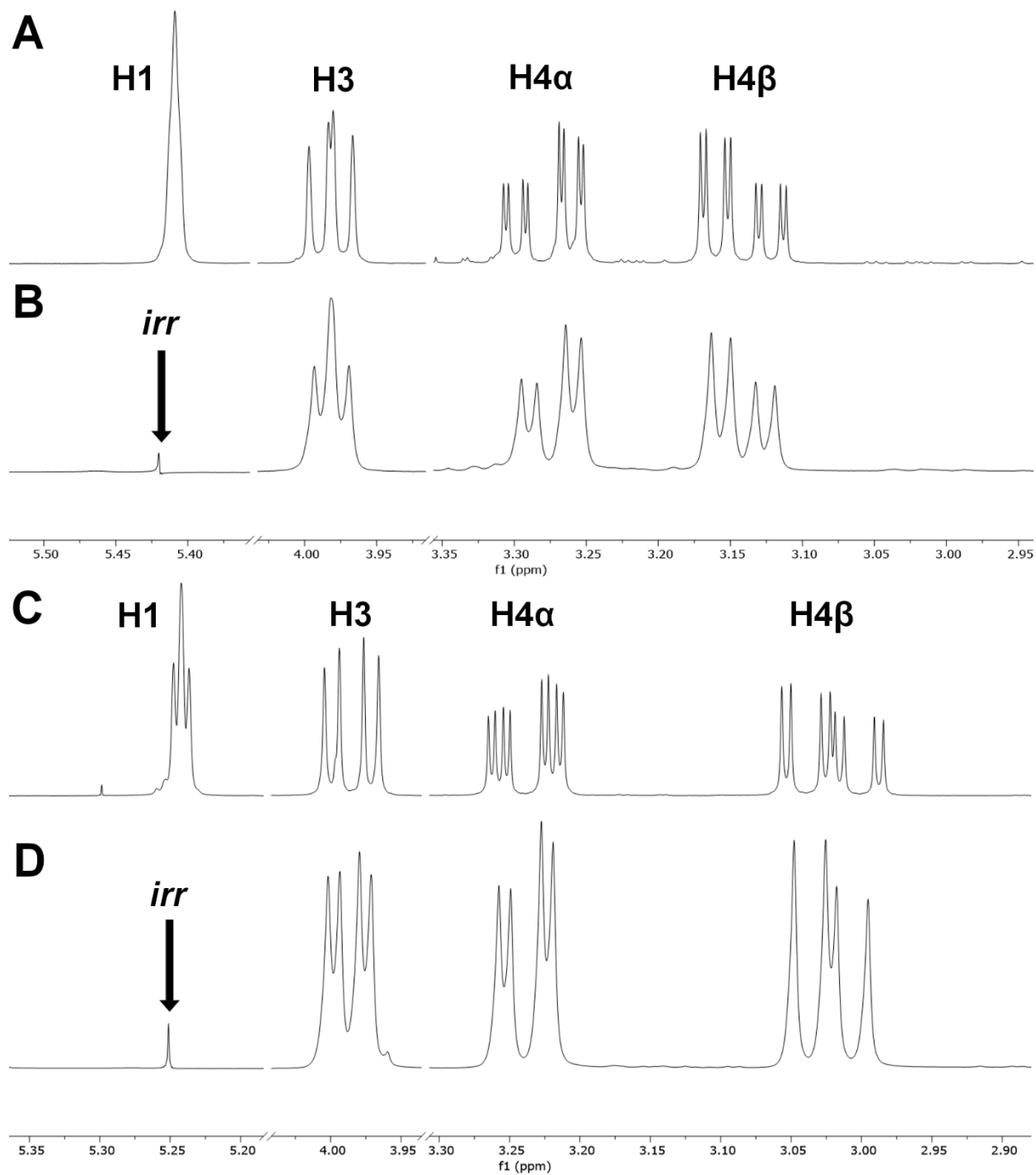
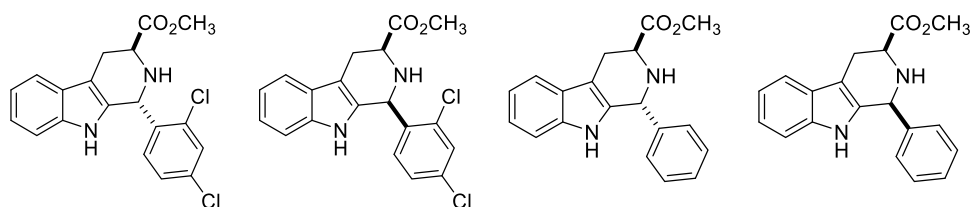


Figure 2.6 Five-bond coupling of H1 to H4 α and H4 β in **4b** and **5b**. **A**) H1, H3, H4 α , and H4 β resonances in the ^1H NMR spectrum of **4b**; **B**) Single-frequency decoupling of H1 in **4b**; **C**) H1, H3, H4 α , and H4 β resonances in the ^1H NMR spectrum of **5b**; **D**) Single-frequency decoupling of H1 in **5b**. Cagašová, K.; Ghavami, M.; Yao, Z.-K.; Carlier, P. R., Questioning the γ -gauche effect: stereoassignment of 1,3-disubstituted-tetrahydro- β -carboline using ^1H - ^1H coupling constants. *Org. Biomol. Chem.* **2019**, *17* (27), 6687-6698. - Reproduced by permission of The Royal Society of Chemistry.

2.4 Density functional theory conformational analysis

As described above, values of ${}^3J_{4\beta-3}$ effectively distinguish *trans*-esters **4a-ar** from *cis*-esters **5a-ar**. Furthermore, the observed values of ${}^3J_{4\beta-3}$ in these compounds appear reasonable based on a first-principles conformational analysis (Figure 2.4). To further substantiate our method for the stereochemical assignment, we undertook computational studies of the possible conformers of **4a/5a** and **4b/5b**. Multiple automated conformer searches were performed at the MMFF94 level, starting from at least two initial geometries of each compound. These structures were then optimized at B3LYP/6-31G(d)^{48, 49} to give 16 conformers of **4a**, 14 conformers of **5a**, and eight conformers each for **4b** and **5b**. As shown in Table 2.5, these conformers can be classified with respect to four structural features and grouped into eight conformational ensembles.

Table 2.5 The number of B3LYP/6-31G(d) potential energy minima found for **4a/5a**, **4b/5b** within each conformational ensemble.



Conformer	4a	5a	4b	5b
ψ_{ax} -CO ₂ Me	8	6	4	4
ψ_{eq} -CO ₂ Me	8	8	4	4
<i>exo</i> -2'-Cl	8	8	—	—
<i>endo</i> -2'-Cl	8	6 ^a	—	—
<i>ax</i> -H ₂	8	6	4	4
<i>eq</i> -H ₂	8	8	4	4
H-bond ^b	12	12	6	6
No H-bond ^c	4	4	2	2
Total	16	14	8	8

^aTwo conformers, namely ψ_{ax} -CO₂Me, *endo*-2'-Cl, *ax*-H₂, were not found in the initial conformational search, likely due to their expected high energy (conformer search was limited to 40 kJ/mol). ^bIntramolecular H-bonding of H₂ to C=O or OMe deduced from H₂...O distances ranging from 2.3 - 2.7 Å. ^cLack of H-bond deduced from H₂...O > 3.7 Å.

First, the approximate half-chair conformation of the tetrahydropyridine ring can be classified as having a ψ_{ax} - or ψ_{eq} -CO₂Me substitution. Representative calculated structures of **4a**

exhibiting these features are shown in Figure 2.7 (**I** and **II**, respectively). Interestingly, the orientation of the 1-aryl groups in **4a** and **4b** does not significantly differ among the different tetrahydropyridine conformers. For **4a**, the C1'-C1-C9a-N9 dihedral angle ϕ in **II** (66.8°) is only slightly larger than those seen in **I** and **III** (52.7 and 46.1° , respectively), despite the expectation that the 1-aryl group would be pseudoaxial in **II** and pseudoequatorial in **I** and **III**. The larger than expected ϕ value in **I** and **III** is likely a consequence of allylic strain of the 1-aryl group and N9.

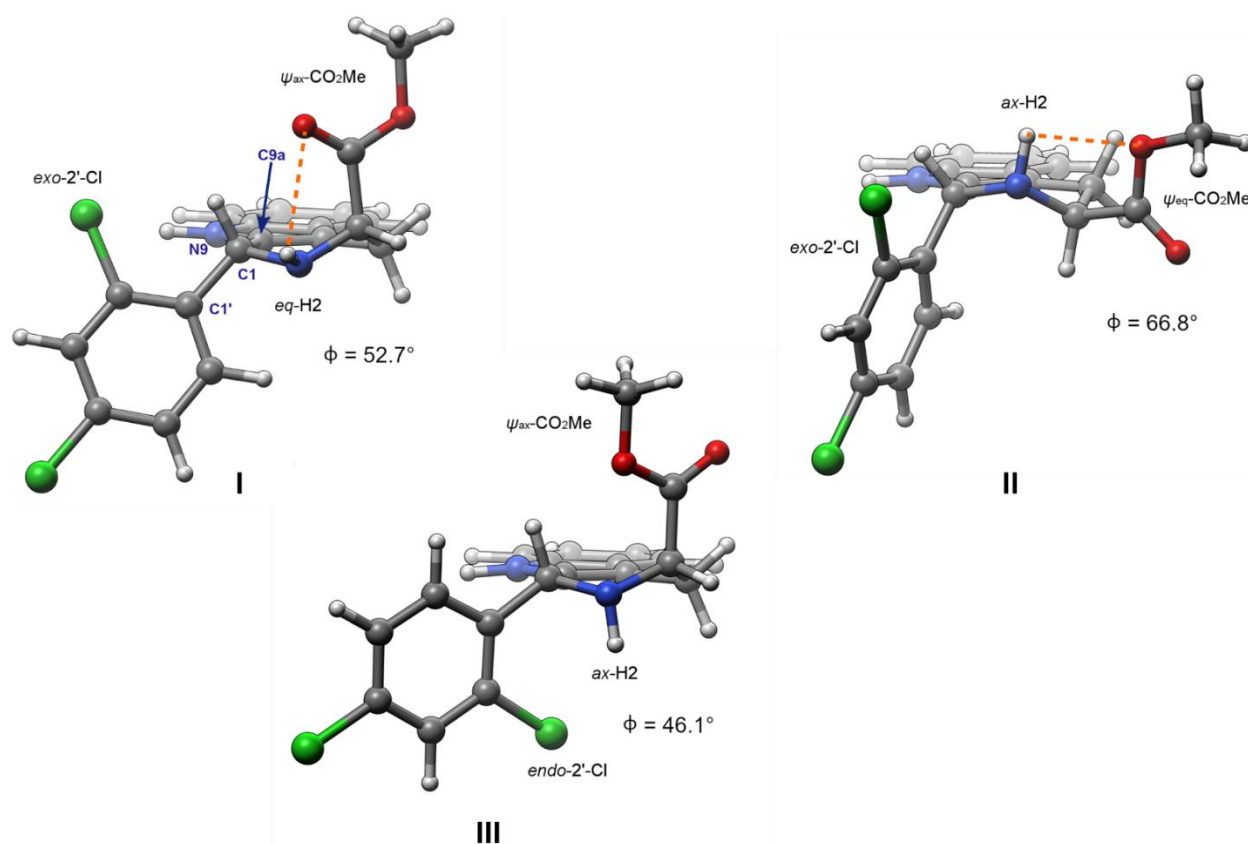


Figure 2.7 Representative calculated (B3LYP/6-31G(d)) structures of **4a** illustrating the orientation of the CO₂Me, NH, and 2'-Cl groups. The C1'-C1-C9a-N9 dihedral angle is represented by ϕ . In conformers **I** and **II**, internal hydrogen bonding between H2 and the carbonyl or methoxy O atoms are depicted with an orange dashed line. Note that intramolecular hydrogen bonding is geometrically impossible in conformer **III**. Conformers **I**, **II**, and **III** are described as **4a-01**, **4a-09**, and **4a-10**, respectively, in Chapter 5 (Table 5.6 and Table 5.7). Graphics rendered using Chimera.⁵⁰ Čagašová, K.; Ghavami, M.; Yao, Z.-K.; Carlier, P. R., Questioning the γ -gauche effect: stereoassignment of 1,3-disubstituted-tetrahydro- β -carbolines using ¹H-¹H coupling constants. *Org. Biomol. Chem.* **2019**, *17* (27), 6687-6698. - Adapted by permission of The Royal Society of Chemistry.

Second, the 2'-Cl of **4a** and **5a** can be oriented either *exo*- or *endo*- to the tetrahydropyridine ring (Figure 2.7: **I/II** (*exo*-) vs. **III** (*endo*-)). This isomerism is absent in **4b** and **5b**, which feature an unsubstituted phenyl ring. Third, the N-H can be axial or equatorial, and fourth, the CO₂Me group can be geometrically aligned for possible hydrogen bonding to the NH or not. These last two features are illustrated in the representative computed structures of **4a** in Figure 2.7. In *trans*-ester **4a**, eight ψ_{ax} -CO₂Me and eight ψ_{eq} -CO₂Me conformations were predicted by MMFF94 calculation (cf. **B** and **C**, Figure 2.4). In the *cis*-isomer **5a**, only six ψ_{ax} -CO₂Me conformers and eight ψ_{eq} -CO₂Me conformations were found. As expected, the six ψ_{ax} -CO₂Me conformers of **5a** are much higher in energy than the ψ_{eq} -CO₂Me conformations due to severe 1,3-diaxial interactions with the C1-aryl group. As depicted in Figure 2.7, for **4a** and **5a**, the 2'-Cl group can adopt an *exo*- or *endo*-orientation with respect to the tetrahydropyridine ring, whereas the *exo*-orientation is energetically preferred. The axial and equatorial orientations of the NH hydrogen (H2) are roughly equally represented among the conformers. In conformations featuring a ψ_{eq} -CO₂Me group, both ax-H2 and eq-H2 can hydrogen-bond to the CO₂Me group via the C=O or OMe oxygen atoms. In contrast, for conformations featuring a ψ_{ax} -CO₂Me group, only eq-H2 can form an intramolecular H-bond via the C=O or OMe oxygen atoms. In ψ_{ax} -CO₂Me/ax-H2 conformations, an intramolecular H-bond is geometrically impossible (e.g., structure **III**, Figure 2.7).

2.4.1 Energetic distribution of calculated conformers

To calculate the free energies of these conformers at 298 K, single-point energies were calculated using the mPW1PW91⁵¹ and B3LYP functionals at a larger basis set (6-311+G(2d,p)) and with PCM⁵² implicit solvation (CHCl₃). The 6-311+G(2d,p) basis set, mPW1PW91 functional, and PCM solvation model were chosen based on their suitability for ¹³C NMR shift calculations.⁵³ In

addition, we also calculated single point energies at M06-2X/def2-TZVP (with PCM solvation) since the M06-2X functional^{54, 55} has been recommended for accurate energies of conformers, especially in conjunction with the def2-TZVP basis set.^{56, 57} Free energy corrections (based on B3LYP/6-31G(d) frequencies) were then applied to these single-point energies (Table 5.6 – Table 5.13).

Boltzmann distributions of the conformers of **4a/5a**, **4b/5b** calculated using mPW1PW91/6-311+G(2d,p) (PCM, CHCl₃) free energies were very similar to those based on B3LYP/6-311+G(2d,p) (PCM, CHCl₃) free energies (Table 5.14). M06-2X/def2-TZVP (PCM, CHCl₃) free energy-based Boltzmann distributions largely follow these trends, but for **5a** and **5b** show a diminished preference for conformers in the $\psi_{\text{eq}}\text{-CO}_2\text{Me}$ ensemble (Figure 2.4A, Table 5.14). Consequently, mPW1PW91 and B3LYP/6-311+G(2d,p)-based Boltzmann distributions give a superior prediction of $^3J_{4\beta-3}$, relative to those based on M06-2X/def2-TZVP. Furthermore, the calculations at mPW1PW91/6-311+G(2d,p) give an improved prediction of ¹³C NMR chemical shifts relative to those based on B3LYP/6-311+G(2d,p). Thus, results presented in this Chapter are based on mPW1PW91/6-311+G(2d,p) (PCM, CHCl₃) Boltzmann weights of the conformers, and complete sets of data from all three methods are included in Chapter 5. Structures of the lowest energy conformers of **4a/4b** and **5a/5b** are presented in Figure 2.8.

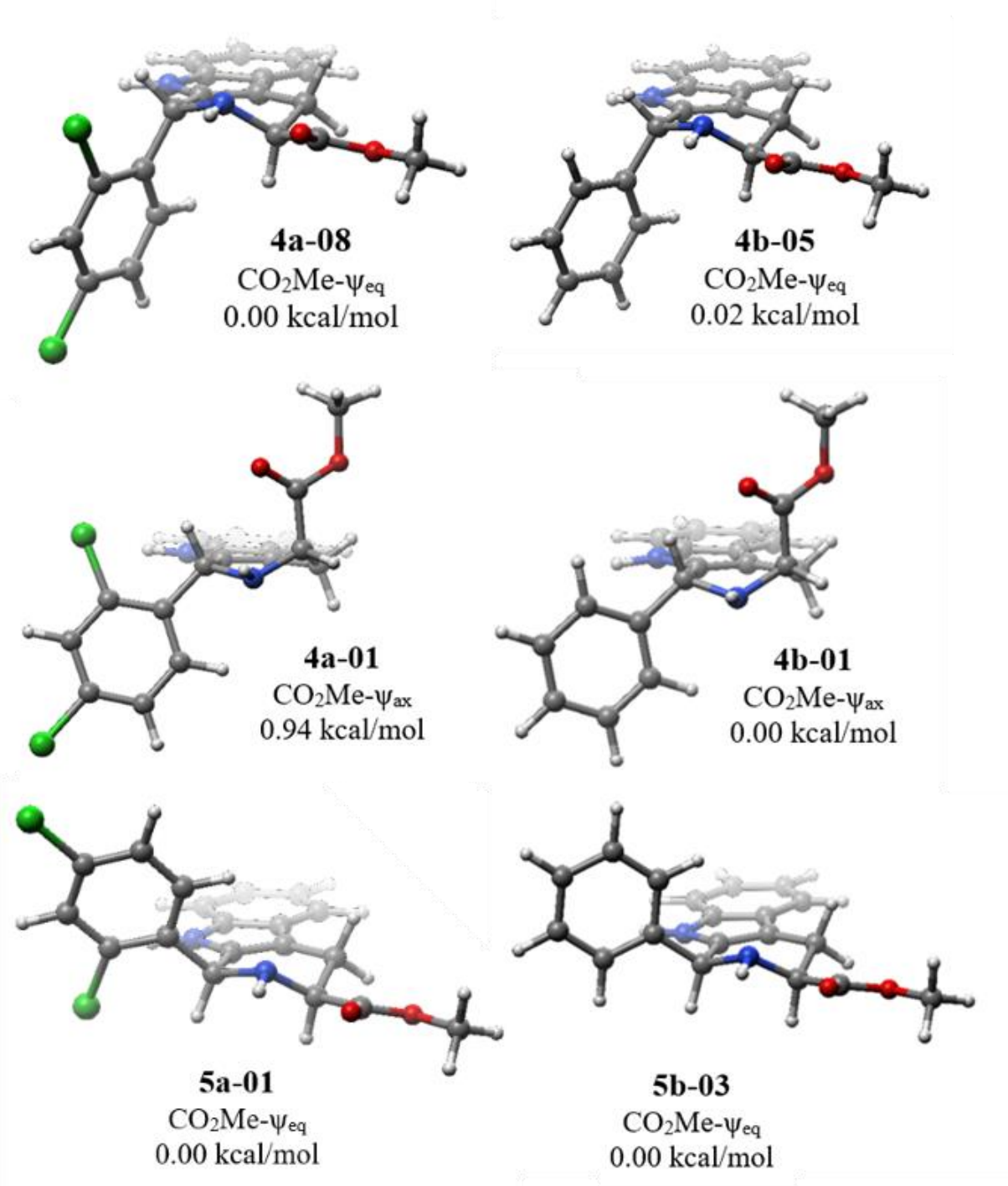
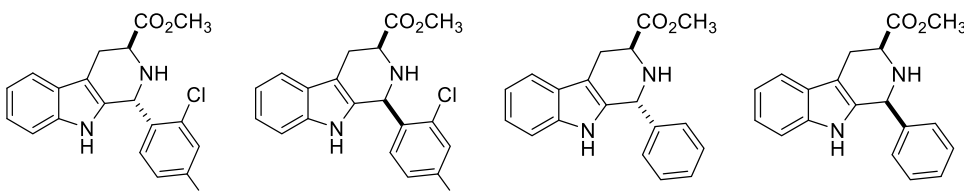


Figure 2.8 The lowest ΔG (298 K) ψ_{eq} - and ψ_{ax} - conformers of **4a** and the global minimum of **5a**. Geometries were obtained by B3LYP/6-31G(d) optimization; free energies were calculated from single-point energies using mPW1PW91/6-311+G(2d,p) – shown here, B3LYP/6-311+G(2d,p), or M06-2X/def2-TZVP (SCRF: PCM = CHCl₃) – the results of latter two methods are shown in Chapter 5 (Figure 5.1 and Figure 5.2). Free energy correction was obtained from the B3LYP/6-31G(d) frequencies.

As anticipated, *trans*-esters **4a** and **4b** significantly populate both the ψ_{ax} -CO₂Me and ψ_{eq} -CO₂Me conformational ensembles (cf. **B** and **C**, Figure 2.3). For **4a**, the lowest energy ψ_{ax} -CO₂Me conformation (**4a-01**) is only 0.94 kcal/mol higher in energy than the global minimum ψ_{eq} -CO₂Me structure (**4a-08**, Figure 2.8, Table 5.7). For **4b**, the lowest energy ψ_{ax} -CO₂Me conformation (**4b-01**) and lowest energy ψ_{eq} -CO₂Me conformation (**4b-05**) are within 0.02 kcal/mol of each other (Figure 2.8, Table 5.9). In contrast, *cis*-esters **5a** and **5b** adopt >99% and ~100% ψ_{eq} -CO₂Me conformations respectively (Table 2.6). As noted above, at M06-2X/def2-TZVP (PCM, CHCl₃)/B3LYP/6-31G(d), **5a** and **5b** show less energetic differentiation of the ψ_{eq} - and ψ_{ax} -CO₂Me conformations, populating only 85 and 99% of the ψ_{eq} -CO₂Me conformation **A** (Figure 2.4), respectively (Table 5.14). For **5a** and **5b**, the lowest energy ψ_{ax} -CO₂Me conformations are 3.1 kcal/mol (**5a-04**) and 4.6 kcal/mol (**5b-05**) higher in energy than global minimum ψ_{eq} -CO₂Me structures (**5a-01** and **5b-03**, Figure 2.8, Table 5.11 and Table 5.13). As discussed at the outset, ψ_{ax} -CO₂Me conformations of **5a** would be unstable by virtue of 1,3-diaxial interactions with the ψ_{ax} -aryl group at C1. Thus, the energy distribution of conformers calculated using DFT methods (Table 2.6) supports not only the first-principles conformational analysis (Figure 2.4) but also satisfactorily reflects the $^3J_{4\beta-3}$ values reported in Table 2.4.

Table 2.6 Boltzmann distribution of conformational ensembles in **4a/b** and **5a/b**, based on mPW1PW91/6-311+G(2d,p) (PCM, CHCl₃)/B3LYP/6-31G(d) free energies at 298 K.



	4a [%]	5a [%]	4b [%]	5b [%]
$\psi_{ax}\text{-CO}_2\text{Me}$	14.0	0.3	38.1	0.0
$\psi_{eq}\text{-CO}_2\text{Me}$	86.0	99.7	61.9	100.0
<i>exo</i> -2'-Cl	98.5	92.3	–	–
<i>endo</i> -2'-Cl	1.5	7.7	–	–
<i>ax</i> -H2	38.9	46.6	32.3	39.0
<i>eq</i> -H2	61.1	53.4	67.7	61.0
H-bond	99.0	100.0	98.3	100.0
No H-bond	1.0	0.0	1.7	0.0

Other noteworthy features of our calculations are: 1) in **4a** and **5a** there is a significant preference for the *exo*-2'-Cl orientation, which appears to be steric in origin; 2) *ax*-H2 and *eq*-H2 conformations are similar in energy for all four compounds; 3) intramolecularly H-bonded structures are much more favorable than non-H-bonded structures for all four compounds.

2.4.2 Calculation of $^3J_{\text{HH}}$ coupling constants

Using mPW1PW91/6-311+G(2d,p) (PCM, CHCl₃) Boltzmann weights, we then calculated select ^1H - ^1H coupling constants at B3LYP/6-31G(d,p)u+1s//B3LYP/6-31G(d), which has been found to be economical and accurate as demonstrated by root-mean-square deviation (RMSD, Equation 2.1) lower than 0.5 Hz for a wide range of organic molecules.⁵⁸ As shown in Table 2.7, this method worked very well for **4a/5a** and **4b/5b**. For the five coupling constants previously presented in Table 2.4, over four compounds, excellent accuracy (RMSD < 0.5 Hz, Table 5.15, and Table 5.16) was obtained. Most importantly, the close correspondence of calculated and observed values of $^3J_{4\beta-3}$ and $^3J_{4\alpha-3}$ suggests that the mPW1PW91/6-311+G(2d,p) (PCM, CHCl₃) Boltzmann weights accurately capture the distribution of $\psi_{ax}\text{-CO}_2\text{Me}$ and $\psi_{eq}\text{-CO}_2\text{Me}$ conformers of the

tetrahydropyridine ring in **4a/5a** and **4b/5b**. In contrast, the M06-2X/def2-TZVP Boltzmann distributions in these calculations gave less accurate values of ${}^3J_{4\beta-3}$ for **5a** and **5b** (8.8 and 10.2 Hz, respectively, Table 5.16) as a consequence of the diminished energetic difference between the ψ_{ax} -CO₂Me and ψ_{ax} -CO₂Me conformers.

Equation 2.1 Formula for root-mean-square deviation (RMSD)

$$\text{RMSD} = \sqrt{\frac{\sum_1^n (x_i - x_0)^2}{n}} \quad (2.1)$$

Where x_i is the calculated value, x_0 is the experimentally observed value, and n is the number of x values within the studied set.

Table 2.7 Calculated (B3LYP/6-31(d,p)u+1s//B3LYP/6-31G(d))^a vs experimental (CDCl₃) ¹H-¹H coupling constants for **4a/5a** and **4b/5b**.

J [Hz]	4a			5a		
	Calculated	Experimental	$ \Delta_{\text{calc-exp}} $	Calculated	Experimental	$ \Delta_{\text{calc-exp}} $
${}^3J_{4\beta-3}$	9.6	7.8	1.8	10.7	11.0	0.3
${}^3J_{4\alpha-3}$	4.2	5.0	0.8	3.8	4.1	0.3
${}^2J_{4\alpha-4\beta}^b$	15.2	15.4	0.2	15.0	15.1	0.1
${}^5J_{4\beta-1}$	1.8	1.5	0.3	3.0	2.5	0.5
${}^5J_{4\alpha-1}$	0.9	1.2	0.3	2.0	1.9	0.1
J [Hz]	4b			5b		
	Calculated	Experimental	$ \Delta_{\text{calc-exp}} $	Calculated	Experimental	$ \Delta_{\text{calc-exp}} $
${}^3J_{4\beta-3}$	6.7	6.8	0.1	10.8	11.2	0.4
${}^3J_{4\alpha-3}$	5.0	5.4	0.2	3.9	4.3	0.4
${}^2J_{4\alpha-4\beta}^b$	15.2	15.4	0.2	15.0	15.2	0.2
${}^5J_{4\beta-1}$	1.9	1.6	0.3	3.0	2.6	0.4
${}^5J_{4\alpha-1}$	1.6	1.4	0.2	2.1	1.9	0.2

^aWeighted average over all conformations, based on mPW1PW91/6-311+G(2d,p)//B3LYP/6-31G(d) Boltzmann distribution (298 K). ^b ${}^2J_{\text{HH}}$ values for sp^3 C-H are calculated to be negative, as expected;⁵⁹ the absolute values are shown here.

2.4.3 Calculation of ¹³C NMR chemical shifts

With the B3LYP/6-31G(d) geometries and mPW1PW91/6-311+G(2d,p) (PCM, CHCl₃) Boltzmann distribution of the conformers of **4a/5a** and **4b/5b** validated by the calculated ¹H-¹H coupling constants in Table 2.7, we were positioned to determine whether the distinctive C1 and C3 chemical shifts of the *cis*- and *trans*-diastereomers could be reproduced by computation. We

thus calculated ^{13}C NMR chemical shifts (δ) for each conformer of **4a**, **4b**, **5a**, and **5b** from the B3LYP/6-31G(d) geometries at the B3LYP/6-311+G(2d,p) (PCM, CHCl_3), and mPW1PW91/6-311+G(2d,p) (PCM, CHCl_3) levels of theory (Table 5.17 – Table 5.20). These functionals, basis set, and solvation model were selected based on their excellent performance in a recent study of colchicine.⁵³ The weighted average ^{13}C NMR chemical shifts of each carbon in **4a**, **4b**, **5a**, and **5b** were then calculated using the calculated Boltzmann populations (Equation 2.2) and the mean average deviations (MAD) of the calculated chemical shifts from the observed values were calculated to assess the performance of each functional (Equation 2.3).

Equation 2.2 Formula for Boltzmann distribution

$$\% = \frac{e^{\frac{(E_i - E_{\min})}{k \cdot T}}}{\sum e^{\frac{(E_i - E_{\min})}{k \cdot T}}} \cdot 100 \quad (2.2)$$

Where k is Boltzmann constant ($k = 0.00198 \text{ kcal mol}^{-1} \text{ K}^{-1}$), T is temperature [K], E_i is the free energy of conformer i [kcal/mol], and E_{\min} is the free energy of the lowest energy conformer [kcal/mol].

Equation 2.3 Formula for mean average deviation (MAD)

$$MAD = \frac{\sum_1^n |x_i - x_0|}{n} \quad (2.3)$$

Where x_i is the calculated value, x_0 is the experimentally observed value, and n is the number of x values within the studied set.

Both functionals predict ^{13}C NMR chemical shifts well, giving MAD of ~ 2 ppm or less. However, mPW1PW91 performed slightly better over the set of examined compounds (Table 2.8). This observation agrees with a recent study of the calculated ^{13}C NMR spectrum of colchicine (CDCl_3), whose authors reported mPW1PW91 MAD = 1.9 ppm and B3LYP MAD = 1.9 ppm.⁵³ The slightly smaller MAD values seen for **4b/5b** relative to **4a/5a** result from inaccurate

calculation of the ^{13}C chemical shifts for Cl-bearing carbons C2' and C4' in **4a** and **5a** (Table 5.17 and Table 5.19).

Table 2.8 All-carbon^a mean absolute deviation (MAD) in calculated ^{13}C NMR resonances for **4a/4b** and **5a/5b**.

	B3LYP/6-311+G(2d,p)	mPW1PW91/6-311+G(2d,p)
4a	2.1 ppm	1.7 ppm
4b	1.5 ppm	1.1 ppm
5a	2.0 ppm	1.6 ppm
5b	1.4 ppm	1.0 ppm
Average	1.8 ppm	1.4 ppm

^aMean absolute deviation in ^{13}C NMR chemical shift for all 19 carbons in each compound. ^bAverage of MAD for compounds **4a**, **4b**, **5a**, and **5b**. All calculations used PCM solvation (CHCl_3) and were based on geometries obtained from B3LYP/6-31G(d) (gas phase).

^{13}C NMR chemical shifts for C3, C1, C=O, and C1' calculated by mPW1PW91/6-311+G(2d,p) method closely match the observed values for all four compounds, with deviations generally less than 2 ppm. Looking at the difference in the chemical shift for a particular carbon between diastereomers ($\Delta\delta_{4.5}$), the congruity is even better (Table 2.9). For example, the C1 and C3 $\Delta\delta_{4.5}$ values for **4a/5a** are predicted to be -4.1 and -2.9 ppm, respectively, and correspond well with the observed $\Delta\delta_{4.5}$ values (-4.4 and -2.6 ppm, respectively). Furthermore, this DFT method also recapitulates the observed slight downfield shifts of C=O and C1' in the *trans*-isomers (+0.5 to +1.3 ppm, respectively). Thus, DFT predicts both the observed upfield shifts of C1 and C3 in **4a-b** relative to **5a-b** and the slight downfield shifts of C=O and C1'.

Table 2.9 Calculated vs. observed ^{13}C NMR chemical shifts (δ [ppm]) for selected carbons in **4a/4b** and **5a/5b**, and corresponding differences in δ between diastereomers ($\Delta_{\delta 4-5}$).

	Experimental ^a δ [ppm]			Calculated ^b δ [ppm]		
	4a	5a	$\Delta_{\delta 4a-5a}$	4a	5a	$\Delta_{\delta 4a-5a}$
C1	51.3	53.9	-2.6	52.7	55.2	-2.5
C3	52.3	56.7	-4.4	52.5	57.7	-4.9
C=O	173.8	173.1	+0.7	175.4	175.1	+0.3
C1'	137.9	137.4	+0.5	139.2	138.8	+0.4
	4b	5b	$\Delta_{\delta 4b-5b}$	4b	5b	$\Delta_{\delta 4b-5b}$
C1	55.1	58.8	-3.7	56.5	59.8	-3.3
C3	52.7	57.0	-4.3	53.8	57.7	-3.9
C=O	174.3	173.3	+1.0	176.0	175.3	+0.7
C1'	142.1	140.8	+1.3	143.9	142.2	+1.7

^aChemical shifts observed experimentally in ^{13}C NMR (CDCl_3). ^bBoltzmann weighted mPW1PW91/6-311+G(2d,p) (PCM, CHCl_3)/B3LYP/6-31G(d) ^{13}C NMR chemical shifts.

2.4.4 Computational evaluation of the role of steric compression in the ^{13}C chemical shifts of C1 and C3 in **4a** and **4b**

Upon establishing the accuracy of DFT-derived ^{13}C NMR chemical shifts for **4a/5a** and **4b/5b**, we were in a position to ask whether these upfield shifts of C1 and C3 in **4a** and **4b** relative to **5a** and **5b** can be attributed to “steric compression”, which is believed to be the major contributor to the so-called γ -effect. *If so, the chemical shifts of C1 and C3 in **4a** and **4b** should depend on the conformation of the tetrahydropyridine ring.* Therefore, by grouping the individual conformers of **4a** and **4b** into two overall $\psi_{\text{eq-}}$ and $\psi_{\text{ax-CO}_2\text{Me}}$ tetrahydropyridine conformational ensembles (i.e., **B** and **C**, Figure 2.4), and recalculating the weighted average ^{13}C NMR chemical shifts at C1 and C3, we can assess the effect of γ -gauche-associated steric compression (Figure 2.9, Table 5.21 and Table 5.22).

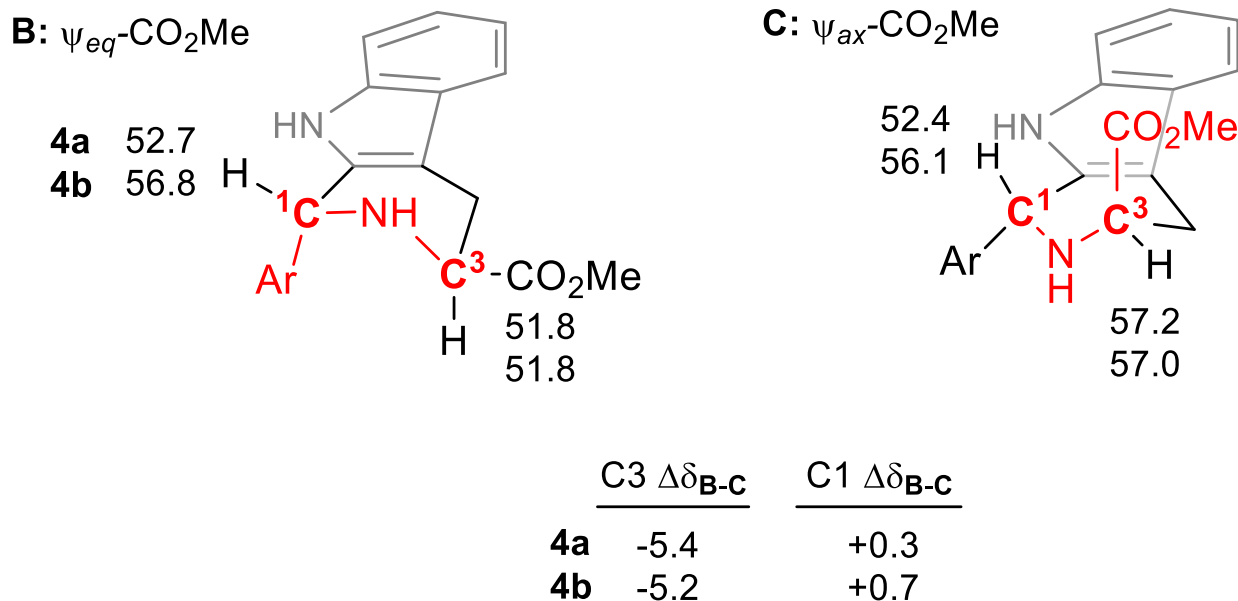


Figure 2.9 Weighted (mPW1PW91/6-311+G(2d,p) (PCM,CHCl₃)/B3LYP/6-31G(d)) ¹³C NMR chemical shifts for C1 & C3 of **4a** and **4b** in the ψ_{eq} - and ψ_{ax} -CO₂Me tetrahydropyridine conformational ensembles **B** and **C**. Gauche interactions of ring substituents with C1 and C3 are highlighted in red. Cagašová, K.; Ghavami, M.; Yao, Z.-K.; Carlier, P. R., Questioning the γ -gauche effect: stereoassignment of 1,3-disubstituted-tetrahydro- β -carboline using ¹H-¹H coupling constants. *Org. Biomol. Chem.* **2019**, *17* (27), 6687-6698. - Adapted by permission of The Royal Society of Chemistry.

The calculated ¹³C chemical shifts of C3 in **4a** and **4b** in ensemble **B** are considerably upfield of the values in ensemble **C** (C3 $\Delta\delta_{B-C}$ = -5.4 and -5.2 ppm, respectively). These calculated upfield shifts could be consistent with steric compression of C3 resulting from γ -gauche interaction with the C1-aryl group in ensemble **B** (cf. Figure 2.4). However, no significant differences are seen in the chemical shifts of C1 in **4a** and **4b** between ensembles **B** and **C** (C1 $\Delta\delta_{B-C}$ = +0.3 and +0.7 ppm, respectively), despite its γ -gauche orientation to the ψ_{ax} -C3-CO₂Me group in ensemble **C**. These observations are also replicated at the B3LYP/6-311+G(2d,p) (PCM, CHCl₃)/B3LYP/6-31G(d) level (Table 5.21 and Table 5.22). Thus, the uniform upfield shift of C1 in **4a-ar** relative to **5a-ar** (Table 2.2) cannot be simply attributed to the steric compression between gauche oriented carbons, since the C1 chemical shifts remain unchanged whether the C1-CO₂Me group is gauche- (ensemble **C**) or anti- (ensemble **B**).

2.4.5 Conclusions

In summary, we demonstrated that the *trans*- and *cis*-configuration of 1,3-disubstituted TH β Cs can be reliably assigned by ^1H NMR spectroscopy, based on a particular coupling constant ($^3J_{4\beta-3}$). In the set of 34 *cis*-esters compounds **5a-ar**, the value of $^3J_{4\beta-3}$ is 11.1 ± 0.1 Hz, indicating that they nearly exclusively populate a tetrahydropyridine conformational ensemble that features a ψ_{eq} -CO₂Me group at C3 (**A**, Figure 2.4). In contrast, the average value of $^3J_{4\beta-3}$ for the set of 34 *trans*-esters **4a-ar** is 7.3 ± 1.2 , indicating that these compounds populate two nearly equienergetic tetrahydropyridine conformational ensembles: one featuring a ψ_{eq} -CO₂Me group at C3 (**B**, Figure 2.4), and one featuring a ψ_{ax} -CO₂Me group at C3 (**C**, Figure 2.4).

Our assignments match those made by the ^{13}C NMR chemical shift method of Ungemach et al. in every case,⁷ but this ^1H NMR assignment method has several benefits. In addition to reduced sample quantity and experiment time requirements, it can be applied when only one stereoisomer is in hand. Furthermore, extensive DFT calculations support the conformational analysis undergirding the ^1H NMR assignment method, including accurate (RMSD = 0.5 Hz) calculation of $^3J_{4\beta-3}$ and other ^1H - ^1H coupling constants. Furthermore, these calculations show that the presence or absence of a γ -gauche substituent does not affect the ^{13}C NMR chemical shift of C1 in **4a** and **4b** (Figure 2.9). This calculated result, combined with the observed failure of C1 and C3 to exert reciprocal upfield shifts of the C=O and C1' carbons in **4a-ar** (Table 2.3), thus challenges the conceptual foundation of the traditional ^{13}C NMR chemical shift assignment method for 1,3-disubstituted TH β Cs. With this foundation in doubt, one cannot predict scenarios under which the method would fail to assign *trans*- and *cis*-TH β Cs properly. Since biological activity within the medicinally important 1,3-disubstituted-TH β C scaffold is typically very sensitive to configuration,^{43, 44, 60, 61} a missed assignment could muddy emerging structure-activity

relationships and mislead investigators. In contrast, the sound theoretical foundation of the ${}^3J_{4\beta-3}$ assignment method described herein allows one to use standard conformational analysis tools to anticipate conditions under which the assignment might fail. This important feature and the other advantages listed above commends its use to synthetic and medicinal chemists.

References

1. Cagašová, K.; Ghavami, M.; Yao, Z.-K.; Carlier, P. R., Questioning the γ -gauche effect: stereoassignment of 1,3-disubstituted-tetrahydro- β -carbolines using ^1H - ^1H coupling constants. *Org. Biomol. Chem.* **2019**, *17* (27), 6687-6698.
2. Coddington, P. W., Structure-activity studies of β -carbolines. 1. Molecular structure and conformation of *cis*-3-carboxylic acid-1,2,3,4-tetrahydroharmane dihydrate. *Can. J. Chem.* **1983**, *61* (3), 529-532.
3. Behm, H.; Beurskens, P. T.; Plate, R.; Ottenheijm, H. C. J., Crystal Structure Determination of 1-[*N*-benzyloxycarbonyl-1-amino-(*S*-4-methoxybenzyl)-2-thio-ethyl] -2-hydroxy-3-ethoxycarbonyl-1,2,3,4 -tetrahydro- β -carboline, $\text{C}_{32}\text{H}_{35}\text{N}_3\text{O}_6\text{S}$. *Recl. Trav. Chim. Pays-Bas* **1986**, *105* (7-8), 238-240.
4. Singh, K.; Deb, P. K.; Venugopalan, P., Modified Pictet-Spengler reaction. A highly diastereoselective approach to 1,2,3-trisubstituted-1,2,3,4-tetrahydro- β -carbolines using perhydro-1,3-heterocycles. *Tetrahedron* **2001**, *57* (37), 7939-7949.
5. Jiang, W.; Alford, V. C.; Qiu, Y.; Bhattacharjee, S.; John, T. M.; Haynes-Johnson, D.; Kraft, P. J.; Lundeen, S. G.; Sui, Z., Synthesis and SAR of tetracyclic pyrroloquinolones as phosphodiesterase 5 inhibitors. *Bioorganic & Medicinal Chemistry* **2004**, *12* (6), 1505-1515.
6. Everett, J. H.; Reynolds, C. D.; Sparks, C. A.; Pangborn, W.; Bailey, P. D.; Dauter, Z.; Helliwell, M.; Hollinshead, S. P., Crystal and molecular structure of a *N*(2)-benzyl-1,3-disubstituted-1,2,3,4-tetrahydro- β -carboline. *J. Crystallogr. Spectrosc. Res.* **1990**, *20* (2), 109-115.
7. Ungemach, F.; Soerens, D.; Weber, R.; DiPierro, M.; Campos, O.; Mokry, P.; Cook, J. M.; Silvertown, J. V., General Method for the Assignment of Stereochemistry of 1,3-Disubstituted 1,2,3,4-Tetrahydro- β -carbolines by Carbon-13 Spectroscopy. *J. Am. Chem. Soc.* **1980**, *102* (23), 6976-6984.
8. Pindur, U., ^1H - und ^{13}C -NMR-spektroskopische Zuordnung der *cis*- und *trans*-Isomere einiger 1-Aryl-1,2,3,4-tetrahydro- β -carbolin-3-carbonsäuren bzw. deren Methylester. *Arch. Pharm.* **1980**, *313* (4), 361-368.
9. Bailey, P. D.; Hollinshead, S. P., On the Assignment of Stereochemistry of 1,3-Disubstituted Tetrahydro- β -carbolines using ^{13}C N.M.R. Spectroscopy. *J. Chem. Soc., Chem. Commun.* **1985**, (22), 1575-1576.
10. Bringmann, G.; Hille, A.; Stäblein, M.; Peters, K.; Von Schnering, H. G., Potential Tryptophan-Derived Alkaloids in Chloral-Treated Patients: Synthesis and Stereostructure. *Liebigs Ann. Chem.* **1991**, *1991* (11), 1189-1194.
11. Pulka, K.; Kulis, P.; Tymecka, D.; Frankiewicz, L.; Wilczek, M.; Kozminski, W.; Misicka, A., Diastereoselective Pictet-Spengler condensation of tryptophan with α -amino aldehydes as chiral carbonyl components. *Tetrahedron* **2008**, *64* (7), 1506-1514.
12. Bertamino, A.; Ostacolo, C.; Medina, A.; Di Sarno, V.; Lauro, G.; Ciaglia, T.; Vestuto, V.; Pepe, G.; Basilicata, M. G.; Musella, S.; Smaldone, G.; Cristiano, C.; Gonzalez-Rodriguez, S.; Fernandez-Carvajal, A.; Bifulco, G.; Campiglia, P.; Gomez-Monterrey, I.; Russo, R., Exploration of TRPM8 Binding Sites by β -Carboline-Based Antagonists and Their In Vitro Characterization and In Vivo Analgesic Activities. *J. Med. Chem.* **2020**, *63* (17), 9672-9694.

13. Xiao, S.; Shi, X.-X.; Ni, F.; Xing, J.; Yan, J.-J.; Liu, S.-L., An Efficient and General Method for the Stereodivergent Syntheses of Tadalafil-Like Tetracyclic Compounds. *Eur. J. Org. Chem.* **2010**, 2010 (9), 1711-1716.
14. Mohamed, H. A.; Girgis, N. M. R.; Wilcken, R.; Bauer, M. R.; Tinsley, H. N.; Gary, B. D.; Piazza, G. A.; Boeckler, F. M.; Abadi, A. H., Synthesis and Molecular Modeling of Novel Tetrahydro- β -carboline Derivatives with Phosphodiesterase 5 Inhibitory and Anticancer Properties. *J. Med. Chem.* **2011**, 54 (2), 495-509.
15. Brossi, A.; Focella, A.; Teitel, S., Alkaloids in Mammalian Tissues. 3. Condensation of L-Tryptophan and L-5-Hydroxytryptophan with Formaldehyde and Acetaldehyde. *J. Med. Chem.* **1973**, 16 (4), 418-420.
16. Rashid, N.; Alam, S.; Hasan, M.; Khan, N.; Khan, K. M.; Duddeck, H.; Pescitelli, G.; Kenéz, Á.; Antus, Sándor; Kurtán, T., *Cis*-Diastereoselectivity in Pictet–Spengler Reactions of L-Tryptophan and Electronic Circular Dichroism Studies. *Chirality* **2012**, 24 (10), 789-795.
17. Shimizu, M.; Ishikawa, M.; Komoda, Y.; Nakajima, T.; Yamaguchi, K.; Sakai, S., Asymmetric Synthesis of (1*S*)-(-)-Trypargine. *Chem. Pharm. Bull.* **1982**, 30 (9), 3453-3456.
18. Abadi, A. H.; Gary, B. D.; Tinsley, H. N.; Piazza, G. A.; Abdel-Halim, M., Synthesis, molecular modeling and biological evaluation of novel tadalafil analogues as phosphodiesterase 5 and colon tumor cell growth inhibitors, new stereochemical perspective. *Eur. J. Med. Chem.* **2010**, 45 (4), 1278-1286.
19. Grant, D. M.; Cheney, B. V., Carbon-13 Magnetic Resonance. VII. Steric Perturbation of the Carbon-13 Chemical Shift. *J. Am. Chem. Soc.* **1967**, 89 (21), 5315-5318.
20. Dalling, D. K.; Grant, D. M., Carbon-13 magnetic resonance. IX. The Methylcyclohexanes. *J. Am. Chem. Soc.* **1967**, 89 (25), 6612-6622.
21. Dalling, D. K.; Grant, D. M., Carbon-13 Magnetic Resonance. XXI. Steric Interactions in the Methylcyclohexanes. *J. Am. Chem. Soc.* **1972**, 94 (15), 5318-5324.
22. Woolfenden, W. R.; Grant, D. M., Carbon-13 Magnetic Resonance. V. Conformational Dependence of the Chemical Shifts in the Methylbenzenes. *J. Am. Chem. Soc.* **1966**, 88 (7), 1496-1502.
23. Seidman, K.; Maciel, G. E., Proximity and Conformational Effects on ^{13}C Chemical Shifts at the γ Position in Hydrocarbons. *J. Am. Chem. Soc.* **1977**, 99 (3), 659-671.
24. Buchanan, G. W.; Preusser, S. H.; Webb, V. L., Deshielding γ -*gauche* effects in ^{13}C magnetic resonance: a comparison of the conformational behaviour of the acetyl group in cyclohexane and 5-substituted-1,3-dioxane systems. *Can. J. Chem.* **1984**, 62 (7), 1308-1311.
25. Buchanan, G. W., Low temperature carbon-13 magnetic resonance detection of axial conformers in vinyl- and formylcyclohexane: a deshielding γ -*gauche* effect. *Can. J. Chem.* **1982**, 60 (23), 2908-2913.
26. Schneider, H. J.; Hoppen, V., Carbon-13 Nuclear Magnetic Resonance Substituent-Induced Shieldings and Conformational Equilibria in Cyclohexanes. *J. Org. Chem.* **1978**, 43 (20), 3866-3873.
27. Subbotin, O.; Sergeev, N., Pulsed ^{13}C Fourier Transform Nuclear Magnetic Resonance Spectra of Monohalo-Substituted Cyclohexanes at Low Temperatures. *J. Am. Chem. Soc.* **1975**, 97 (5), 1080-1084.
28. Manoharan, M.; Eliel, E. L., ^{17}O NMR Spectra of Tertiary Alcohols, Ethers, Sulfoxides and Sulfones in the Cyclohexyl and 5-Substituted 1,3-Dioxanyl Series and Related Compounds. *Magn. Reson. Chem.* **1985**, 23 (4), 225-231.

29. Roberts, J. D.; Weigert, F. J.; Kroschwitz, J. I.; Reich, H. J., Nuclear Magnetic Resonance Spectroscopy. Carbon-13 Chemical Shifts in Acyclic and Alicyclic Alcohols. *J. Am. Chem. Soc.* **1970**, *92* (5), 1338-1347.
30. Rajan, K. P.; Manimekalai, A., Influence of *gauche* Interactions on the Substituent Effects on Carbon-13 Chemical Shifts in Six-Membered Ring Compounds. *Magn. Reson. Chem.* **1991**, *29* (9), 904-911.
31. Eggert, H.; Djerassi, C., Carbon-13 Nuclear Magnetic Resonance Spectra of Acyclic Aliphatic Amines. *J. Am. Chem. Soc.* **1973**, *95* (11), 3710-3718.
32. Carcenac, Y.; Diter, P.; Wakselman, C.; Tordeux, M., Influence of the spatial position of a trifluoromethyl group on the ^{13}C chemical shifts in the cyclohexane series. *Magn. Reson. Chem.* **2006**, *44* (6), 617-623.
33. Eliel, E. L.; Wilen, S. H.; Mander, L. N., *Stereochemistry of Organic Compounds*. Wiley: New York, 1994.
34. Jung, S.; Podlech, J., Stereoelectronic Effects: The γ -Gauche Effect in Sulfoxides. *J. Phys. Chem. A* **2018**, *122* (26), 5764-5772.
35. Wang, B.; Yu, D.; Zhao, D.; Rong, C.; Liu, S., Nature and origin of γ -gauche effect in sulfoxides: A density functional theory and information-theoretic approach study. *Chem. Phys. Lett.* **2019**, *730*, 451-459.
36. Vavsari, V. F.; Dianati, V.; Ramezani, S.; Balalaie, S., Stereoselective Synthesis of Functionalized Tetrahydro- β -Carbolines via Pictet–Spengler Reaction. *Synlett* **2015**, *26* (14), 1955-1960.
37. Ahmed, N. S.; Gary, B. D.; Tinsley, H. N.; Piazza, G. A.; Laufer, S.; Abadi, A. H., Design, Synthesis and Structure–Activity Relationship of Functionalized Tetrahydro- β -carboline Derivatives as Novel PDE5 Inhibitors. *Arch. Pharm. Chem. Life Sci.* **2011**, *344* (3), 149-157.
38. El-Gamil, D. S.; Ahmed, N. S.; Gary, B. D.; Piazza, G. A.; Engel, M.; Hartmann, R. W.; Abadi, A. H., Design of Novel β -Carboline Derivatives with Pendant 5-Bromothienyl and Their Evaluation as Phosphodiesterase-5 Inhibitors. *Arch. Pharm. Chem. Life Sci.* **2013**, *346* (1), 23-33.
39. Mizuno, T.; Oonishi, Y.; Takimoto, M.; Sato, Y., Total Synthesis of (–)-Corynantheidine by Nickel-Catalyzed Carboxylative Cyclization of Enynes. *Eur. J. Org. Chem.* **2011**, *2011* (14), 2606-2609.
40. Zhang, H.; Timmermann, B. N., Withanolide Structural Revisions by ^{13}C NMR Spectroscopic Analysis Inclusive of the γ -Gauche Effect. *J. Nat. Prod.* **2016**, *79* (4), 732-742.
41. London, R. E.; Wingad, B. D.; Mueller, G. A., Dependence of Amino Acid Side Chain ^{13}C Shifts on Dihedral Angle: Application to Conformational Analysis. *J. Am. Chem. Soc.* **2008**, *130* (33), 11097-11105.
42. Hansen, D. F.; Kay, L. E., Determining Valine Side-Chain Rotamer Conformations in Proteins from Methyl ^{13}C Chemical Shifts: Application to the 360 kDa Half-Proteasome. *J. Am. Chem. Soc.* **2011**, *133* (21), 8272-8281.
43. Yao, Z.-K.; Krai, P. M.; Merino, E. F.; Simpson, M. E.; Slobodnick, C.; Cassera, M. B.; Carlier, P. R., Determination of the active stereoisomer of the MEP pathway-targeting antimalarial agent MMV008138, and initial structure–activity studies. *Bioorg. Med. Chem. Lett.* **2015**, *25* (7), 1515-1519.
44. Ghavami, M.; Merino, E. F.; Yao, Z.-K.; Elahi, R.; Simpson, M. E.; Fernández-Murga, M. L.; Butler, J. H.; Casasanta, M. A.; Krai, P. M.; Totrov, M. M.; Slade, D. J.; Carlier, P. R.;

- Cassera, M. B., Biological Studies and Target Engagement of the 2-C-Methyl-D-Erythritol 4-Phosphate Cytidylyltransferase (IspD)-Targeting Antimalarial Agent (1*R*,3*S*)-MMV008138 and Analogs. *ACS Infect. Dis.* **2018**, *4* (4), 549-559.
45. Nakamura, T.; Ishida, A.; Irie, K.; Ohishi, T., A New Method for the Preparation of 3,4-Dihydro and 1,2,3,4-Tetrahydro- β -carbolines. *Chem. Pharm. Bull.* **1984**, *32* (7), 2859-2862.
46. Guenther, H.; Jikeli, G., ¹H Nuclear Magnetic Resonance Spectra of Cyclic Monoenes: Hydrocarbons, Ketones, Heterocycles, and Benzo Derivatives. *Chem. Rev.* **1977**, *77* (4), 599-637.
47. Barfield, M.; Sternhell, S., Conformational Dependence of Homoallylic H-H Coupling Constants. *J. Am. Chem. Soc.* **1972**, *94* (6), 1905-1913.
48. Becke, A. D., Density-functional thermochemistry. III. The role of exact exchange. *J. Chem. Phys.* **1993**, *98* (7), 5648-5652.
49. Lee, C.; Yang, W.; Parr, F., Development of the Colle-Salvetti correlation-energy formula into a functional of the electron density. *Phys. Rev. B* **1988**, *37* (2), 785-789.
50. Pettersen, D.; Marcolini, M.; Bernardi, L.; Fini, F.; Herrera, R. P.; Sgarzani, V.; Ricci, A., Direct Access to Enantiomerically Enriched α -Amino Phosphonic Acid Derivatives by Organocatalytic Asymmetric Hydrophosphonylation of Imines. *Journal of Organic Chemistry* **2006**, *71* (16), 6269-6272.
51. Adamo, C.; Barone, V., Exchange functionals with improved long-range behavior and adiabatic connection methods without adjustable parameters: The mPW and mPW1PW models. *J. Chem. Phys.* **1998**, *108* (2), 664-675.
52. Miertuš, S.; Scrocco, E.; Tomasi, J., Electrostatic interaction of a solute with a continuum. A direct utilization of AB initio molecular potentials for the prevision of solvent effects. *Chem. Phys.* **1981**, *55* (1), 117-129.
53. Pierens, G. K.; Venkatachalam, T.; Reutens, D. C., NMR and DFT investigations of structure of colchicine in various solvents including density functional theory calculations. *Sci. Rep.* **2017**, *7* (1), 5605.
54. Zhao, Y.; Truhlar, D. G., The M06 suite of density functionals for main group thermochemistry, thermochemical kinetics, noncovalent interactions, excited states, and transition elements: two new functionals and systematic testing of four M06-class functionals and 12 other functionals. *Theor. Chem. Acc.* **2008**, *120* (1), 215-241.
55. Zhao, Y.; Truhlar, D. G., Applications and validations of the Minnesota density functionals. *Chem. Phys. Lett.* **2011**, *502* (1), 1-13.
56. Weigend, F.; Ahlrichs, R., Balanced basis sets of split valence, triple zeta valence and quadruple zeta valence quality for H to Rn: Design and assessment of accuracy. *Phys. Chem. Chem. Phys.* **2005**, *7* (18), 3297-3305.
57. Aliev, A. E.; Karu, K.; Mitchell, R. E.; Porter, M. J., The structure of tagetitoxin. *Org. Biomol. Chem.* **2016**, *14* (1), 238-245.
58. Bally, T.; Rablen, P. R., Quantum-Chemical Simulation of ¹H NMR Spectra. 2. Comparison of DFT-Based Procedures for Computing Proton-Proton Coupling Constants in Organic Molecules. *J. Org. Chem.* **2011**, *76* (12), 4818-4830.
59. Friebolin, H., Indirect Spin-Spin Coupling. In *Basic One- and Two-Dimensional NMR Spectroscopy*, Wiley-VCH: 1998; pp 85-88.
60. Dagan, A.; Grondin, P.; Ruault, C.; Le Monnier de Gouville, A.-C.; Coste, H.; Linget, J. M.; Kirilovsky, J.; Hyafil, F.; Labaudinière, R., The Discovery of Tadalafil: A Novel and

Highly Selective PDE5 Inhibitor. 2: 2,3,6,7,12,12a-hexahydropyrazino[1',2':1,6]pyrido[3,4-b]indole-1,4-dione Analogues. *J. Med. Chem.* **2003**, *46* (21), 4533-4542.

61. Beghyn, T. B.; Charton, J.; Leroux, F.; Laconde, G.; Bourin, A.; Cos, P.; Maes, L.; Deprez, B., Drug to genome to drug: discovery of new antiplasmodial compounds. *J. Med. Chem.* **2011**, *54* (9), 3222-3240.

3 Tetrazole and phosphonate analogs of MMV008138

The carboxylic acid functionality present in our lead compound **1a** (Figure 3.1) is a common feature of many approved drugs on the market (more than 450 examples found in 2013¹, 13% of FDA approved drugs between 2015 and 2018),² which could significantly improve binding to the molecular targets via ionic interactions and hydrogen bonding.³ It can also improve the solubility of the drug in aqueous media. On the other hand, the ionic character of carboxylic acids under biological pH also leads to a decreased ability to penetrate cell membranes.⁴

The approximately 5-fold difference in potency of **1a** in growth inhibition assay and *Pf*lspD inhibition assay could be at least partially attributed to loss of the active species during the transfer to the apicoplast – the only organelle in *Plasmodium sp.* that contains MEP pathway enzymes.^{5, 6} First of all, it was necessary to confirm whether the C3-COOH substitution was a part of an active pharmacophore. Among compounds identified within Malaria Box,⁷ the only other tetrahydro- β -carboline was the compound MMV019690 (Figure 3.1), which lacked both the carboxylic acid moiety and the anti-apicoplast activity.⁸ Unfortunately, a direct comparison of the two molecules was not possible due to a considerable variation in D-ring substitution between MMV008138 and MMV019690, rendering synthesis of more closely related species necessary.

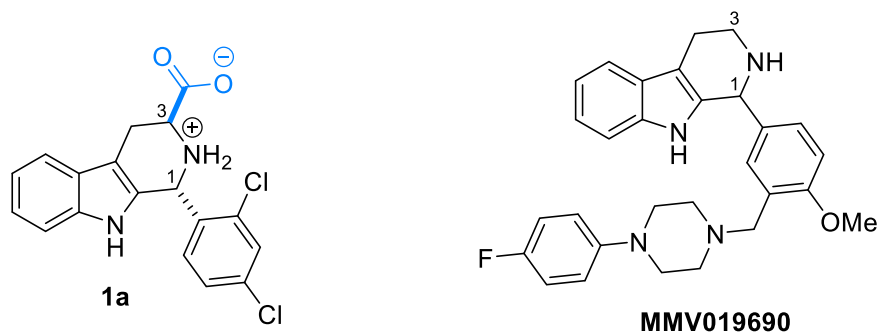
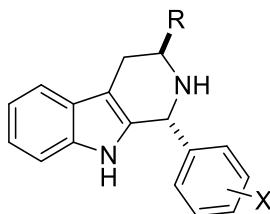


Figure 3.1 Tetrahydro- β -carbolines included in Malaria Box compound library. Compound **1a** is an amino acid and is expected to be a zwitterion in the solid-state. Its charge state in water is discussed below.

3.1 Structure-activity relationship of MMV008138 and carboxylic acid derivatives

To explore the importance of the carboxylic acid moiety in **1a**, Dr. Yao in the Carrier group synthesized decarboxylated analog (\pm)-**6a** and the 1° alcohol analog **7a**. The *P. falciparum* growth inhibition assay clearly shows the importance of the C3 carboxylate for the antimalarial activity of **1a**, as both decarboxylation ((\pm)-**6a**) and removal of the carbonyl group (**7a**) led to a complete loss of potency. The initial investigation of C3-isosteres of **1a** focused on a series of amides and a hydrazide, which could be easily obtained from the reaction of methyl ester **4a** with appropriate amine or hydrazine.⁹

Table 3.1 Growth inhibition activity of MMV008138 modified on position C3.⁹

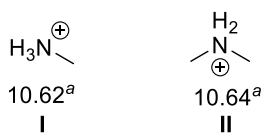


Compound	R	X	<i>P. falciparum</i> Dd2 strain growth inhibition IC ₅₀ (nM)
1a	CO ₂ H	2', 4'-Cl ₂	250 ± 70
1e	CO ₂ H	2'-Cl, 4'-Me	410 ± 40
1j	CO ₂ H	2'-Cl, 4'-Br	320 ± 60
1k	CO ₂ H	2'-Br, 4'-Cl	360 ± 40
4a	CO ₂ Me	2', 4'-Cl ₂	6800 ± 1400
(\pm)- 6a	H	2', 4'-Cl ₂	10,000 ± 1600
7a	CH ₂ OH	2', 4'-Cl ₂	> 10,000
8a	CONH ₂	2', 4'-Cl ₂	1200 ± 100
9a	CONHMe	2', 4'-Cl ₂	190 ± 30
9e	CONHMe	2'-Cl, 4'-Me	340 ± 50
9j	CONHMe	2'-Cl, 4'-Br	300 ± 40
9k	CONHMe	2'-Br, 4'-Cl	340 ± 60
10a	CONHEt	2', 4'-Cl ₂	~ 5,000
11a	CONHiPr	2', 4'-Cl ₂	50% inhibition at 10,000
12a	CONHBu	2', 4'-Cl ₂	80% inhibition at 10,000
13a	CONHCy	2', 4'-Cl ₂	2830 ± 500
14a	CONMe ₂	2', 4'-Cl ₂	> 20,000
15a	CONHNHMe	2', 4'-Cl ₂	1940 ± 200

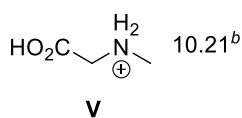
While the 1° amide **8a** retains some antimalarial activity compared to **1a**, the methyl amides **9a**, **9e**, **9j**, and **9k** show excellent potency equivalent to their appropriate carboxylic acid analogs (Table 3.1).⁹ At first glance, the pK_a of a protonated secondary amine is estimated at 10 – 11, and thus we would expect compounds **8a** and **9a** to be positively charged at physiological pH due to lack of carboxylic acid, while compound **1a** would be expected in the form of zwitterion. However, this initial estimate does not consider the environment of the secondary amine functionality. As we will show below, the pK_a of the protonated 2° amine in these compounds is significantly lower than 10-11, and this affects the expected charge states of these compounds at pH 7.4.

As depicted in Figure 3.2 below, attachment of a benzyl group to an amine lowers the pK_a by approximately one unit relative to its aliphatic counterpart (cf. **III** and **IV** with **I** and **II**).¹⁰ The experimental pK_a value of unsubstituted 1,2,3,4-tetrahydro-β-carboline (**XII**) is well aligned with this expectation.^{11, 12} The pK_a of protonated amines is further lowered by approximately 0.5 unit by the presence of an α-carboxylic acid (cf. **V** with **II** and **VI** with **III**), as is confirmed in tryptophan (**XIII**) and 1,2,3,4-tetrahydro-β-carboline-3-carboxylic acid (**XIV**).¹²⁻¹⁴ Thus, the pK_a of the protonated amine in our lead compound **1a** was calculated by our collaborator Dr. Maxim Totrov to be 7.1, where the 1.6 log difference from 1,2,3,4-tetrahydro-β-carboline-3-carboxylic acid (**XIV**, experimental pK_a = 8.7) can be attributed to an additional benzyl substitution and electron-withdrawing effect of chlorines (cf. **VII** with **VIII-X**).^{10, 15, 16} In case of compound **9a**, the amine pK_a was calculated by Dr. Totrov to be 5.6. While this value might seem very low, the difference between **1a** and **9a** (ΔpK_a = 1.5) aligns well with comparable pair of tryptophan (**XIII**) and tryptophanamide (**XV**, ΔpK_a = 1.8).^{11, 17}

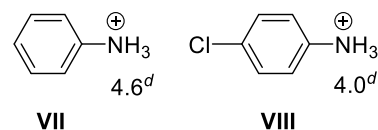
Aliphatic amines (pK_a ~ 10 - 11)



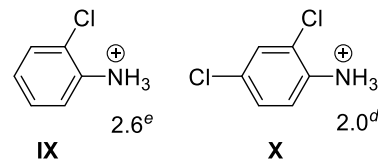
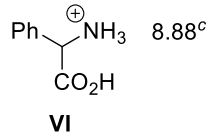
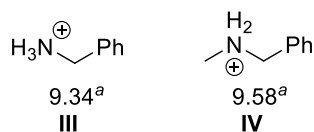
Adjacent -CO₂H decreases pK_a



Chlorine substitution decreases pK_a



Benzyl substitution decreases pK_a



Application in more complex systems and effect of amide substitution on amine pK_a

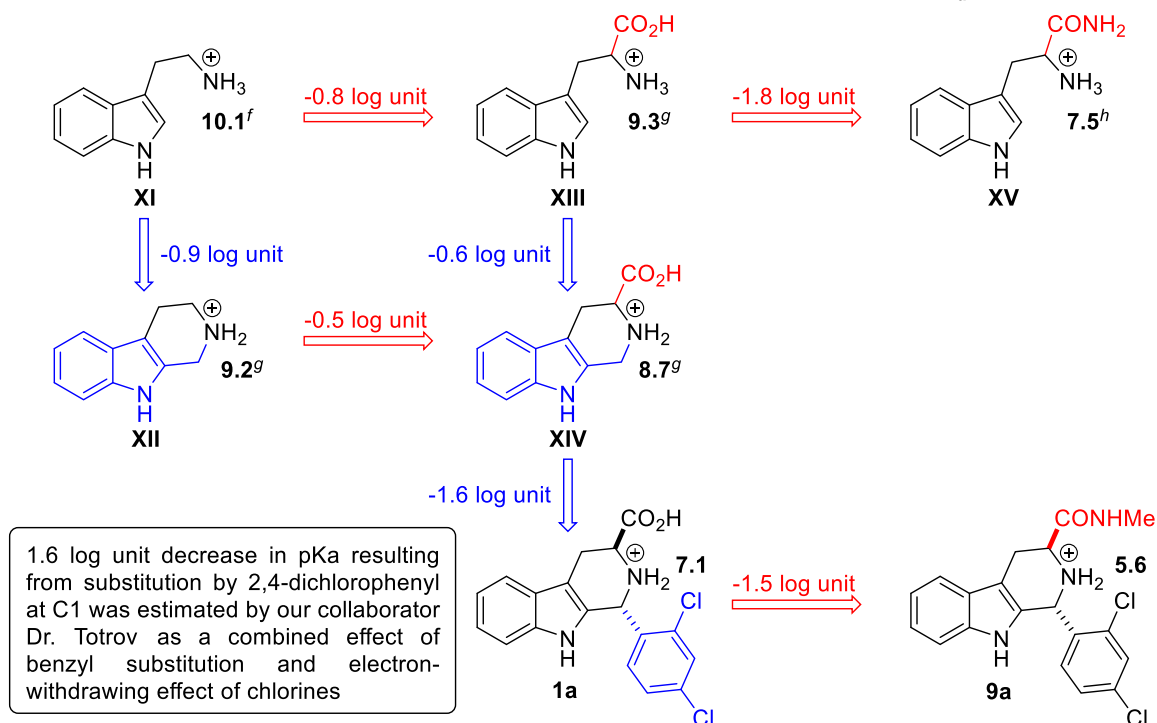


Figure 3.2 Effect of various substituents on pK_a of amines. All values, except for compounds **1a** and **9a**, were experimentally determined in aqueous conditions and are cited as found in the literature. Amine pK_a in compounds **1a** and **9a** were calculated by our collaborator Dr. Totrov. References for literature pK_a values: ^aHall, H. (1957)¹⁰, ^bHamborg et al. (2007)¹³, ^cKudelko et al. (2011)¹⁴, ^dLi, J. (2004)¹⁵, ^eKaljurand et al. (2005)¹⁶, ^fLlinas et al. (2008)¹¹, ^gEftink et al. (1995)¹², ^hFujikawa et al. (2005).¹⁷

With the more accurately estimated pK_a values for compounds **1a** and **9a**, we can calculate approximate charge composition using the Henderson-Hasselbalch equation (Equation 3.1). At physiological pH of 7.4, compound **1a** will therefore exist in approximately 2:1 ratio of carboxylate anion and zwitterion species, while amides such as **9a** will be found predominantly

(>98%) in neutral form. While the protonation state of the enzyme-bound compound cannot be directly related to the protonation state of the free compound in buffered solution, the preference for deprotonated amine in both **1a** and **9a** might be important for the compound's potency.

Equation 3.1 Henderson-Hasselbalch equation

$$pH = pK_a + \log \left(\frac{[base]}{[acid]} \right) \quad (3.1)$$

Additionally, it can be argued that the exact match in size of substituents does not guarantee comparable potency. As can be seen in Figure 3.3A, the carboxylic acid moiety is sterically more similar to the (less potent) 1° amide than to the (more potent) 2° methyl amide. Also, primary amides, unlike methyl amides, can be metabolized (via amidases) to carboxylic acids in vivo,¹⁸ and if such amidases were present in *P. falciparum*, we might expect **8a** to be more potent than **9a** (assuming the activity is due solely to **1a**). Confusingly, the potent secondary methyl amides **9a**, **e**, **f**, **k** are sterically comparable to the inactive methyl ester **4a** (Figure 3.3B). Note that the inactivity of **4a** indicates that there are no esterases¹⁸ present in *P. falciparum* that can deliver effective concentrations of acid **1a**. Therefore, we can conclude that while the carbonyl group seems to play an essential role for antimalarial action of **1a**, the exact size and acidity of the C3 substituent does not necessarily need to match that of a carboxylic acid.

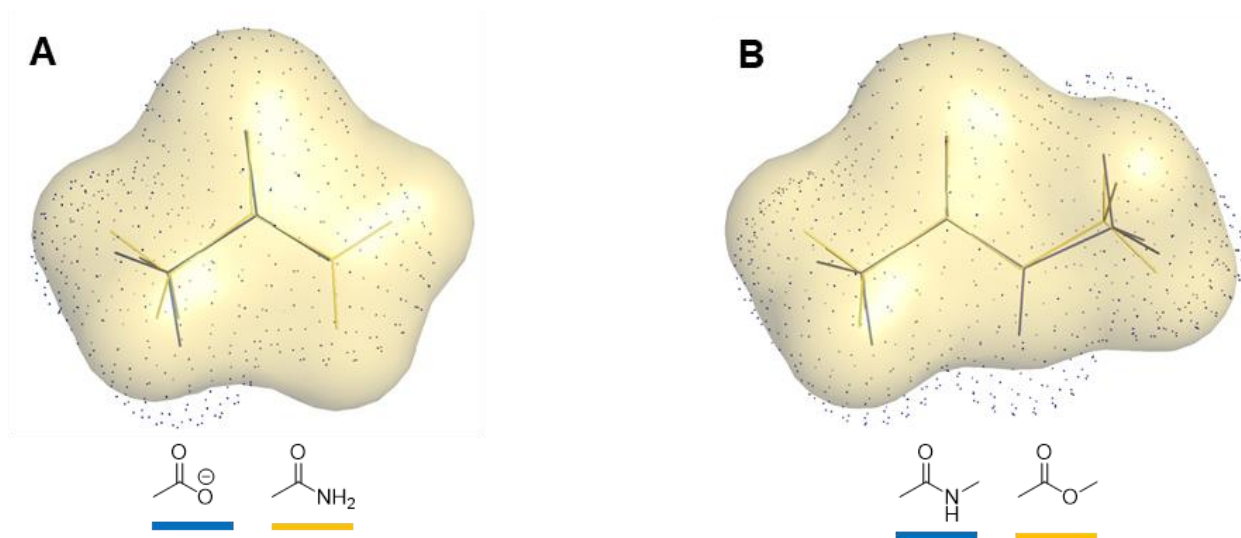


Figure 3.3 Structural comparison of C3-substituents in analogs **8a** and **4a** with potent **1a** and **9a**. **A**) Alignment of acetic acid anion and acetamide shows a good steric match of C3-substituent present in the potent analog **1a** and 5-fold less potent amide **8a**. **B**) Methyl ester aligned with methyl amide shows close spatial similarity, despite over 30-fold difference in potency between **9a** and **4a**. All structures were generated via B3LYP/6-31G (gas phase) geometry optimization in Gaussian and visualized in PyMOL.

Larger substituents in compounds **10a-15a** performed poorly in the growth inhibition assay (Table 3.1). Both cyclohexylamide (**13a**) and hydrazine (**15a**) derivatives showed approximately 10-fold decreases in potency, while ethyl, *iso*-propyl, and butyl amides (**10a-12a**) showed even greater loss of antimalarial activity. Furthermore, the tertiary dimethyl amide analog (**14a**) does not exhibit any antimalarial activity. Comparison of the groups present in non-active analogs **10a-15a** with groups in potent compounds **1a** and **9a** suggests that the carboxylate binding site must be fairly small.

Despite their relatively high potency, the methyl amide derivatives **9a**, **9e**, **9j**, and **9k** face a significant challenge in the form of poor solubility (thermodynamic solubility of **9a** in aqueous buffer at pH = 7.4 was only 0.6 $\mu\text{g/mL}$, while the solubility of **1a** under identical conditions is 1.05 mg/mL as determined by Pharmaron).¹⁹ Consequently, the focus of the Carrier group turned to derivatives promising improved aqueous solubility with some retained properties common to both **1a** and **9a**, such as comparable size, hydrogen bonding ability, and presence of carbonyl.

Further C3-derivatives of **1a** were synthesized by Dr. Maryam Ghavami (PhD, June 2018) and Ms. Lixuan Liu (M.S., April 2018). These analogs still contained -CONRR' motif, but additional polar groups promised improved aqueous solubility. Dr. Ghavami successfully synthesized analogs **16a-19a** by coupling reactions of **1a** (Table 3.2). To further expand the library of C3-analogs, Ms. Liu used similar reaction conditions as Dr. Ghavami to obtain analogs **20a-22a** (Table 3.2).²⁰

Table 3.2 Bioisosteres synthesized from **1a** by Dr. Ghavami and Ms. Liu.^{19, 20}

1a \longrightarrow **16a-22a**

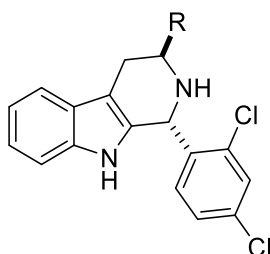
	R	R'	coupling agent	reagent	base	solvent	yield
16a	OH	H	T ₃ P	NH ₂ OH·HCl	NMM	DMF/CH ₃ CN	46%
17a	OMe	H	HATU	NHOMe·HCl	DIPEA	DMF	84%
18a	OMe	Me	HATU	NMeOMe·HCl	DIPEA	DMF	64%
19a	CH ₂ SO ₃ H	H	T ₃ P	NH ₂ CH ₂ SO ₃ H	DIPEA	DMF	15%
20a	SO ₂ Me	H	HBTU	NHSO ₂ Me	Et ₃ N	DMF	63%
21a	(CH ₂) ₂ CN	H	HBTU	NH ₂ (CH ₂) ₂ CN	DIPEA	DMF	63%
22a			HBTU	HCl·HN	DIPEA	DMF	83%

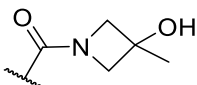
T₃P = propylphosphonic anhydride

Growth inhibition potency of compounds **16a-22a** against the Dd2 strain of *P. falciparum* was analyzed in the laboratory of Dr. Cassera. The methoxyamide **17a** showed promising growth inhibition, as well as inhibition of isolated *Pf*lspD (117 ± 44 nM), and was selected for further studies of its D-ring analogs.¹⁹ Unfortunately, the biological data for methoxyamides **17a** and D-ring analogs showed highly inconsistent results depending on the length of the compound's storage

prior to the testing. The stability of **17a** in mouse plasma was determined to be very low ($t_{1/2} \sim 8$ min, Pharmaron), suggesting that the methoxyamide structure was not suitable for in vivo administration. In contrast, acid **1a** and methyl amide **9a** are quite stable in mouse plasma (no loss of parent over 2 h, Pharmaron). Thus, the methoxyamide derivatives were abandoned (Table 3.3).^{19,20}

Table 3.3 *P. falciparum* growth inhibition of compounds **16a-22a**.^{19,20}



Compound	R	<i>P. falciparum</i> Dd2 strain growth inhibition IC ₅₀ (nM)
16a	CONHOH	2050 ± 360
17a	CONHOMe	540 ± 30
18a	CONMeOMe	~ 4200
19a	CONHCH ₂ SO ₃ H	> 10,000
20a	CONHSO ₂ Me	3000 – 5000 ± 1000
21a	CONH(CH ₂) ₂ CN	> 5000
22a		> 5000

The groups present in non-active analogs **18a-22a**, similarly to inactive secondary amides listed above, are also likely too bulky to be accommodated by the carboxylate binding site of *Pf*IspD. The decreased potency of **16a** compared to **17a**, similarly to **8a** and **9a**, cannot be explained based on the size as inactive **16a** is sterically comparable to active **9a**, while potent **17a** is larger than either **9a** or **1a** (Figure 3.4). Moreover, both **16a** and **17a** are expected to lack the negative charge present in **1a** at physiological pH, resulting in overall neutral or positively charged species. It is likely that, to a certain extent, the increase in the bulk of the C3 substituent can be

compensated by an increase in the lipophilicity of the molecule. Lastly, potentially poor chemical stability of **16a**, similar to **17a**, could lead to the observed decrease in potency.

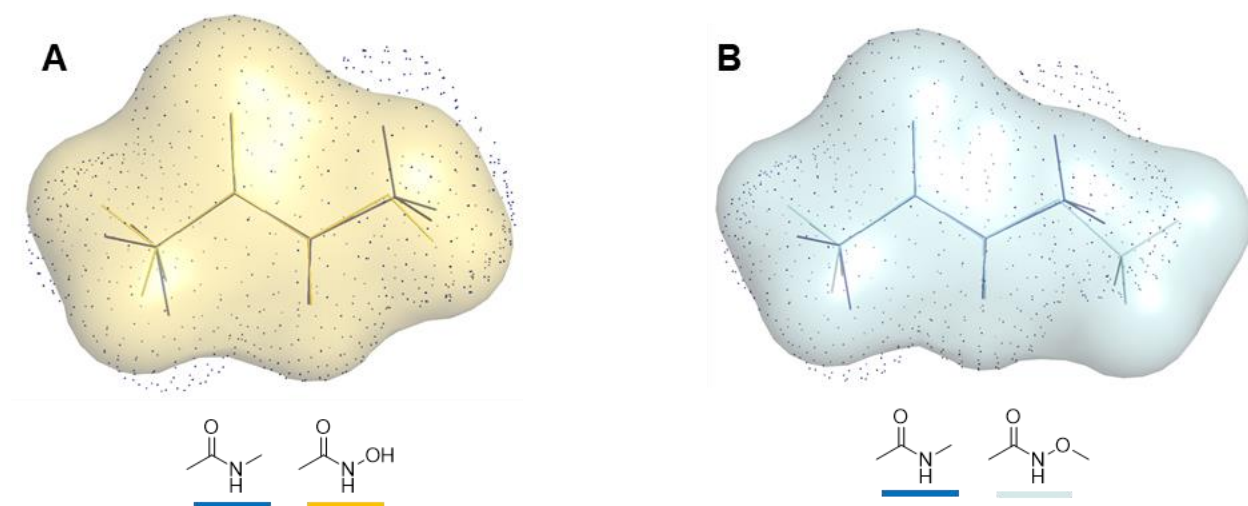


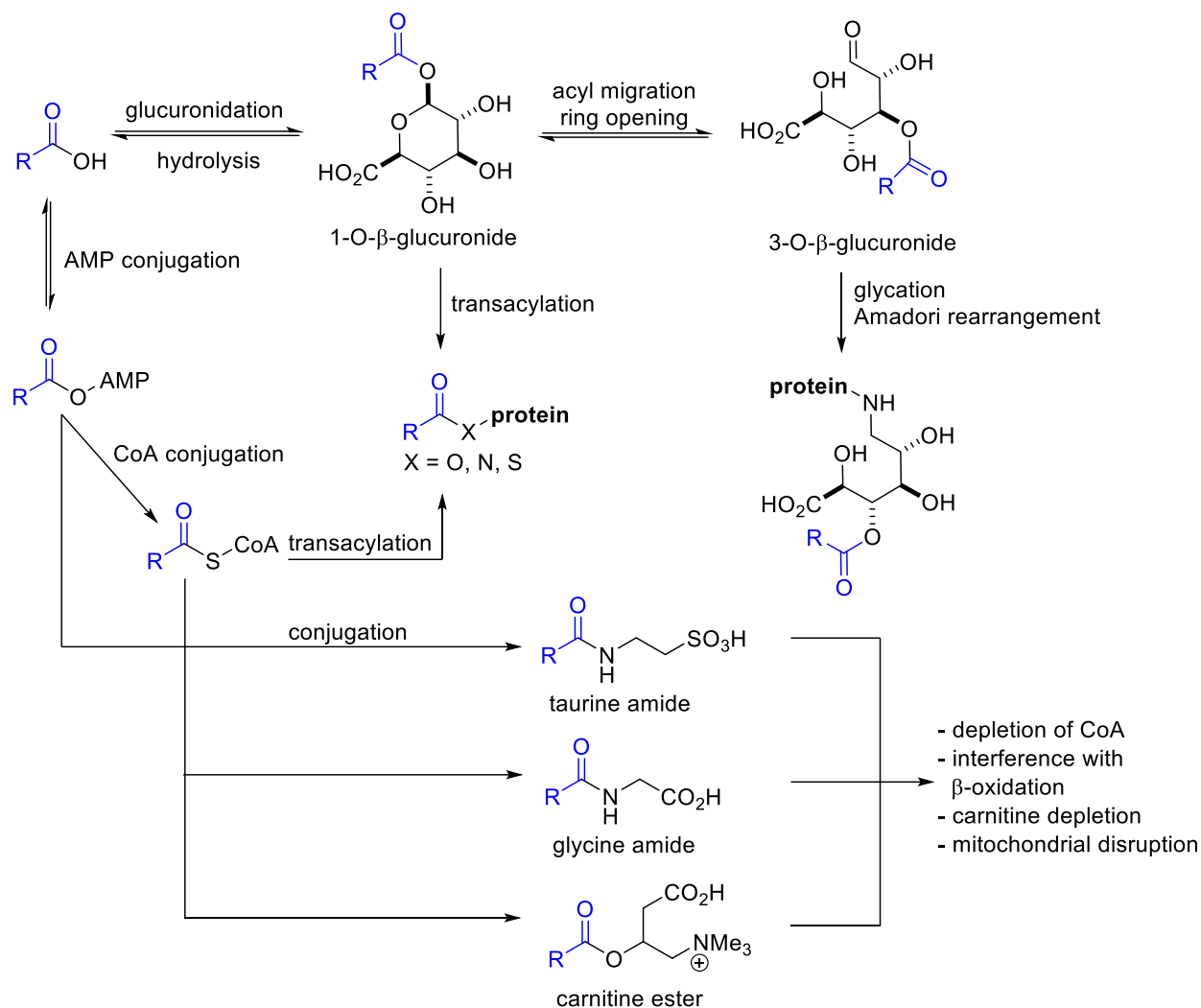
Figure 3.4 Structural comparison of C3-substituents in analogs **16a** and **17a** with potent **9a**. **A**) Alignment of methylamide group in potent analog **9a** (blue) with inactive hydroxamic acid present in **16a** (yellow). **B**) Alignment of methylamide group in potent analog **9a** (blue) with potent methoxyamide found in **17a** (cyan). Structures were generated by B3LYP/6-31G (gas phase) geometry optimization in Gaussian and visualized in PyMOL.

3.2 The usefulness of carboxylic isosteres and their possible application to MMV008138

The evaluation of the antimalarial activity of compounds **6a-22a** revealed some valuable information for further structure-activity relationship studies of MMV008138. As mentioned in the beginning of this chapter, the carboxylic acid functionality can be a source of both beneficial and detrimental characteristics to a potential drug candidate. Some of the MMV008138's problems likely related to the carboxylic acid moiety are the previously mentioned disconnect between growth and enzyme inhibition potency (250 ± 70 nM and 44 ± 15 nM, respectively),²¹ lack of oral efficacy in *P. berghei* infected mice, and poor metabolic stability (half-life of 14.5 min as determined in mouse liver microsomes by Pharmaron).¹⁹

In addition to the issues observed in MMV008138 mentioned above, carboxylic acid-containing drugs also suffer from toxicity resulting from the formation of acyl glucuronides and

coenzyme A (CoA) conjugates in phase II of metabolism (Scheme 3.1).²² The phase II metabolism converts a xenobiotic compound to water-soluble species, which can then be excreted either in urine or bile. These conjugation metabolites are in many cases highly electrophilic, and to avoid harmful reactivity, glucuronidation or conjugation with CoA is usually followed by conjugation to glutathione, a highly nucleophilic scavenger molecule located predominantly in liver and kidney tissue.²³ If, however, the phase II metabolites are not intercepted by glutathione, they can react with other cellular metabolites, such as proteins or DNA, leading to potentially toxic outcomes.²² It should be noted that while hydroxamic acids are sometimes used in lieu of a carboxylic acid group, they suffer the same metabolic fate as carboxylic acids.¹



Scheme 3.1 Phase II metabolism of carboxylic acids might lead to a toxic effect on the organism. AMP = adenosine monophosphate, CoA = coenzyme A. Scheme modified based on Lassila et al.²²

Replacement of a carboxylic acid with another functional group mimicking some of its characteristics can improve the potency, selectivity, bioavailability, and/or toxicological profile of the drug. Such surrogate groups are commonly called bioisosteres (or just isosteres). A few representative examples of successful bioisosteric substitution are shown in Figure 3.5.

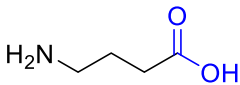
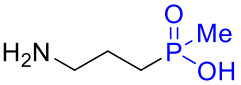
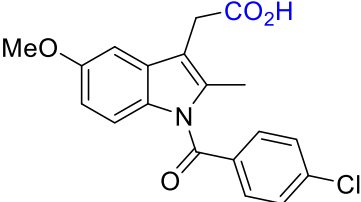
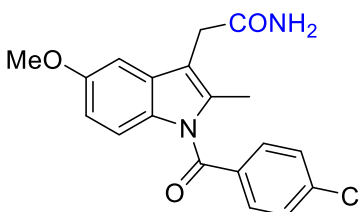
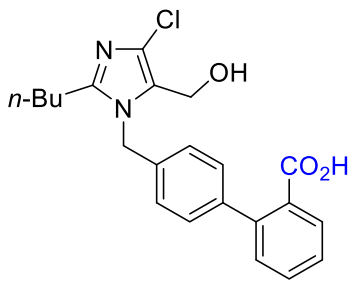
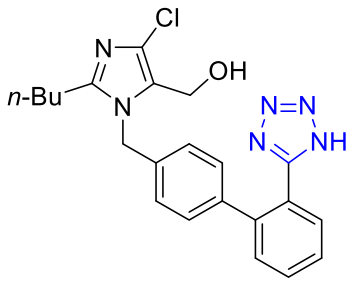
Parent compound	Bioisostere
 <p>γ-aminobutyric acid non-selective GABA agonist</p>	 <p>increased potency increased selectivity for GABA_A over GABA_B receptor</p>
 <p>indomethacin non-selective COX inhibitor ulcerogenic</p>	 <p>selective COX-2 inhibitor non-ulcerogenic</p>
 <p>angiotensin II antagonist IC₅₀ = 230 nM oral EC₃₀ = 11 mg/kg</p>	 <p>Losartan angiotensin II antagonist IC₅₀ = 20 nM oral EC₃₀ = 0.6 mg/kg</p>

Figure 3.5 Examples of improved pharmacokinetic properties of selected carboxylic acid bioisosteres.^{1, 24, 25}

Langmuir originally defined isosteres as compounds or groups that contain the same number and arrangement of atoms.²⁶ This definition was later expanded to its current version, according to which isosteres are understood as groups of similar size and physical properties. In the context of medicinal chemistry, the isostere definition can be further expanded to compounds that share similar biological activity. Such compounds are then called bioisosteres.²⁷ Bioisosteres were initially formally defined by Friedman as structurally similar compounds with similar or antagonistic biological properties. Later, Thornber formulated a more flexible definition of

bioisosteres as “*groups or molecules which have chemical and physical similarities producing broadly similar biological properties*”.²⁸ This work will follow Thornber’s definition when discussing carboxylic acid bioisosteres because, despite the lack of structural and/or chemical similarity, reasonable assumptions of biological likeliness were made based on existing literature and good steric alignment with potent analogs previously developed in the Carrier group. With the hope to solve at least one of the aforementioned issues of MMV008138, we have turned our attention to more structurally diverse analogs of carboxylic acids. The rest of this chapter will specifically focus on synthesis of tetrazolic and phosphonic acid bioisosteres of **1a**.

A tetrazolic acid is a popular surrogate for carboxylic acid, which matches in acidity (pK_a of tetrazole $\sim 4.5 - 4.9$ vs. pK_a of carboxylic acid $\sim 4 - 5$), planarity, and size (*2H*-tetrazole is about 1 Å larger).^{1, 25} On the other hand, the resonance-stabilized negative charge is distributed over a larger area which may either facilitate or hinder interaction with the target based on the structure of the active site.²⁵ The tetrazole ring is also reported to be significantly more lipophilic than a carboxylic acid group (Figure 3.6), which often improves biological membrane permeability of tetrazole-bearing compounds.^{1, 25} However, the exact effect of the substitution is hard to predict simply based on calculated physical properties. For example, Lassalas *et al.* determined using Parallel Artificial Membrane Permeability Assay (PAMPA) for a series of carboxylic acid bioisosteres that the tetrazole substituted analog was less permeable, despite being more lipophilic.²⁹

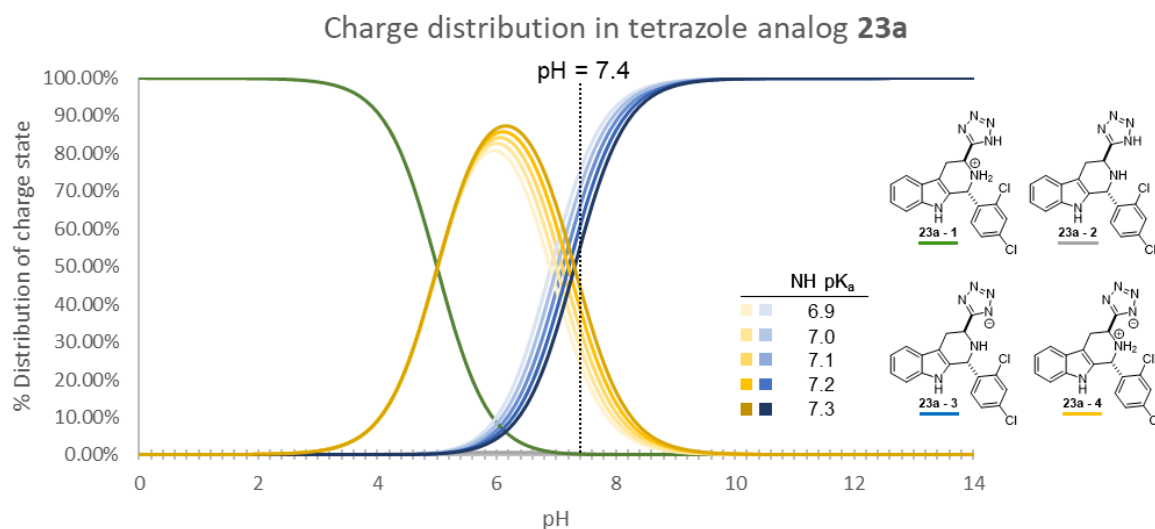
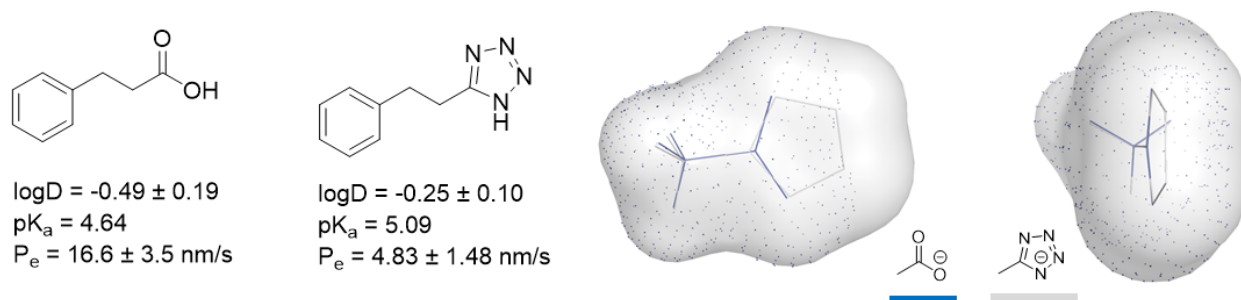


Figure 3.6 Comparison of physical properties and structural alignment of the carboxylic acid group (present in our lead compound **1a**) and tetrazole ring, present in proposed analog **23a**. Data for phenylpropionic acid and its tetrazole analog were experimentally obtained by Lassalas *et al.*²⁹ LogD values were determined at $pH = 7.4$. Charge distribution in proposed analog **23a** is calculated using the Henderson-Hasselbalch equation. While the pK_a of tetrazole is expected in the range of 4.5 – 5.0 and the moiety is expected to be negatively charged at physiological pH, the data are shown only for the upper limit of the range ($pK_a = 5.0$). The pK_a value of secondary amine is estimated in the same way as for previously discussed compound **1a** and shown as a range of $pK_a = 7.1 \pm 0.2$. Structures of acetate and deprotonated methyl tetrazole were generated via B3LYP/6-31G (gas phase) geometry optimization in Gaussian and visualized in PyMOL.

When metabolized, tetrazole is susceptible to glucuronidation, similarly to the metabolism of carboxylic acids depicted in Scheme 3.1 (*vide supra*). However, the *N*-glucuronides formed from tetrazole are less reactive than *O*-glucuronides and thus do not suffer from comparable *in vivo* toxicity.¹ In fact, glucuronidation of the tetrazole group is suspected to be responsible for a long half-life common to a number of tetrazole-containing drugs administered orally.²⁵ In the proposed enterohepatic recirculation mechanism, the tetrazole *N*-glucuronide is reabsorbed in the

intestines and hydrolyzed by local microflora back to the parent drug, which can then re-enter the liver in the second pass of metabolism (Figure 3.7).²⁵ Increased metabolic stability possibly offered by the tetrazole surrogate would greatly benefit our attempts to improve the lead compound **1a** (half-life = 14.5 min). However, it is unclear how the metabolic clearance might be affected by other functional groups present in the structure.

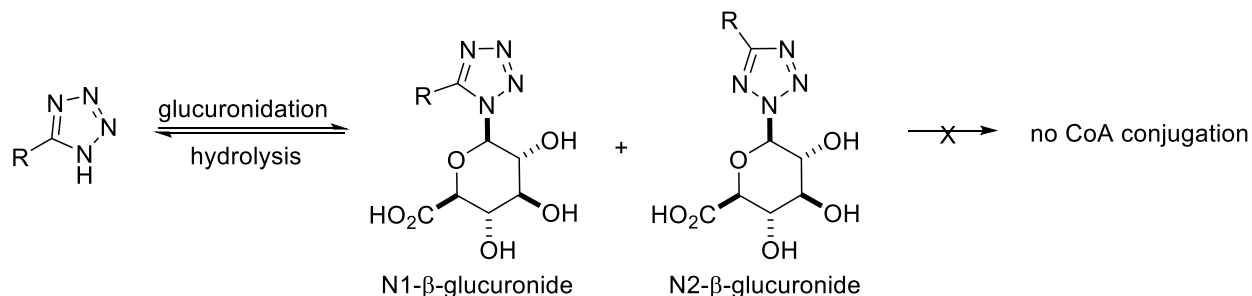


Figure 3.7 Metabolic products of tetrazolic acid glucuronidation do not progress to form toxic conjugates known in the metabolism of carboxylic acids. The tetrazole N-glucuronides are either excreted in urine or can get hydrolyzed back to the parent drug and undergo a second pass of the liver, prolonging the effective half-life of the drug.²⁵

The phosphonic acid bioisostere of the carboxylic acid is not as widely used as the tetrazolic acid one; however, it presents an intriguing possibility of modifying our lead compound **1a**. In fact, the phosphonic acid group is larger than the carboxylic acid and adopts tetrahedral rather than planar geometry. Phosphonic acids are also more acidic than carboxylic acids ($pK_{a1} \sim 0-2$ and $pK_{a2} \sim 5-8$).^{29, 30} The α -aminophosphonic acids are typically more acidic than aliphatic phosphonic acids, and thus we expect the phosphonate to be fully deprotonated at physiological pH (Figure 3.8).^{31, 32} Furthermore, we expect the pK_a of the protonated amine in (\pm)-**62a** to be higher than in **1a** by approximately 1 log unit (cf. **V** and **VI**, pK_a ((\pm)-**62a**) ~ 8.1 vs. pK_a (**1a**) ~ 7.1).³¹ The range of decreased acidity of protonated amine in α -aminophosphonic acids can be seen in the specific example of glycine and aminomethylphosphonic acid (**IV**, $\Delta pK_a \sim 0.2$) and glyphosate (**III**) and its dicarboxylic acid counterpart, iminodiacetic acid ($\Delta pK_a \sim 1.9$).³³⁻³⁵ Thus, the proposed analog (\pm)-**62a** is expected to exist predominantly in the form of species (\pm)-**62a-3**,

as depicted in Figure 3.8. Even though (\pm)-**62a** is expected to be less lipophilic than **1a**, the formal charge of -1 might mimic the dominant anionic form of **1a** at pH = 7.4.

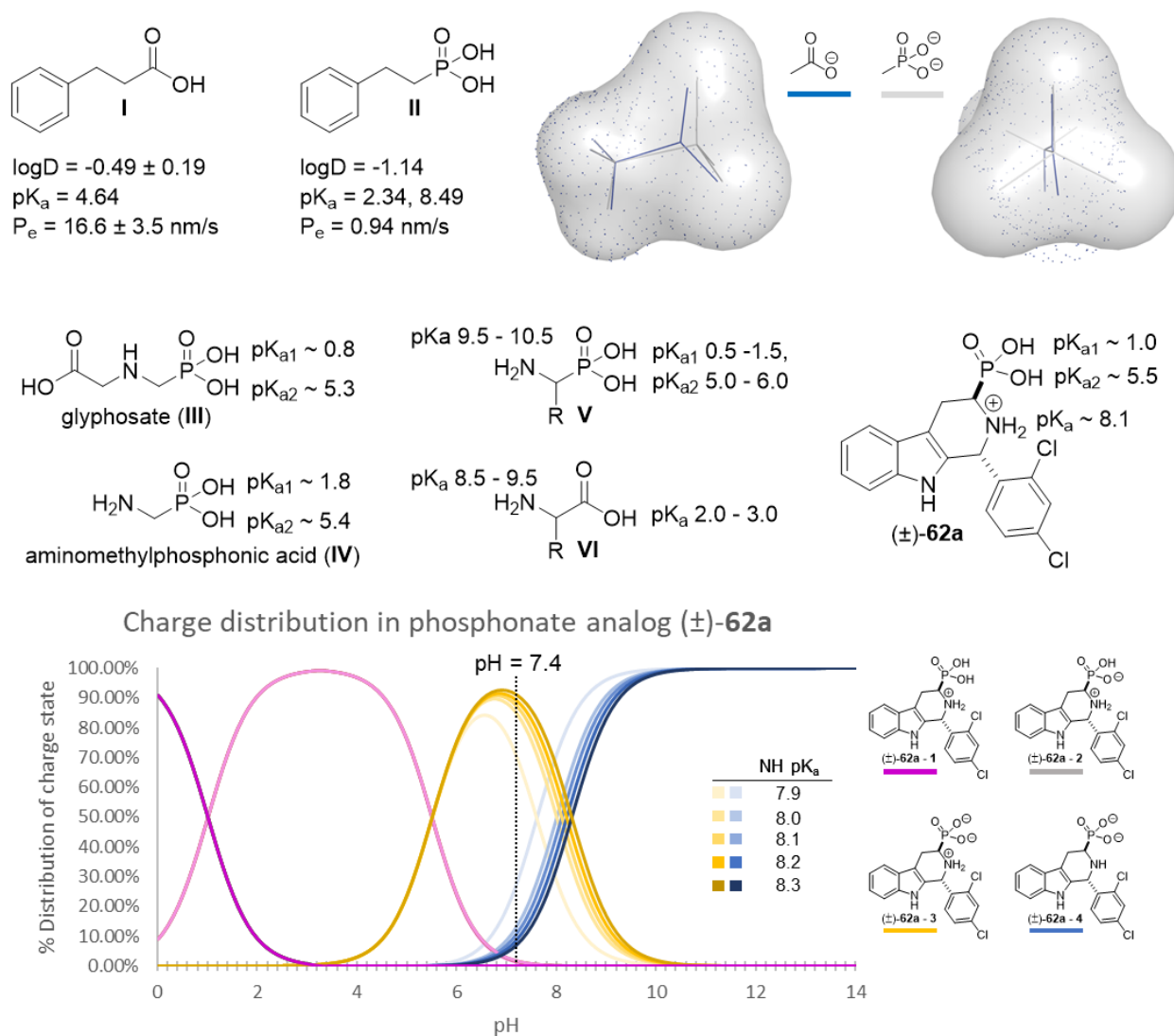


Figure 3.8 Comparison of physical properties and structural alignment of the carboxylic acid group (present in our lead compound **1a**) and phosphonic acid, present in proposed analog (\pm)-**62a**. Data for phenylpropionic acid and its phosphonic acid analog were experimentally obtained by Lassalas *et al.*²⁹ LogD values are determined for pH = 7.4. The expected pK_a values for α -aminophosphonic acids are presented on examples of glyphosate and aminomethylphosphonic acid.³⁴ Comparison of pK_a estimates in general structures of α -aminophosphonic acid and α -aminocarboxylic acid³¹ led to the conclusion that the pK_a of amine in (\pm)-**62a** can be expected on average about 1 log unit higher than in parent compound **1a**. The charge distribution in the proposed analog (\pm)-**62a** is calculated using the Henderson-Hasselbalch equation. The pK_a value of secondary amine is depicted as a range of pK_a = 8.1 ± 0.2 . Structures of acetate and deprotonated methyl tetrazole were generated via B3LYP/6-31G (gas phase) geometry optimization in Gaussian and visualized in PyMOL.

However, not only is the structure of the *PfIspD* active site unknown, and therefore improved interaction with phosphonic rather than carboxylic acid might be a possibility, but also the native substrates of IspD – CTP and MEP, both contain phosphate groups that are being accommodated for in the active site. Moreover, unlike our lead compound **1a**, all substrates of the MEP pathway are negatively charged at physiological pH. Lastly, compounds known to target the *PfIspC* enzyme of *P. falciparum*'s MEP pathway, such as fosmidomycin, contain a phosphonic acid moiety (Figure 3.9).^{21, 36}

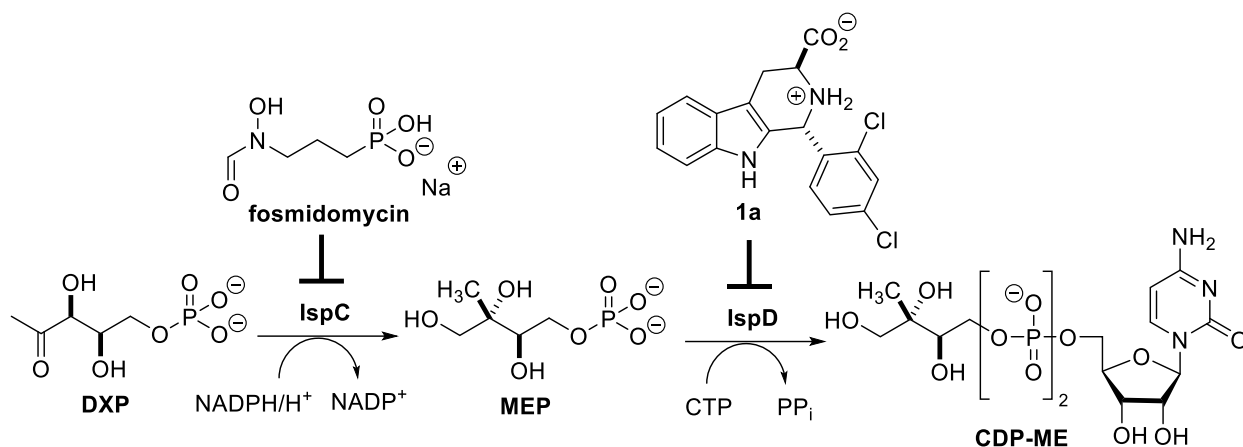


Figure 3.9 Steps of MEP pathway catalyzed by IspC (reductoisomerase) and IspD (cytidyltransferase) enzymes. Phosphonic acid-containing fosmidomycin is a substrate inhibitor of IspC, mimicking 1-deoxy-D-xylulose-5-phosphate (DXP). While neither 2-C-Methyl-D-erythritol 4-phosphate (MEP) nor cytidine triphosphate (CTP) shares structural similarity to the active enantiomer of MMV008138 (**1a**), the **1a** acts as a CTP-competitive inhibitor of IspD. The lack of structural similarity with native substrates suggests that **1a** is likely an allosteric competitive inhibitor of *PfIspD*.

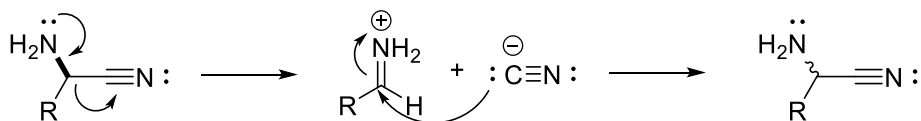
3.3 Synthesis of the enantiopure *trans*-tetrazole analog

The preliminary work towards the synthesis of the tetrazole analog (**23a**) was performed by Mr. Parth Vaghani (undergraduate researcher) under the supervision of Dr. Ghavami. First, Mr. Vaghani prepared the unprotected tetrazole analog of tryptophan (**29**) which then provided an inseparable mixture of *cis*-/*trans*- diastereomers of **23a**. Later, Ms. Liu took over the project and synthesized product **23a** as a mixture of diastereomers from cyanoethyl-protected tetrazole analog

of tryptophan (**33**).²⁰ The final product was isolated and purified via HPLC by Dr. Ghavami; however, isolation of pure *trans* diastereomer was not successful, and the antimalarial activity of **23a** was evaluated from a mixture.¹⁹ The growth inhibition potency of 1250 – 2500 nM, coupled with a lack of certainty on the identification of the predominant stereoisomer, motivated me to prepare diastereomerically pure *trans*-**23a** by another route. My successful completion of this goal is discussed in this chapter.

3.3.1 Approaches to the tetrazole analog by previous group members

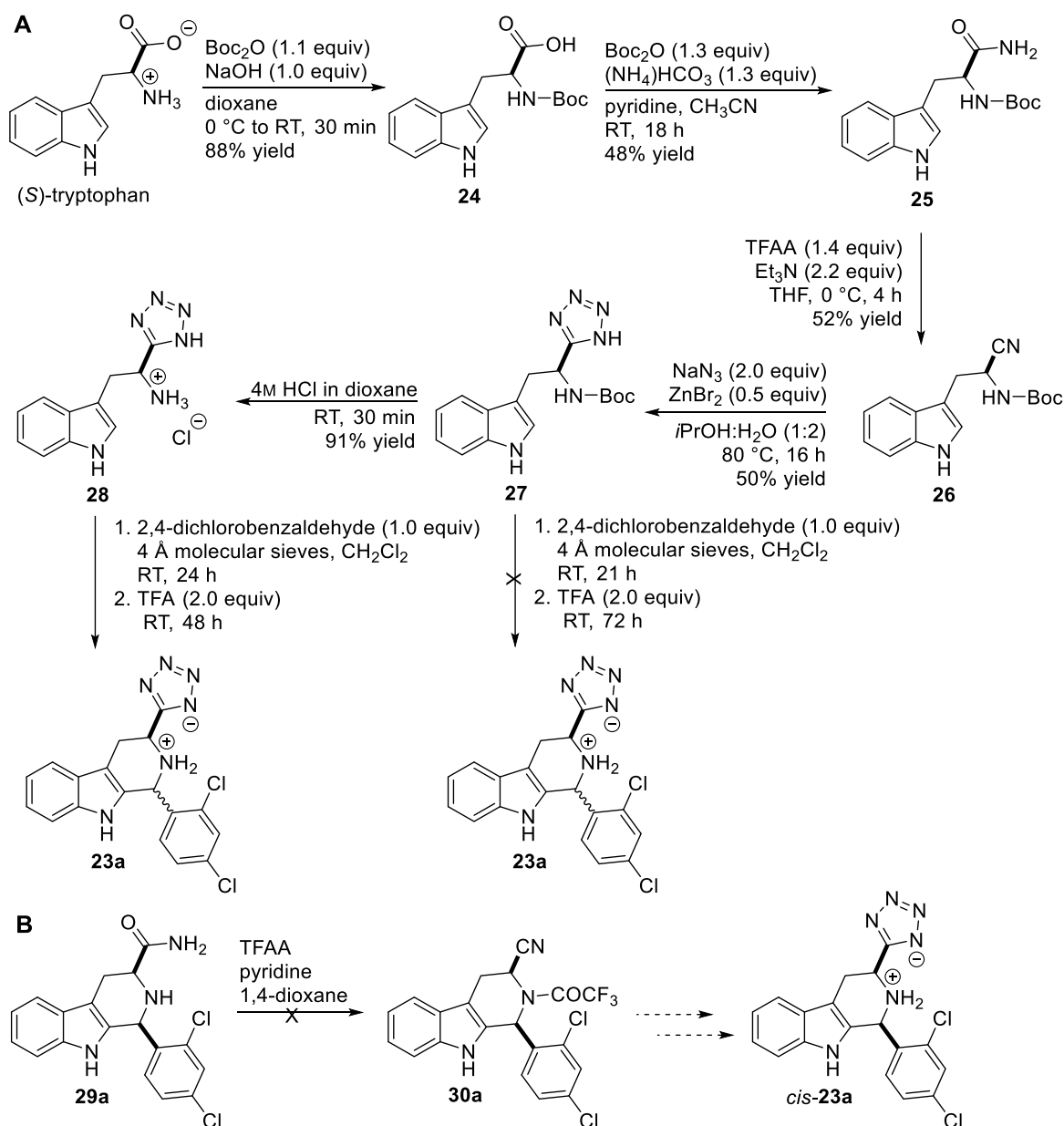
Unlike previous C3-derivatives of **1a**, the tetrazole ring cannot be introduced either to **1a** or **4a** by a simple coupling reaction. Instead, the most common method for tetrazole preparation is based on the reaction of a nitrile group with an azide, usually at a high temperature.²⁵ Unfortunately, direct synthesis of **23a** from the nitrile analog of **1a** would not be possible due to the instability of α -amino nitriles, which can be easily racemized via iminium ions, even under mild conditions (Scheme 3.2).³⁷ The formation of imine can be avoided by protecting the amine as an amide or carbamate.



Scheme 3.2 Racemization of α -amino nitriles.

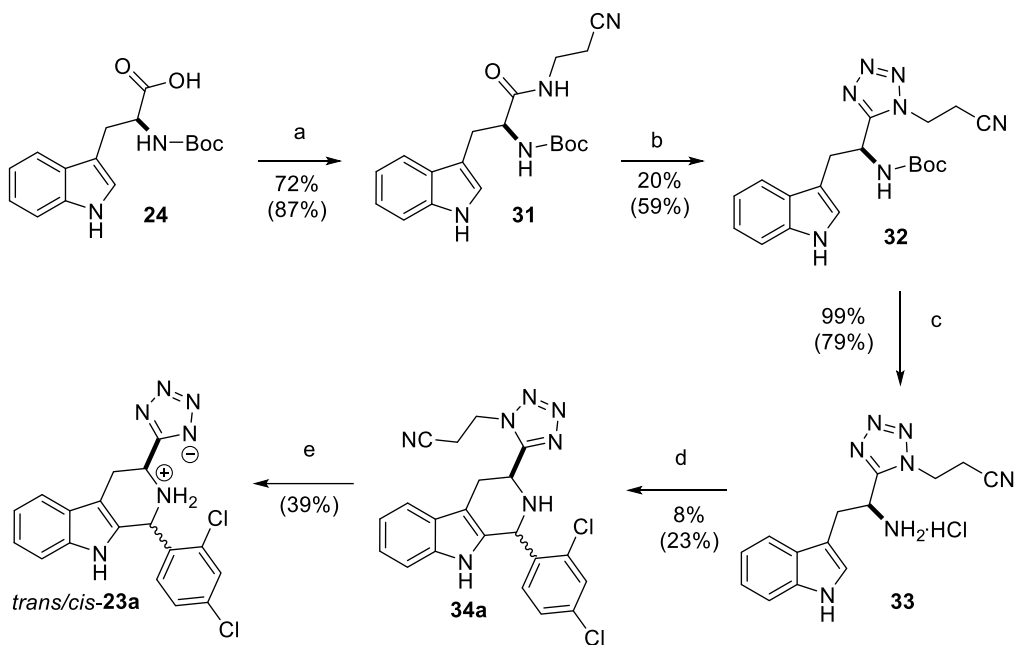
Mr. Vaghani successfully synthesized the tetrazole analog of tryptophan (**28**) from *N*-Boc protected tryptophan (**24**). Compound **28** was then reacted with 2,4-dichlorobenzaldehyde to afford a diastereomeric mixture of *cis*-/*trans*-**23a**, which proved to be inseparable by conventional chromatography techniques (Scheme 3.3A). Concurrently, Dr. Ghavami attempted to synthesize enantiopure *cis*-**23a** by simultaneous dehydration and N2-protection of **29a**. She envisioned following the formation of protected nitrile by reaction with azide analogously to the preparation

of **27**. Unfortunately, the trifluoroacetamide-protected **30a** was not obtained, even though a similar reaction was previously reported in a closely related substrate (Scheme 3.3B).^{19, 38}



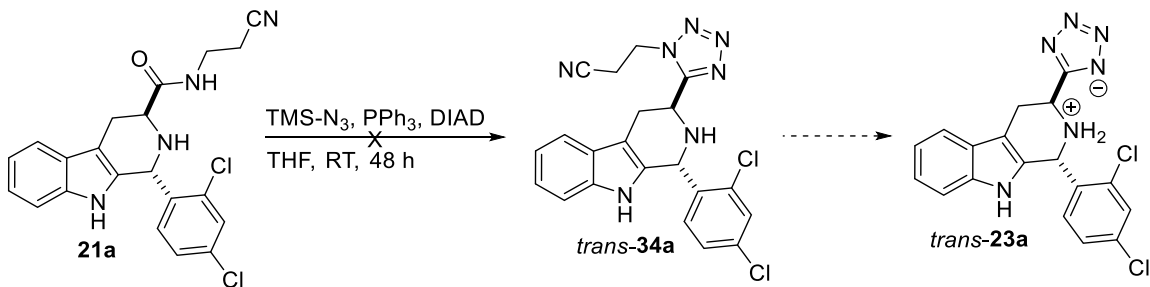
Scheme 3.3 First attempts of tetrazole bioisostere synthesis. **A**) Synthesis of unprotected tetrazole analog of tryptophan (**28**) and subsequent Pictet-Spengler reaction to form *cis-trans*-**23a** performed by Mr. Vaghani. It should be noted that the *N*-Boc protected **27** did not afford desired product in the Pictet-Spengler reaction, and only starting material was recovered. **B**) Attempt of stereoselective synthesis of *cis*-**23a** from amide **29a** via nitrile intermediate **30a** performed by Dr. Ghavami. This scouting reaction was attempted from **29a** (*cis*) rather than **8a** (*trans*) for reasons of convenience.¹⁹

Ms. Liu, who took over the project later, aspired to obtain *trans*-**23a** by hydrolysis of cyanoethyl-protected tetrazole analog (**34a**), which was expected to be more easily purifiable. The procedure was inspired by a synthesis of cyanoethyl-protected tetrazole developed by Duncia *et al.* (Scheme 3.4).³⁹ Starting from enantiopure *N*-Boc protected (*S*)-tryptophan (**24**), a modified Mitsunobu reaction was employed to generate the *N*-2-cyanoethyltetrazole analog of (*S*)-tryptophan (**32**).³⁹ After removal of the protecting group, compound **33** was reacted under standard Pictet-Spengler conditions to generate a mixture of *cis*- and *trans*-TH β Cs (**34a**). However, despite all our efforts, the diastereomers could not be separated by column chromatography. The diastereomeric mixture was then converted to tetrazole analogs (*trans/cis*-**23a**) by the removal of the cyanoethyl protecting group under basic conditions (Scheme 3.4).²⁰ Dr. Ghavami purified *trans/cis*-**23a** via HPLC but could not obtain a pure sample of the *trans*-diastereomer **23a**, and a mixture of *cis*- and *trans*-diastereomers (estimated to be 3:7 *cis*-: *trans*-) was eventually submitted for growth inhibition assay.



Scheme 3.4 Synthesis of cyanoethyl-tetrazole analog **34a** with use of modified Mitsunobu reaction. Ms. Liu obtained yields in parentheses; yields in the plain text were obtained by me. Reagents and conditions: a) $\text{H}_2\text{N}(\text{CH}_2)_2\text{CN}$, DCC, HOBt, DMF, RT, 50 h, b) TMS- N_3 , PPh_3 , DIAD, THF, RT, 48 h, c) 4M HCl in 1,4-dioxane (79% yield) or 1M HCl in EtOAc (99% yield), d) i: 2,4-dichlorobenzaldehyde, 4 Å molecular sieves, CH_2Cl_2 , RT, 24 h, ii: TFA, RT, 48 h, e) i: NaOH, THF, MeOH, RT, 12 h, ii: Amberlyst A26, THF, MeOH, H_2O , RT, 12 h.

Ms. Liu also attempted to apply conditions shown in Scheme 3.4 (step b) to enantiopure **21a** in order to isolate pure *trans*-**34a**. Unfortunately, the reaction did not proceed, and only starting material **21a** was recovered (Scheme 3.5).²⁰



Scheme 3.5 Attempted synthesis of *trans*-**23a** directly from **21a** by Ms. Liu.²⁰

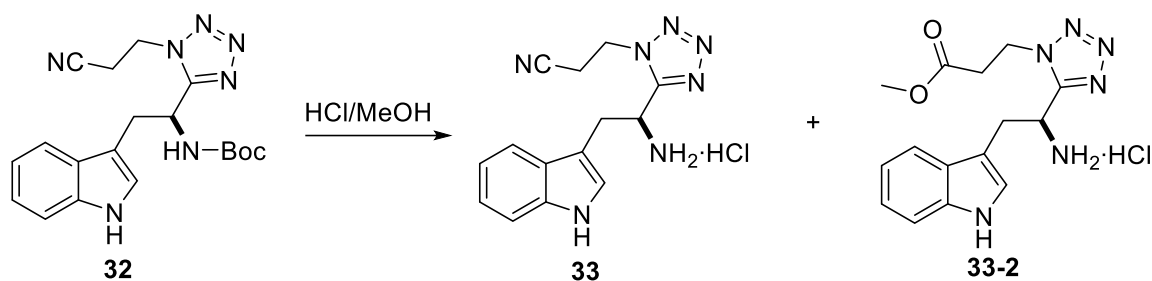
With Ms. Liu's work as the foundation, I began preparing a diastereomerically and enantiomerically pure form of the tetrazole **34a**. Initially, my strategy was to retain the tetrazole protecting group and make additional attempts to isolate pure (1*R*,3*S*)-**34a** before deprotection

rather than purifying mixture of diastereomeric tetrazoles **23a** by HPLC, as was done previously by Dr. Ghavami. Unfortunately, none of the attempted chromatography methods were successful.

Additionally, several problematic aspects of the procedure depicted in Scheme 3.4 should be noted. First, even though the Mitsunobu reaction successfully generates compound **32**, the yield is low in comparison with literature precedence (23% vs. 58% after deprotection of the cyanoethyl group reported by Duncia *et al.*).^{20, 39} The main reason for the poor yield of the Mitsunobu reaction is troublesome removal of triphenylphosphine oxide byproduct, which cannot be precipitated from non-polar solvent due to high polarity of compound **32** itself, and because it at least partially co-elutes with the desired product during column purification. Consequently, multiple consecutive column purifications were necessary to obtain intermediate **32** in acceptable purity, rendering the isolation both uneconomical and unecological.

The deprotection of the Boc group to intermediate **33** was found to be highly dependent on freshness and solvent type of HCl solution. A freshly prepared saturated solution of hydrochloric acid in anhydrous ethyl acetate or a newly opened bottle of commercially available 1M HCl in ethyl acetate gave the best results with regards to yield, purity, and reaction time. Solution of 4M HCl in 1,4-dioxane was originally used by Ms. Liu, but to our surprise, removing the solvent from the product in vacuo proved challenging. When the removal of the Boc group was attempted in a freshly prepared saturated solution of HCl in anhydrous methanol, a significant formation of a side product **33-2** was observed (Scheme 3.6). The by-product **33-2** arose from the Pinner reaction between the nitrile and methanol, resulting in a methyl acrylate-protected tetrazole side product. Upon retrospective evaluation of NMR data of **33** previously synthesized by both Ms. Liu and me, impurity **33-2** was found in the majority of them, suggesting that the nitrile group in compound **33**

is particularly labile and reacts readily with methanol even after short contact (e.g., when methanol was used to dissolve and transfer material between containers).



Scheme 3.6 Removal of Boc protecting group from **32** and formation of by-product **33-2** in contact with methanol .

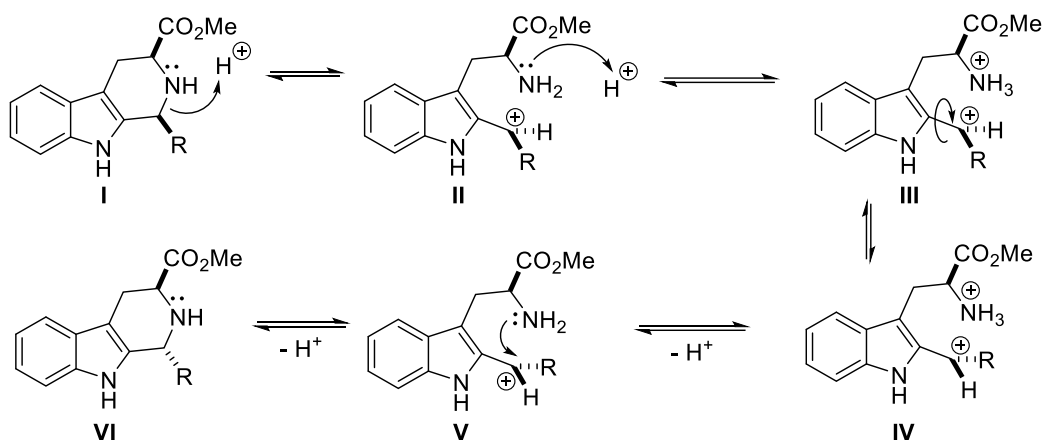
Lastly, the yield of the Pictet-Spengler reaction is lower than was observed for methyl ester analogs (Ms. Liu was able to isolate 23% of the mixture **34a**,²⁰ while I only obtained 8% in the same procedure). Furthermore, the *cis*- and *trans*- products **34a** exhibit poor solubility, complicating the purification attempts. The inability to separate mixture **34a** by conventional methods and the aforementioned concerns pertaining to the synthetic method led to the development of a procedure that would selectively generate the *trans* diastereomer of **23a**.

3.3.2 An attempt of stereoselective synthesis using N-allyl substitution

Many publications in past decades discussed the topic of stereoselective Pictet-Spengler reaction; however, most of these methods focus on the preparation of the *cis* diastereomer.⁴⁰⁻⁴⁴ A selective synthesis of either *cis*- or *trans*-TH β C diastereomer in one step can be achieved via the crystallization-induced asymmetric transformation method (CIAT).^{45, 46} Unfortunately, the stereochemistry of the product generated by the CIAT method depends on solubility difference within the diastereomeric pair, and thus, the outcome cannot be easily predicted.

The Pictet-Spengler reaction of tryptophan esters typically has a mild preference for the *cis*-1,3-disubstituted- TH β C (2:1 – 3:1 ratio to the *trans*- diastereomer). In the presence of an acid, the equilibrium between *cis*- and *trans*- diastereomers can be achieved via C1-N2 bond cleavage

(Scheme 3.7, structure **II**), followed by C9a-C1 bond rotation (Scheme 3.7, structures **III** and **IV**), and ring closure (Scheme 3.7, structure **V**). The mild preference for *cis*- diastereomer under thermodynamic conditions can be explained by the fact that the *cis*- isomer features 1,3-dipseudoequatorial substitution, while the *trans*- isomer must feature one pseudo-axial substituent. In 1979, the Cook Group presented a method for the stereoselective synthesis of *trans*-1,3-disubstituted-TH β Cs, which relied on the introduction of a sterically large substituent on the N2 position to form 1,3-*trans*-1,2,3-trisubstituted-TH β C, followed by deprotection of benzyl substituent.^{47, 48} Multiple publications showed the stereoselective formation of 1,3-*trans*-1,2,3-trisubstituted-TH β Cs from Pictet-Spengler reaction of NH-Bn protected tryptophan methyl ester with an aldehyde under both kinetic and thermodynamic control.⁴⁹⁻⁵²



Scheme 3.7 Mechanism of acid-catalyzed TH β C epimerization. Formation of dication intermediate is supported by kinetic studies reported by van Linn *et al.*⁵³

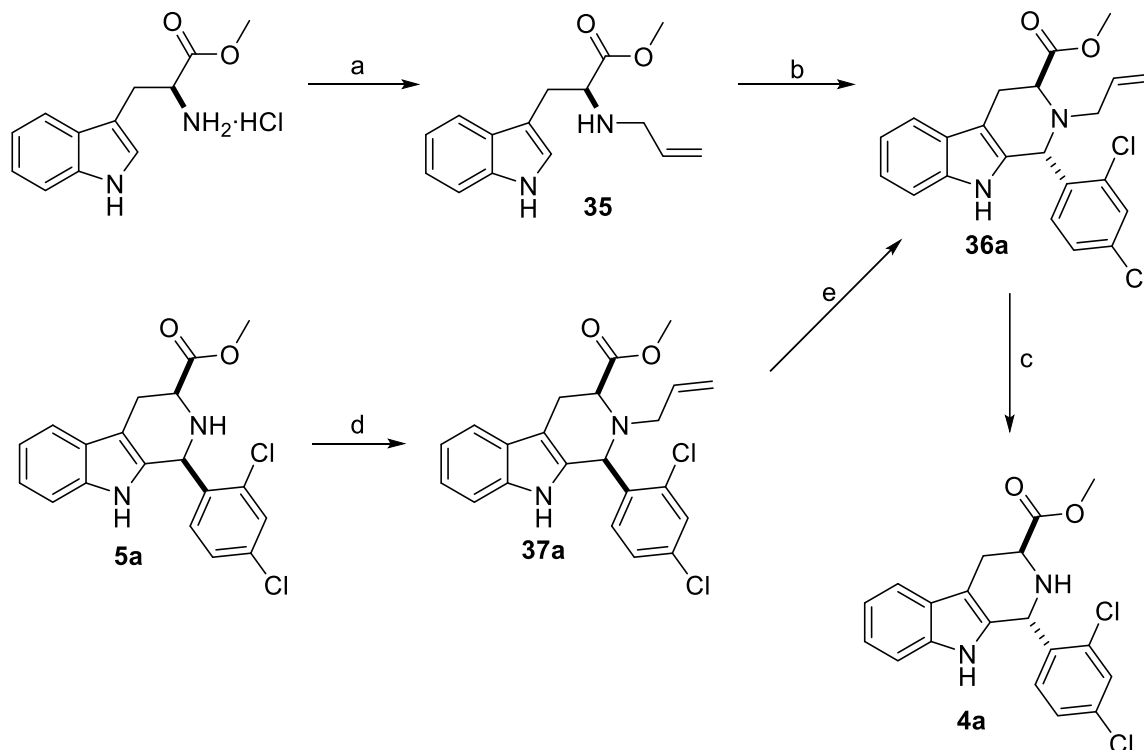
Whereas the rationale for high kinetic selectivity for the *trans*-diastereomer is not fully clear, the rationale for the high thermodynamic selectivity can be explained by examination of X-ray structures.⁵⁰ Interestingly, the presence of an N2-substituent forces the C1-substituent to be pseudoaxial in both *cis*- and *trans*-diastereomers. Thus, for *cis*-diastereomers, the N2-substitution causes both the C1 and C3 substituents to be axial, creating a destabilizing 1,3-diaxial interaction.

However, for *trans*-diastereomers, the axial orientation of the C1-substituent places the C3-substituent in a pseudoequatorial position. Therefore, in the case of N2-substitution, the *trans*-diastereomer is considerably more stable than the *cis*-diastereomer. Why the N2-substituent drives a C1-substituent to favor axial orientation is not known. Bailey wrote, “*It is difficult to find a convincing argument to explain the dramatic effect of the benzyl substituent, particularly as it appears to have little axial/equatorial preference itself.*” However, the effects are clear: “*But the general rule is clear: an N(2)-benzyl substituent strongly favours the 1-substituent being axial, and 1,3-diaxial interactions favour 3-substituents being equatorial and thus trans.*”⁵⁰

Since *cis*-/*trans* Pictet-Spengler adducts can equilibrate in acidic conditions via reversible C1-N2 cleavage, the N2-substituted *trans*-Pictet Spengler adducts can be obtained in good yield. Alternatively, the N2-H *cis*-TH β C diastereomer can be isolated, alkylated at the N2 position, and converted into the *trans* diastereomer via treatment by dilute acid.⁵³

Unfortunately, the benzyl protecting group cannot be applied to the analogs of **1a** due to the presence of chlorine substitution in the D-ring. The catalytic hydrogenation used to remove the benzyl group also competitively cleaves chlorines from the molecule (hydrodehalogenation). This process is supported by both literature examples^{54, 55} and experimentally observed cleavage of chlorines from other **1a** analogs synthesized by Dr. Sha Ding (PhD, July 2020) under catalytic hydrogenation conditions.

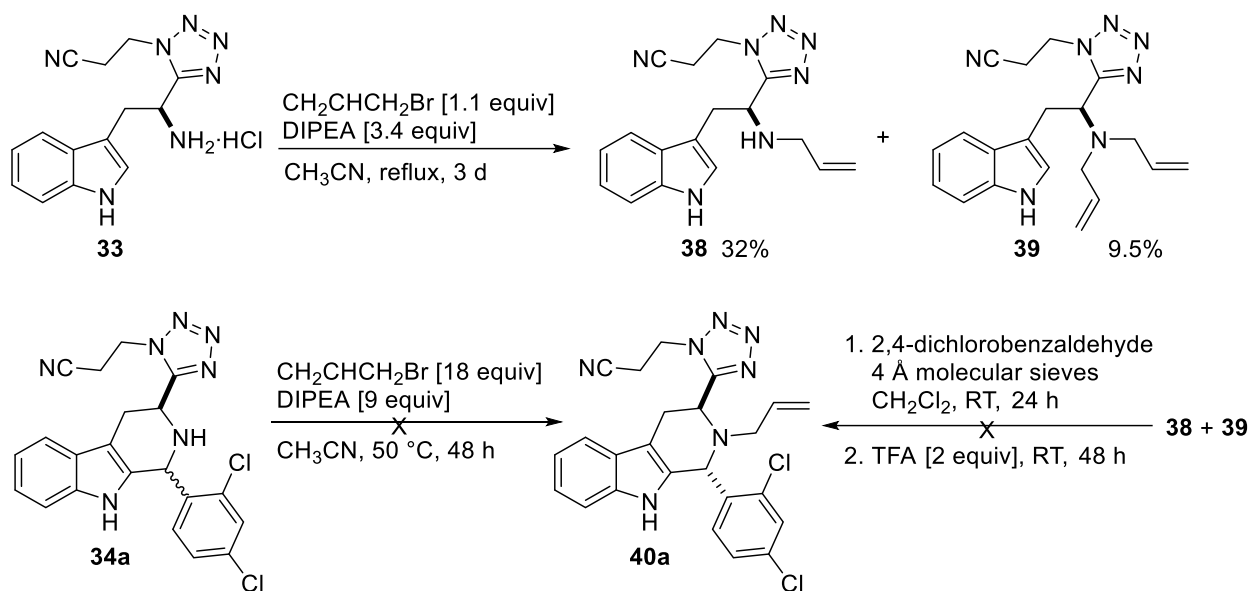
Concurrently with my work on the tetrazole derivative, Ms. Hanan AlMolhim (graduate student in the Carlier group) was exploring a stereoselective synthesis of **1a** analogs using an *N*-allyl protecting group. Not only was she able to obtain >95:5 diastereomeric ratio of *trans*:*cis* products, but the allyl chain could also be removed from the molecule without loss of halogens by treatment with 1,3-dimethylbarbituric acid under Pd catalysis (Scheme 3.8).



Scheme 3.8 Selective synthesis of *trans* diastereomer using N-allyl protection developed by Ms. AlMolhim. a) K_2CO_3 (2 equiv), allyl bromide (1.1 equiv), DMF, 0 °C to RT, 1 h, 60% yield (14% of di-allyl substituted by-product was also isolated); b) i: 2,4-dichlorobenzaldehyde, 4 Å molecular sieves, CH_2Cl_2 , RT, 24 h, ii: TFA, RT, 3 h, 68% yield; c) 1,3-dimethylbarbituric acid (2 equiv), $Pd(PH_3)_4$ (2 mol%), CH_2Cl_2 , reflux, 24 h, 90% yield; d) DIPEA (1.5 equiv), allyl bromide (3 equiv), anhydrous acetonitrile, 85 °C, 24 h, 90% yield; e) diluted TFA in CH_2Cl_2 , RT, 3 d, 34% yield (97:3 dr *trans:cis*).

Following the literature precedent and the previous work by Ms. AlMolhim, I attempted to install an allyl group both before and after the Pictet-Spengler reaction to allow the thermodynamically controlled formation of the desired *trans*-tetrazole (Scheme 3.9). Direct allylation of **33**, the protected tetrazole analog of tryptophan, yielded both mono- (**38**) and di-allyl amine (**39**). The separation of **38** and **39** proved to be complicated both due to the relatively small difference in polarity between the species and the presence of reaction by-products originating from impurity **33-2**. When separation of **38** and **39** failed, the mixture of **38+39** was used in the Pictet-Spengler reaction directly. However, the desired product **40a** could not be isolated. Thus, direct allylation of **34a** was attempted in the hope of generating *cis-/trans-40a*, which could then

be epimerized using dilute TFA (Scheme 3.8). Unfortunately, the *N*-allyl Pictet-Spengler adduct **40a** was not obtained. Due to the lack of selective reactivity and laboriousness of the process to obtain compound **33**, this method for tetrazole analog synthesis was abandoned, and late-stage formation of tetrazole ring was considered instead.



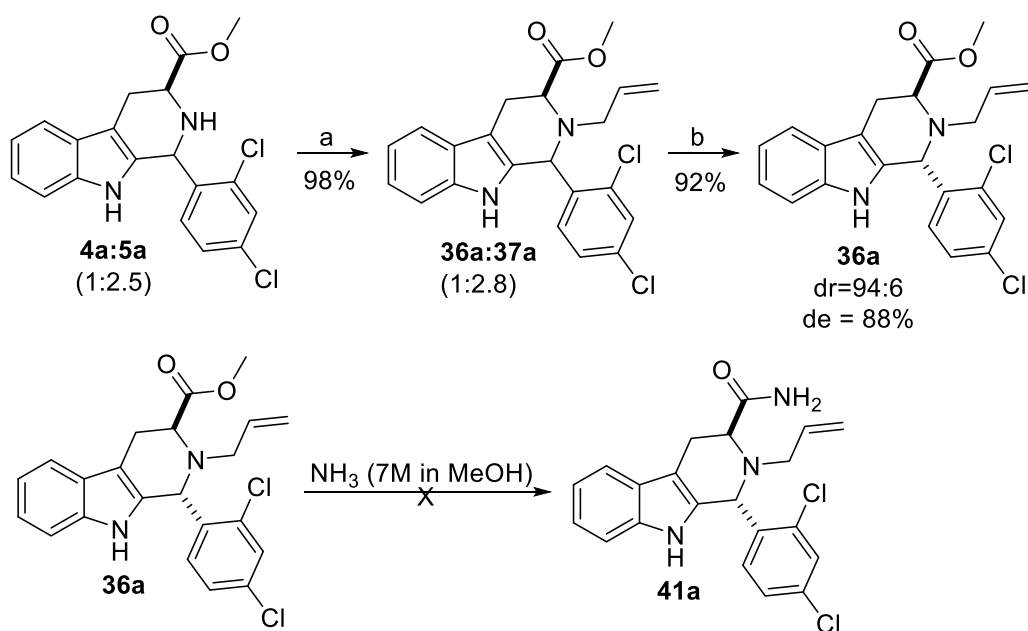
Scheme 3.9 Attempt of *trans*-selective synthesis of *N*2-allyl protected **40a**.

3.3.3 Stereoselective synthesis of tetrazole derivative via nitrile intermediate

As mentioned previously, the most common method for tetrazole synthesis consists of treating a nitrile group with an azide.^{25, 56-60} The initial reports of this synthesis used hydrazoic acid,⁶¹ however, soon methods employing azide salts in high boiling point solvents (e.g., DMF, DMSO) were developed.⁶² Use of azide salts is beneficial not only to avoid handling of both highly toxic and explosive hydrazoic acid but also because these reactions provide higher yields after a shorter reaction time without a need for pressurized equipment.⁶² In the early 2000s, the Sharpless group reported the use of ZnBr_2 to facilitate the reaction of nitriles with sodium azide to give tetrazoles.⁶³ ⁶⁴ Importantly, the second of these papers⁶⁴ focused on the preparation of tetrazoles from protected

α -aminonitriles, which were themselves synthesized from protected α -amino acids. Therefore, our first goal was to prepare a suitably protected *trans*- α -aminonitrile derivative of MMV008138 **1a**.

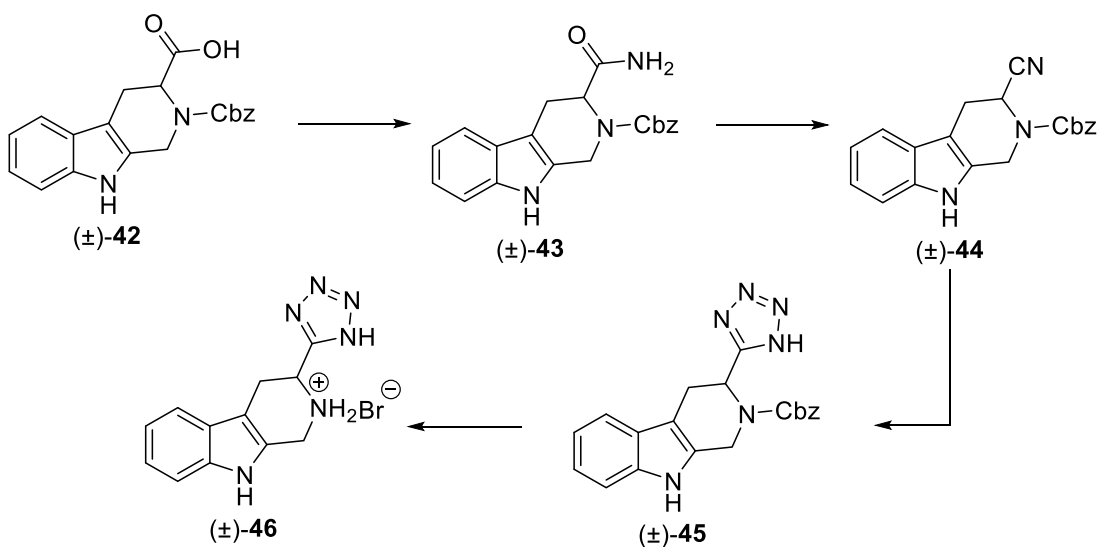
Initially, the *N*-allyl protected compound **36a** was prepared from a mixture of **4a** and **5a** (2.5:1 ratio determined by ^1H NMR) by slightly modifying the procedures developed by Ms. AlMolhim (Scheme 3.8) as shown in Scheme 3.10. Allyl protection was selected for its stability to both acids and bases⁶⁵ and the option to remove the protecting group without hydrodehalogenation side reaction. However, to our surprise, unlike the facile quantitative conversion of ester **4a** to a primary amide **8a**, compound **36a** did not react with ammonia to form **41a**, and only starting material was recovered (Scheme 3.10).



Scheme 3.10 Synthesis of *N*-allyl protected **36a** and an attempt to convert **36a** to its primary amide analog **41a**. a) DIPEA (1.5 equiv), allyl bromide (4.3 equiv), anhydrous acetonitrile, 85 °C, sealed tube, 1 h; e) diluted TFA in CH_2Cl_2 , RT, 2.5 h. Conversion of **36a** to **41a** was attempted for 24 h at RT and 24 h refluxing in a sealed tube – in both cases, only **36a** was isolated.

Other protecting groups commonly seen in relevant literature are *N*-Boc (*tert*-butyl carbamate) or *N*-Cbz (carboxybenzyl carbamate).^{56, 57, 59, 66} The latter was selected for our synthesis for two reasons. Firstly, Boc is more susceptible to cleavage under acidic conditions than Cbz⁶⁵

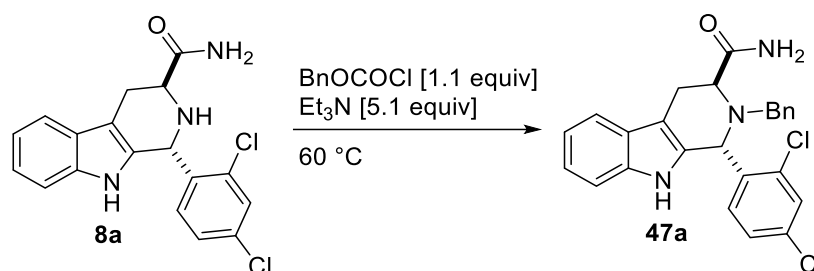
and its steric bulk located closer to the reaction site might hinder the reactivity. Secondly, the Cbz group was used in a literature reference where C3-tetrazole was introduced into a broadly similar TH β C structure (Scheme 3.11). Notably, the Cbz-deprotection of tetrazole-substituted Pictet-Spengler adduct ((\pm)-**45**) presented by Saiga *et al.* was carried out under strongly acidic conditions, rather than by catalytic hydrogenation. Even though the exposure of the TH β C to acidic conditions might induce epimerization on C1 position (Scheme 3.7), we selected this cleavage method because it would not lead to hydrodehalogenation.⁶⁶



Scheme 3.11 Installation of tetrazole group on an *N*-Cbz protected TH β C as presented by Saiga *et al.*⁶⁶

Primary amide **8a** was then synthesized according to the aforementioned literature procedure⁹ and reacted with benzyl chloroformate (Cbz-Cl) to protect the N2 position of the tetrahydropyridine ring. Curiously, both HRMS and ¹H NMR confirmed that only the *N*-benzyl protected product (**47a**) was recovered instead of the expected *N*-Cbz analog. In addition, both the identity and purity of the Cbz-Cl reagent were confirmed by NMR. The reaction was also repeated with newly purchased reagent; however, in all cases, only *N*-benzyl product **47a** was formed (Table 3.4).

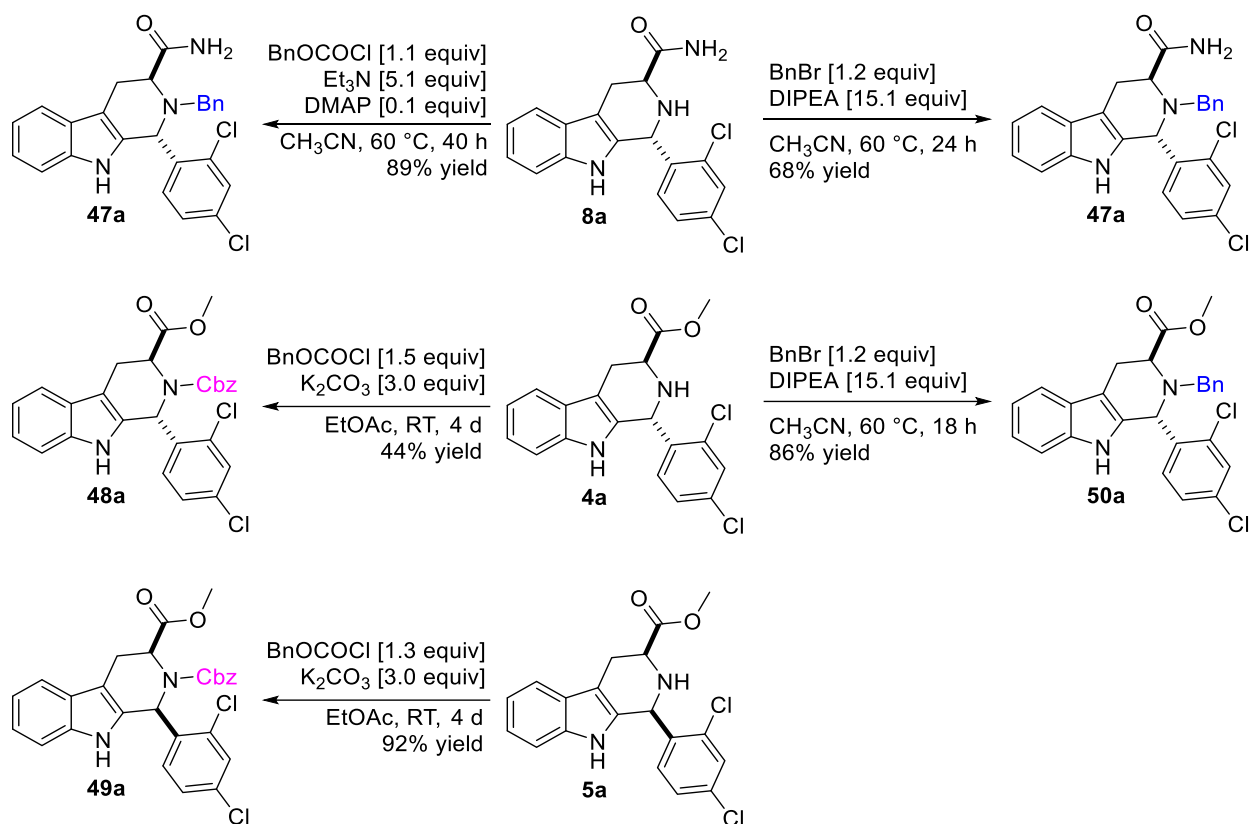
Table 3.4 Attempt to protect secondary amine in **8a** with Cbz group.



Entry	Solvent	Et ₃ N	Additive	Time	% Yield
1	CH ₃ CN:CHCl ₃ (1:1 v/v)	7.0 equiv	—	10 d	58%
2	CH ₃ CN:CHCl ₃ (1:1 v/v)	5.0 equiv	DMAP [0.6 equiv]	92 h	78%
3	CH ₃ CN	5.1 equiv	DMAP [0.1 equiv]	40 h	89%

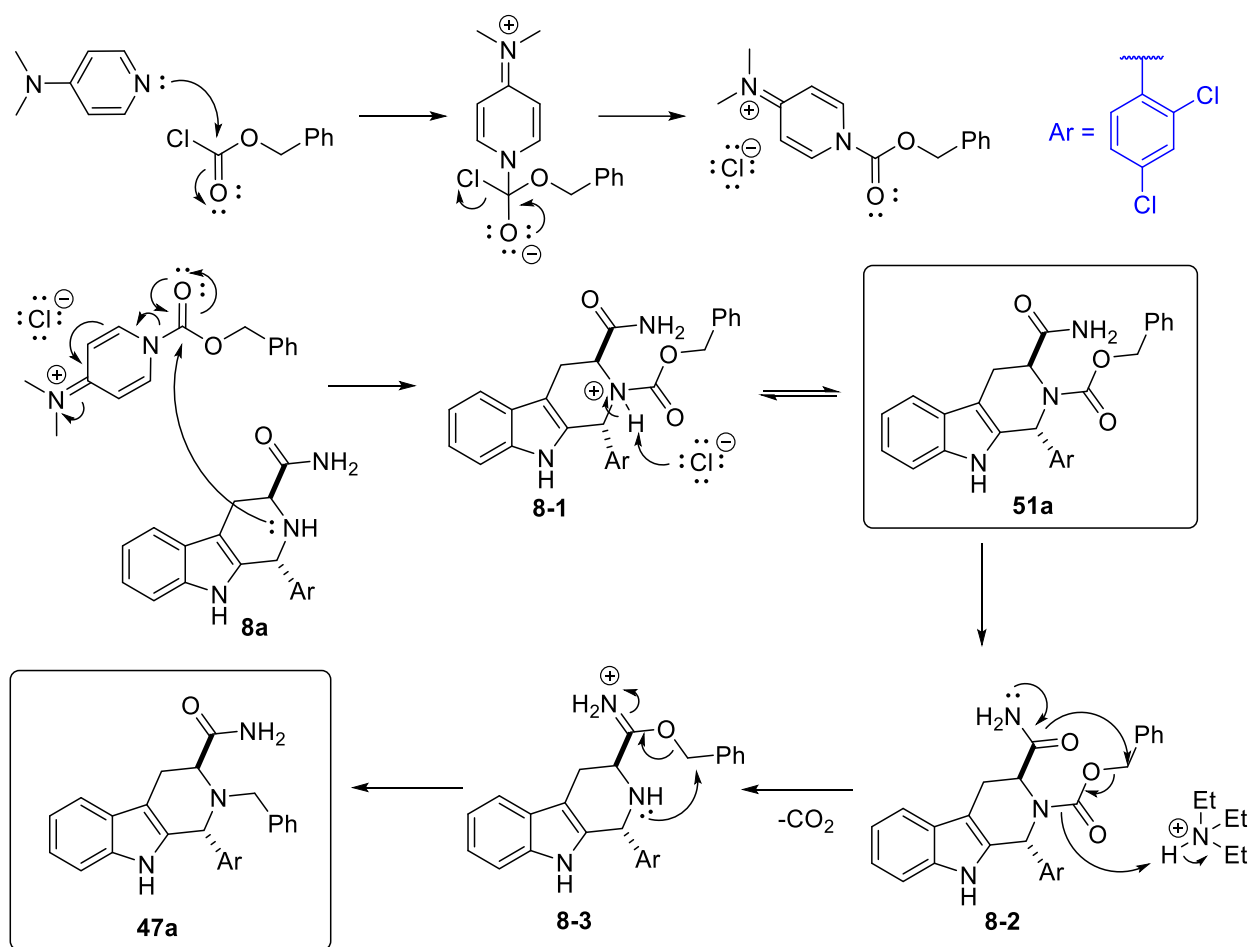
Compound **47a** was also prepared intentionally from **8a** in 68% yield under the following conditions: 1.2 equiv benzyl bromide, 15.1 equiv DIPEA, CH₃CN, 60 °C, 24 h. Spectra of compound **47a** obtained by reaction with benzyl bromide and from procedures in entries 1 – 3 were compared and found to be identical. HRMS analysis also confirmed the identity of **47a**.

To gain an inside into the surprising reaction outcome of **8a** (Table 3.4), Cbz-Cl was also reacted with *trans*-ester **4a** and *cis*-ester **5a** to yield only the *trans*-*N*-Cbz ester (**48a**) and its *cis*-isomer (**49a**). *N*-benzyl protected compounds **47a** and **50a** were also synthesized from a reaction with benzyl bromide. No observable amount of *N*-benzyl protected species (**50a**) was obtained from reactions of **4a**, while the compound **47a** obtained by reactions of **8a** with Cbz-Cl and **8a** with benzyl bromide were found identical by both NMR and HRMS (Scheme 3.12).



Scheme 3.12 Synthesis of *N*-Bn protected analogs **47a** and **50a**, and *N*-Cbz protected esters **48a** and **49a**.

Later, when we obtained the desired *N*-Cbz protected amide analog **51a** (Table 3.6), TLC monitoring of reaction depicted in Table 3.4 gave us further insight into the reaction. A trace amount of desired product **51a** was observed together with the formation of **47a** and disappeared when the reaction reached completion –suggesting a decarboxylative conversion of **51a** to **47a**. The mechanism of this conversion is not clear, but a possible reaction pathway is proposed in Scheme 3.13.

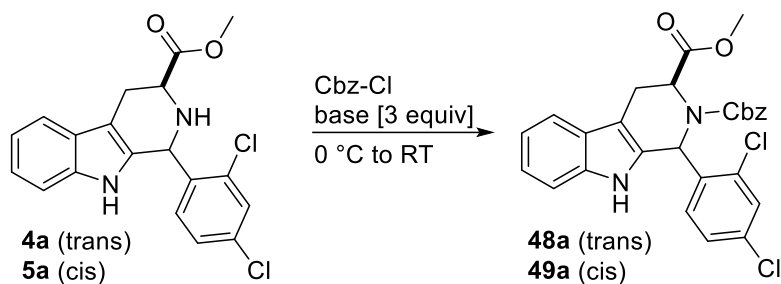


Scheme 3.13 Proposed mechanism for the formation of **47a** from **8a**.

An alternative approach to the synthesis of desired *N*-Cbz protected amide **51a** was via conversion of *N*-Cbz protected ester **48a**. Initially, the *N*-Cbz protected esters **48a** and **49a** were prepared under anhydrous conditions following literature precedence.⁶⁷ While the desired products **48a** and **49a** were formed, the reaction suffered from long reaction time and problematic monitoring due to the heterogenous nature of the reaction mixture (Table 3.5, Entries 1-2). We hypothesized that the culprit of the reaction is the low solubility of potassium carbonate in ethyl acetate, and thus triethylamine was selected as a more soluble alternative base. Unfortunately, only a trace amount of the desired product was obtained even after a prolonged reaction time (Table 3.5, Entry 3). Further reaction optimization allowed us to shorten the reaction time by introducing

a biphasic solvent system (Table 3.5, Entries 4-5, Schotten-Baumann reaction conditions).⁶⁸ The product was obtained in nearly quantitative yield in a significantly shorter time and, after removal of Cbz-Cl side-products by trituration, could be used in the next step without further purification. The observed reactivity of *cis*- and *trans*- isomers was comparable under both anhydrous and biphasic conditions.

Table 3.5 Optimization of Cbz-protection reaction for **4a** and **5a**.



Entry	Substrate	Solvent	Base	Cbz-Cl	Time	% Yield
1	4a	EtOAc	K ₂ CO ₃	1.5 equiv	4 d	44%
2	5a	EtOAc	K ₂ CO ₃	1.3 equiv	4 d	92%
3	5a	EtOAc	Et ₃ N + 10 mol% DMAP	1.4 equiv	4 d	trace
4	4a	EtOAc:H ₂ O (2:1 v/v)	K ₂ CO ₃	1.1 equiv	4 h	93%
5	5a	EtOAc:H ₂ O (2:1 v/v)	K ₂ CO ₃	1.2 equiv	4 h	94%

The conversion of **4a** (*trans*-) and **5a** (*cis*-) to the N2-Cbz derivatives **48a** and **49a** was stereospecific (no epimerization detected). Initially, the ¹H NMR spectra were analyzed to determine if the relative stereochemistry remained unchanged. However, the analysis of coupling constants discussed in Chapter 2 cannot be directly applied in this case because the conformation of the C-ring is strongly affected by the presence of a Cbz group at N2. Nevertheless, the ³J_{HH} couplings observed in the respective ¹H NMR spectra suggested that the *trans* diastereomer **48a** would have a predominantly pseudo-axial C3-ester group (H3 signal appeared as an apparent triplet with ³J_{HH} = 4.5 Hz, while the two accidentally equivalent H4 protons appeared as a doublet with ³J_{HH} = 4.3 Hz, suggesting nearly equal dihedral angle between H3 and both H4s). In contrast,

the *cis* diastereomer **49a** showed $^3J_{\text{HH}}$ (H3-H4) of 7.2 and 2.4 Hz, which led us to believe that the *cis*-interconverts between conformations featuring both pseudo-equatorial and pseudo-axial C3-esters. Evaluation of through-space interaction via NOE NMR, which is normally useful for identification of the *cis*-diastereomer (e.g., **5a**), did not show any correlation between H1 and H3 in either **48a** or **49a**. To reach a final conclusion regarding the relative stereochemistry of **48a** and **49a**, both compounds were crystallized and submitted for X-ray diffraction analysis (performed by Dr. Carla Slebodnick). With the crystallographic data in hand, we were able to confirm the retention of stereochemistry in both compounds (Figure 3.10).

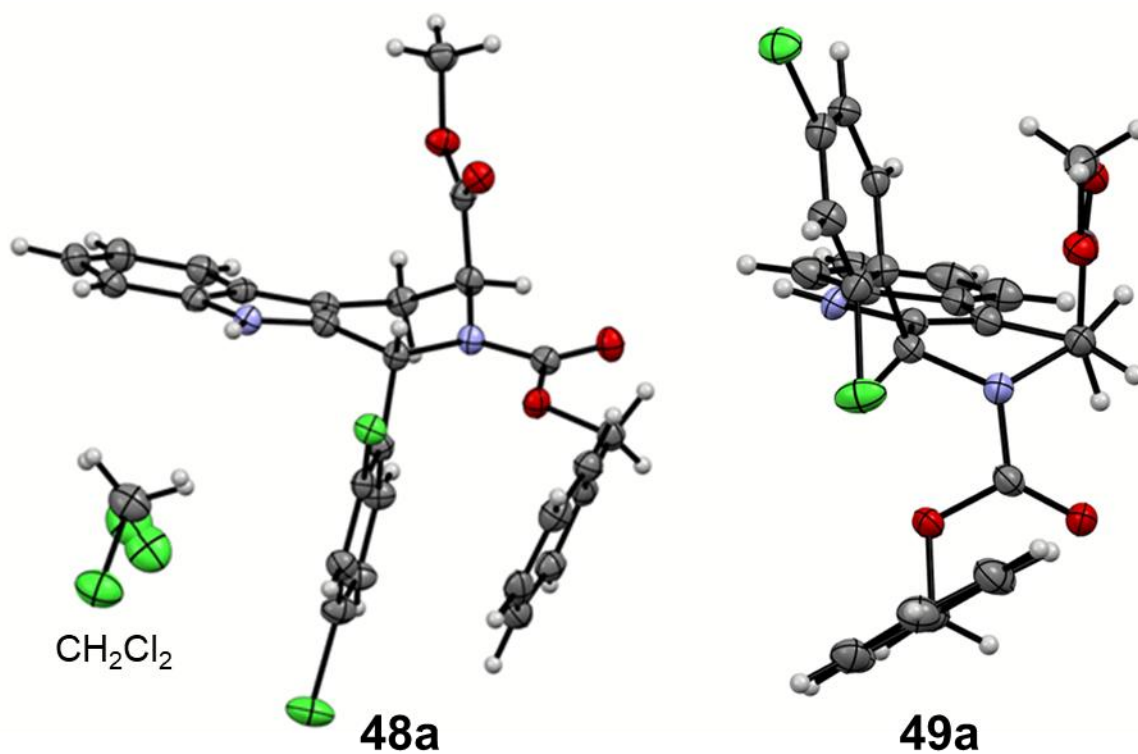


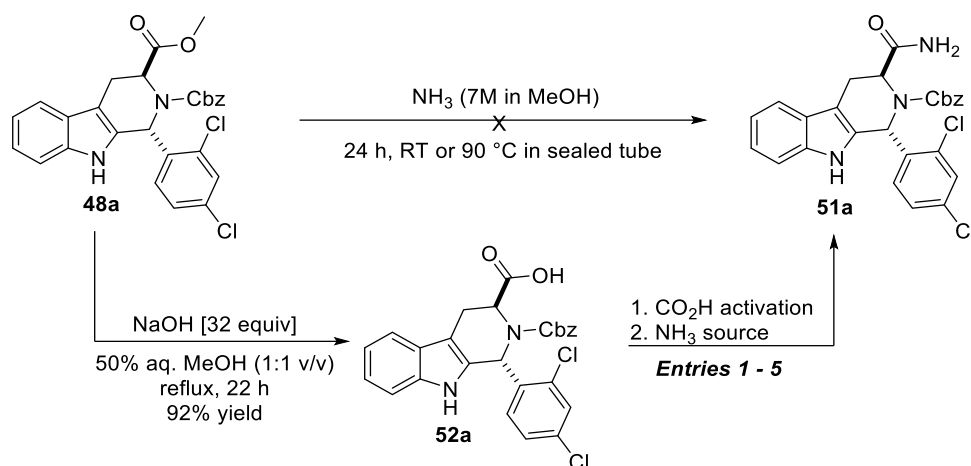
Figure 3.10 Anisotropic displacement ellipsoid drawing of X-ray structures of compounds **48a** and **49a**. Both molecules were crystallized from methylene chloride:hexanes mixture, and the crystallographic data were visualized with Mercury.

As can be seen in both X-ray structures, the N2-carbamate substituent adopts a roughly pseudoequatorial orientation. The *trans*-isomer **48a** has a pseudo-axial ester with dihedral angles between H3-H4 α and H3-H4 β +52.5° and -67.4°, respectively in the solid-state. Thus, the X-ray structure correlates well with the observed coupling constants in the solution, which are expected to be nearly equivalent due to the dihedral angles being comparable in size. Interestingly, in the solid-state, the C1 aryl and C3-CO₂Me groups in **49a** are roughly pseudo-axial. To the extent that this conformation exists in the solution, it will weaken the NOE correlation between H1 and H3 since they are so far apart. The observed dihedral angles of H3-H4 α (+40.1°) and H3-H4 β (-78.7°) in the X-ray structure, resulting from steric repulsion of diaxial substitution, also match the NMR observation as they would be expected to show $^3J_{\text{HH}}$ of 7-8 and 1-2 Hz, respectively (calculated using MestReJ software).⁶⁹

Direct conversion of ester **48a** to primary amide **51a** was attempted by treatment with methanolic ammonia, but even in a sealed tube at 90 °C, only starting material was recovered (Table 3.6).⁶⁵ The *N*-Cbz protected ester **48a** was then hydrolyzed into respective carboxylic acid **52a**, which was, upon activation, converted into amide **51a**. Several reaction conditions were tried, and the best results were achieved when **52a** reacted with EDC and HOBT (Table 3.6, Entry 5).⁶⁶

70

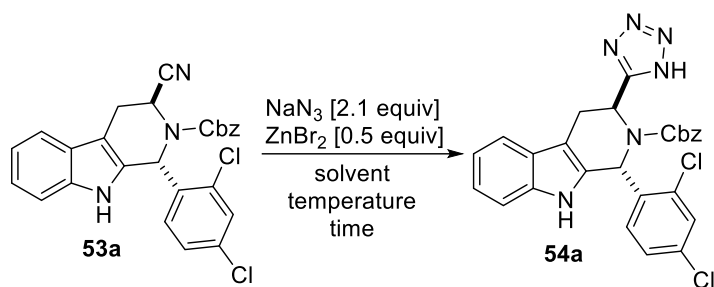
Table 3.6 Optimization of primary amide **51a** synthesis.



Entry	CO ₂ H Activation	NH ₃ source	Solvent	Temp.	Time	Yield
1	Et ₃ N [5.4 equiv] EtOCOCl [2.0 equiv]	NH ₄ Cl	THF	0 – 5 °C	2.5 h	23%
2	Et ₃ N [1.2 equiv] EtOCOCl [1.1 equiv]	NH ₄ OH	THF	-10 °C	2.5 h	42%
3	CDI [1.2 equiv]	NH ₃ (7M in MeOH)	CH ₂ Cl ₂	0 – 5 °C	24 h	53%
4	DIPEA [3.1 equiv] HATU [1.3 equiv]	NH ₃ (7M in MeOH)	DMF:CH ₂ Cl ₂ (1:2 v/v)	RT	3 d	79%
5	DIPEA [3.2 equiv] EDC·HCl [2.0 equiv] HOBT [2.0 equiv]	NH ₃ (7M in MeOH)	DMF	RT	21 h	90%

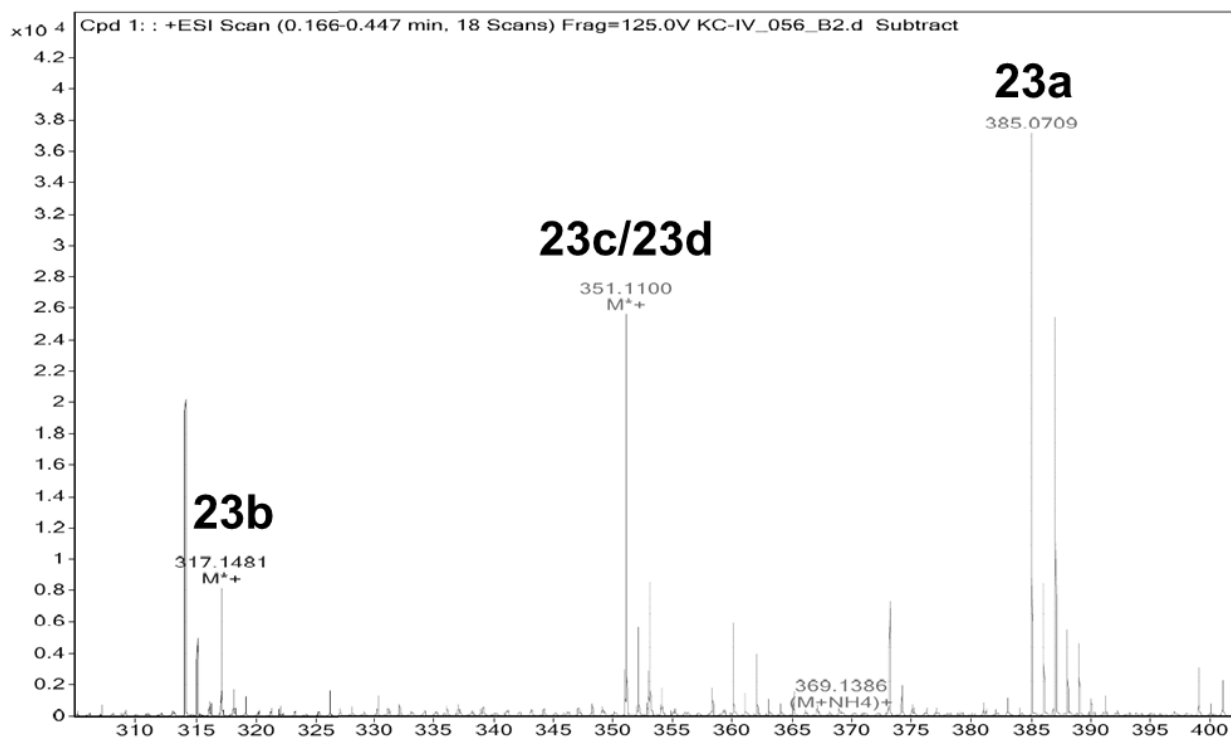
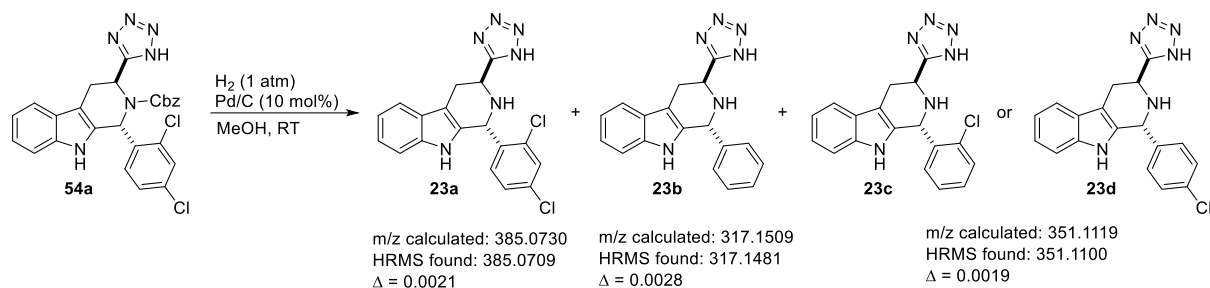
The dehydration of amide **51a** to nitrile **53a** was achieved in high yield with POCl₃ in pyridine according to the literature procedure.⁶⁶ The product was sufficiently pure to use in the next step without further purification. The tetrazole formation was attempted with NaN₃ and ZnBr₂ in DMF and water/propan-2-ol mixture according to literature procedures.^{64, 66} However, both reactions suffered from low yields and long reaction times. Further optimization of the Sharpless procedure⁶⁴ revealed that the best results are obtained in absolute propan-2-ol. The protected tetrazole analog **54a** is either isolated in sufficient purity for a deprotection step or can be purified by column chromatography if needed (Table 3.7).

Table 3.7 Optimization of tetrazole **54a** synthesis.



Entry	Solvent	Temperature	Time	Yield	Notes
1	DMF	100 °C	2 d	ND	Product detected with a large variety of impurities by TLC, not isolated
2	<i>i</i> PrOH:H ₂ O (1:3 v/v)	reflux	3 d	26%	Purified by column chromatography
3	<i>i</i> PrOH:H ₂ O (3:1 v/v)	reflux	3 d	85%	Purity after work up ~ 96 wt%
4	<i>i</i> PrOH	reflux	25 h	89%	Purity after work up ~ 95 wt%

The deprotection of the Cbz group presented yet another challenge for the synthesis. The most common method for Cbz cleavage is catalytic hydrogenation, treatment with strong acid, or dissolving metal reduction in ammonia.⁷¹ Despite our observations of competitive hydrodehalogenation in the removal of benzyl from *N*-Bn analogs of **1a** (*vide supra*), we did attempt catalytic hydrogenation of compound **54a**. However, as feared, the reaction gave hydrodehalogenation concurrent with Cbz-removal. HRMS revealed that the desired product **23a** was formed in an inseparable mixture with the monochloro-analog (**23c** or **23d** – the regiochemistry was not determined) and the unsubstituted phenyl analog **23b** (Scheme 3.14). The use of Na/NH₃ or Li/NH₃ protocol^{72, 73} was avoided because the reductive nature of the process was likely to result in hydrodehalogenation analogously to catalytic hydrogenation.^{74, 75}

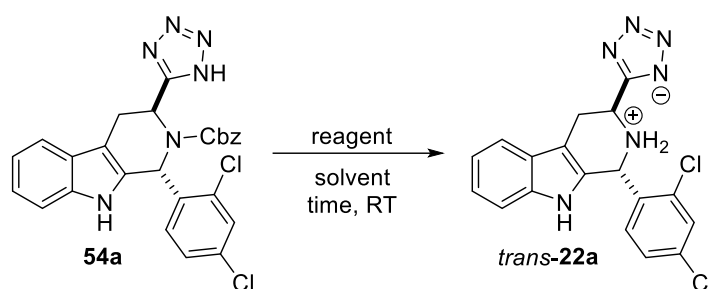


Scheme 3.14 Hydrodehalogenation as a side reaction of **54a** with H₂ over Pd/C in methanol. The HRMS confirmed the presence of dehalogenated products.

Lastly, the treatment of **54a** with strong Brønsted or Lewis acid was attempted according to methods presented in the literature (Table 3.8).^{66, 71, 76, 77} Lewis acids TMSI and TMSCl⁷⁶ reacted with **54a** in acetonitrile but did not produce the desired product (Table 3.8, Entries 1-2). Reaction with TMSI was also attempted in CDCl₃ (for an NMR monitored reaction) and in CHCl₃.⁷⁷ Reaction in CDCl₃ was quenched after 30 minutes due to heavy precipitation forming in the sample, and analysis of the isolated product suggested 62:37 molar ratio of desired product **23a** to unreacted **54a**, along with a number of impurities. When the same reaction was performed in

CHCl₃ and monitored by TLC, the reaction failed to reach full conversion after 24 hours. Meanwhile, HRMS analysis showed that the product of NMR-monitored reaction did not match expected m/z for compound **23a** and the method was abandoned (Table 3.8, Entry 3). Use of strongly acidic resin Amberlyst 15 was also attempted, based on literature describing its use for removal of *N*-Boc protecting group.⁷⁸ However, no conversion of **54a** was observed after 24 hours, and the starting material was recovered (Table 3.8, Entry 4). The deprotection using HBr in acetic acid provided the most satisfactory results. Prolonged contact with acid in a more dilute reaction mixture led to an increased rate of epimerization, producing both desired *trans*-**23a** and the undesired *cis* diastereomer *cis*-**23a** (Table 3.8, Entry 5). However, when the reaction was carried out in concentrated HBr/AcOH, the diastereomeric ratio of isolated crude product was 95:5 in favor of *trans* diastereomer. After careful purification via column chromatography (80:20 CH₂Cl₂:propan-2-ol), the desired product *trans*-**23a** (>98% *trans*-) was obtained in a 30% yield. The overall yield of *trans*-**23a** from (*S*)-tryptophan methyl ester hydrochloride was 4.9%.

Table 3.8 Optimization of Cbz-deprotection in the formation of **23a**.



Entry	Reagent	Solvent	Time	Yield	Note
1	TMSI	CH ₃ CN	24 h	0%	54a not recovered
2	TMSCl	CH ₃ CN	24 h	0%	54a and other products
3	TMSI	CHCl ₃	24 h	0%	54a and other products
4	Amberlyst 15	MeOH	24 h	0%	54a recovered
5	HBr (33% in AcOH)	AcOH	23 h	50%	dr = 81:29 <i>trans</i> : <i>cis</i>
6	HBr (33% in AcOH)	—	15 min	56% [30%]	dr = 95:5 <i>trans</i> : <i>cis</i> purified [dr > 98:2 <i>trans</i> : <i>cis</i>]

The pure diastereomer *trans*-**23a** was evaluated for its growth inhibition potency against the Dd2 strain of *P. falciparum* in the laboratory of Prof. Cassera. Unfortunately, the potency of *trans*-**23a** ($IC_{50} = 1850 \pm 63$ nM) did not improve in comparison to the for 7:3 dr mixture of *trans*-/*cis*-**23a** ($IC_{50} = 1470 \pm 62$ nM, Figure 3.11). The similarity of growth inhibition results suggests that both diastereomers are likely equally non-potent.

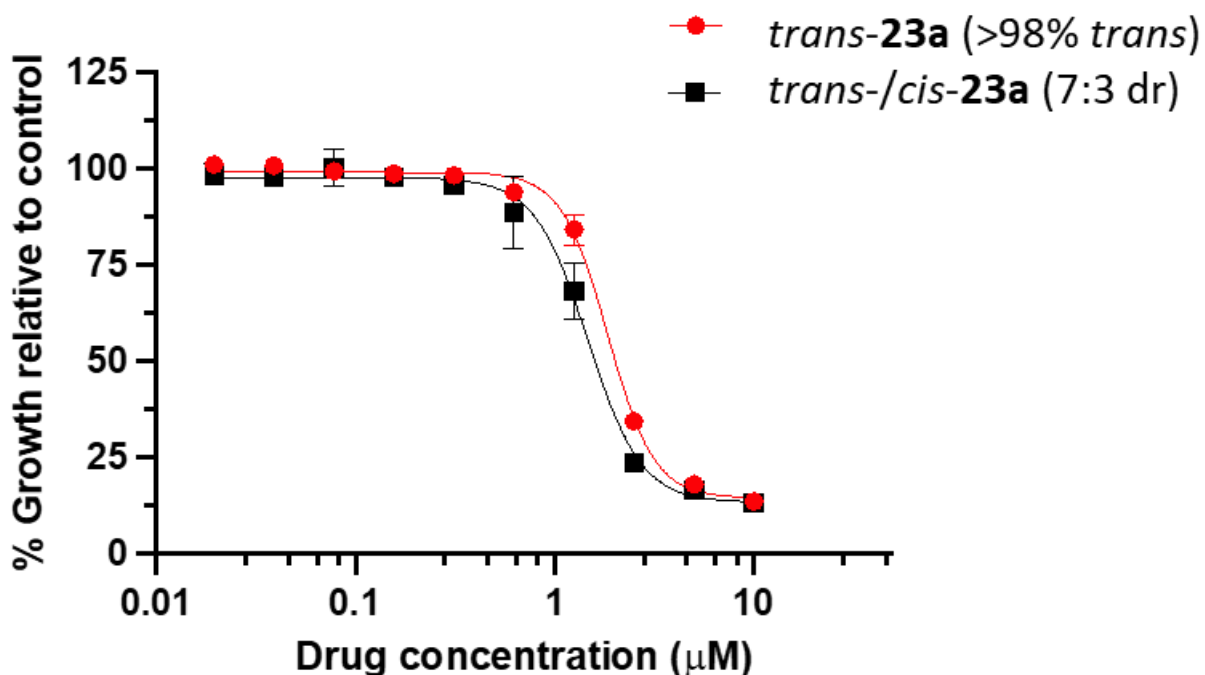
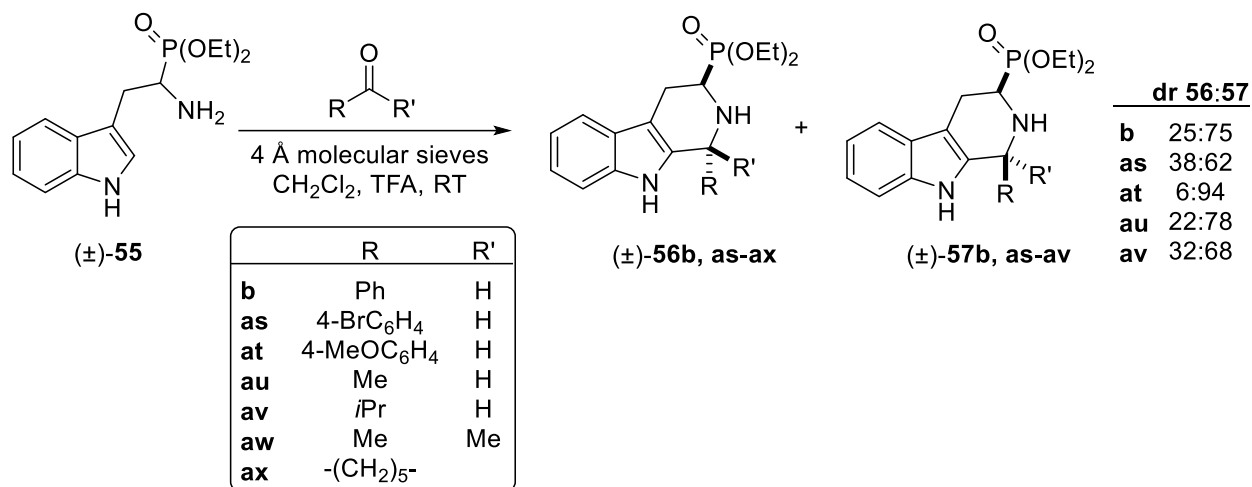


Figure 3.11 Growth inhibition of *P. falciparum* (Dd2 strain) induced by pure diastereomer *trans*-**23a** (red circles) and a sample of *trans*-/*cis*-**23a** (7:3 dr, black squares). Growth inhibition was determined by the SYBR Green assay after 72 hours of exposure. Data and plot are courtesy of Prof. Cassera.

3.4 Synthesis of the racemic phosphonic acid derivative

The literature search revealed that the most feasible approach to the synthesis of phosphonic acid bioisostere of **1a** would be via a diethyl ester phosphonate analog of tryptophan ((±)-**55**). Preparation of this compound has been presented in several publications,^{79, 80} including one example of compound (±)-**55** reacting under Pictet-Spengler conditions to afford aromatic and

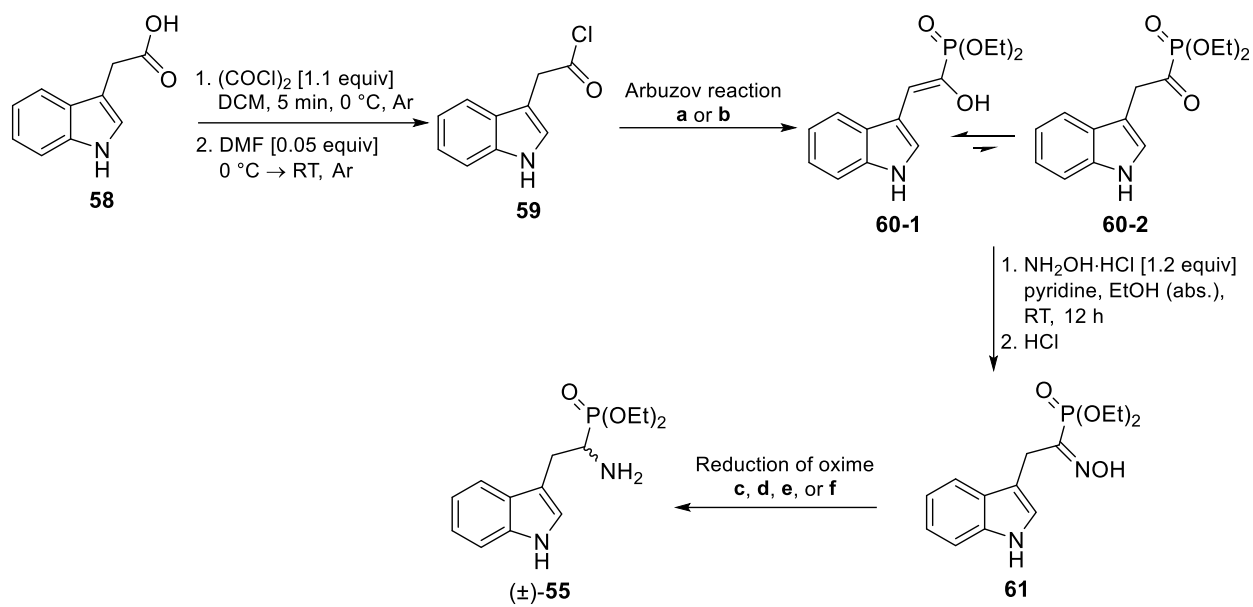
aliphatic TH β Cs.⁸¹ However, the Pictet-Spengler adducts presented by Viveros-Ceballos *et al.*⁸¹ were not further hydrolyzed, and to the best of my knowledge, there is no literature precedence for C3-phosphonic acid substituted TH β Cs.



Scheme 3.15 Diethyl phosphonate TH β Cs synthesized from (±)-**55** by Viveros-Ceballos *et al.*⁸¹

3.4.1 Synthesis of diethylphosphonate analog of tryptophan

The exact reproduction of literature procedures for the synthesis of (±)-**55** in our laboratory proved to be challenging, and optimization of several individual steps was required. The synthetic scheme for literature precedents is shown in Scheme 3.16. It should be noted that in our hands, the purification of intermediates **59-61** proved to be both detrimental to their stability and unnecessary for a satisfactory yield of desired tryptophan analog (±)-**55** and, consequently, the intermediates were isolated and carried to the next step without purification. The final yield of 49% of (±)-**55** was then calculated over four steps from the initial indole-3-acetic acid (**58**), which is identical with 49% yield obtained by Viveros-Ceballos *et al.*, who also omitted purification of intermediates **59-61**,⁸¹ and superior to 29% yield obtained by Rogers and Stern⁸⁰ and 30-33% yield obtained by Subotkowski *et al.* (Scheme 3.16).⁷⁹



Scheme 3.16 Literature pathway to diethyl phosphonate analog of tryptophan (\pm)-**55**. Conditions: **a**) POEt_3 (1.0 equiv), Et_2O (anh.), 0-5 °C for 1 h, RT for 4 h, 64%⁷⁹ and 56%⁸⁰ isolated yield from **59**; **b**) POEt_3 (1.0 equiv), THF (anh.), 0 °C for 5 min, reflux for 15 min, Ar, product was not purified in this step; **c**) Zn (2.6 equiv), CuSO_4 (1.4 equiv) couple, EtOH (65% aq.), 60 °C, 3 h, 69%⁸⁰ isolated yield from **61**; **d**) Raney-Ni (150 g/mol of **61**), EtOH (anh.), H_2 (100-120 atm), 100 °C, 1 h, 75%⁷⁹ isolated yield from **61**; **e**) Al-Hg (300 g/mol of **60**), EtOH (83 wt% aq.), RT, 8 h, 70%⁷⁹ isolated yield from **61**; **f**) Zn (4.0 equiv), HCO_2H (equiv), RT, overnight, 49% isolated yield over 4 steps from **58**. Compound **59** was carried to the Arbuzov reaction without isolation^{80, 81} and compound **61** was isolated in 68%⁷⁹ and 76%⁸⁰ yield, respectively. Conditions for formation of **59** and **61** were nearly identical in all three referenced procedures.

The activation of carboxylic acid **58** was achieved via reaction with oxalyl chloride to yield compound **59** (crude yield: 118%). The conversion to the desired product was confirmed by comparison of ^{13}C NMR, where the starting material was no longer observed, and the carbonyl resonance shifted noticeably upfield (Figure 3.12), which agrees with literature examples.⁸² The acyl chloride **59** appeared to be moderately stable for several hours and was used without purification in Arbuzov reaction with triethyl phosphite.

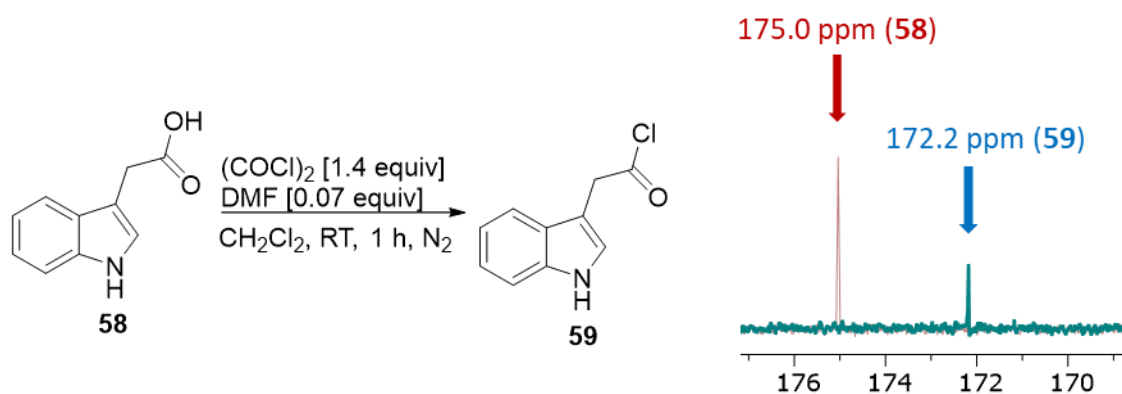


Figure 3.12 Synthesis of acetyl chloride **59** and confirmation of product formation by ^{13}C NMR.

The choice of triethyl phosphite was based on its dominant position in the existing literature.^{79-81, 83-87} Alternative phosphites – trimethyl phosphite and larger alkyl or aryl phosphites were ruled out for possible hydrolysis issues (trimethylphosphite)⁸⁸ and steric hindrance issues (longer alkyl chains and aromatic substituents). The Arbuzov reaction was finished nearly instantaneously as monitored by TLC; however, the reaction subjected to 15 minutes of reflux afforded the cleanest product as determined by ^{31}P NMR (crude yield: 111% over two steps from **58**). When Et_2O was used as an alternative solvent to THF, the acyl chloride **59** readily degraded at low temperature, and no desired product was isolated. In agreement with previous literature, only the enol tautomer **60-1** was detected by NMR spectroscopy.⁷⁹ Handling of **60-1** required special care because the product is highly unstable and cannot be efficiently stored for longer than several hours. Any attempts to purify **60-1** led to complete degradation of the product.

Compound **60-1** was thus immediately subjected to a reaction with hydroxylamine hydrochloride in pyridine to generate a mixture of E/Z isomers of oxime **61** (crude yield: 96% over three steps from **58**, dr = 1:0.6, stereochemistry was not determined). Attempts to isolate individual isomers led to diminished yield via crystallization and to degradation of material when column

chromatography was used. However, if stored dry, the crude mixture of oximes **61** exhibits a shelf life of at least several months (determined by ^1H and ^{31}P NMR). Moreover, the ^{31}P NMR shows a complete conversion of **60-1** to **61**, while the majority of phosphorus-containing impurities remain unchanged (Figure 3.13).

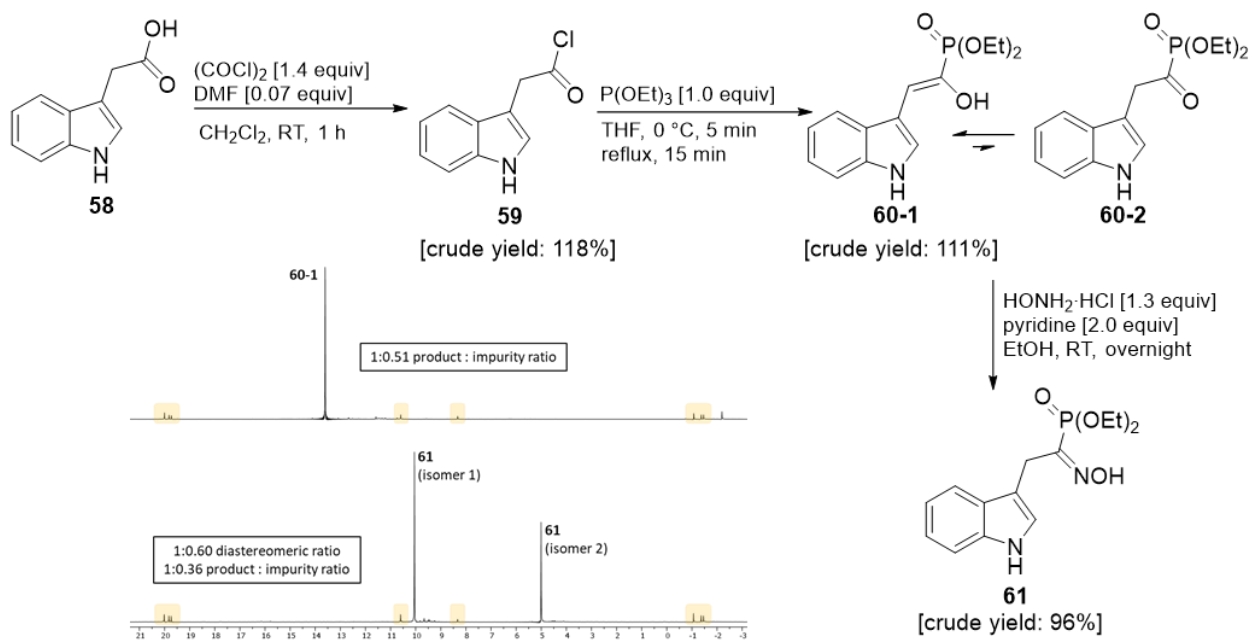
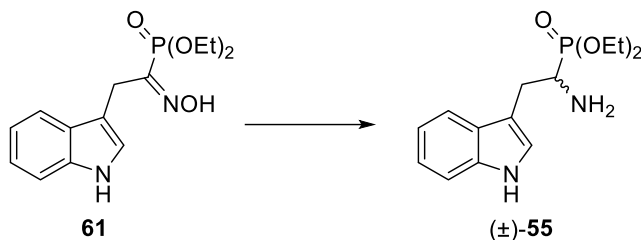


Figure 3.13 Synthesis of oxime **61** from **58** and comparison of purity of crude products **60-1** and **61** by ^{31}P NMR. Impurities highlighted in yellow are identical by ^{31}P NMR between **60-1** and **61**.

The reduction of oxime **61** to amine (\pm)-**55** proved to be the most challenging step of the process. Several methods were attempted (Table 3.9) with mostly negative results.^{80, 83, 89} In the end, the use of 88% aqueous formic acid and the addition of activated zinc powder in several portions gave the highest yield. Still, a wide range of side products can be detected by TLC (not characterized), and it is reasonable to assume that this reduction step is responsible for an overall low yield of this synthesis. However, it should be noted that the yield obtained in our laboratory is comparable with literature data.⁸¹ Interestingly, when anhydrous formic or trifluoroacetic acid was

used, the reaction gave a very low or no yield of (\pm)-**55** accompanied by a variety of degradation products.

Table 3.9 Reduction of oxime **61** to tryptophan analog (\pm)-**55**.

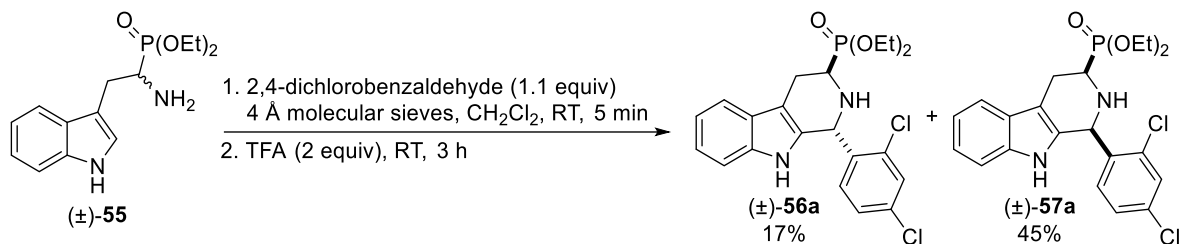


Entry	Reducing agent	Solvent	Temperature	Time	Yield ^a	Ref.
1	NaBH ₄	MeOH	RT	48 h	0%	83
2	BH ₃	THF	RT	48 h	0%	89
3	Zn-Cu	EtOH	60 – 70 °C	24 h	0%	80
4	Zn	HCO ₂ H (88% aq.)	RT	24 h	0%	81
5	Zn	TFA (99.9%)	RT	24 h	0%	
6	Zn	HCO ₂ H (88% aq.)	45 – 55 °C	48 h	49%	
7	Zn	HCO ₂ H (99.7%)	45 – 55 °C	48 h	5%	

^aYield was determined as overall yield over four steps from indole-3-acetic acid (**58**). For previous steps of the synthesis, see Figure 3.13.

3.4.2 Synthesis of the phosphonic acid derivative of MMV008138

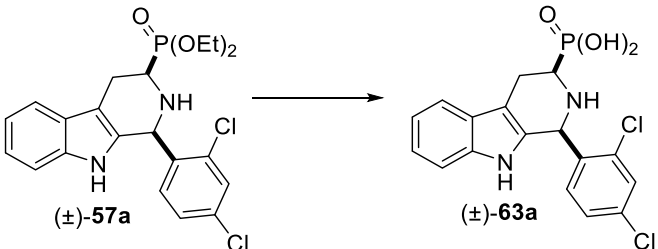
With the racemic diethylphosphonate analog of tryptophan ((\pm)-**55**) in hand, the Pictet-Spengler reaction was carried out under standard conditions used in our laboratory. The reaction time was much shorter than 1-3 days typically required for methyl ester analogs, as the diethylphosphonate products were formed within 3 hours (Scheme 3.17). The diastereomers (\pm)-**56a** (*trans*) and (\pm)-**57a** (*cis*) were successfully isolated by column chromatography in 17% and 45% yield, respectively. The stereochemistry was confirmed by a 1D NOE experiment.



Scheme 3.17 Preparation of diethylphosphonate TH β Cs from (\pm)-**55** via Pictet-Spengler reaction.

While the Pictet-Spengler reaction progressed smoothly, the hydrolysis of the final intermediate presented a challenge in the form of reaction monitoring. Similarly to esters of carboxylic acids, phosphonate esters can be hydrolyzed under both acid and base conditions. However, in basic conditions, the hydrolysis proceeds only to mono-deprotection, while in acidic conditions, both alkyl chains can be cleaved.³⁰ A variety of acidic conditions were applied to hydrolyze the *cis*- Pictet-Spengler adducts (\pm)-**57a** to its respective phosphonic acid analog (\pm)-**63a**.^{30, 79, 80} TLC did not prove successful in reaction monitoring (Table 3.10), which was not surprising, as the most frequently used monitoring method for similar reactions in literature was reverse phase HPLC, rather than normal phase TLC. NMR analysis of samples from reactions shown in Table 3.10 showed either degradation of starting material, but no product formation (entries 2 and 3), or the hydrolyzed product was detected albeit as a mixture of diastereomers together with other side products (entries 1 and 4).

Table 3.10 Attempts of (\pm)-**57a** hydrolysis under acidic conditions monitored by TLC.

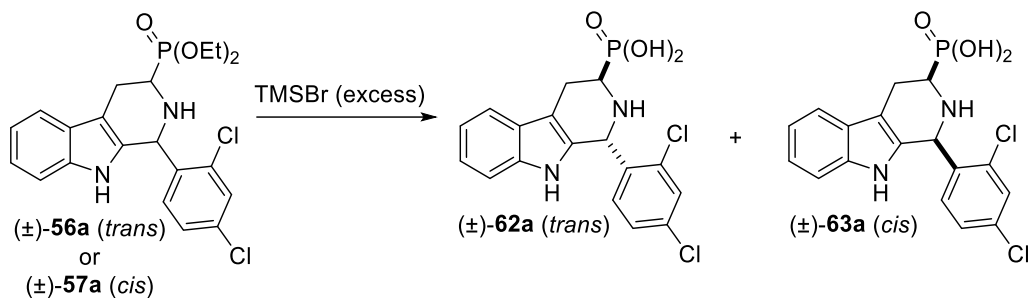


Product was not successfully isolated from any of the reactions in entries 1-4.

Entry	Reagent	Solvent	Temperature	Time	Observations from ³¹ P NMR
1	TMSBr	CH ₂ Cl ₂	RT	24 h	2.4:1 product : impurities ratio product in 1:1.9 dr (<i>trans:cis</i>)
2	TMSCl, NaBr	NMP	50 °C	24 h	no product observed starting material degraded
3	HCl (12M)	H ₂ O	RT	24 h	no product observed starting material degraded
4	HBr	AcOH	45 °C	4 d	1:2.6 product : impurities ratio product in 2:3 dr (<i>trans:cis</i>)

Another monitoring option was to observe the reaction progress in ^1H and/or ^{31}P NMR (Figure 3.14).³⁰ To explore this monitoring method, the reaction most suitable for carrying out in deuterated solvent was selected to be the one with TMSBr (Table 3.10, Entry 1). Optimization of the hydrolysis reaction was performed on the *cis* diastereomer (\pm)-**57a** (Table 3.11, Entries 1-3). When the optimized conditions were applied to the *trans* diastereomer (\pm)-**56a**, epimerization was observed, resulting in *trans*- (\pm)-**62a** and *cis*- (\pm)-**63a** hydrolyzed products (Table 3.11, Entries 4-5). In retrospect, non-negligible amounts of *trans* product (\pm)-**62a** were found in NMR spectra of *cis* compound (\pm)-**57a** reacted in CDCl_3 (Table 3.11, Entry 2). When the *trans* diethylphosphonate (\pm)-**56a** was hydrolyzed in CDCl_3 , the *trans* product (\pm)-**62a** was obtained in significant excess (dr [**62a**:**63a**] = 96:4) (Table 3.11, Entry 6). In all cases, the products (\pm)-**62a** and (\pm)-**63a** were isolated in quantitative yield by in vacuo concentration from methanol.

Table 3.11 Hydrolysis of (\pm)-**56a** /(\pm)-**57a** with TMSBr monitored by ^1H and ^{31}P NMR.



Entry	Substrate	Solvent	Temperature	Time	dr (61a : 62a)
1	(\pm)- 57a	CDCl_3	RT	48 h	incomplete conversion
2	(\pm)- 57a	CDCl_3	45 – 55 °C	27 h	77:23
3	(\pm)- 57a	CD_3CN	45 – 55 °C	8 h	3:97
4	(\pm)- 56a	CD_3CN	RT	12 h	83:17
5	(\pm)- 56a	CD_3CN	45 – 55 °C	8 h	83:17
6	(\pm)- 56a	CDCl_3	40 – 50 °C	48 h	96:4

The majority of ^1H NMR signals are broad throughout the de-ethylation process and thus not easy to interpret, but the ^{31}P NMR offers valuable insights into the reaction mechanism (Figure

3.14) and the epimerization process (Figure 3.15). In Figure 3.14, which depicts reaction from Table 3.11, Entry 6, we can see that the coordination of TMS to the diethyl phosphonate of (\pm)-**56a** (**A**) occurs nearly instantaneously and results in ~ 10 ppm upfield shift due to deshielding of the phosphorus. The two diastereomeric mono-deethylated species (**B**) appear as signals close to 5 ppm, and the fully deethylated bis-TMS ester (**C**) can be found around -1 ppm. ^1H NMR, on the other hand, clearly shows the formation of ethyl bromide and the disappearance of P-O-Et signals. The stereochemistry of *trans*- product (\pm)-**62a** was confirmed by 1D NOE.

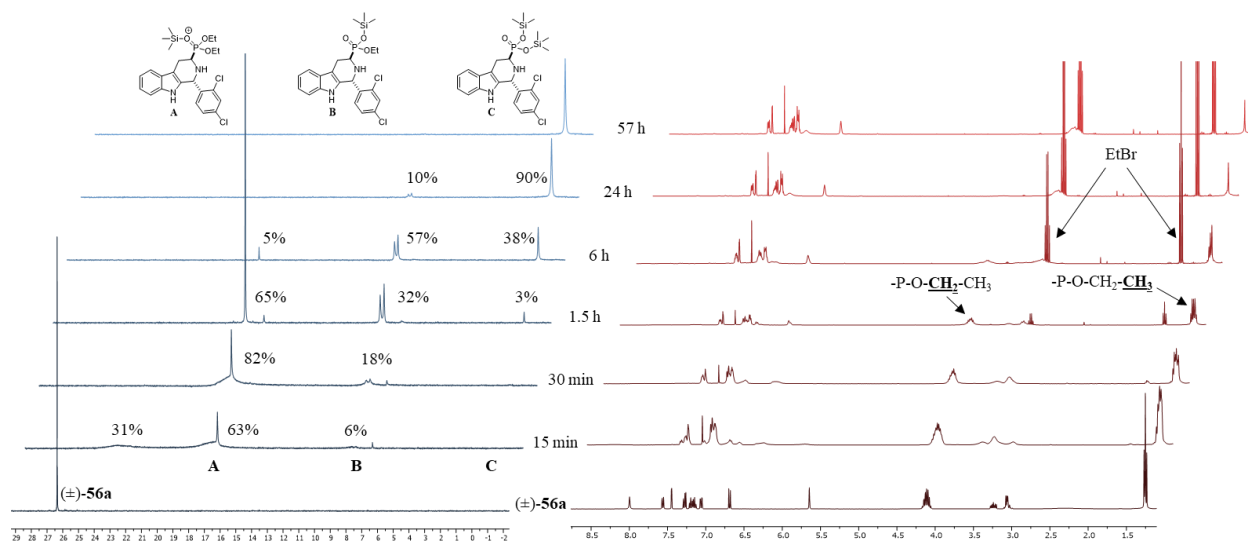


Figure 3.14 Monitoring of reaction between (\pm)-**56a** and TMSBr in CDCl_3 (Table 3.1, Entry 6) via ^{31}P NMR (left) and ^1H NMR (right). In the ^1H NMR, the formation of ethyl bromide is readily apparent.

The epimerization observed in CDCl_3 for *cis*- (\pm)-**63a** and in CD_3CN for *trans*- (\pm)-**62a** (Table 3.11, Entries 2, 4, and 5) can most likely be attributed to C1-N2 bond cleavage (Scheme 3.7) due to acidic environment caused by TMSBr. The solvation in acetonitrile seems to favor the *cis*- diastereomer (\pm)-**63a**, while the *trans*- diastereomer (\pm)-**62a** is preferred in chloroform (Figure 3.15A). Even though both aforementioned solvents are considered aprotic, chloroform is known to be capable of both hydrogen and halogen bonding, and acetonitrile, with its considerable dielectric moment, can exert strong dipole interactions.⁹⁰ It is possible that the variability in

solvent-solute interactions between CD₃CN and CDCl₃ results in the opposite thermodynamic preference for the final product. This can be experimentally confirmed by conducting the diethyl phosphonate hydrolysis under thermodynamic conditions in both CD₃CN and CDCl₃. Heating of *cis*- (±)-**57a** in CD₃CN resulted in retention of stereochemistry (dr = 97:3 *cis:trans*), while *trans*- (±)-**56a** yielded a mixture of *cis*- ((±)-**63a**) and *trans*- ((±)-**62a**) products (dr = 17:83 *cis:trans*, Table 3.11, Entries 3 and 5, Figure 3.15 A-1 and A-2, respectively) under the same conditions. On the other hand, heating of *cis*- (±)-**57a** and *trans*- (±)-**56a** in CDCl₃ led to a noticeable inversion of configuration in *cis*- but retention of stereochemistry in *trans*- (Table 3.11, Entries 2 and 6, Figure 3.15 A-3 and A-4, respectively). To further test thermodynamic preference for *trans*- configuration in CDCl₃, a sample of *cis*- (±)-**57a** was allowed to equilibrate at room temperature in CDCl₃ for seven days. The diastereomeric ratio of *cis:trans* de-ethylated species was 71:29. The mixture was then heated to 60 °C, and after 28 hours, the *cis*- diastereomer was no longer detectable by ³¹P NMR (Figure 3.15B).

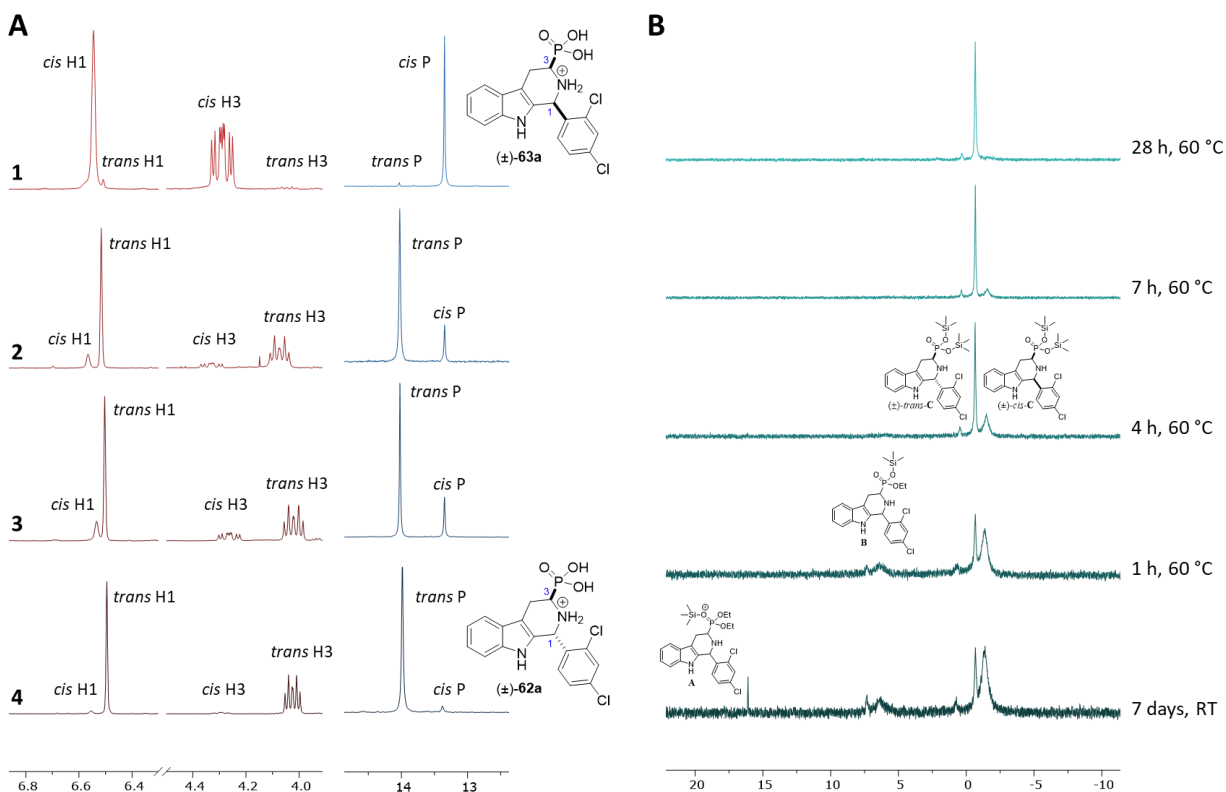


Figure 3.15 Solvent related stereochemical preference seen in the hydrolysis of (\pm)-56a and (\pm)-57a **A**: Comparison of hydrolyzed products from reactions shown in Table 3.11 and extent of epimerization under various conditions. Depicted spectra are taken in CD₃OD. **A-1** corresponds to Entry 3 of Table 3.11, where *cis* stereochemistry of starting material is mostly retained when reacted in CD₃CN. **A-2** corresponds to Entry 5 of Table 3.11, where *trans* configured starting material shows significant epimerization to its *cis* isomer when reacted in CD₃CN. **A-3** corresponds to Entry 2 of Table 3.11, where *cis* configured starting material shows significant epimerization to its *trans* counterpart when reacted in CDCl₃. **A-4** corresponds to Entry 6 of Table 3.11, where *trans* stereochemistry of starting material is mostly retained when reacted in CDCl₃. **B**: Epimerization of *cis* product of deethylation reaction in CDCl₃ into the *trans* stereoisomer by heating confirms thermodynamic preference of *trans* product in CDCl₃.

The growth inhibition potency of (\pm)-62a (de = 92%) against the Dd2 strain of *P. falciparum* was evaluated in the laboratory of Prof. Cassera, and unfortunately, the IC₅₀ was determined to be >10,000 nM. However, it is not clear if the lack of potency derives from a failure to inhibit *Pf*lspD or the inability of the negatively charged (\pm)-62a to pass through cellular membranes into the apicoplast.

3.5 Conclusions

Both the tetrazole (*trans*-**23a**) and the phosphonic acid bioisosteres (\pm)-**62a** of compound **1a** were successfully synthesized in predominantly *trans*- stereochemistry (>98% and 96:4 dr, respectively, as determined by $^1\text{H NMR}$). Unfortunately, neither compound *trans*-**23a** nor (\pm)-**62a** showed a satisfactory inhibition potency when tested against the Dd2 strain of *P. falciparum*.

References

1. Ballatore, C.; Huryn, D. M.; Smith, A. B., Carboxylic Acid (Bio)Isosteres in Drug Design. **2013**, *8* (3), 385-395.
2. Ferri, M.; Alunno, M.; Greco, F. A.; Mammoli, A.; Saluti, G.; Carotti, A.; Sardella, R.; Macchiarulo, A.; Camaioni, E.; Liscio, P., Fragment based drug design and diversity-oriented synthesis of carboxylic acid isosteres. *Bioorg. Med. Chem.* **2020**, *28* (22), 115731.
3. Silverman, R. B.; Holladay, M. W., Receptors. In *The Organic Chemistry of Drug Design and Drug Action (Third Edition)*, Silverman, R. B.; Holladay, M. W., Eds. Academic Press: Boston, 2014; pp 123-163.
4. Bazzini, P.; Wermuth, C. G., Substituent Groups. In *The Practice of Medicinal Chemistry (Fourth Edition)*, Wermuth, C. G.; Aldous, D.; Raboisson, P.; Rognan, D., Eds. Academic Press: San Diego, 2008; pp 319-357.
5. Yeh, E.; DeRisi, J. L., Chemical Rescue of Malaria Parasites Lacking an Apicoplast Defines Organelle Function in Blood-Stage *Plasmodium falciparum*. *PLoS Biol.* **2011**, *9* (8), e1001138.
6. Wiley, J. D.; Merino, E. F.; Krai, P. M.; McLean, K. J.; Tripathi, A. K.; Vega-Rodríguez, J.; Jacobs-Lorena, M.; Klemba, M.; Cassera, M. B., Isoprenoid Precursor Biosynthesis Is the Essential Metabolic Role of the Apicoplast during Gametocytogenesis in *Plasmodium falciparum*. *Eukaryotic Cell* **2015**, *14* (2), 128-139.
7. Spangenberg, T.; Burrows, J. N.; Kowalczyk, P.; McDonald, S.; Wells, T. N.; Willis, P., The open access malaria box: a drug discovery catalyst for neglected diseases. *PloS One* **2013**, *8* (6), e62906.
8. Bowman, J. D.; Merino, E. F.; Brooks, C. F.; Striepen, B.; Carlier, P. R.; Cassera, M. B., Antiapicoplast and Gametocytocidal Screening To Identify the Mechanisms of Action of Compounds within the Malaria Box. *Antimicrob. Agents Chemother.* **2014**, *58* (2), 811-819.
9. Yao, Z.-K.; Krai, P. M.; Merino, E. F.; Simpson, M. E.; Slobodnick, C.; Cassera, M. B.; Carlier, P. R., Determination of the active stereoisomer of the MEP pathway-targeting antimalarial agent MMV008138, and initial structure-activity studies. *Bioorg. Med. Chem. Lett.* **2015**, *25* (7), 1515-1519.
10. Hall Jr, H., Correlation of the base strengths of amines1. *J. Am. Chem. Soc.* **1957**, *79* (20), 5441-5444.
11. Llinas, A.; Glen, R. C.; Goodman, J. M., Solubility challenge: can you predict solubilities of 32 molecules using a database of 100 reliable measurements? *J. Chem. Inf. Model.* **2008**, *48* (7), 1289-1303.
12. Eftink, M. R.; Jia, J.; Hu, D.; Ghiron, C. A., Fluorescence studies with tryptophan analogs: excited state interactions involving the side chain amino group. *J. Phys. Chem.* **1995**, *99* (15), 5713-5723.
13. Hamborg, E. S.; Niederer, J. P.; Versteeg, G. F., Dissociation constants and thermodynamic properties of amino acids used in CO₂ absorption from (293 to 353) K. *J. Chem. Eng. Data* **2007**, *52* (6), 2491-2502.
14. Kudelko, A.; Zieliński, W.; Ejsmont, K., The reaction of optically active α -aminocarboxylic acid hydrazides with triethyl orthoesters. *Tetrahedron* **2011**, *67* (40), 7838-7845.

15. Li, J., Prediction of internal standards in reversed-phase liquid chromatography. *Chromatographia* **2004**, *60* (1), 63-71.
16. Kaljurand, I.; Kütt, A.; Sooväli, L.; Rodima, T.; Mäemets, V.; Leito, I.; Koppel, I. A., Extension of the self-consistent spectrophotometric basicity scale in acetonitrile to a full span of 28 p K a units: unification of different basicity scales. *J. Org. Chem.* **2005**, *70* (3), 1019-1028.
17. Fujikawa, M.; Ano, R.; Nakao, K.; Shimizu, R.; Akamatsu, M., Relationships between structure and high-throughput screening permeability of diverse drugs with artificial membranes: Application to prediction of Caco-2 cell permeability. *Bioorg. Med. Chem.* **2005**, *13* (15), 4721-4732.
18. Choi-Sledeski, Y. M.; Wermuth, C. G., Designing Prodrugs and Bioprecursors. In *The Practice of Medicinal Chemistry (Fourth Edition)*, Wermuth, C. G.; Aldous, D.; Raboisson, P.; Rognan, D., Eds. Academic Press: San Diego, 2015; pp 657-696.
19. Ghavami, M. Antimalarial Agents: New Mechanisms of Action for Old and New Drugs. Virginia Polytechnic Institute and State University, Blacksburg, VA, 2018.
20. Liu, L. MMV008138 and analogs: potential novel antimalarial agents for *P. falciparum*. Virginia Polytechnic Institute and State University, Blacksburg, VA, 2018.
21. Ghavami, M.; Merino, E. F.; Yao, Z.-K.; Elahi, R.; Simpson, M. E.; Fernández-Murga, M. L.; Butler, J. H.; Casasanta, M. A.; Krai, P. M.; Totrov, M. M.; Slade, D. J.; Carlier, P. R.; Cassera, M. B., Biological Studies and Target Engagement of the 2-C-Methyl-D-Erythritol 4-Phosphate Cytidylyltransferase (IspD)-Targeting Antimalarial Agent (1*R*,3*S*)-MMV008138 and Analogs. *ACS Infect. Dis.* **2018**, *4* (4), 549-559.
22. Lassila, T.; Hokkanen, J.; Aatsinki, S.-M.; Mattila, S.; Turpeinen, M.; Tolonen, A., Toxicity of Carboxylic Acid-Containing Drugs: The Role of Acyl Migration and CoA Conjugation Investigated. *Chem. Res. Toxicol.* **2015**, *28* (12), 2292-2303.
23. Silverman, R. B.; Holladay, M. W., Drug Metabolism. In *The Organic Chemistry of Drug Design and Drug Action (Third Edition)*, Silverman, R. B.; Holladay, M. W., Eds. Academic Press: Boston, 2014; pp 357-422.
24. Kalgutkar, A. S.; Scott Daniels, J., Carboxylic Acids and their Bioisosteres. In *Metabolism, Pharmacokinetics and Toxicity of Functional Groups: Impact of Chemical Building Blocks on ADMET*, The Royal Society of Chemistry: 2010; pp 99-167.
25. Herr, R. J., 5-Substituted-1*H*-tetrazoles as Carboxylic Acid Isosteres: Medicinal Chemistry and Synthetic Methods. *Bioorg. Med. Chem.* **2002**, *10* (11), 3379-3393.
26. Langmuir, I., Isomorphism, Isosterism and Covalence. *J. Am. Chem. Soc.* **1919**, *41* (10), 1543-1559.
27. Ciapetti, P.; Giethlen, B., Molecular Variations Based on Isosteric Replacements. In *The Practice of Medicinal Chemistry (Fourth Edition)*, Wermuth, C. G.; Aldous, D.; Raboisson, P.; Rognan, D., Eds. Academic Press: San Diego, 2008; pp 181-241.
28. Thornber, C. W., Isosterism and Molecular Modification in Drug Design. *Chem. Soc. Rev.* **1979**, *8* (4), 563-580.
29. Lassalas, P.; Gay, B.; Lasfargeas, C.; James, M. J.; Tran, V.; Vijayendran, K. G.; Brunden, K. R.; Kozlowski, M. C.; Thomas, C. J.; Smith, A. B.; Huryn, D. M.; Ballatore, C., Structure Property Relationships of Carboxylic Acid Isosteres. *J. Med. Chem.* **2016**, *59* (7), 3183-3203.
30. Sevrain, C. M.; Berchel, M.; Couthon, H.; Jaffrès, P.-A., Phosphonic acid: preparation and applications. *Beilstein J. Org. Chem.* **2017**, *13*, 2186-2213.

31. Kukhar, V. P.; Romanenko, V. D., Chemistry of Aminophosphonic Acids and Phosphonopeptides. In *Amino Acids, Peptides and Proteins in Organic Chemistry*, pp 189-260.
32. Freedman, L. D.; Doak, G., The preparation and properties of phosphonic acids. *Chem. Rev.* **1957**, 57 (3), 479-523.
33. Chaberek Jr, S.; Martell, A., Stability of metal chelates. I. Iminodiacetic and iminodipropionic acids. *J. Am. Chem. Soc.* **1952**, 74 (20), 5052-5056.
34. Chen, Z.; He, W.; Beer, M.; Megharaj, M.; Naidu, R., Speciation of glyphosate, phosphate and aminomethylphosphonic acid in soil extracts by ion chromatography with inductively coupled plasma mass spectrometry with an octopole reaction system. *Talanta* **2009**, 78 (3), 852-856.
35. Rumble, J. R.; Bruno, T. J.; Doa, M., *CRC handbook of chemistry and physics : a ready-reference book of chemical and physical data*. 2020.
36. Wiesner, J.; Ortmann, R.; Jomaa, H.; Schlitzer, M., New Antimalarial Drugs. *Angew. Chem., Int. Ed.* **2003**, 42 (43), 5274-5293.
37. Enders, D.; Shilvock, J. P., Some recent applications of α -amino nitrile chemistry. *Chem. Soc. Rev.* **2000**, 29 (5), 359-373.
38. Overman, L. E.; Robichaud, A. J., Total Syntheses of (+)-Geissoschizine, (\pm)-Geissoschizine, and (\pm)-(*Z*)-Isositsirikine. Stereocontrolled Synthesis of Exocyclic Double Bonds by Stereospecific Iminium Ion-Vinylsilane Cyclizations. *J. Am. Chem. Soc.* **1989**, 111 (1), 300-308.
39. Duncia, J. V.; Pierce, M. E.; Santella, J. B., Three Synthetic Routes to a Sterically Hindered Tetrazole. A New One-Step Mild Conversion of an Amide into a Tetrazole. *J. Org. Chem.* **1991**, 56 (7), 2395-2400.
40. Bailey, P. D.; McLay, N. R., Use of the Kinetically Controlled Pictet–Spengler Reaction in the Asymmetric Synthesis of Indole Alkaloids: Formal Syntheses of (–)-Ajmaline, (–)-Koumine, (–)-Taberpsychine, (–)-Koumidine and (–)-Suavoline. *J. Chem. Soc., Perkin Trans. 1* **1993**, (4), 441-449.
41. Bailey, P. D.; Cochrane, P. J.; Lorenz, K.; Collier, I. D.; Pearson, D. P. J.; Rosair, G. M., A concise, efficient route to fumitremorgins. *Tetrahedron Lett.* **2001**, 42 (1), 113-115.
42. Brokamp, R.; Bergmann, B.; Müller, I. B.; Bienz, S., Stereoselective preparation of pyridoxal 1,2,3,4-tetrahydro- β -carboline derivatives and the influence of their absolute and relative configuration on the proliferation of the malaria parasite *Plasmodium falciparum*. *Bioorg. Med. Chem.* **2014**, 22 (6), 1832-1837.
43. Vavsari, V. F.; Dianati, V.; Ramezanpour, S.; Balalaie, S., Stereoselective Synthesis of Functionalized Tetrahydro- β -Carbolines via Pictet–Spengler Reaction. *Synlett* **2015**, 26 (14), 1955-1960.
44. Alberch, L.; Bailey, Patrick D.; Clingan, Paul D.; Mills, Timothy J.; Price, Richard A.; Pritchard, Robin G., The *cis*-Specific Pictet–Spengler Reaction. *Eur. J. Org. Chem.* **2004**, 2004 (9), 1887-1890.
45. Xiao, S.; Lu, X.; Shi, X.-X.; Sun, Y.; Liang, L.-L.; Yu, X.-H.; Dong, J., Syntheses of chiral 1,3-disubstituted tetrahydro- β -carbolines via CIAT process: highly stereoselective Pictet–Spengler reaction of D-tryptophan ester hydrochlorides with various aldehydes. *Tetrahedron: Asymmetry* **2009**, 20 (4), 430-439.
46. Meng, T.-Z.; Shi, X.-X.; Qu, H.-Y.; Zhang, Y.; Huang, Z.-S.; Fan, Q.-Q., Highly diastereoselective crystallization-induced asymmetric transformation of 1,3-disubstituted-tetrahydro- β -carbolines in water. *RSC Adv.* **2017**, 7 (75), 47753-47757.

47. Soerens, D.; Sandrin, J.; Ungemach, F.; Mokry, P.; Wu, G. S.; Yamanaka, E.; Hutchins, L.; DiPierro, M.; Cook, J. M., Study of the Pictet-Spengler Reaction in Aprotic Media: Synthesis of the β -Galactosidase Inhibitor, Pyridindolol. *J. Org. Chem.* **1979**, *44* (4), 535-545.
48. Ungemach, F.; DiPierro, M.; Weber, R.; Cook, J. M., Stereospecific synthesis of trans-1,3-disubstituted-1,2,3,4-tetrahydro β -carbolines. *Tetrahedron Lett.* **1979**, *20* (35), 3225-3228.
49. Cook, J.; Zhang, L.-h., *Pictet-Spengler Reactions in Aprotic Media. N_b-Benzyl Promoted Retention of Optical Activity in the Synthesis of an Indole Substituted Azabicyclo[3.3.1]nonane, a Key Template for the Synthesis of Macroline Alkaloids.* 1988; Vol. 27.
50. Bailey, P. D.; Hollinshead, S. P.; McLay, N. R.; Morgan, K.; Palmer, S. J.; Prince, S. N.; Reynolds, C. D.; Wood, S. D., Diastereo- and Enantio-selectivity in the Pictet-Spengler Reaction. *J. Chem. Soc., Perkin Trans. I* **1993**, (4), 431-439.
51. Cox, E. D.; Hamaker, L. K.; Li, J.; Yu, P.; Czerwinski, K. M.; Deng, L.; Bennett, D. W.; Cook, J. M.; Watson, W. H.; Krawiec, M., Enantiospecific Formation of *Trans* 1,3-Disubstituted Tetrahydro- β -carbolines by the Pictet-Spengler Reaction and Conversion of *Cis* Diastereomers into Their *Trans* Counterparts by Scission of the C-1/N-2 Bond. *J. Org. Chem.* **1997**, *62* (1), 44-61.
52. Zhao, S.; Liao, X.; Wang, T.; Flippen-Anderson, J.; Cook, J. M., The Enantiospecific, Stereospecific Total Synthesis of the Ring-A Oxygenated Sarpagine Indole Alkaloids (+)-Majvinine, (+)-10-Methoxyaffinisine, and (+)-N_a-Methylsarpagine, as Well as the Total Synthesis of the *Alstonia* Bisindole Alkaloid Macralstonidine. *J. Org. Chem.* **2003**, *68* (16), 6279-6295.
53. Van Linn, M. L.; Cook, J. M., Mechanistic Studies on the *Cis* to *Trans* Epimerization of Trisubstituted 1,2,3,4-Tetrahydro- β -carbolines. *J. Org. Chem.* **2010**, *75* (11), 3587-3599.
54. Ma, X.; Liu, S.; Liu, Y.; Gu, G.; Xia, C., Comparative study on catalytic hydrodehalogenation of halogenated aromatic compounds over Pd/C and Raney Ni catalysts. *Sci. Rep.* **2016**, *6* (1), 25068.
55. Ukisu, Y., Hydrogen-transfer hydrodehalogenation of aromatic halides with a silica-supported palladium catalyst in alkaline 2-propanol: comparison between brominated and chlorinated anisoles. *React. Kinet., Mech. Catal.* **2019**, *128* (1), 41-52.
56. Subramanian, V.; Knight, J. S.; Parelkar, S.; Anguish, L.; Coonrod, S. A.; Kaplan, M. J.; Thompson, P. R., Design, Synthesis, and Biological Evaluation of Tetrazole Analogs of Cl-Amidine as Protein Arginine Deiminase Inhibitors. *J. Med. Chem.* **2015**, *58* (3), 1337-1344.
57. Pícha, J.; Vaněk, V.; Buděšínský, M.; Mládková, J.; Garrow, T. A.; Jiráček, J., The development of a new class of inhibitors for betaine-homocysteine *S*-methyltransferase. *Eur. J. Med. Chem.* **2013**, *65*, 256-275.
58. Mani, P.; Singh, A. K.; Awasthi, S. K., AgNO₃ catalyzed synthesis of 5-substituted-1*H*-tetrazole via [3+2] cycloaddition of nitriles and sodium azide. *Tetrahedron Lett.* **2014**, *55* (11), 1879-1882.
59. Aureggi, V.; Franckevičius, V.; Kitching, M. O.; Ley, S. V.; Longbottom, D. A.; Oelke, A. J.; Sedelmeier, G., (*S*)-5-Pyrrolidin-2-yl-1*H*-Tetrazole. *Org. Synth.* **2003**, *85*, 72-87.
60. Leal, J. G.; Sauer, A. C.; Mayer, J. C. P.; Stefanello, S. T.; Gonçalves, D. F.; Soares, F. A. A.; Iglesias, B. A.; Back, D. F.; Rodrigues, O. E. D.; Dornelles, L., Synthesis and electrochemical and antioxidant properties of chalcogenocyanate oxadiazole and 5-heteroarylchalcogenomethyl-1*H*-tetrazole derivatives. *New J. Chem.* **2017**, *41* (13), 5875-5883.
61. Herbst, R. M.; Froberger, C. F., Synthesis of Iminotetrazoline Derivatives as Trichomonacidal and Fungicidal Agents. *J. Org. Chem.* **1957**, *22* (9), 1050-1053.

62. Finnegan, W. G.; Henry, R. A.; Lofquist, R., An Improved Synthesis of 5-Substituted Tetrazoles. *J. Am. Chem. Soc.* **1958**, *80* (15), 3908-3911.
63. Demko, Z. P.; Sharpless, K. B., Preparation of 5-Substituted 1*H*-Tetrazoles from Nitriles in Water. *J. Org. Chem.* **2001**, *66* (24), 7945-7950.
64. Demko, Z. P.; Sharpless, K. B., An Expedient Route to the Tetrazole Analogues of α -Amino Acids. *Org. Lett.* **2002**, *4* (15), 2525-2527.
65. Reactivities, Reagents, and Reactivity Charts. In *Greene's Protective Groups in Organic Synthesis*, 2014; pp 1263-1332.
66. Saiga, Y.; Iijima, I.; Ishida, A.; Miyagishima, T.; Homma, K.; Oh-Ishi, T.; Matsumoto, M.; Matsuoka, Y., Synthesis of 1,2,3,4-Tetrahydro- β -carboline Derivatives as Hepatoprotective Agents. III. Introduction of Substituents onto Methyl 1,2,3,4-Tetrahydro- β -carboline-2-carbodithioate. *Chem. Pharm. Bull.* **1987**, *35* (8), 3284-3291.
67. Xiao, S.; Shi, X.-X.; Xing, J.; Yan, J.-J.; Liu, S.-L.; Lu, W.-D., Synthesis of tadalafil (Cialis) from L-tryptophan. *Tetrahedron: Asymmetry* **2009**, *20* (18), 2090-2096.
68. Lawrence, S. A., *Amines: Synthesis, Properties and Applications*. Cambridge University Press: 2004; p 371.
69. Navarro-Vázquez, A.; Cobas, J. C.; Sardina, F. J.; Casanueva, J.; Díez, E., A Graphical Tool for the Prediction of Vicinal Proton-Proton $^3J_{HH}$ Coupling Constants. *J. Chem. Inf. Comput. Sci.* **2004**, *44* (5), 1680-1685.
70. Ezawa, T.; Kawashima, Y.; Noguchi, T.; Jung, S.; Imai, N., Amidation of carboxylic acids via the mixed carbonic carboxylic anhydrides and its application to synthesis of antidepressant (1*S*,2*R*)-tranylcypromine. *Tetrahedron: Asymmetry* **2017**, *28* (12), 1690-1699.
71. Protection for the Amino Group. In *Greene's Protective Groups in Organic Synthesis*, 2014; pp 895-1193.
72. Schon, I.; Szirtes, T.; Überhardt, T.; Rill, A.; Csehi, A.; Hegedus, B., Reexamination of sodium-liquid ammonia reduction in the peptide chemistry. *Int. J. Pept. Protein Res.* **1983**, *22* (1), 92-109.
73. Williams, R. M.; Sinclair, P. J.; Zhai, D.; Chen, D., Practical Asymmetric Syntheses of α -Amino Acids through Carbon-Carbon Bond Constructions on Electrophilic Glycine Templates. *J. Am. Chem. Soc.* **1988**, *110* (5), 1547-1557.
74. Mackenzie, K.; Kopinke, F.-D.; Remmler, M., Reductive destruction of halogenated hydrocarbons in liquids and solids with solvated electrons. *Chemosphere* **1996**, *33* (8), 1495-1513.
75. Sun, G.-R.; He, J.-B.; Pittman, C. U., Destruction of halogenated hydrocarbons with solvated electrons in the presence of water. *Chemosphere* **2000**, *41* (6), 907-916.
76. Ihara, M.; Taniguchi, N.; Noguchi, K.; Fukumoto, K.; Kametani, T., Total Synthesis of Hydrocinchonidine and Hydrocinchonine via Photo-oxygenation of an Indole Derivative. *J. Chem. Soc., Perkin Trans. 1* **1988**, (5), 1277-1281.
77. Lott, R. S.; Chauhan, V. S.; Stammer, C. H., Trimethylsilyl Iodide as a Peptide Deblocking Agent. *J. Chem. Soc., Chem. Commun.* **1979**, (11), 495-496.
78. Liu, Y.-S.; Zhao, C.; Bergbreiter, D. E.; Romo, D., Simultaneous Deprotection and Purification of BOC-amines Based on Ionic Resin Capture. *J. Org. Chem.* **1998**, *63* (10), 3471-3473.
79. Subotkowski, W. a. K., Janusz and Tyka, Roman and Mastalerz, Przemyslaw, The phosphonic analog of tryptophan. *Pol. J. Chem.* **1981**, *55* (4), 853-857.

80. Rogers, R. S.; Stern, M. K., An Improved Synthesis of the Phosphonic Acid Analog of Tryptophan. *Synlett* **1992**, 1992 (09), 708-708.
81. Viveros-Ceballos, J. L.; Sayago, F. J.; Cativiela, C.; Ordóñez, M., First Practical and Efficient Synthesis of 3-Phosphorylated β -Carboline Derivatives Using the Pictet–Spengler Reaction. *Eur. J. Org. Chem.* **2015**, 2015 (5), 1084-1091.
82. Pretsch, E.; Bühlmann, P.; Badertscher, M., ^{13}C NMR Spectroscopy. In *Structure Determination of Organic Compounds: Tables of Spectral Data*, Springer Berlin Heidelberg: Berlin, Heidelberg, 2009; pp 1-88.
83. Demir, A. S.; Tanyeli, C.; Şeşenoğlu, Ö.; Demic, Ş.; Evin, Ö. Ö., A simple synthesis of 1-aminophosphonic acids from 1-hydroxyiminophosphonates with NaBH_4 in the presence of transition metal compounds. *Tetrahedron Lett.* **1996**, 37 (3), 407-410.
84. Guo, Y.-C.; Li, J.; Ma, J.-L.; Yu, Z.-R.; Wang, H.-W.; Zhu, W.-J.; Liao, X.-C.; Zhao, Y.-F., Synthesis and antitumor activity of α -aminophosphonate derivatives containing thieno[2,3-d]pyrimidines. *Chin. Chem. Lett.* **2015**, 26 (6), 755-758.
85. McDonald, S. L., Copper-Catalyzed α -Amination of Phosphonates and Phosphine Oxides: A Direct Approach to α -Amino Phosphonic Acids and Derivatives. In *Copper-Catalyzed Electrophilic Amination of sp^2 and sp^3 C–H Bonds*, Springer International Publishing: Cham, 2016; pp 61-95.
86. Pettersen, D.; Marcolini, M.; Bernardi, L.; Fini, F.; Herrera, R. P.; Sgarzani, V.; Ricci, A., Direct Access to Enantiomerically Enriched α -Amino Phosphonic Acid Derivatives by Organocatalytic Asymmetric Hydrophosphonylation of Imines. *Journal of Organic Chemistry* **2006**, 71 (16), 6269-6272.
87. Ramakrishna, K.; Thomas, J. M.; Sivasankar, C., A Green Approach to the Synthesis of α -Amino Phosphonate in Water Medium: Carbene Insertion into the N–H Bond by Cu(I) Catalyst. *J. Org. Chem.* **2016**, 81 (20), 9826-9835.
88. Fakhraian, H.; Mirzaei, A., Reconsideration of the Base-Free Batch-Wise Esterification of Phosphorus Trichloride with Alcohols. *Organic Process Research & Development* **2004**, 8 (3), 401-404.
89. Green, D.; Patel, G.; Elgendy, S.; Baban, J. A.; Claeson, G.; Kakkar, V. V.; Deadman, J., The Facile Synthesis of *O,O*-Dialkyl 1-Aminoalkanephosphonates. *Tetrahedron Lett.* **1993**, 34 (43), 6917-6920.
90. Davis, M. M., *Acid-base behavior in aprotic organic solvents*. U.S. National Bureau of Standards: Washington, D.C., 1968.

4 Experimental

4.1 General

Compounds were purchased from Sigma-Aldrich, Fisher Scientific, Alfa Aesar, Astatech, Enamine, Combi-blocks, Oakwood Chemicals, and Cambridge Chemicals and were used without purification unless stated otherwise. NMR spectra were performed on 400 MHz, 500 MHz, or 600 MHz instruments. ^{13}C NMR spectra were correspondingly recorded at 101 MHz, 126 MHz, or 151 MHz. ^{19}F NMR spectra were correspondingly recorded at 376 MHz or 471 MHz. ^{31}P NMR spectra were recorded at 162 MHz or 202 MHz. Chemical shifts for ^1H and ^{13}C are presented in ppm against tetramethylsilane with an internal standard as a reference. Chemical shifts for ^{31}P NMR are presented in ppm against triphenylphosphine oxide as an internal standard (-6.00 ppm). The chemical shifts are reported in δ (ppm), and coupling constants are given in Hz. Deuterated solvents were purchased from Cambridge Isotope Laboratories. High-resolution mass spectroscopy (HRMS) was performed on an Agilent 6220 LC/MS time-of-flight mass spectrometer using either electrospray ionization (ESI). Optical rotation was performed on a Jasco P-2000 digital polarimeter using a cylindrical glass cell (3.5 mm D x 100 mm L). Column chromatography was performed by using flash grade silica gel (SiO_2 , 32-63 μm). Thin layer chromatography (TLC) was performed on Sorbtech Silica XG TLC plates w/UV254.

Compounds prepared for bioassays were >95% pure as judged by ^1H , ^{13}C , ^{19}F , and ^{31}P NMR unless otherwise stated.

Computational

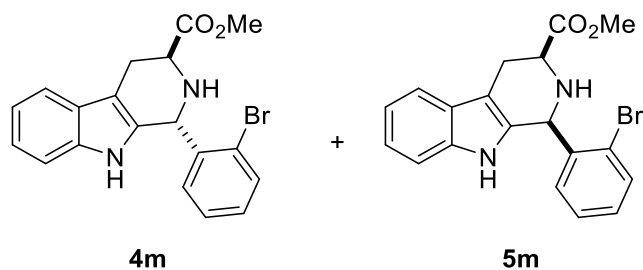
To extensively probe the conformational space available to compounds **4a**, **4b**, **5a**, and **5b**, automated conformer searches (MMFF94) were performed using Spartan '16,¹ starting from at least two different geometries. These MMFF94 minima were then optimized at B3LYP/6-31G(d)

using Gaussian 09,² giving the numbers of conformers listed in Table 2.5. In each case, vibrational frequency analysis (NIMAG=0) confirmed that each stationary point was a minimum. Individual conformers of **4a**, **4b**, **5a**, and **5b** are identified in Chapter 5 as **4a-01** to **4a-16**, **4b-01** to **4b-08**, **5a-01** to **5a-14**, **5b-01** to **5b-08**, respectively. Single point energies of each conformer were calculated with three different functionals and larger basis sets, as described above: B3LYP/6-311+G(2d,p), mPW1PW91/6-311+G(2d,p) and M06-2X/def2-TZVP each with implicit solvation SCRF=(PCM,Solvent=Chloroform). Free energies were calculated by adding the free energy (298 K) corrections derived from unscaled B3LYP/6-31G(d) frequencies to these single point energies, to derive the corresponding Boltzmann distributions. The overall population of each of the eight conformational ensembles described in Table 2.6 (and Table 5.14) was calculated by summing the Boltzmann populations of the appropriate individual conformers.

Calculated J_{HH} coupling constants shown in Table 2.7 were obtained using the B3LYP functional with core-augmented 6-31G(d,p) basis set (“6-31G(d,p)u+1s”). Note that only Fermi contact terms were evaluated, and only couplings between the hydrogen atoms of interest (H4 β , H4 α , H3, H1) were specified for calculation. This approach was selected based on its high accuracy (RMSD <0.5 Hz over a large test set) and low computational cost.³ Interestingly, although ¹H chemical shift modeling benefits from the inclusion of implicit solvation, this study demonstrated that implicit solvation does not improve the accuracy of calculated J_{HH} values;³ thus, we calculated values in the gas phase. The coupling constants (³ $J_{4\beta-3}$, ³ $J_{4\alpha-3}$, ² $J_{4\beta-4\alpha}$, ⁵ $J_{4\beta-1}$, ⁵ $J_{4\alpha-1}$) in each conformer of **4a**, **5a**, **4b**, and **5b**, (scaled by the recommend factor of 0.9117) are given in Table 5.15, which includes a sample Gaussian route section to perform these calculations. To obtain weighted average J_{HH} coupling constants, various Boltzmann distributions were applied (Table 5.16).

Shielding tensors σ for each carbon in each conformer were calculated from the B3LYP/6-31G(d) geometries at the B3LYP/6-311+G(2d,p) (PCM, CHCl₃) and mPW1PW91/6-311+G(2d,p) (PCM, CHCl₃) levels of theory. These functionals, basis set, and solvation model were selected based on their excellent performance in a recent study of the ¹H and ¹³C NMR solution spectra of colchicine.⁴ The corresponding ¹³C NMR chemical shifts were calculated according to the formula $\delta = (\sigma - b)/a$, where a = slope and b = intercept.⁵ The values of a and b were taken from the aforementioned study of colchicine,⁴ and were $a = -1.043$, $b = 181.717$ for B3LYP/6-311+G(2d,p) (PCM=CHCl₃), and $a = -1.042$, $b = 186.357$ for mPW1PW91/6-311+G(2d,p) (PCM=CHCl₃). The weighted average ¹³C chemical shifts of each carbon were then determined using the calculated Boltzmann distributions and compared to experimental chemical shifts to obtain the MAD for each compound studied.

4.2 Chapter 1 – Synthesis of D-ring variants of 1a



Methyl-1-(2-bromophenyl)-2,3,4,9-tetrahydro-1H-pyrido[3,4-b]indole-3-carboxylate:

To a mixture of L-tryptophan methyl ester hydrochloride (1.2727 g, 5.00 mmol), 4Å molecular sieves (2.5 g, powdered), and 2-bromobenzaldehyde (0.6 mL, 5.14 mmol), CH₂Cl₂ (16 mL) was added under nitrogen. The resulting mixture was stirred at room temperature for 48 hours. Next, TFA (0.77 mL, 9.99 mmol) was added dropwise. The reaction mixture was further stirred at room temperature for additional 24 hours. The reaction was cooled to 0 °C, and a saturated aqueous solution of NaHCO₃ (16 mL) was added, followed by the addition of EtOAc (16 mL). After stirring for 30 min at 0 °C, the molecular sieves were filtered, and phases of the filtrate were partitioned, and the aqueous layer was extracted with EtOAc (3 x 20 mL). The combined organic layers were washed with water and saturated aqueous NaCl solution (30 mL), dried over Na₂SO₄ and concentrated in vacuo. Compounds **4m** and **5m** were separated from the crude material by flash chromatography (5:5:1 CH₂Cl₂:hexane:EtOAc) to give **5m** (877.2 mg, 46%, first-eluting, light orange powder) and **4m** (505.7 mg, 26%, second-eluting, off-white powder).

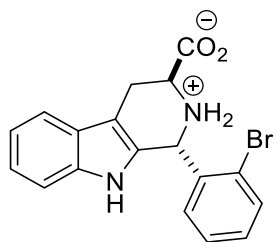
Methyl (1*R*,3*S*)-1-(2-bromophenyl)-2,3,4,9-tetrahydro-1H-pyrido[3,4-*b*]indole-3-carboxylate (**4m**):

¹H NMR (400 MHz, CDCl₃) δ 7.68 (s, 1H), 7.64 (m, 1H), 7.57 (d, *J* = 7.0 Hz, 1H), 7.27 (d, *J* = 6.0 Hz, 1H), 7.17 (dddd, *J* = 8.6, 7.1, 6.4, 1.3 Hz, 4H), 6.95 (m, 1H), 5.87 (s, 1H), 3.88 (dd, *J* =

7.8, 5.0 Hz, 1H), 3.74 (s, 3H), 3.27 (ddd, $J = 15.3, 5.0, 1.2$ Hz, 1H), 3.11 (ddd, $J = 15.3, 7.9, 1.6$ Hz, 1H). ^{13}C NMR (126 MHz, CDCl_3) δ 173.9, 140.7, 136.3, 133.4, 132.1, 130.4, 129.7, 127.6, 126.9, 124.3, 122.2, 119.7, 118.4, 111.1, 109.6, 54.2, 52.3, 52.2, 25.0.

Methyl (1*S*,3*S*)-1-(2-bromophenyl)-2,3,4,9-tetrahydro-1*H*-pyrido[3,4-*b*]indole-3-carboxylate (5*m*):

^1H NMR (400 MHz, CDCl_3) δ 7.64 (dd, $J = 7.9, 1.2$ Hz, 1H), 7.54 (m, 2H), 7.41 (dd, $J = 7.7, 1.7$ Hz, 1H), 7.28 (d, $J = 6.3$ Hz, 1H), 7.25 (s, 1H), 7.21 (ddd, $J = 8.0, 1.9, 0.6$ Hz, 1H), 7.14 (m, 2H), 5.82 (s, 1H), 4.01 (dd, $J = 11.0, 4.1$ Hz, 1H), 3.24 (ddd, $J = 15.1, 4.1, 1.7$ Hz, 2H), 3.03 (ddd, $J = 15.0, 11.0, 2.5$ Hz, 1H). ^{13}C NMR (126 MHz, CDCl_3) δ 173.1, 140.4, 136.2, 133.8, 133.0, 130.7, 130.0, 128.3, 127.0, 124.1, 122.1, 119.7, 118.3, 111.0, 109.2, 57.0, 56.7, 52.4, 25.6.



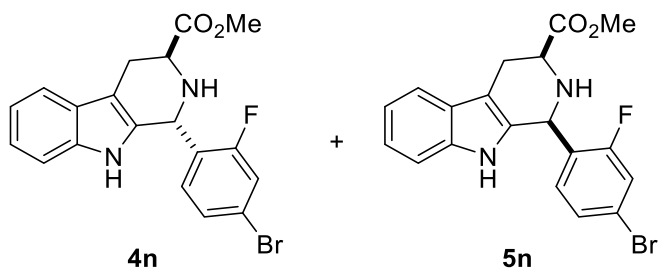
1m

(1*R*,3*S*)-1-(2-bromophenyl)-2,3,4,9-tetrahydro-1*H*-pyrido[3,4-*b*]indol-2-ium-3-carboxylate (1*m*):

A reaction vessel was charged with **4m** (137.4 mg, 0.36 mmol) and Amberlyst A26 resin (1.33 g, 5.60 mmol) under nitrogen atmosphere. Freshly distilled anhydrous THF (3.6 mL), degassed CH_3OH (3.6 mL), and degassed de-ionized water (3.6 mL) were added, and the reaction was stirred at ambient temperature for 28 hours. The reaction mixture was filtered and washed alternately with CH_3OH and CH_2Cl_2 (3x10 mL/each). The product was then cleaved from the resin with 50% (v/v) aqueous acetic acid (40 mL). Collected filtrate was concentrated in vacuo to yield 0.24g of crude

yellow glass-like solid. The crude material was purified by precipitation from CH₃OH:Et₂O:hexanes (1:10:50 mL) to yield **1m** as a light yellow powder (40.5 mg, 31% yield).

¹H NMR (400 MHz, CD₃OD) δ 7.79 (m, 1H), 7.56 (d, *J* = 7.8 Hz, 1H), 7.36 (m, 2H), 7.27 (dt, *J* = 8.1, 0.9 Hz, 1H), 7.14 (ddd, *J* = 8.2, 7.1, 1.2 Hz, 1H), 7.07 (ddd, *J* = 8.0, 7.1, 1.1 Hz, 1H), 7.00 (m, 1H), 6.36 (s, 1H), 3.92 (t, *J* = 7.2 Hz, 1H), 3.47 (dd, *J* = 16.4, 4.8 Hz, 1H), 3.21 (dd, *J* = 16.2, 8.8 Hz, 1H). ¹³C NMR (126 MHz, CD₃OD) δ 174.4, 138.7, 136.4, 134.7, 132.65, 132.64, 129.3, 128.4, 127.3, 126.6, 123.6, 120.5, 119.3, 112.3, 109.8, 55.9, 54.9, 24.2. HRMS (ESI) [M+H]⁺ calculated for C₁₈H₁₆BrN₂O₂⁺: 371.0390 Found: 371.0380.



Methyl-1-(4-bromo-2-fluorophenyl)-2,3,4,9-tetrahydro-1H-pyrido[3,4-b]indole-3-carboxylate:

To a mixture of L-tryptophan methyl ester hydrochloride (1.2741 g, 5.00 mmol), 4Å molecular sieves (2.5 g, powdered), and 4-bromo-2-fluorobenzaldehyde (1.0214 g, 5.03 mmol), CH₂Cl₂ (13 mL) was added under nitrogen. The resulting mixture was stirred at room temperature for 25 hours. TFA (0.8 mL, 10.45 mmol) was added dropwise. The reaction mixture was further stirred at room temperature for additional 72 hours. The reaction was cooled to 0 °C, and a saturated aqueous solution of NaHCO₃ (15 mL) was added, followed by the addition of EtOAc (15 mL). After stirring for 1 h at 0 °C, the molecular sieves were filtered, and phases of the filtrate were partitioned, and the aqueous layer was extracted with EtOAc (3 x 10 mL). The combined organic layers were washed with water (3 x 20 mL) and saturated aqueous NaCl solution (1 x 20 mL), dried over

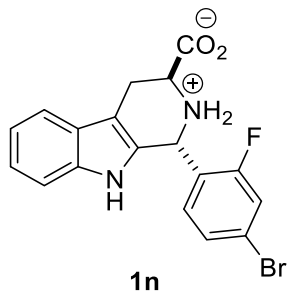
Na₂SO₄ and concentrated in vacuo. Compounds **4n** and **5n** were separated from the crude material by column chromatography (5:5:1 CH₂Cl₂:hexane:EtOAc) to give **5n** (1002.6 mg, 50%, first-eluting, yellow glass-like solid) and **4n** (361.1 mg, 17%, second-eluting, white powder).

Methyl (1R,3S)-1-(4-bromo-2-fluorophenyl)-2,3,4,9-tetrahydro-1H-pyrido[3,4-b]indole-3-carboxylate (4n):

¹H NMR (400 MHz, CDCl₃) δ 7.67 (s, 1H), 7.55 (d, *J* = 7.6 Hz, 1H), 7.32 (dd, *J* = 9.7, 1.9 Hz, 1H), 7.28 (ddd, *J* = 8.1, 1.3, 0.8 Hz, 1H), 7.16 (m, 3H), 6.92 (t, *J* = 8.1 Hz, 1H), 5.76 (s, 1H), 3.90 (dd, *J* = 7.7, 5.1 Hz, 1H), 3.74 (s, 3H), 3.24 (ddd, *J* = 15.4, 5.1, 1.2 Hz, 1H), 3.08 (ddd, *J* = 15.4, 7.7, 1.5 Hz, 1H). ¹⁹F NMR (376 MHz, CDCl₃) δ -116.34 (t, *J* = 8.8 Hz). ¹³C NMR (101 MHz, CDCl₃) δ 173.8, 160.5 (d, ¹*J*_{CF} = 251.3 Hz), 136.3, 131.2, 131.0 (d, ³*J*_{CF} = 4.6 Hz), 128.3 (d, ²*J*_{CF} = 13.7 Hz), 127.4 (d, ⁴*J*_{CF} = 3.6 Hz), 126.8, 122.3, 122.1 (d, ³*J*_{CF} = 9.7 Hz), 119.7, 119.4 (d, ²*J*_{CF} = 24.9 Hz), 118.3, 111.1, 109.5, 53.3, 52.2, 47.9 (d, ³*J*_{CF} = 3.3 Hz), 24.9.

Methyl (1S,3S)-1-(4-bromo-2-fluorophenyl)-2,3,4,9-tetrahydro-1H-pyrido[3,4-b]indole-3-carboxylate (5n):

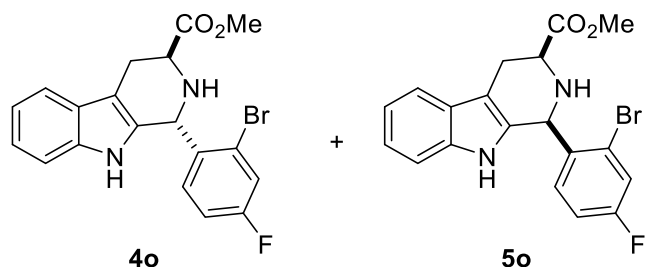
¹H NMR (400 MHz, CDCl₃) δ 7.66 (s, 1H), 7.54 (dd, *J* = 6.6, 2.3 Hz, 1H), 7.33 (dd, *J* = 9.5, 1.9 Hz, 1H), 7.25 (m, 1H), 7.22 (m, 1H), 7.14 (m, 2H), 5.62 (s, 1H), 3.96 (dd, *J* = 11.1, 4.2 Hz, 1H), 3.82 (s, 3H), 3.23 (ddd, *J* = 15.1, 4.2, 1.9 Hz, 1H), 3.00 (ddd, *J* = 15.1, 11.0, 2.5 Hz, 1H), 2.49 (s, 1H). ¹⁹F NMR (376 MHz, CDCl₃) δ -117.43 (m). ¹³C NMR (101 MHz, CDCl₃) δ 173.1, 160.7 (d, ¹*J*_{CF} = 251.0 Hz), 136.3, 133.0, 131.4 (d, ³*J*_{CF} = 4.5 Hz), 128.3 (d, ⁴*J*_{CF} = 3.5 Hz), 127.2 (d, ²*J*_{CF} = 13.0 Hz), 127.0, 122.4 (d, ³*J*_{CF} = 9.7 Hz), 122.3, 119.9, 119.4 (d, ²*J*_{CF} = 25.2 Hz), 118.3, 111.1, 109.5, 56.7, 52.5, 50.6 (d, ³*J*_{CF} = 3.4 Hz), 25.6.



(1*R*,3*S*)-1-(4-bromo-2-fluorophenyl)-2,3,4,9-tetrahydro-1*H*-pyrido[3,4-*b*]indol-2-ium-3-carboxylate (1n**):**

A reaction vessel was charged with **4n** (199.3 mg, 0.49 mmol) and Amberlyst A26 resin (1.78 g, 7.49 mmol) under nitrogen atmosphere. Freshly distilled anhydrous THF (5 mL), degassed CH₃OH (5 mL), and degassed de-ionized water (5 mL) were added, and the reaction was stirred at ambient temperature for 24 hours. The reaction mixture was filtered and washed alternately with CH₃OH and CH₂Cl₂ (5x5 mL/each). The product was then cleaved from the resin with 50% (v/v) aqueous acetic acid (37 mL). Collected filtrate was concentrated in vacuo and purified by precipitation from CH₃OH:Et₂O:hexanes (0.7:7:21 mL) to yield **1n** as a yellow powder (173.3 mg, 90% yield).

¹H NMR (400 MHz, CD₃OD) δ 7.56 (dd, *J* = 9.7, 1.9 Hz, 1H), 7.55 (dt, *J* = 7.7, 1.0 Hz, 1H), 7.38 (dd, *J* = 8.3, 1.9 Hz, 1H), 7.27 (dt, *J* = 8.2, 0.9 Hz, 1H), 7.15 (ddd, *J* = 8.2, 7.1, 1.2 Hz, 1H), 7.08 (ddd, *J* = 8.1, 7.0, 1.1 Hz, 1H), 6.97 (t, *J* = 8.1 Hz, 1H), 6.23 (s, 1H), 3.99 (dd, *J* = 8.5, 5.5 Hz, 1H), 3.47 (dd, *J* = 16.3, 5.5 Hz, 1H), 3.24 (ddd, *J* = 16.3, 8.5, 1.3 Hz, 1H). ¹⁹F NMR (376 MHz, CD₃OD) δ -115.46 (t, *J* = 8.4 Hz). ¹³C NMR (126 MHz, MeOD) δ 173.7, 162.4 (d, ¹*J*_{CF} = 253.6 Hz), 138.7, 133.7, 133.6, 129.4 (d, *J* = 3.7 Hz), 127.3, 125.71 (d, ³*J*_{CF} = 9.9 Hz), 123.8, 123.5 (d, ²*J*_{CF} = 13.0 Hz), 120.8 (d, ²*J*_{CF} = 25.3 Hz), 120.6, 119.3, 112.3, 109.6, 55.1, 24.0. One resonance in the aliphatic region is missing, likely due to overlap with solvent signal at 49.0 ppm.



Methyl-1-(2-bromo-4-fluorophenyl)-2,3,4,9-tetrahydro-1*H*-pyrido[3,4-*b*]indole-3-

carboxylate:

To a mixture of L-tryptophan methyl ester hydrochloride (1.2726 g, 5.00 mmol), 4Å molecular sieves (2.5 g, powdered), and 2-bromobenzaldehyde (1.0173 g, 5.01 mmol), CH₂Cl₂ (15 mL) was added under nitrogen. The resulting mixture was stirred at room temperature for 38 hours. Next, TFA (0.8 mL, 10.45 mmol) was added dropwise. The reaction mixture was further stirred at room temperature for additional 72 hours. The reaction was cooled to 0 °C, and a saturated aqueous solution of NaHCO₃ (15 mL) was added, followed by the addition of EtOAc (15 mL). After stirring for 30 min at 0 °C, the molecular sieves were filtered, and phases of the filtrate were partitioned, and the aqueous layer was extracted with EtOAc (3 x 10 mL). The combined organic layers were washed with water (3 x 20 mL) and saturated aqueous NaCl solution (1 x 20 mL), dried over Na₂SO₄ and concentrated in vacuo. Compounds **4o** and **5o** were separated from the crude material by column chromatography (5:5:2 CH₂Cl₂:hexane:EtOAc) to give **5o** (780 mg, 39%, first-eluting, off-white powder) and **4o** (272.1 mg, 14%, second-eluting, white powder).

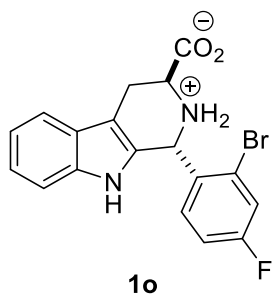
Methyl (1*R*,3*S*)-1-(2-bromo-4-fluorophenyl)-2,3,4,9-tetrahydro-1*H*-pyrido[3,4-*b*]indole-3-carboxylate (4o**):**

¹H NMR (400 MHz, CDCl₃) δ 7.71 (s, 1H), 7.57 (d, *J* = 6.9 Hz, 1H), 7.38 (dd, *J* = 8.1, 2.5 Hz, 1H), 7.26 (m, 1H), 7.17 (m, 2H), 6.92 (m, 2H), 5.82 (s, 1H), 3.85 (dd, *J* = 7.6, 5.0 Hz, 1H), 3.73 (s, 3H), 3.26 (ddd, *J* = 15.4, 5.1, 1.2 Hz, 1H), 3.10 (ddd, *J* = 15.3, 7.7, 1.5 Hz, 1H). ¹⁹F NMR (376

MHz, CDCl₃) δ -111.79 (td, J = 7.9, 6.4 Hz). ¹³C NMR (126 MHz, CDCl₃) δ 173.9, 162.0 (d, ¹ J_{CF} = 252.0 Hz), 136.8 (d, ⁴ J_{CF} = 3.4 Hz), 136.4, 132.0, 131.4 (d, ³ J_{CF} = 8.5 Hz), 126.9, 124.2 (d, ³ J_{CF} = 9.6 Hz), 122.4, 120.6 (d, ² J_{CF} = 24.5 Hz), 119.8, 118.5, 114.7 (d, ² J_{CF} = 20.7 Hz), 111.1, 109.6, 53.5, 52.4, 52.3, 24.9.

Methyl (1*S*,3*S*)-1-(2-bromo-4-fluorophenyl)-2,3,4,9-tetrahydro-1*H*-pyrido[3,4-*b*]indole-3-carboxylate (5o):

¹H NMR (500 MHz, CDCl₃) δ 7.60 (s, 1H), 7.55 (d, J = 7.0 Hz, 1H), 7.39 (m, 2H), 7.24 (dd, J = 6.9, 1.3 Hz, 1H), 7.15 (pd, J = 7.1, 1.3 Hz, 2H), 6.99 (td, J = 8.4, 2.5 Hz, 1H), 5.78 (s, 1H), 4.00 (dd, J = 11.1, 4.1 Hz, 1H), 3.83 (s, 3H), 3.25 (ddd, J = 15.0, 4.1, 1.8 Hz, 1H), 3.03 (ddd, J = 15.0, 11.1, 2.5 Hz, 1H), 2.57 (s, 1H). ¹⁹F NMR (376 MHz, CDCl₃) δ -111.18 (app q, J = 7.7 Hz). ¹³C NMR (126 MHz, CDCl₃) δ 173.1, 162.1 (d, ¹ J_{CF} = 252.1 Hz), 136.4 (br), 136.3, 133.6, 131.9 (br), 127.0, 123.8 (d, ³ J_{CF} = 9.3 Hz), 122.2, 120.1 (br), 119.8, 118.4, 115.7 (d, ² J_{CF} = 21.1 Hz), 111.1, 109.4, 56.7, 56.4 (br), 52.4, 25.5.



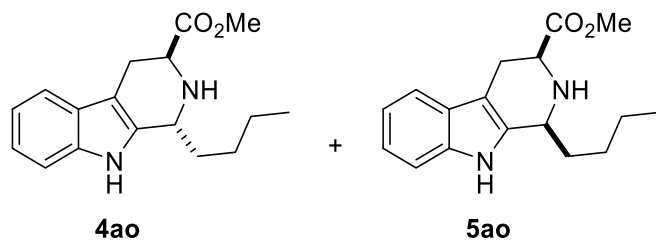
(1*R*,3*S*)-1-(2-bromo-4-fluorophenyl)-2,3,4,9-tetrahydro-1*H*-pyrido[3,4-*b*]indol-2-ium-3-carboxylate (1o):

A reaction vessel was charged with **4o** (117.7 mg, 0.29 mmol) and Amberlyst A26 resin (961 mg, 4.04 mmol) under nitrogen atmosphere. Freshly distilled anhydrous THF (2.5 mL), degassed CH₃OH (2.5 mL), and degassed de-ionized water (2.5 mL) were added, and the reaction was stirred

at ambient temperature for 23 hours. The reaction mixture was filtered and washed alternately with CH₃OH and CH₂Cl₂ (4 x 5 mL/each). The product was then cleaved from the resin with 50% (v/v) aqueous acetic acid (40 mL). Collected filtrate concentrated in vacuo to yield crude yellow glass-like solid. The crude material was purified by precipitation from CH₃OH:Et₂O:hexanes (0.5:5:15 mL) to yield **1o** as a white powder (94.2 mg, 83% yield).

¹H NMR (500 MHz, CD₃OD) δ 7.52 (m, 2H), 7.28 (d, *J* = 8.1 Hz, 1H), 7.13 (t, *J* = 7.5 Hz, 1H), 7.03 (m, 2H), 6.84 (dd, *J* = 8.7, 5.9 Hz, 1H), 5.96 (s, 1H), 3.67 (br s, 1H), 3.36 (br s, 1H), 3.05 (dd, *J* = 15.6, 9.9 Hz, 1H). ¹⁹F NMR (376 MHz, CD₃OD) δ -112.95 (br s). ¹³C NMR (126 MHz, CD₃OD) δ 163.7 (d, ¹*J*_{CF} = 251.3 Hz), 138.6, 135.9, 133.4 (d, ³*J*_{CF} = 8.9 Hz), 130.9, 127.7, 126.0 (d, ³*J*_{CF} = 9.0 Hz), 123.2, 121.5 (d, ²*J*_{CF} = 24.9 Hz), 120.2, 119.1, 115.6 (d, ²*J*_{CF} = 20.9 Hz), 112.2, 110.8, 55.3, 54.0, 25.6. The resonance for carbonyl carbon was not observed in the spectrum.

4.3 Chapter 2 – Synthesis of aliphatic Pictet-Spengler adducts



Methyl 1-butyl-2,3,4,9-tetrahydro-1H-pyrido[3,4-b]indole-3-carboxylate:

To a mixture of L-tryptophan methyl ester hydrochloride (514 mg, 2.02 mmol), 4Å molecular sieves (1 g, powdered), and pentanal (0.24 mL, 2.26 mmol), CH₂Cl₂ (6 mL) was added under nitrogen. The resulting mixture was stirred at room temperature for 24 hours. Next, TFA (0.3 mL, 3.92 mmol) was added dropwise. The reaction mixture was further stirred at room temperature for additional 48 hours. The reaction was cooled to 0 °C, and a saturated aqueous solution of NaHCO₃ (6 mL) was added, followed by the addition of EtOAc (6 mL). After stirring for 30 min at 0 °C, the molecular sieves were filtered, and phases of the filtrate were partitioned, and the aqueous layer was extracted with EtOAc (3 x 15 mL). The combined organic layers were washed with water (2 x 25 mL) and saturated aqueous NaCl solution (1 x 24 mL), dried over Na₂SO₄ and concentrated in vacuo. Following workup, **4ao** and **5ao** were separated from the crude material by flash chromatography (gradient, from 1:1 CH₂Cl₂:hexane to 2:2:1 CH₂Cl₂:hexane:EtOAc) to give **5ao** (190 mg, 33%, first-eluting, off-white solid) and **4ao** (45 mg, 8%, second-eluting, yellow oil). A mixed fraction of **4ao** and **5ao** (162 mg, 28% yield) was also obtained.

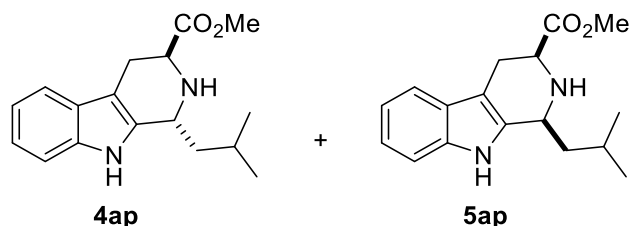
Methyl (1*R*,3*S*)-1-butyl-2,3,4,9-tetrahydro-1H-pyrido[3,4-*b*]indole-3-carboxylate (**4ao**):

¹H NMR (400 MHz, CDCl₃) δ 7.73 (s, 1H), 7.49 (ddd, *J* = 7.6, 1.4, 0.7 Hz, 1H), 7.31 (ddd, *J* = 8.0, 1.2, 0.7 Hz, 1H), 7.15 (ddd, *J* = 8.0, 7.1, 1.4 Hz, 1H), 7.10 (ddd, *J* = 7.6, 7.1, 1.1 Hz, 1H), 4.24 (dd, *J* = 8.3, 4.9 Hz, 1H), 3.99 (dd, *J* = 7.3, 5.3 Hz, 1H), 3.75 (s, 3H), 3.12 (ddd, *J* = 15.3, 5.3, 1.2

Hz, 1H), 2.99 (ddd, $J = 15.3, 7.3, 1.5$ Hz, 1H), 1.93 (s, 1H), 1.84 – 1.68 (m, 2H), 1.58 – 1.44 (m, 2H), 1.43 – 1.35 (m, 2H), 0.94 (t, $J = 7.2$ Hz, 3H). ^{13}C NMR (101 MHz, CDCl_3) δ 174.4, 136.0, 135.8, 127.2, 121.7, 119.5, 118.1, 110.8, 107.0, 52.7, 52.2, 50.4, 35.5, 28.5, 25.1, 22.9, 14.2. This compound has been reported previously without full NMR characterization.⁶

Methyl (1*S*,3*S*)-1-butyl-2,3,4,9-tetrahydro-1*H*-pyrido[3,4-*b*]indole-3-carboxylate (5ao):

^1H NMR (400 MHz, CDCl_3) δ 7.79 (s, 1H), 7.48 (d, $J = 7.7$ Hz, 1H), 7.36 – 7.30 (m, 1H), 7.16 (td, $J = 8.1, 7.6, 1.3$ Hz, 1H), 7.11 (ddd, $J = 7.6, 7.2, 1.2$ Hz, 1H), 4.20 (ddt, $J = 8.3, 4.1, 2.2$ Hz, 1H), 3.83 (s, 3H), 3.80 (dd, $J = 11.2, 4.2$ Hz, 1H), 3.13 (ddd, $J = 15.1, 4.2, 1.9$ Hz, 1H), 2.82 (ddd, $J = 15.1, 11.2, 2.6$ Hz, 1H), 2.00 – 1.91 (m, 1H), 1.72 (dddd, $J = 13.8, 10.5, 8.1, 5.2$ Hz, 1H), 1.52 – 1.44 (m, 2H), 1.39 (dddd, $J = 14.2, 8.7, 6.9, 5.4$ Hz, 2H), 0.94 (t, $J = 7.1$ Hz, 3H). ^{13}C NMR (101 MHz, CDCl_3) δ 173.9, 136.0, 135.8, 127.3, 121.8, 119.7, 118.1, 110.9, 108.2, 56.6, 52.9, 52.3, 34.7, 27.6, 26.1, 23.1, 14.1. This compound has been reported previously without full NMR characterization.⁶



Methyl 1-isobutyl-2,3,4,9-tetrahydro-1*H*-pyrido[3,4-*b*]indole-3-carboxylate:

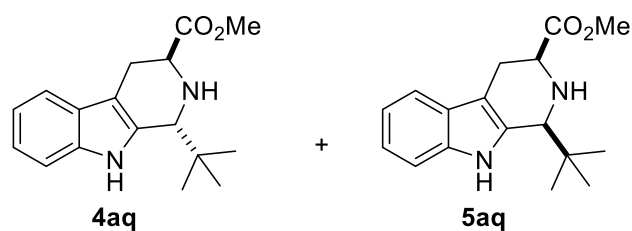
The procedure for **4ao/5ao** above was followed using L-tryptophan methyl ester hydrochloride (502 mg, 1.97 mmol) and 3-methylbutanal (0.23 mL, 2.14 mmol). Purification on column chromatography (5:5:2 CH_2Cl_2 : hexane: EtOAc) to give **5ap** (152.8 mg, 27%, first-eluting, yellow oil) and **4ap** (117.4 mg, 21% yield, second-eluting, yellow oil). A mixed fraction of **4ap** and **5ap** (225.6 mg, 40% yield) was also obtained.

Methyl (1*R*,3*S*)-1-isobutyl-2,3,4,9-tetrahydro-1*H*-pyrido[3,4-*b*]indole-3-carboxylate (4ap):

¹H NMR (400 MHz, CDCl₃) δ 7.74 (s, 1H), 7.48 (ddt, *J* = 7.7, 1.5, 0.8 Hz, 1H), 7.30 (ddd, *J* = 8.0, 1.2, 0.8 Hz, 1H), 7.15 (ddd, *J* = 8.0, 7.1, 1.4 Hz, 1H), 7.10 (ddd, *J* = 7.6, 7.1, 1.2 Hz, 1H), 4.32 (dd, *J* = 10.0, 4.2 Hz, 1H), 3.99 (dd, *J* = 7.4, 5.3 Hz, 1H), 3.75 (s, 3H), 3.13 (ddd, *J* = 15.4, 5.3, 1.2 Hz, 1H), 3.00 (ddd, *J* = 15.4, 7.4, 1.5 Hz, 1H), 1.96 (dddt, *J* = 15.0, 6.6, 4.6, 2.3 Hz, 2H), 1.88 (s, 2H), 1.73 (ddd, *J* = 13.7, 9.9, 4.8 Hz, 1H), 1.53 (ddd, *J* = 13.8, 9.4, 4.2 Hz, 1H), 1.04 (d, *J* = 6.5 Hz, 3H), 1.01 (d, *J* = 6.7 Hz, 3H). ¹³C NMR (101 MHz, CDCl₃) δ 174.4, 136.0, 135.9, 127.2, 121.7, 119.5, 118.1, 110.8, 106.8, 52.5, 52.2, 48.2, 44.5, 25.1, 24.8, 23.8, 21.7. This compound has been previously reported and NMR data are consistent with literature.⁷

Methyl (1*R*,3*S*)-1-isobutyl-2,3,4,9-tetrahydro-1*H*-pyrido[3,4-*b*]indole-3-carboxylate (5ap):

¹H NMR (400 MHz, Chloroform-*d*) δ 7.84 (s, 1H), 7.48 (ddt, *J* = 7.6, 1.5, 0.7 Hz, 1H), 7.33 – 7.30 (m, 1H), 7.19 – 7.14 (m, 1H), 7.11 (ddd, *J* = 7.1, 1.3 Hz, 1H), 4.23 (ddt, *J* = 9.0, 4.4, 2.2 Hz, 1H), 3.83 (s, 3H), 3.80 (dd, *J* = 11.2, 4.2 Hz, 1H), 3.14 (ddd, *J* = 15.0, 4.2, 1.9 Hz, 1H), 2.83 (ddd, *J* = 15.0, 11.2, 2.6 Hz, 1H), 2.10 – 1.97 (m, 2H), 1.75 – 1.60 (m, 2H), 1.04 (d, *J* = 6.6 Hz, 3H), 1.01 (d, *J* = 6.6 Hz, 3H). ¹³C NMR (101 MHz, CDCl₃) δ 173.9, 136.2, 136.0, 127.4, 121.8, 119.7, 118.1, 110.9, 107.9, 56.6, 52.3, 50.7, 44.5, 26.1, 24.4, 24.0, 21.8. This compound has been previously reported and NMR data are consistent with literature.⁷



Methyl 1-(*tert*-butyl)-2,3,4,9-tetrahydro-1*H*-pyrido[3,4-*b*]indole-3-carboxylate:

The procedure for **4ao**/**5ao** above was followed using L-tryptophan methyl ester hydrochloride (514 mg, 2.02 mmol) and trimethylacetaldehyde (0.65 mL, 5.98 mmol). Purification on column chromatography (5:5:2 CH₂Cl₂: hexane: EtOAc) yielded **5aq** (1.9 mg, 0.3%, first-eluting, yellow oil) a mixed fraction of **4aq** and **5aq** (289.7 mg, 50%, yellow oil). Recrystallization of the mixture from EtOAc gave a small quantity of pure **4aq** (17.1 mg, 3%, colorless crystals).

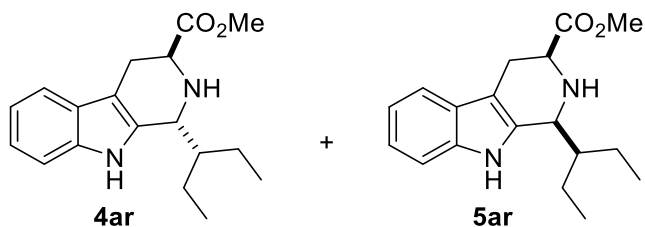
Methyl (1*R*,3*S*)-1-(*tert*-butyl)-2,3,4,9-tetrahydro-1*H*-pyrido[3,4-*b*]indole-3-carboxylate (4aq):

¹H NMR (400 MHz, CDCl₃) δ 7.78 (s, 1H), 7.50 (ddt, *J* = 7.7, 1.5, 0.8 Hz, 1H), 7.35 – 7.28 (m, 1H), 7.18 – 7.13 (m, 1H), 7.10 (ddd, *J* = 7.7, 7.1, 1.2 Hz, 1H), 4.09 (app. t, *J* = 5.2 Hz, 1H), 4.07 (t, *J* = 1.4 Hz, 1H), 3.63 (s, 3H), 3.11 (ddd, *J* = 15.0, 5.1, 1.5 Hz, 1H), 3.08 (ddd, *J* = 15.0, 5.3, 1.6 Hz, 1H), 1.08 (s, 9H). ¹³C NMR (126 MHz, CDCl₃) δ 175.1, 135.9, 133.7, 127.0, 121.8, 119.4, 118.1, 110.7, 109.2, 59.4, 54.4, 52.1, 36.8, 27.3, 24.7. HRMS (ESI) [M+H]⁺ calculated for C₁₇H₂₂N₂O₂: 287.1754. Found: 287.1753. mp = 141.3-142.4 °C

Methyl (1*S*,3*S*)-1-(*tert*-butyl)-2,3,4,9-tetrahydro-1*H*-pyrido[3,4-*b*]indole-3-carboxylate (5aq):

¹H NMR (400 MHz, CDCl₃) δ 7.90 (s, 1H), 7.50 (d, *J* = 8.1 Hz, 1H), 7.33 (dt, *J* = 8.1, 0.9 Hz, 1H), 7.17 (ddd, *J* = 8.1, 7.1, 1.3 Hz, 1H), 7.11 (ddd, *J* = 8.1, 7.1, 1.1 Hz, 1H), 4.03 (s, 1H), 3.83 (s, 3H), 3.68 (dd, *J* = 11.2, 3.6 Hz, 1H), 3.14 (ddd, *J* = 14.6, 3.6, 1.5 Hz, 1H), 2.77 (ddd, *J* = 14.6, 11.2, 2.4

Hz, 1H), 1.13 (s, 9H). ^{13}C NMR (101 MHz, CDCl_3) δ 174.0, 136.0, 134.6, 126.9, 121.9, 119.6, 118.0, 110.8, 109.2, 62.6, 56.5, 52.3, 35.7, 27.1, 26.4. This compound has been previously reported and NMR data are consistent with literature.⁸



Methyl 1-(pentan-3-yl)-2,3,4,9-tetrahydro-1H-pyrido[3,4-b]indole-3-carboxylate:

The procedure for **4ao/5ao** above was followed using L-tryptophan methyl ester hydrochloride (501 mg, 1.97 mmol) and 2-ethylbutanal (0.27 mL, 2.19 mmol). Purification on column chromatography (5:5:2 CH_2Cl_2 :hexane:EtOAc) yielded **5ar** (166.4 mg, 28%, first-eluting, yellow glass) and **4ar** (34.3 mg, 6%, second-eluting, yellow oil). A mixed fraction of **4ar** and **5ar** (312.3 mg, 52.8% yield) was also obtained.

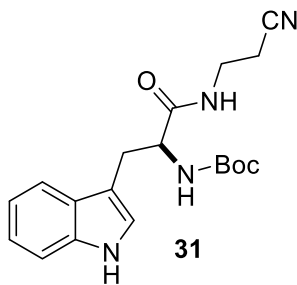
Methyl (1R,3S)-1-(pentan-3-yl)-2,3,4,9-tetrahydro-1H-pyrido[3,4-b]indole-3-carboxylate (4ar):

^1H NMR (400 MHz, CDCl_3) δ 7.74 (s, 1H), 7.49 (ddt, $J = 7.5, 1.5, 0.8$ Hz, 1H), 7.31 (dt, $J = 7.8, 1.1$ Hz, 1H), 7.17 – 7.12 (m, 1H), 7.10 (td, $J = 7.4, 1.2$ Hz, 1H), 4.48 (dt, $J = 3.3, 1.8$ Hz, 1H), 4.05 (t, $J = 5.2$ Hz, 1H), 3.68 (s, 3H), 3.12 (dt, $J = 5.4, 1.7$ Hz, 2H), 1.91 (s, 2H), 1.63 – 1.48 (m, 3H), 1.38 – 1.23 (m, 3H), 1.05 (t, $J = 7.2$ Hz, 3H), 0.84 (t, $J = 7.5$ Hz, 3H). ^{13}C NMR (101 MHz, CDCl_3) δ 174.7, 136.0, 134.7, 127.4, 121.6, 119.4, 118.0, 110.8, 108.2, 54.1, 52.2, 51.0, 46.7, 24.4, 23.1, 22.7, 12.6, 12.3. HRMS (ESI) $[\text{M}+\text{H}]^+$ calculated for $\text{C}_{18}\text{H}_{24}\text{N}_2\text{O}_2$: 301.1911. Found: 301.1910.

Methyl (1*S*,3*S*)-1-(pentan-3-yl)-2,3,4,9-tetrahydro-1*H*-pyrido[3,4-*b*]indole-3-carboxylate (5ar):

¹H NMR (400 MHz, CDCl₃) δ 7.76 (s, 1H), 7.48 (ddt, *J* = 7.7, 1.5, 0.7 Hz, 1H), 7.33 (ddd, *J* = 8.0, 1.2, 0.8 Hz, 1H), 7.18 – 7.13 (m, 1H), 7.11 (ddd, *J* = 7.6, 7.1, 1.2 Hz, 1H), 4.35 (q, *J* = 2.3 Hz, 1H), 3.82 (s, 3H), 3.74 (dd, *J* = 11.2, 4.1 Hz, 1H), 3.12 (ddd, *J* = 15.0, 4.1, 1.9 Hz, 1H), 2.78 (ddd, *J* = 15.0, 11.2, 2.6 Hz, 1H), 1.69 (s, 1H), 1.63 – 1.53 (m, 3H), 1.37 – 1.24 (m, 2H), 1.04 (t, *J* = 7.3 Hz, 3H), 0.89 (t, *J* = 7.5 Hz, 3H). ¹³C NMR (101 MHz, CDCl₃) δ 174.1, 136.0, 135.5, 127.5, 121.7, 119.6, 117.9, 110.9, 109.5, 56.6, 54.6, 52.3, 46.1, 26.2, 23.3, 22.8, 13.2, 12.8. HRMS (ESI) [M+H]⁺ calculated for C₁₈H₂₄N₂O₂: 301.1911. Found: 301.1908.

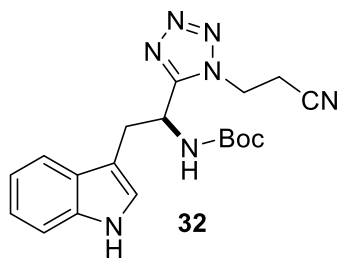
4.4 Chapter 3 – Synthesis of tetrazole and phosphonate bioisosteres of 1a



***tert*-butyl (*S*)-1-((2-cyanoethyl)amino)-3-(1*H*-indol-3-yl)-1-oxopropan-2-ylcarbamate (**31**):**

A reaction vessel was charged with **24** (1.9936 g, 6.55 mmol) prepared by Ms. Liu⁹ and hydroxybenzotriazole hydrate (1.0485 g, 6.83 mmol) in DMF (10 mL) on an ice bath. *N,N'*-dicyclohexylcarbodiimide (1.3729 g, 6.65 mmol) was added to the solution, and the mixture was stirred for an additional 10 min. Next, 3-aminopropanenitrile (0.52 mL, 7.06 mmol) was added dropwise on ice, and the reaction was slowly allowed to reach room temperature. The stirring continued for 50 h. The reaction mixture was then stored in a freezer (-20 °C) for 24 h. After the cooling, white precipitate appeared and was filtered off. The filtrate was treated with cold water (70 mL), and the resulting precipitate was filtered again. The precipitate was then recrystallized from CH₂Cl₂ to yield the first crop of pure product **31** (1.3642 g). The mother liquor was concentrated down and recrystallized from aqueous methanol to yield a second crop of **31** (325.3 mg). The white crystals were combined to provide **31** (1.6895 g, 72% yield).

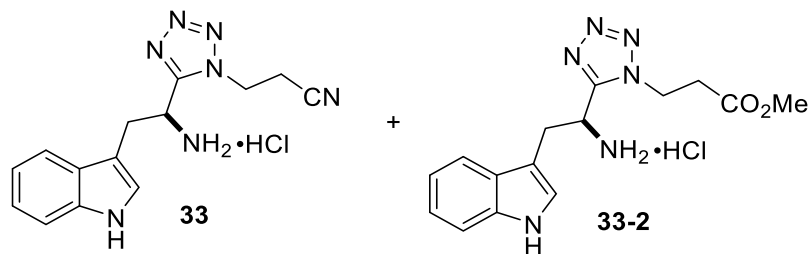
¹H NMR (400 MHz, CD₃OD) δ 7.58 (d, *J* = 7.8 Hz, 1H), 7.34 (s, 1H), 7.11 (s, 1H), 7.08 (d, *J* = 7.1 Hz, 1H), 7.02 (t, *J* = 7.0 Hz, 1H), 4.29 (t, *J* = 7.0 Hz, 1H), 3.38 (dt, *J* = 12.9, 6.4 Hz, 1H), 3.24 (m, 2H), 3.07 (dd, *J* = 14.4, 7.4 Hz, 1H), 2.40 (m, 2H), 1.38 (s, 8H), 1.23 (s, 2H). mp = 171.5 – 172.1 °C (recrystallized from CH₂Cl₂), 171.1 – 172.1 °C (recrystallized from CH₃OH/H₂O). The experimental data are in agreement with data presented by Ms. Liu.⁹



***tert*-butyl (*S*)-1-(1-(2-cyanoethyl)-1*H*-tetrazol-5-yl)-2-(1*H*-indol-3-yl)ethylcarbamate (**32**):**

A Schlenk flask was charged with **31** (2.6054 g, 7.31 mmol) and triphenylphosphine (4.7953 g, 18.28 mmol) in freshly distilled THF (46 mL) under N₂ atmosphere. Flask was cooled on an ice bath, and azidotrimethylsilane (2.4 mL, 18.08 mmol) was added dropwise over 5 min, followed by dropwise addition of DIAD (3.6 mL, 18.28 mmol). The reaction mixture was stirred on an ice bath for an additional 20 min and then was allowed to reach room temperature and continued stirring for 76 h. The reaction was then cooled on an ice bath again, and an aqueous solution of ceric ammonium nitrate (5.5 wt%, 92 mL) was added, followed by extraction with EtOAc (3 x 45 mL). The combined organic layers were washed with saturated aqueous NaHCO₃ solution (3 x 50 mL) and saturated aqueous NaCl solution (1 x 100 mL), dried over Na₂SO₄ and concentrated under reduced pressure. The crude product was purified by four consecutive runs of column chromatography (gradient 100 – 50% hexanes:EtOAc, then isocratic 1:1 hexanes:EtOAc) to afford **32** as off-white solid (1.12 g, 40% yield).

¹H NMR (400 MHz, CD₃OD) δ 7.41 (dd, *J* = 7.9, 1.0 Hz, 1H), 7.34 (d, *J* = 8.2 Hz, 1H), 7.11 (ddd, *J* = 8.2, 7.0, 1.2 Hz, 1H), 7.01 (ddd, *J* = 8.0, 7.0, 1.0 Hz, 1H), 6.93 (s, 1H), 5.17 (dd, *J* = 9.6, 6.3 Hz, 1H), 4.29 (dt, *J* = 14.1, 7.0 Hz, 1H), 4.18 (dt, *J* = 14.1, 6.8 Hz, 1H), 3.50 (dd, *J* = 14.0, 6.4 Hz, 1H), 3.41 (dd, *J* = 14.0, 9.6 Hz, 1H), 2.46 (m, 2H). The experimental data are in agreement with data presented by Ms. Liu.⁹



(S)-3-(5-(1-amino-2-(1H-indol-3-yl)ethyl)-1H-tetrazol-1-yl)propanenitrile hydrochloride (33):

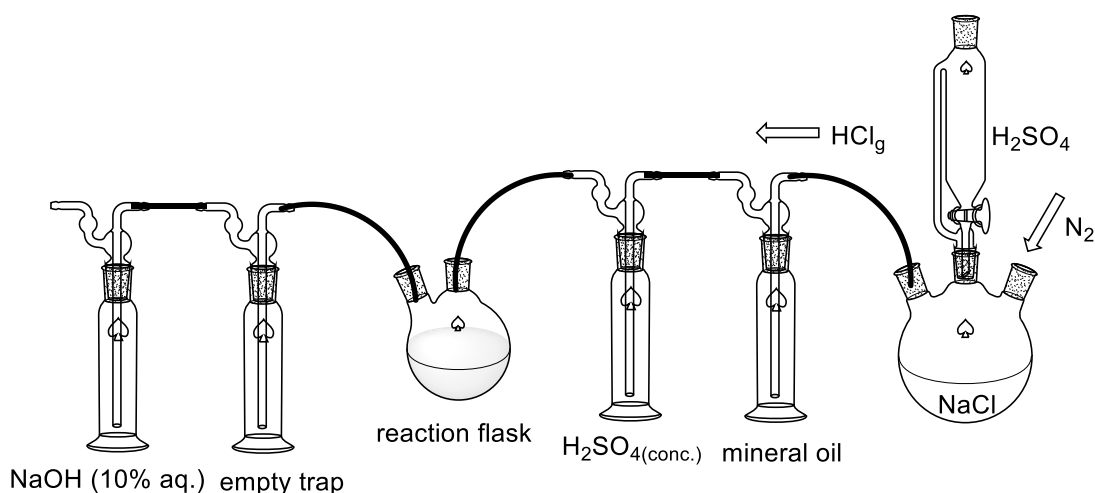
Method 1: A reaction flask was charged with **32** (254 mg, 0.67 mmol), and a solution of 1M HCl in EtOAc (16.6 mL) was added under N₂. The solution was stirred overnight at ambient temperature. Residual HCl and solvent were then removed under reduced pressure. Compound **33** was isolated as light brown solid (180.6 mg, 85% yield adjusted for presence of **33-2**), insoluble in the majority of common solvents, except for methanol. The material was briefly dissolved in CH₃OH for transfer, but even a short contact time resulted in small amounts of **33-2** (12 mol%) detectable by ¹H NMR analysis.

¹H NMR (400 MHz, CD₃OD) δ 7.42 – 7.38 (m, 1H), 7.17 – 7.13 (m, 2H), 7.07 (s, 1H), 7.00 (ddd, *J* = 7.8, 7.1, 1.0 Hz, 1H), 5.13 (dd, *J* = 10.7, 5.2 Hz, 1H), 4.03 (ddd, *J* = 14.6, 8.0, 6.6 Hz, 1H), 3.72 – 3.62 (m, 2H), 3.48 – 3.41 (m, 1H), 2.40 (ddd, *J* = 17.1, 8.0, 6.9 Hz, 1H), 2.21 (ddd, *J* = 17.1, 6.6, 5.8 Hz, 1H).

Method 2: A reaction flask was charged with **32** (190.5 mg, 0.50 mmol) and connected to the apparatus for the development of HCl_g depicted in the scheme below. Anhydrous EtOAc (10 mL, dried over activated 4Å molecular sieves for three days) was added to **32**. The apparatus was kept under N₂ atmosphere, and the HCl was allowed to evolve slowly. The reaction reached completion overnight. Compound **33** was isolated in the same manner as in *Method 1* and then was converted to a form of a free base by treatment with saturated NaHCO₃ solution. The free base of **33** was

isolated by extraction in CH₂Cl₂ (102.5 mg, 55% yield adjusted for presence of **33-2**, which was detected in 23 mol%).

¹H NMR (400 MHz, CDCl₃) δ 8.32 (s, 1H), 7.40 (d, *J* = 7.2 Hz, 1H), 7.39 (dt, *J* = 7.3, 1.1 Hz, 1H), 7.22 (ddd, *J* = 8.2, 7.1, 1.0 Hz, 1H), 7.11 (ddd, *J* = 7.9, 7.1, 1.0 Hz, 1H), 6.99 (d, *J* = 2.3 Hz, 1H), 4.62 (t, *J* = 7.0 Hz, 1H), 4.32 (m, 2H), 3.39 (tdd, *J* = 14.3, 7.0, 0.7 Hz, 2H), 2.73 (ddd, *J* = 16.9, 7.4, 6.8 Hz, 1H), 2.56 (ddd, *J* = 16.9, 7.3, 6.6 Hz, 1H), 1.82 (s, 2H). ¹³C NMR (126 MHz, CDCl₃) δ 170.7, 158.1, 136.3, 127.0, 123.6, 122.8, 120.3, 118.3, 116.1, 111.7, 110.5, 48.3, 42.8, 33.7, 18.2.

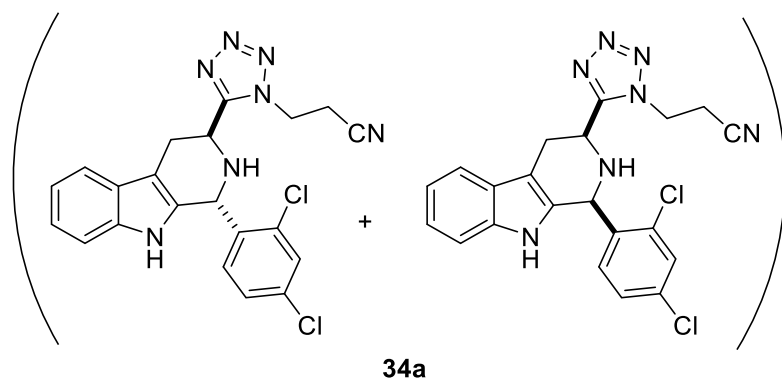


Method 3: A reaction flask was charged with **32** (528.6 mg, 1.39 mmol), and the procedure from *Method 2* was repeated with anhydrous CH₃OH (15 mL). The reaction was stopped after 1 h and isolated in the same manner as for *Method 1*. Compound **33-2** was the primary reaction product (**33**:**33-2** molar ratio = 0.4:1 as observed in ¹H NMR), combined yield of **33** and **33-2** was 412.1 mg (87%).

Methyl (S)-3-(5-(1-amino-2-(1*H*-indol-3-yl)ethyl)-1*H*-tetrazol-1-yl)propanoate hydrochloride (33-2**):**

¹H NMR (400 MHz, CD₃OD) δ 7.37 (dt, *J* = 8.2, 0.8 Hz, 1H), 7.22 (dt, *J* = 8.0, 0.9 Hz, 1H), 7.17 – 7.07 (m, 2H), 7.06 (s, 1H), 7.02 – 6.96 (m, 1H), 5.23 (dd, *J* = 10.3, 5.5 Hz, 1H), 3.95 (ddd, *J* =

14.3, 8.6, 5.7 Hz, 1H), 3.74 – 3.64 (m, 1H), 3.60 (dt, $J = 14.3, 5.8$ Hz, 3H), 3.52 – 3.39 (m, 2H), 2.61 (ddd, $J = 17.8, 8.6, 5.9$ Hz, 1H), 2.43 – 2.32 (m, 1H), 2.24 (dt, $J = 17.7, 5.6$ Hz, 1H). ^{13}C NMR (126 MHz, CD_3OD) δ 172.4, 154.6, 138.0, 127.8, 125.7, 123.2, 120.8, 118.3, 112.9, 107.5, 52.5, 47.6, 43.6, 33.5, 30.8.

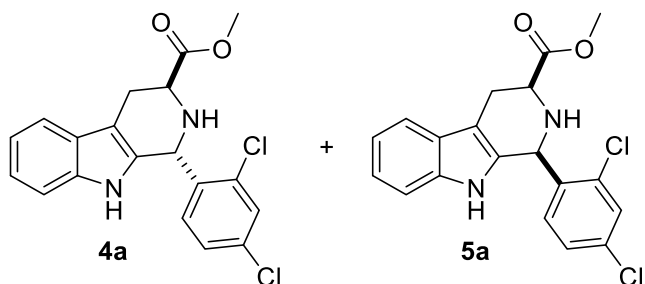


3-(5-(1-(2,4-dichlorophenyl)-2,3,4,9-tetrahydro-1H-pyrido[3,4-b]indol-3-yl)-1H-tetrazol-1-yl)propanenitrile (3a):

A round bottom flask was charged with **33** (182.0 mg, 0.46 mmol), 4Å activated molecular sieves (1 g, powdered), 2,4-dichlorobenzaldehyde (106.4 mg, 0.61 mmol), and CH_2Cl_2 (anh., 5.2 mL) under N_2 atmosphere. The mixture was stirred for 18 h at ambient temperature, followed by the addition of TFA (0.15 mL, 1.96 mmol). The reaction continued stirring at room temperature for 23 h. The reaction mixture was cooled on an ice bath, and saturated aqueous NaHCO_3 solution (3 mL) was added together with EtOAc (6 mL). Stirring continued on an ice bath for an additional 40 min. Molecular sieves were filtered off, and the aqueous layer was partitioned from EtOAc. The organic layer was washed with water (3 x 10 mL), and saturated aqueous NaCl solution (1 x 20 mL), dried over Na_2SO_4 and concentrated in vacuo to afford light yellow solid (213.4 mg, 103% crude yield). The crude material suffered from poor solubility but was eventually dissolved in CH_3OH and was purified by column chromatography (solid loading, isocratic 3:1:1

CH₂Cl₂:hexanes:EtOAc) to afford **34a** as light yellow solid (18.5 mg, 9% yield, dr = 65:35 *trans*:*cis*).

¹H NMR (400 MHz, DMSO) δ 10.84 (s, 1H, *trans*), 10.61 (s, 0.55H, *cis*), 7.72 (d, *J* = 2.2 Hz, 1H, *trans*), 7.71 (d, *J* = 2.2 Hz, 0.5H, *cis*), 7.58 (d, *J* = 7.2 Hz, 1H, *trans*), 7.53 (d, *J* = 7.5 Hz, 0.55H, *cis*), 7.35 (m, 1.5H), 7.29 (dt, *J* = 8.0, 1.0 Hz, 1H, *trans*), 7.25 (dt, *J* = 8.0, 1.1 Hz, 0.55H, *cis*), 7.05 (m, 3.7H), 6.77 (d, *J* = 8.3 Hz, 1H, *trans* H6'), 5.79 (d, *J* = 9.3 Hz, 0.55H, *cis*), 5.52 (d, *J* = 5.5 Hz, 1H, *trans*), 4.95 (dt, *J* = 13.9, 6.8 Hz, 0.55H, *cis*), 4.81 (m, 1.1H, *cis*), 4.57 (dt, *J* = 14.1, 7.1 Hz, 1H, *trans*), 4.31 (m, 2H, *trans*), 3.82 (dd, *J* = 12.1, 5.6 Hz, 1H, *trans*), 3.25 (m, 5H), 2.96 (m, 2H). The stereochemistry was assigned based on position of H6' doublet which is observed significantly upfield in *trans* relative to *cis* in a range of 2',4'-Cl₂ substituted analogs (cf. **4a** and **5a**). The experimental data are in agreement with data presented by Ms. Liu.⁹



Methyl 1-(2,4-dichlorophenyl)-2,3,4,9-tetrahydro-1H-pyrido[3,4-*b*]indole-3-carboxylate:

To a mixture of L-tryptophan methyl ester hydrochloride (2.0553 g, 7.91 mmol), 4Å molecular sieves (3.2 g, powdered), and 2,4-dichlorobenzaldehyde (1.5411 g, 8.72 mmol), CH₂Cl₂ (15 mL) was added under nitrogen. The resulting mixture was stirred at room temperature for 24 hours. TFA (1.2 mL, 15.52 mmol) was added dropwise. The reaction mixture was further stirred at room temperature for additional 3 hours. The reaction was cooled to 0 °C, and a saturated aqueous solution of NaHCO₃ (15 mL) was added, followed by the addition of EtOAc (15 mL). After stirring

for 30 min at 0 °C, the molecular sieves were filtered, phases of the filtrate were partitioned, and the aqueous layer was extracted with EtOAc (3 x 20 mL). The combined organic layers were washed with water (2 x 40 mL) and saturated aqueous NaCl solution (1 x 30 mL), dried over MgSO₄ and concentrated *in vacuo*. Compounds **4a** and **5a** were separated from the crude material by flash chromatography (95:5 CH₂Cl₂:EtOAc) to give **5a** (1.9616 g, 66%, first-eluting, off-white powder) and **4a** (732.3 mg, 25%, second-eluting, off-white powder).

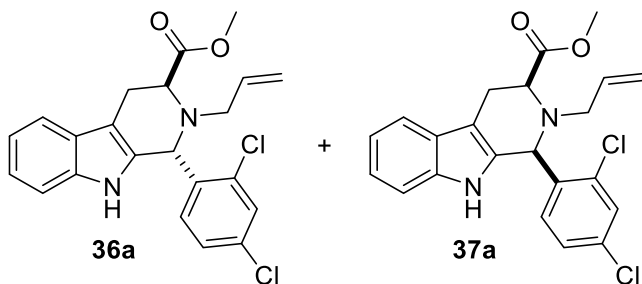
Methyl (1R,3S)-1-(2,4-dichlorophenyl)-2,3,4,9-tetrahydro-1H-pyrido[3,4-*b*]indole-3-carboxylate (4a):

¹H NMR (400 MHz, CDCl₃) δ 7.68 (s, 1H), 7.56 (ddt, *J* = 7.4, 1.6, 0.7 Hz, 1H), 7.47 (d, *J* = 2.1 Hz, 1H), 7.27 (m, 1H), 7.17 (m, 2H), 7.11 (ddd, *J* = 8.3, 2.1, 0.4 Hz, 1H), 6.92 (d, *J* = 8.3 Hz, 1H), 3.84 (dd, *J* = 7.7, 5.0 Hz, 1H), 3.73 (s, 3H), 3.26 (ddd, *J* = 15.4, 5.0, 1.2 Hz, 1H), 3.10 (ddd, *J* = 15.3, 7.8, 1.5 Hz, 1H), 2.79 (s, 1H). ¹³C NMR (101 MHz, CDCl₃) δ 173.8, 137.9, 136.3, 134.5, 134.5, 131.6, 131.0, 129.9, 127.3, 126.9, 122.4, 119.9, 118.5, 111.1, 109.8, 52.4, 52.3, 51.3, 24.9. The compound was published previously and the experimental data are in agreement with literature.¹⁰

Methyl (1S,3S)-1-(2,4-dichlorophenyl)-2,3,4,9-tetrahydro-1H-pyrido[3,4-*b*]indole-3-carboxylate (5a):

¹H NMR (400 MHz, CDCl₃) δ 7.59 (s, 1H), 7.57 – 7.53 (m, 1H), 7.48 (d, *J* = 2.1 Hz, 1H), 7.38 (d, *J* = 8.4 Hz, 1H), 7.25 – 7.22 (m, 1H), 7.22 – 7.18 (m, 1H), 7.17 – 7.11 (m, 2H), 5.79 (s, 1H), 3.99 (dd, *J* = 11.0, 4.1 Hz, 1H), 3.83 (s, 3H), 3.25 (ddd, *J* = 15.1, 4.1, 1.8 Hz, 1H), 3.02 (ddd, *J* = 15.1, 11.0, 2.5 Hz, 1H), 2.62 (s, 1H). ¹³C NMR (101 MHz, CDCl₃) δ 173.08, 137.40, 136.27, 134.72, 134.21, 133.27, 131.52, 129.47, 128.12, 126.96, 122.29, 119.88, 118.36, 111.07, 109.47, 77.16,

56.68, 53.91, 52.46, 25.53. The compound was published previously and the experimental data are in agreement with literature.¹⁰



Methyl-2-allyl-1-(2,4-dichlorophenyl)-2,3,4,9-tetrahydro-1H-pyrido[3,4-b]indole-3-carboxylate:

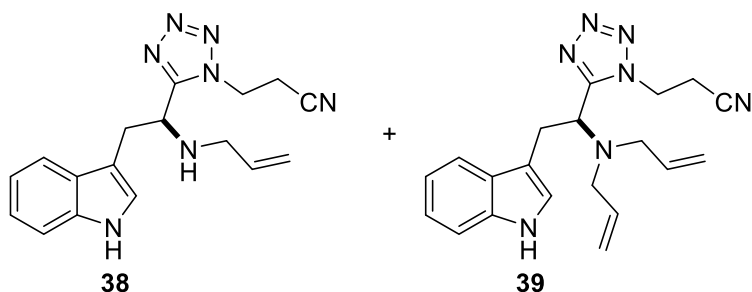
Mixture of of **4a:5a** (dr = 0.4:1, 504.8 mg, 1.35 mmol) was added into a sealed tube, followed by CH₃CN (anh., 3 mL), DIPEA (0.35 mL, 2.01 mmol), and allyl bromide (0.5 mL, 5.78 mmol). The tube was tightly closed, and the mixture was heated at 115 °C for 1.5 h. Ethyl acetate (10 mL) was added to the cooled reaction mixture, and the precipitate was removed. This step was repeated once more. The organic filtrate was then washed with water (2 x 15 mL), saturated NaCl solution (1 x 12 mL), dried over Na₂SO₄, and concentrated in vacuo. Products **36a** and **37a** were obtained as a yellow powder (547.6 mg, 98% yield) and used in the next reaction step without separation of the diastereomers.

Methyl-(1R,3S)-2-allyl-1-(2,4-dichlorophenyl)-2,3,4,9-tetrahydro-1H-pyrido[3,4-b]indole-3-carboxylate (36a):

The mixture of **36a** and **37a** (dr = 0.4:1.0, 541.0 mg, 1.30 mmol) was dissolved in CH₂Cl₂ (anh., 10 mL) under N₂, followed by addition of TFA (0.3 mL, 3.92 mmol). The reaction proceeded at ambient temperature, and the progress was monitored by TLC analysis (15:15:1 CH₂Cl₂:hexanes:EtOAc). After 1.5 h, the reaction was cooled on an ice bath, and a saturated

solution of NaHCO₃ (10 mL) was added, followed by stirring for an additional 10 min. The organic layer was partitioned from the aqueous phase and washed with water (1 x 20 mL) and saturated NaCl solution (1 x 15 mL), dried over Na₂SO₄ and concentrated *in vacuo*. The product **36a** was isolated as a light yellow powder (481.2 mg, 89% yield, 89% de).

¹H NMR (400 MHz, CDCl₃) δ 7.59 (s, 1H), 7.49 (d, *J* = 6.9 Hz, 1H), 7.46 (d, *J* = 8.5 Hz, 1H), 7.44 (d, *J* = 2.1 Hz, 1H), 7.20 (m, 1H), 7.15 (dd, *J* = 8.5, 2.1 Hz, 1H), 7.10 (m, 2H), 6.04 (s, 1H), 5.72 (dddd, *J* = 17.2, 10.1, 8.1, 4.4 Hz, 1H), 5.19 (dq, *J* = 17.2, 1.9 Hz, 1H), 5.10 (dq, *J* = 10.1, 1.0 Hz, 1H), 4.19 (t, *J* = 4.2 Hz, 1H), 3.61 (s, 3H), 3.45 (dd, *J* = 14.4, 7.7 Hz, 1H), 3.28 (dd, *J* = 4.3, 1.8 Hz, 2H), 3.19 (ddt, *J* = 14.6, 4.2, 1.9 Hz, 1H).

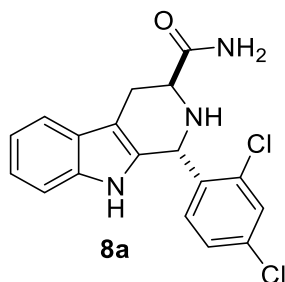


(S)-3-(5-(1-(allylamino)-2-(1H-indol-3-yl)ethyl)-1H-tetrazol-1-yl)propanenitrile (38) and (S)-3-(5-(1-(diallylamino)-2-(1H-indol-3-yl)ethyl)-1H-tetrazol-1-yl)propanenitrile (39):

Sealed tube was charged with **33** (111.6 mg, 69:31 **33**:**33-2** ratio, 0.34 mmol), DIPEA (0.2 mL, 1.15 mmol), and allyl bromide (31 μL, 0.36 mmol) in CH₃CN (anh., 0.7 mL). The reaction was heated to reflux for three days. When cooled, the mixture was partitioned with 1M HCl (2 mL) and EtOAc (2 mL). The aqueous layer was extracted with EtOAc (2 x 1 mL). The combined organic layers were washed with saturated aqueous NaHCO₃ solution (2 x 2 mL), water (2 x 2 mL), and saturated aqueous NaCl solution (1 x 2 mL), dried over Na₂SO₄, and concentrated *in vacuo* to

afford the product as a brown oil (63.1 mg composed of **38** and **39** together with products resulting from **33-2**: **38-2** and **39-2**). The molar ratio of products detected by ^1H NMR was **38**:**39**:**38-2**:**39-2** = 1:0.3:0.3:0.1, and thus, the calculated yield of desired product **38** was 32%. Attempts to separate the mixture of products by chromatographic techniques were not successful. The ^1H NMR spectrum is reported for the signals of major product **38**. Side products **38-2** and **39-2** were identified by comparison with products of reaction starting from 25:75 mixture of **33**:**33-2**.

^1H NMR (400 MHz, CDCl_3) δ 8.19 (s, 1H), 7.37 (m, 2H), 7.22 (ddd, $J = 8.2, 7.1, 1.2$ Hz, 2H), 7.12 (ddd, $J = 8.0, 7.1, 1.0$ Hz, 2H), 6.93 (d, $J = 2.4$ Hz, 1H), 5.78 (m, 2H), 5.11 (m, 3H), 4.51 (dd, $J = 7.9, 6.4$ Hz, 2H), 4.14 (m, 3H), 3.29 (ddd, $J = 14.2, 7.9, 0.7$ Hz, 1H), 3.18 (dt, $J = 5.6, 1.5$ Hz, 1H), 3.11 (dt, $J = 6.3, 1.3$ Hz, 1H), 2.53 (ddd, $J = 16.8, 8.3, 6.8$ Hz, 1H), 2.29 (ddd, $J = 16.9, 8.2, 6.0$ Hz, 2H).

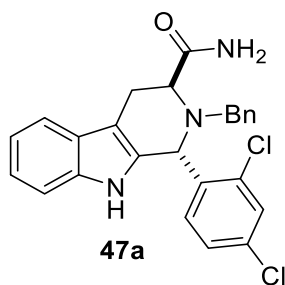


(1R,3S)-1-(2,4-dichlorophenyl)-2,3,4,9-tetrahydro-1H-pyrido[3,4-b]indole-3-carboxamide

(8a):

The reaction flask was charged with **4a** (305.2 mg, 0.81 mmol), and a solution of NH_3 (7M in CH_3OH , 7.5 mL, 52.5 mmol) was added to it under N_2 . The solution was stirred overnight at ambient temperature. Solvent and residual ammonia were removed under reduced pressure to afford **8a** as a white solid (279.1 mg, 96% yield).

^1H NMR (500 MHz, DMSO) δ 10.72 (s, 1H), 7.69 (d, J = 2.2 Hz, 1H), 7.48 (d, J = 7.7 Hz, 1H), 7.31 (dd, J = 8.4, 2.2 Hz, 1H), 7.27 (s, 1H), 7.25 (d, J = 8.0 Hz, 1H), 7.08 (s, 1H), 7.06 (ddd, J = 8.2, 7.0, 1.3 Hz, 1H), 6.99 (ddd, J = 8.0, 7.0, 1.1 Hz, 1H), 6.69 (d, J = 8.3 Hz, 1H), 3.08 (dd, J = 8.8, 4.9 Hz, 2H), 3.03 (dd, J = 15.1, 4.5 Hz, 1H), 2.69 (dd, J = 14.3, 9.8 Hz, 1H). ^{13}C NMR (126 MHz, DMSO) δ 174.6, 139.0, 136.2, 134.4, 132.7, 132.6, 131.2, 129.1, 126.8, 126.5, 121.1, 118.5, 117.7, 111.2, 109.2, 51.3, 50.8, 25.1. The compound was published previously and the experimental data are in agreement with literature.¹⁰



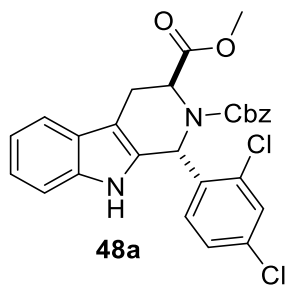
(1R,3S)-2-benzyl-1-(2,4-dichlorophenyl)-2,3,4,9-tetrahydro-1H-pyrido[3,4-b]indole-3-carboxamide (47a):

Method 1: A reaction vessel was charged with **8a** (101.7 mg, 0.28 mmol) in CH_3CN (anh., 1.5 mL), benzyl chloroformate (0.19 mL, 1.34 mmol), Et_3N (0.20 mL, 1.43 mmol), and DMAP (3.8 mg, 0.03 mmol) under N_2 atmosphere. The reaction mixture was heated to 60 °C for 24 h and then to reflux for an additional 17 h. Water (12 mL), 1M HCl (3 mL), and EtOAc (10 mL) and the phases were partitioned. The aqueous layer was further extracted with EtOAc (2 x 10 mL). The combined organic layers were washed with water (2 x 10 mL), saturated NaCl solution (1 x 10 mL), dried over MgSO_4 , and concentrated under reduced pressure. The crude product was purified by column chromatography (95:5 CH_2Cl_2 :2-propanol) to afford **47a** as a white powder (124.1 mg, 89% yield).

^1H and ^{13}C NMR spectra are identical between *Method 1* and *Method 2* and are listed after *Method 2*. HRMS (ESI) $[\text{M}+\text{H}]^+$ calculated for $\text{C}_{25}\text{H}_{22}\text{Cl}_2\text{N}_3\text{O}^+$: 450.1134. Found: 450.1124.

Method 2: A reaction vessel was charged with **8a** (72.8 mg, 0.20 mmol) in CH_3CN (anh., 0.7 mL), benzyl bromide (29 μL , 0.24 mmol), and DIPEA (0.53 mL, 3.05 mmol) under N_2 atmosphere. The reaction mixture was heated to 60 $^\circ\text{C}$ for 24 h. The solvent was removed under reduced pressure, and the residue was extracted with 1M HCl (2 mL) and EtOAc (1 mL). The aqueous layer was extracted further with EtOAc (3 x 1 mL). Combined organic layers were washed with water (2 x 2 mL), saturated NaCl solution (1 x 2 mL), dried over Na_2SO_4 , and concentrated under reduced pressure. The crude product was purified by column chromatography (95:5 CH_2Cl_2 :2-propanol) to afford **47a** as a white powder (61.9 mg, 68% yield).

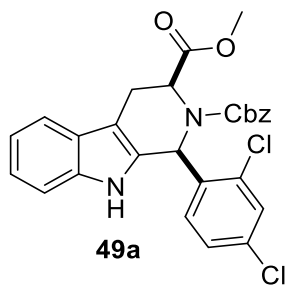
^1H NMR (500 MHz, CDCl_3) δ 7.81 (s, 1H), 7.66 (d, $J = 7.7$ Hz, 1H), 7.33 (m, 7H), 7.25 (td, $J = 8.1, 7.6, 1.4$ Hz, 2H), 7.21 (td, $J = 7.5, 1.1$ Hz, 1H), 7.04 (dd, $J = 8.4, 2.1$ Hz, 1H), 6.75 (s, 1H), 6.73 (d, $J = 8.4$ Hz, 1H), 5.68 (s, 1H), 5.39 (s, 1H), 3.87 (d, $J = 12.7$ Hz, 1H), 3.80 (t, $J = 7.8$ Hz, 1H), 3.64 (d, $J = 12.7$ Hz, 1H), 3.21 (d, $J = 7.8$ Hz, 2H). ^{13}C NMR (126 MHz, CDCl_3) δ 174.9, 137.4, 136.7, 136.7, 135.4, 134.7, 132.4, 130.8, 130.2, 130.1, 128.3, 127.9, 127.0, 126.9, 122.7, 120.1, 118.8, 111.3, 110.4, 56.7, 55.8, 53.2, 18.6. HRMS (ESI) $[\text{M}+\text{H}]^+$ calculated for $\text{C}_{25}\text{H}_{22}\text{Cl}_2\text{N}_3\text{O}^+$: 450.1134. Found: 450.1127.



2-benzyl 3-methyl (1R,3S)-1-(2,4-dichlorophenyl)-1,3,4,9-tetrahydro-2H-pyrido[3,4-b]indole-2,3-dicarboxylate (48a):

A reaction vessel was charged with **4a** (693.8 mg, 1.83 mmol) and dissolved in EtOAc (11 mL) under N₂. The solution was placed on an ice bath, and an aqueous solution of K₂CO₃ was added (764.2 mg, 5.52 mmol, 5.5 mL of water), and the mixture was stirred for 5 min. Benzyl chloroformate (0.35 mL, 2.09 mmol) was then added in one portion. The reaction was stirred for 10 min on ice and then allowed to warm to room temperature. After 3.5 h, the organic layer was partitioned from the aqueous phase, dried over MgSO₄, and concentrated *in vacuo*. Product **48a** was precipitated from CH₂Cl₂/hexanes as a white powder (869.6 mg, 93% yield). No further purification was necessary.

¹H NMR (600 MHz, DMSO, 70 °C) δ 10.41 (s, 1H), 7.47 (d, *J* = 7.5 Hz, 2H), 7.28 (d, *J* = 8.1 Hz, 4H), 7.24 (t, *J* = 5.2 Hz, 2H), 7.18 – 7.02 (m, 3H), 6.99 (t, *J* = 7.2 Hz, 1H), 6.46 (s, 1H), 5.19 (t, *J* = 4.5 Hz, 1H), 5.12 (d, *J* = 12.5 Hz, 1H), 4.98 (d, *J* = 12.5 Hz, 1H), 3.52 (s, 3H), 3.41 (d, *J* = 4.3 Hz, 2H). ¹³C NMR (151 MHz, DMSO, 70 °C) δ 171.3, 155.1, 136.5, 136.2, 135.8, 134.2, 132.7, 131.0, 130.2, 128.6, 127.9, 127.5, 127.3, 126.6, 125.6, 121.2, 118.6, 117.6, 111.2, 105.8, 67.1, 52.8, 51.7, 51.3, 21.4. IR (neat, cm⁻¹): 1728 (ester C=O), 1698 (Cbz C=O). HRMS (ESI) [M+H]⁺ calculated for C₂₇H₂₃Cl₂N₂O₄⁺: 509.1029. Found: 509.1022. [α]_D^{23.6} = -8.09 (c = 0.025 M in CH₂Cl₂).

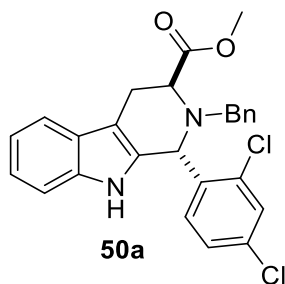


2-benzyl 3-methyl (1*S*,3*S*)-1-(2,4-dichlorophenyl)-1,3,4,9-tetrahydro-2*H*-pyrido[3,4-*b*]indole-2,3-dicarboxylate (49a):

A reaction vessel was charged with **5a** (1.9176 g, 5.09 mmol) and dissolved in EtOAc (20 mL) under N₂. The solution was placed on an ice bath, and an aqueous solution of K₂CO₃ was added (2.2074 g, 15.96 mmol, 10 mL of water), and the mixture was stirred for 5 min. Benzyl chloroformate (1.0 mL, 5.97 mmol) was then added in one portion. The reaction was stirred for 10 min on ice and then allowed to warm to room temperature. After 3.5 h, the organic layer was partitioned from the aqueous phase, dried over MgSO₄, and concentrated *in vacuo*. Product **49a** was precipitated from CH₂Cl₂/hexanes as a white powder (2.4344 g, 94% yield). No further purification was necessary.

¹H NMR (600 MHz, DMSO, 70 °C) δ 10.48 (s, 1H), 7.55 (m, 1H), 7.52 (d, *J* = 7.8 Hz, 1H), 7.31 (td, *J* = 12.2, 10.9, 4.2 Hz, 5H), 7.25 (d, *J* = 6.6 Hz, 2H), 7.18 (d, *J* = 8.5 Hz, 1H), 7.09 (t, *J* = 7.9 Hz, 1H), 7.03 (t, *J* = 7.4 Hz, 1H), 6.63 (s, 1H), 5.35 (dd, *J* = 7.2, 2.5 Hz, 1H), 5.17 (d, *J* = 12.5 Hz, 1H), 5.11 (d, *J* = 12.5 Hz, 1H), 3.45 (dd, *J* = 15.8, 2.4 Hz, 1H), 3.32 (s, 3H), 3.16 (dd, *J* = 15.8, 7.2 Hz, 1H). ¹³C NMR (151 MHz, DMSO, 70 °C) δ 171.3, 155.1, 136.5, 136.2, 135.8, 134.2, 132.7, 131.0, 130.2, 128.6, 127.9, 127.5, 127.3, 126.6, 125.6, 121.2, 118.6, 117.6, 111.2, 105.8, 67.1, 52.8, 51.7, 51.3, 21.4. IR (neat, cm⁻¹): 1737 (ester C=O), 1667 (Cbz C=O). HRMS (ESI)

$[M+H]^+$ calculated for $C_{27}H_{23}Cl_2N_2O_4^+$: 509.1029. Found: 509.1023. $[\alpha]_D^{24.0} = +10.78$ (c = 0.026 M in CH_2Cl_2).

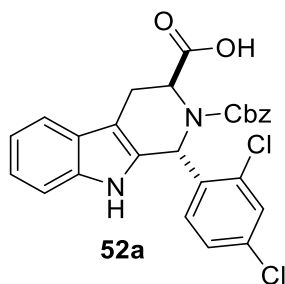


Methyl (1*R*,3*S*)-2-benzyl-1-(2,4-dichlorophenyl)-2,3,4,9-tetrahydro-1*H*-pyrido[3,4-*b*]indole-3-carboxylate (50a):

A reaction vessel was charged with **4a** (63.7 mg, 0.17 mmol) in CH_3CN (anh., 0.5 mL), benzyl bromide (25 μ L, 0.20 mmol), and DIPEA (0.45 mL, 2.56 mmol) under N_2 atmosphere. The reaction mixture was heated to 60 $^\circ C$ overnight. The solvent was removed under reduced pressure, and the residue was extracted with 1M HCl (2 mL) and EtOAc (1 mL). The aqueous layer was extracted further with EtOAc (3 x 1 mL). Combined organic layers were washed with water (2 x 2 mL), saturated NaCl solution (1 x 2 mL), dried over Na_2SO_4 , and concentrated under reduced pressure. The crude product was purified by column chromatography (8:2 hexanes:EtOAc) to afford **50a** as a white powder (67.8 mg, 86% yield).

1H NMR (500 MHz, $CDCl_3$) δ 7.58 (d, $J = 8.5$ Hz, 1H), 7.57 (s, 1H), 7.49 (d, $J = 7.7$ Hz, 1H), 7.45 (d, $J = 2.1$ Hz, 1H), 7.25 (m, 7H), 7.13 (td, $J = 8.1, 7.6, 1.3$ Hz, 1H), 7.09 (td, $J = 7.5, 1.1$ Hz, 1H), 6.18 (s, 1H), 4.01 (d, $J = 13.9$ Hz, 1H), 3.97 (dd, $J = 4.8, 3.5$ Hz, 1H), 3.77 (d, $J = 13.9$ Hz, 1H), 3.61 (s, 3H), 3.23 (dd, $J = 5.1, 1.8$ Hz, 2H). ^{13}C NMR (126 MHz, $CDCl_3$) δ 173.5, 138.92, 138.86, 136.6, 134.8, 134.3, 134.2, 131.8, 129.3, 128.6, 128.2, 127.4, 126.8, 122.0, 119.6, 118.4, 111.0, 106.5, 56.6, 56.3, 55.1, 51.6, 25.2. HRMS (ESI) $[M+H]^+$ calculated for $C_{26}H_{23}Cl_2N_2O_2^+$: 465.1131.

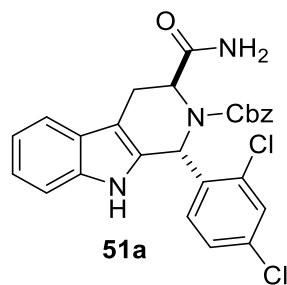
Found: 465.1119. One ^{13}C resonance is missing in aromatic region, this can be likely attributed to equivalent chemical shift of two positions in unsubstituted phenyl ring.



(1R,3S)-2-((benzyloxy)carbonyl)-1-(2,4-dichlorophenyl)-2,3,4,9-tetrahydro-1H-pyrido[3,4-b]indole-3-carboxylic acid (52a):

A reaction vessel was charged with **48a** (814.4 mg, 1.57 mmol) in CH_3OH (20 mL), followed by the addition of aqueous NaOH (20 mL, 2.5M). The reaction mixture was kept under reflux for 22 h. When cooled to ambient temperature, the mixture was acidified by 1M HCl (aq.) to pH \sim 2, extracted with CH_2Cl_2 (3 x 20 mL), dried over MgSO_4 . The solvent was removed *in vacuo* to afford **52a** as light yellow solid (727.3 mg, 92% yield). No further purification was necessary.

^1H NMR (600 MHz, DMSO, 70 $^\circ\text{C}$) δ 10.35 (s, 1H), 7.47 (d, $J = 7.8$ Hz, 1H), 7.44 (s, 1H), 7.29 (m, 6H), 7.22 (d, $J = 8.4$ Hz, 1H), 7.07 (m, 2H), 7.05 (t, $J = 7.1$ Hz, 1H), 6.99 (t, $J = 7.4$ Hz, 1H), 6.43 (s, 1H), 5.21 (dd, $J = 5.6, 2.7$ Hz, 1H), 5.11 (d, $J = 12.6$ Hz, 1H), 4.96 (d, $J = 12.2$ Hz, 1H), 3.45 (dd, $J = 15.6, 2.8$ Hz, 1H), 3.40 (dd, $J = 15.3, 6.1$ Hz, 1H). ^{13}C NMR (151 MHz, DMSO, 70 $^\circ\text{C}$) δ 172.5, 155.9, 140.0, 136.7, 135.8, 132.6, 132.3, 131.8, 129.5, 128.3, 127.8, 127.4, 127.2, 127.1, 125.5, 121.2, 118.6, 117.5, 111.4, 104.5, 66.6, 55.3, 53.0, 22.5. HRMS (ESI) $[\text{M}+\text{H}]^+$ calculated for $\text{C}_{26}\text{H}_{21}\text{Cl}_2\text{N}_2\text{O}_4^+$: 495.0873. Found: 495.9857. $[\alpha]_{\text{D}}^{24.4} = -8.59$ (c = 0.025 M in CH_2Cl_2).

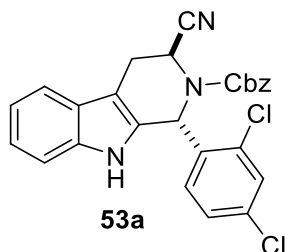


Benzyl (1*R*,3*S*)-3-carbamoyl-1-(2,4-dichlorophenyl)-1,3,4,9-tetrahydro-2*H*-pyrido[3,4-*b*]indole-2-carboxylate (51a):

A round bottom flask was charged with **52a** (451.0 mg, 0.89 mmol) in DMF (anh., 2 mL). A mixture of EDC·HCl (350.0 mg, 1.79 mmol), HOBt hydrate (291.1 mg, 1.81 mmol), and DIPEA (0.5 mL, 2.86 mmol) was dissolved in DMF (0.8 mL) and added to the solution of **52a** under N₂ on an ice bath. The mixture was stirred for 10 min before methanolic NH₃ was added (7M in CH₃OH, 0.2 mL, 1.4 mmol). The reaction was stirred for an additional 20 min on an ice bath before warming up to ambient temperature. Stirring continued at room temperature for 20 h. The reaction was quenched by the addition of water (30 mL) and EtOAc (10 mL), followed by a partition of the two phases. The aqueous layer was extracted with EtOAc (3 x 10 mL), the combined organic layers were washed with water (3 x 10 mL), a saturated aqueous solution of NH₄Cl (3 x 10 mL), a saturated aqueous solution of NaHCO₃ (3 x 10 mL), a saturated aqueous solution of NaCl (1 x 10 mL), dried over Na₂SO₄, and concentrated *in vacuo*. Compound **51a** was obtained as an off-white powder (394.6 mg, 85% yield). No further purification was necessary.

¹H NMR (600 MHz, DMSO, 70 °C) δ 10.27 (s, 1H), 7.41 (d, *J* = 7.9 Hz, 2H), 7.32 (d, *J* = 8.5 Hz, 1H), 7.28 (m, 5H), 7.21 (dd, *J* = 8.5, 1.8 Hz, 1H), 7.08 (s, 2H), 7.02 (t, *J* = 7.4 Hz, 1H), 6.97 (t, *J* = 7.4 Hz, 1H), 6.74 (s, 1H), 6.52 (s, 1H), 5.17 (dd, *J* = 5.3, 2.7 Hz, 1H), 5.08 (d, *J* = 12.7 Hz, 1H), 4.94 (d, *J* = 12.5 Hz, 1H), 3.43 (m, 2H). ¹³C NMR (151 MHz, DMSO, 70 °C) δ 172.7, 155.9,

140.6, 136.6, 135.9, 132.9, 132.5, 131.5, 129.4, 128.2, 127.7, 127.3, 127.1, 126.9, 125.6, 120.9, 118.4, 117.3, 111.3, 103.9, 66.4, 55.9, 53.3, 23.5. HRMS (ESI) $[M+H]^+$ calculated for $C_{26}H_{22}Cl_2N_3O_3^+$: 494.1033. Found: 494.1035. $[\alpha]_D^{24.7} = -8.03$ (c = 0.022 M in CH_2Cl_2).

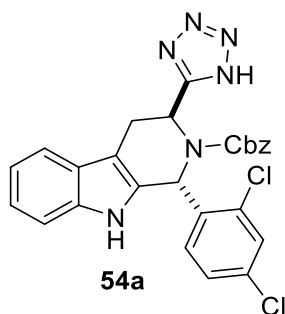


Benzyl (1R,3S)-3-cyano-1-(2,4-dichlorophenyl)-1,3,4,9-tetrahydro-2H-pyrido[3,4-b]indole-2-carboxylate (53a):

Prior to the reaction, pyridine was dried by reflux over KOH (0.1g/mL of pyridine), followed by simple distillation (bp = 111 °C). Collected pyridine was stored over 4Å molecular sieves under N_2 atmosphere for 24 h. Phosphoryl chloride was freshly distilled (bp = 102 °C) shortly prior to the reaction.

A round bottom flask was charged with **51a** (253.1 mg, 0.49 mmol) in dry pyridine (2 mL, 24.73 mmol) under N_2 . The mixture was cooled on ice bath and $POCl_3$ (0.25 mL, 2.68 mmol) was added dropwise. The reaction was kept on ice bath for 20 min, followed by stirring at ambient temperature for additional 100 min. 1M HCl (30 mL) and EtOAc (10 mL) were added and the mixture was stirred for additional 10 min. The organic and aqueous phases were partitioned and the aqueous layer was extracted with EtOAc (2 x 10 mL). The combined organic layers were washed with water (2 x 25 mL) and saturated aqueous NaCl solution (1 x 30 mL), dried over $MgSO_4$, and concentrated *in vacuo* to afford **53a** as light yellow solid (226.1 mg, 96% yield). No further purification was necessary.

^1H NMR (500 MHz, CDCl_3) δ 8.00 (s, 1H), 7.51 (d, $J = 7.8$ Hz, 1H), 7.30 (m, 5H), 7.19 (m, 1H), 7.14 (td, $J = 7.6, 1.1$ Hz, 1H), 7.04 (s, 4H), 6.47 (s, 1H), 5.76 (s, 1H), 5.19 (d, $J = 11.8$ Hz, 1H), 4.98 (d, $J = 11.5$ Hz, 1H), 3.40 (m, 2H). ^{13}C NMR (126 MHz, CDCl_3) δ 155.8, 139.0, 136.8, 134.8, 133.9, 132.2, 131.7, 129.7, 128.7, 128.6, 128.5, 128.2, 127.9, 126.0, 123.2, 120.5, 118.5, 118.4, 111.5, 104.7, 69.1, 52.9, 44.7, 25.1. HRMS (ESI) $[\text{M}+\text{H}]^+$ calculated for $\text{C}_{26}\text{H}_{20}\text{Cl}_2\text{N}_3\text{O}_2^+$: 476.0927. Found: 476.0906.

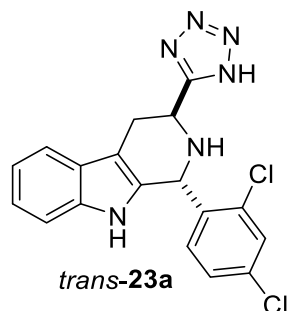


Benzyl (1R,3S)-1-(2,4-dichlorophenyl)-3-(1H-tetrazol-5-yl)-1,3,4,9-tetrahydro-2H-pyrido[3,4-b]indole-2-carboxylate (54a):

A sealed tube was charged with **53a** (76.5 mg, 0.16 mmol), ZnBr_2 (19.0 mg, 0.08 mmol), NaN_3 (23.0 mg, 0.35 mmol), and 2-propanol (3 mL). Reaction mixture was heated to 100 °C for 25 h. When cooled to ambient temperature, 1M HCl (3 mL) and EtOAc (2 mL) were added and the layers were partitioned. Aqueous layer was then extracted with EtOAc (3 x 2 mL), combined organic layers were washed with water (2 x 4 mL) and saturated NaCl solution (1 x 4 mL), dried over Na_2SO_4 , and concentrated *in vacuo* to afford **54a** as off-white powder (76.4 mg, 89%).

^1H NMR (500 MHz, CDCl_3) δ 8.01 (s, 1H), 7.46 (d, $J = 7.8$ Hz, 1H), 7.22 (m, 5H), 7.09 (m, 3H), 6.95 (s, 2H), 6.59 (s, 1H), 6.25 (dd, $J = 5.4, 2.6$ Hz, 1H), 5.15 (d, $J = 11.9$ Hz, 1H), 4.93 (d, $J = 12.0$ Hz, 1H), 3.67 (ddd, $J = 15.9, 2.6, 1.0$ Hz, 1H), 3.60 (dd, $J = 15.9, 5.3$ Hz, 1H). ^{13}C NMR (126 MHz, CDCl_3) δ 157.0, 140.0, 136.6, 135.0, 133.7, 132.3, 132.2, 129.6, 128.50, 128.46, 128.24,

128.16, 128.0, 126.1, 122.8, 120.1, 118.5, 111.5, 104.5, 68.8, 53.4, 49.2, 25.5. HRMS (ESI) $[M+H]^+$ calculated for $C_{26}H_{21}Cl_2N_6O_2^+$: 519.1098. Found: 519.1091.

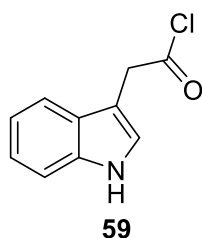


(1*R*,3*S*)-1-(2,4-dichlorophenyl)-3-(1*H*-tetrazol-5-yl)-2,3,4,9-tetrahydro-1*H*-pyrido[3,4-*b*]indole (*trans*-23a):

A reaction vessel was charged with **54a** (91.4 mg, 0.17 mmol) and HBr in AcOH (33 wt%, 0.45 mL, 2.61 mmol). The mixture was stirred at ambient temperature for 15 min (until all effervescence seized). Reaction mixture was then added dropwise to a saturated NaHCO₃ solution (3 mL) on ice, followed by addition of EtOAc (4 mL). Additional NaHCO₃ solution was added dropwise to pH = 5.5-6.0. The aqueous and organic layers were partitioned and aqueous layer was extracted with EtOAc (2 x 4 mL). Combined organic layers were dried over MgSO₄, concentrated in vacuo, and precipitated from Et₂O/hexanes to afford 56.8 mg of crude **23a**. The crude product was purified by column chromatography (crude material:silica = 1:132, gradient 100 – 90% CH₂Cl₂ : 2-propanol). Collected fractions were analyzed by TLC under both short- and long-wave UV light. The pure product *trans*-**23a** was isolated as light yellow solid (23.3 mg, 36% yield). No *cis*-**23a** was observed in the pure fraction by ¹H NMR, however a mixed fraction of *cis*-/*trans*-**23a** was also obtained from the column purification (14.0 mg, dr = 15:85 *cis*:*trans*).

¹H NMR (500 MHz, CD₃OD) δ 7.66 (d, J = 2.1 Hz, 1H), 7.57 (d, J = 7.8 Hz, 1H), 7.34 (dd, J = 8.4, 2.1 Hz, 1H), 7.28 (d, J = 8.1 Hz, 1H), 7.14 (ddd, J = 8.2, 7.1, 1.1 Hz, 1H), 7.08 (ddd, J = 7.9,

7.1, 1.0 Hz, 2H), 7.06 (d, $J = 8.4$ Hz, 1H), 6.13 (s, 1H), 4.85 (dd, $J = 9.3, 4.9$ Hz, 1H), 3.51 (dd, $J = 15.9, 4.7$ Hz, 1H), 3.38 (ddd, $J = 16.2, 9.3, 1.3$ Hz, 1H). ^{13}C NMR (126 MHz, CD_3OD) δ 160.1, 138.6, 136.9, 135.7, 133.3, 131.0, 129.8, 128.7, 127.5, 123.5, 120.5, 119.2, 112.3, 109.7, 53.1, 47.3, 27.1. HRMS (ESI) $[\text{M}+\text{H}]^+$ calculated for $\text{C}_{18}\text{H}_{15}\text{Cl}_2\text{N}_6^+$: 385.0730. Found: 385.0713. The ^{13}C resonance at $\delta = 129.8$ corresponds to two accidentally equivalent carbons as confirmed by HMBC.

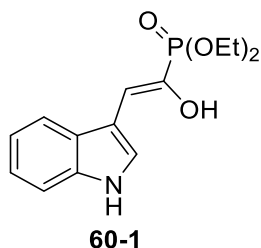


2-(1*H*-indol-3-yl)acetyl chloride (**59**):

A 100 mL round bottom flask was charged with 3.03 g (17.3 mmol) of indole-3-acetic acid (**58**). CH_2Cl_2 (30 mL) was added under N_2 . The mixture was left to cool on ice bath for 5 min before oxalyl chloride (2 mL, 23.6 mmol) was added dropwise, followed by addition of dimethyl formamide (0.1 mL, 1.3 mmol) in one portion. Stirring on ice continued for another 10 minutes and then the reaction was allowed to warm up to ambient temperature. The reaction was stirred until no more effervescence was observable (1 h) and then was concentrated in vacuo to give 3.97g of **59** as brown oil (118% crude yield). Product formation was confirmed by ^1H and ^{13}C NMR. The material was carried to the next step immediately without further purification. This procedure was performed according to literature precedence with slight modifications.¹¹

^1H NMR (400 MHz, CDCl_3) δ 8.56 (s, 1H), 7.55 (ddd, $J = 7.7, 1.4, 0.7$ Hz, 1H), 7.38 (dt, $J = 8.0, 0.9$ Hz, 1H), 7.21 (ddd, $J = 8.2, 7.0, 1.4$ Hz, 1H), 7.16 (ddd, $J = 7.6, 7.1, 1.2$ Hz, 1H), 7.14 (s, 1

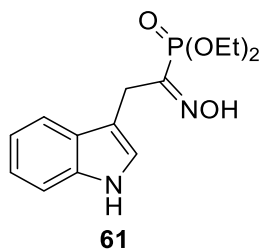
H), 4.29 (s, 2H). ^{13}C NMR (126 MHz, CDCl_3) δ 172.2, 136.1, 126.8, 124.1, 122.8, 120.4, 118.6, 111.6, 106.3, 43.7. The literature did not provide experimental data for **59** to compare.¹¹



Diethyl (1-hydroxy-2-(1*H*-indol-3-yl)vinyl)phosphonate (**60-1**):

Freshly distilled THF (10 mL) was added to crude oil of **59** under N_2 and the mixture was stirred at ambient temperature to dissolve. Then, the solution was cooled on ice bath and triethyl phosphite (3 mL, 17.5 mmol) in freshly distilled THF (2 mL) was added dropwise (1 mL/min). After the addition was completed, the ice bath was removed, and the reaction mixture was heated to reflux. After 15 min of reflux, the reaction mixture was concentrated *in vacuo* to yield 5.68 g of **60-1** as brown oil (111% crude yield). Product formation was confirmed by ^1H , ^{13}C , and ^{31}P NMR and by HRMS. Only enol tautomer was detected by NMR. The material was carried to the next step immediately without further purification. This procedure was performed according to literature precedence with modifications.¹¹

^1H NMR (400 MHz, CDCl_3) δ 8.95 (s, 1H), 7.98 (d, $J = 2.0$ Hz, 1H), 7.71 (d, $J = 7.1$ Hz, 1H), 7.38 (d, $J = 7.2$ Hz, 1H), 7.17 (m, 2H), 6.56 (d, $J = 11.0$ Hz, 1H), 4.19 (m, 4H), 1.37 (t, $J = 7.1$ Hz, 6H). ^{31}P NMR (162 MHz, CDCl_3) δ 13.6 ^{13}C NMR (101 MHz, CDCl_3) δ 137.2 (d, $^1J_{\text{CP}} = 210.1$ Hz), 135.5, 127.2, 126.6, 122.4, 120.2, 118.5, 111.5, 110.2 (d, $^3J_{\text{CP}} = 18.1$ Hz), 110.0 (d, $^2J_{\text{CP}} = 28.8$ Hz), 63.1 (d, $^2J_{\text{CP}} = 5.2$ Hz), 16.4 (d, $^3J_{\text{CP}} = 6.5$ Hz). The literature did not provide experimental data for **60-1** to compare.¹¹

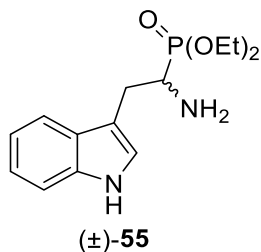


Diethyl (1-(hydroxyimino)-2-(1*H*-indol-3-yl)ethyl)phosphonate (61):

Hydroxylamine hydrochloride (1.59 g, 22.6 mmol) was added to the crude oil **60-1** followed by addition of anhydrous ethanol (12 mL) and freshly dried pyridine (2 mL) under N₂. The mixture was stirred at ambient temperature for 13 hours. After the reaction reached completion as indicated by TLC analysis, the solvents were removed in vacuo. The crude brown oil was dissolved and partitioned between 1M HCl (30 mL) and EtOAc (30 mL). The aqueous layer was then extracted with EtOAc (2x 10 mL). Combined organic layers were washed with water (2x 20 mL), saturated sodium chloride solution (1x 20 mL), dried over Na₂SO₄, filtered, concentrated *in vacuo* to yield 5.15 g of **61** as golden brown solid (96% crude yield). Product formation was confirmed by ¹H, ¹³C, and ³¹P NMR and by HRMS. Two isomers were detected by NMR in 1:0.6 ratio, but the stereochemistry was not determined. The material was carried to the next step without further purification. This procedure was performed according to literature precedence with modifications.¹¹

¹H NMR (400 MHz, CDCl₃, mixture of isomers) δ 8.68 (s, 0.6H), 8.51 (s, 1H), 7.68 (d, *J* = 7.8 Hz, 1H), 7.59 (d, *J* = 8.0 Hz, 0.6H), 7.30 (d, *J* = 8.0 Hz, 1.6H), 7.10 (m, 5H), 3.93 (m, 16H), 1.12 (t, *J* = 7.1 Hz, 3H), 1.07 (t, *J* = 7.1 Hz, 6H). ¹H NMR (400 MHz, CDCl₃, major isomer) δ 9.42 (s, 1H), 8.29 (s, 1H), 7.71 (d, *J* = 7.9 Hz, 1H), 7.32 (dt, *J* = 8.1, 0.9 Hz, 1H), 7.19 (d, *J* = 2.4 Hz, 1H), 7.16 (ddd, *J* = 8.1, 7.1, 1.2 Hz, 1H), 7.09 (ddd, *J* = 8.0, 7.1, 1.1 Hz, 1H), 4.04 (dd, *J* = 14.3, 1.0 Hz, 2H), 3.92 (m, 4H), 1.11 (td, *J* = 7.1, 0.7 Hz, 6H). ³¹P NMR (162 MHz, CDCl₃) δ 9.5 (s, 1P), 5.2 (s,

0.6P). ^{13}C NMR (126 MHz, CDCl_3 , mixture of isomers) δ 153.7 (d, $^1J_{\text{CP}} = 211.9$ Hz), 150.8 (d, $^1J_{\text{CP}} = 152.0$ Hz), 136.4, 136.1, 127.4, 127.3, 124.3, 124.0, 121.9, 121.8, 119.3, 119.0, 118.8, 111.4, 111.2, 110.2, 108.8, 63.1 (d, $^2J_{\text{CP}} = 5.8$ Hz), 63.0 (d, $^2J_{\text{CP}} = 5.9$ Hz), 29.0 (d, $^2J_{\text{CP}} = 18.3$ Hz), 22.0 (d, $^2J_{\text{CP}} = 15.9$ Hz), 16.2 (d, $^3J_{\text{CP}} = 6.4$ Hz), 16.1 (d, $^3J_{\text{CP}} = 6.6$ Hz). The literature did not provide experimental data for **61** to compare.¹¹



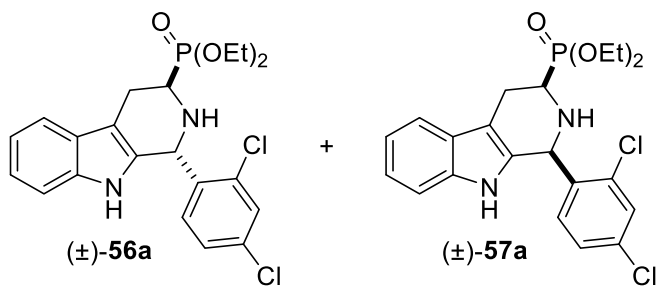
Diethyl (1-amino-2-(1*H*-indol-3-yl)ethyl)phosphonate ((±)-55):

Powdered zinc was activated prior to reduction of **61** by following procedure. Powdered zinc was added to a round bottom flask followed by addition of 1.5M HCl (35 mL/g of Zn). Mixture was stirred vigorously for 5 min and the HCl was decanted. Zinc was then washed with water (4 x 70 mL/g). The used water was decanted after each wash. Absolute ethanol (17 mL/g) was added to the zinc and the solid was vacuum filtered using water aspirator. Solid was then washed on the filter with acetone (1 x 35 mL/g) and anhydrous Et_2O (2 x 17 mL/g). Zinc was then transferred to flask and dried on a vacuum line with heating for 15 min. Activated zinc (Zn^*) was then stored under N_2 .

Crude **60** was dissolved in 17 mL of 88% formic acid (aqueous) and transferred into a two-neck round bottom flask. Activated zinc was added to the solution (1 equiv, ~ 800 mg) under positive N_2 pressure every 2 hours until 7 equivalents were added, while the reaction was heated to 45 °C. After addition of last Zn^* portion, the reaction was allowed to stir overnight. Reaction was stopped after 24 h since the addition of first Zn^* portion. The slurry was filtered and washed with

chloroform (30 mL). Filtrate was basified with 1M NaOH to pH 10-11 and partitioned. Aqueous layer was extracted with CH₃Cl (2 x 15 mL) and combined organic layers were washed with saturated NaCl solution (1 x 30 mL), dried over MgSO₄, and concentrated in vacuo to afford crude (±)-**55** as dark brown oil in 101% yield. The pure product was then separated by column chromatography (gradient 100 – 80% CH₂Cl₂ with 2-propanol + 0.5% methanolic ammonia, the silica gel used for the column was prepared in 99.5:0.5 CH₂Cl₂:NH₃ (in MeOH)) to yield 2.49 g of golden oil. Yield over four steps calculated from indole-3-acetic acid (**58**) was 49%.

¹H NMR (400 MHz, CDCl₃) δ 8.60 (s, 1H), 7.60 (ddt, *J* = 7.9, 1.4, 0.8 Hz, 1H), 7.37 (dt, *J* = 8.1, 0.9 Hz, 1H), 7.18 (ddd, *J* = 8.2, 7.1, 1.2 Hz, 1H), 7.10 (m, 2H), 4.20 (m, 4H), 3.39 (m, 2H), 2.86 (m, 1H), 1.35 (tdd, *J* = 7.1, 1.5, 0.4 Hz, 6H). ³¹P NMR (162 MHz, CDCl₃) δ 27.9. ¹³C NMR (126 MHz, CDCl₃) δ 136.6, 127.3, 123.3, 122.3, 119.6, 118.8, 111.6 (d, ³*J*_{CP} = 17.3 Hz), 111.4, 62.5 (d, ²*J*_{CP} = 7.2 Hz), 62.4 (d, ²*J*_{CP} = 7.0 Hz), 49.3 (d, ¹*J*_{CP} = 154.9 Hz), 27.8, 16.7 (d, ³*J*_{CP} = 5.5 Hz). The compound was published previously and the experimental data are in agreement with literature.¹¹



Diethyl (1-(2,4-dichlorophenyl)-2,3,4,9-tetrahydro-1H-pyrido[3,4-b]indol-3-yl)phosphonate:

To a mixture of (±)-**55** (264.3 mg, 0.79 mmol), 4Å molecular sieves (1 g, powdered), and 2,4-dichlorobenzaldehyde (142.3 mg, 0.81 mmol), CH₂Cl₂ (8 mL) was added under nitrogen. The resulting mixture was stirred at room temperature for 5 minutes. TFA (0.15 mL, 1.96 mmol) was added dropwise. Reaction mixture was further stirred at room temperature for additional 3 hours.

Reaction was cooled to 0 °C and saturated aqueous solution of NaHCO₃ (10 mL) was added, followed by addition of EtOAc (10 mL). After stirring for 30 min at 0 °C, the molecular sieves were filtered, phases of the filtrate were partitioned, and the aqueous layer was extracted with EtOAc (3 x 10 mL). The combined organic layers were washed with water (2 x 10 mL) and saturated aqueous NaCl solution (1 x 15 mL), dried over MgSO₄, and concentrated *in vacuo*. Compounds (±)-**56a** and (±)-**57a** were separated from the crude material by flash chromatography (gradient, from 100% CH₂Cl₂ to 95:5 CH₂Cl₂ : 2-propanol) to give (±)-**57a** (163.2 mg, 45%, first-eluting, off-white powder) and (±)-**56a** (61.7 mg, 17%, second-eluting, off-white powder).

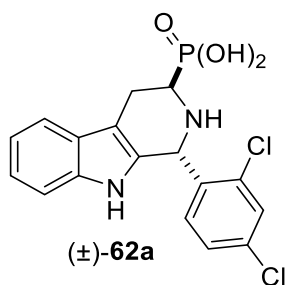
Diethyl (trans-1-(2,4-dichlorophenyl)-2,3,4,9-tetrahydro-1H-pyrido[3,4-b]indol-3-yl)phosphonate ((±)-56a):

¹H NMR (500 MHz, CDCl₃) δ 7.87 (s, 1H), 7.57 (d, *J* = 7.7 Hz, 1H), 7.46 (d, *J* = 2.1 Hz, 1H), 7.29 (d, *J* = 8.0 Hz, 1H), 7.20 (ddd, *J* = 8.1, 7.1, 1.3 Hz, 1H), 7.15 (td, *J* = 7.4, 1.1 Hz, 1H), 7.07 (dd, *J* = 8.3, 2.1 Hz, 1H), 6.69 (d, *J* = 8.3 Hz, 1H), 5.65 (s, 1H), 4.12 (m, 4H), 3.24 (ddd, *J* = 15.7, 9.8, 5.4 Hz, 1H), 3.06 (m, 2H), 1.25 (t, *J* = 7.1 Hz, 6H). ³¹P NMR (162 MHz, CDCl₃) δ 25.9. ¹³C NMR (126 MHz, CDCl₃) δ 137.3, 136.1, 134.9, 134.6, 131.2 (d, ⁴*J*_{CP} = 2.3 Hz), 131.1, 129.9, 126.9, 126.8 (d, ⁴*J*_{CP} = 2.2 Hz), 122.6, 119.9, 118.5, 111.2, 110.3 (d, ³*J*_{CP} = 15.4 Hz), 63.1 (d, ²*J*_{CP} = 6.7 Hz), 62.5 (d, ²*J*_{CP} = 6.7 Hz), 51.9 (d, ³*J*_{CP} = 16.7 Hz), 45.9 (d, ¹*J*_{CP} = 159.5 Hz), 22.7, 16.6 (d, ³*J*_{CP} = 5.7 Hz), 16.5 (d, ³*J*_{CP} = 5.9 Hz). HRMS (ESI) [M+H]⁺ calculated for C₂₁H₂₄Cl₂N₂O₃P⁺: 453.0896. Found: 453.0882.

Diethyl (cis-1-(2,4-dichlorophenyl)-2,3,4,9-tetrahydro-1H-pyrido[3,4-b]indol-3-yl)phosphonate ((±)-57a):

¹H NMR (500 MHz, CDCl₃) δ 7.58 (s, 1H), 7.53 (d, *J* = 7.6 Hz, 1H), 7.47 (d, *J* = 2.0 Hz, 1H), 7.31 (d, *J* = 8.4 Hz, 1H), 7.24 (d, *J* = 7.7 Hz, 1H), 7.19 (dd, *J* = 8.4, 1.9 Hz, 1H), 7.15 (td, *J* = 8.0, 7.5,

1.5 Hz, 1H), 7.12 (td, $J = 7.5, 1.2$ Hz, 1H), 5.72 (s, 1H), 4.26 (m, 4H), 3.56 (ddd, $J = 14.3, 10.9, 4.5$ Hz, 1H), 3.08 (m, 2H), 2.20 (s, 1H), 1.39 (td, $J = 7.1, 4.5$ Hz, 6H). ^{31}P NMR (162 MHz, CDCl_3) δ 25.3. ^{13}C NMR (126 MHz, CDCl_3) δ 137.4, 136.0, 134.8, 134.6, 133.1 (d, $^4J_{\text{CP}} = 2.2$ Hz), 131.2, 129.7, 128.0, 126.96 (d, $^4J_{\text{CP}} = 2.4$ Hz), 122.4, 119.9, 118.4, 111.1, 109.3 (d, $^3J_{\text{CP}} = 17.0$ Hz), 62.94 (d, $^2J_{\text{CP}} = 2.7$ Hz), 62.89 (d, $^2J_{\text{CP}} = 2.7$ Hz), 54.5, 51.8 (d, $^1J_{\text{CP}} = 159.6$ Hz), 23.0, 16.7 (d, $^3J_{\text{CP}} = 5.7$ Hz).. HRMS (ESI) $[\text{M}+\text{H}]^+$ calculated for $\text{C}_{21}\text{H}_{24}\text{Cl}_2\text{N}_2\text{O}_3\text{P}^+$: 453.0896. Found: 453.0878.

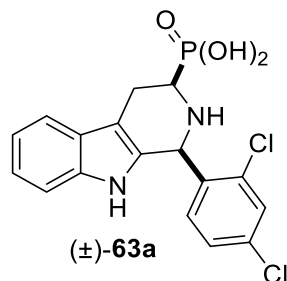


(*trans*-1-(2,4-dichlorophenyl)-2,3,4,9-tetrahydro-1*H*-pyrido[3,4-*b*]indol-3-yl)phosphonic acid ((±)-62a**):**

17.2 mg of (±)-**56a** was dissolved in 0.6 mL of CDCl_3 and added to an NMR tube closed with rubber septum. The solution was cooled on ice bath for 5 minutes before 0.1 mL of trimethylsilyl bromide was added. The reaction mixture stayed on ice for additional 5 minutes before allowing to warm up to room temperature. Reaction was then heated to 50 °C and monitored for progress by ^1H and ^{31}P NMR. Completion was reached after 48 hours of heating. Reaction mixture was then concentrated under reduced pressure, washed three times with 1 mL CH_3OH and dried *in vacuo*. Compound (±)-**62a** was obtained in 94% yield (14.2 mg, dr = 96:4) as a yellow powder.

^1H NMR (400 MHz, CD_3OD) δ 7.78 (d, $J = 2.1$ Hz, 1H), 7.59 (d, $J = 7.8$ Hz, 1H), 7.44 (dd, $J = 8.4, 2.2$ Hz, 1H), 7.30 (d, $J = 8.1$ Hz, 1H), 7.23 (d, $J = 8.4$ Hz, 1H), 7.18 (ddd, $J = 8.2, 7.0, 1.2$ Hz, 1H), 7.11 (ddd, $J = 8.0, 7.1, 1.1$ Hz, 1H), 6.50 (s, 1H), 4.02 (ddd, $J = 15.1, 7.1, 6.1$ Hz, 1H), 3.56

(dddd, $J = 16.8, 13.9, 6.1, 1.3$ Hz, 1H), 3.37 (m, 1H). ^{31}P NMR (202 MHz, CD_3OD) δ 14.0. ^{13}C NMR (126 MHz, CD_3OD) δ 138.7, 138.5, 137.6, 133.9, 131.5, 131.3, 129.4, 127.0 (d, $^4J_{\text{CP}} = 6.1$ Hz), 124.1, 120.9, 119.3, 112.5, 108.6 (d, $^3J_{\text{CP}} = 7.8$ Hz), 53.5 (d, $^3J_{\text{CP}} = 5.4$ Hz), 49.3 (d, $^1J_{\text{CP}} = 146$ Hz), 49.0, 21.1. HRMS (ESI) $[\text{M}+\text{H}]^+$ calculated for $\text{C}_{17}\text{H}_{16}\text{Cl}_2\text{N}_2\text{O}_3\text{P}^+$: 397.0270. Found: 397.0256.



(cis-1-(2,4-dichlorophenyl)-2,3,4,9-tetrahydro-1H-pyrido[3,4-b]indol-3-yl)phosphonic acid ((±)-63a):

17.0 mg of (±)-57a was dissolved in 0.6 mL of CD_3CN and added to an NMR tube closed with rubber septum. The solution was cooled on ice bath for 5 minutes before 0.1 mL of trimethylsilyl bromide was added. The reaction mixture stayed on ice for additional 5 minutes before allowing to warm up to room temperature. Reaction was then heated to 50 °C and monitored for progress by ^1H and ^{31}P NMR. Completion was reached after 8 hours of heating. Reaction mixture was then concentrated under reduced pressure, washed three times with 1 mL CH_3OH and dried *in vacuo*. Compound (±)-63a was obtained in 98% yield (14.8 mg, dr = 97:3) as a yellow powder.

^1H NMR (400 MHz, CD_3OD) δ 7.76 (s, 1H), 7.55 (d, $J = 7.8$ Hz, 1H), 7.49 (m, 2H), 7.28 (d, $J = 8.1$ Hz, 1H), 7.16 (ddd, $J = 8.2, 7.0, 1.3$ Hz, 1H), 7.10 (ddd, $J = 8.0, 7.0, 1.1$ Hz, 1H), 6.55 (s, 1H), 4.29 (ddd, $J = 14.4, 12.2, 5.0$ Hz, 1H), 3.48 (m, 1H), 3.37 (m, 1H). ^{31}P NMR (162 MHz, CD_3OD) δ 13.3.

References

1. Shao, Y.; Molnar, L.; Jung, Y.; Kussmann, J.; Ochsenfeld, C.; Brown, S.; Gilbert, A.; Slipchenko, L.; Levchenko, S.; O'Neill, D., *Phys. Chem. Chem. Phys.* **2006**.
2. Frisch, M. J. T., G. W.; Schlegel, H. B.; Scuseria, G. E.; Robb, M. A.; Cheeseman, J. R.; Scalmani, G.; Barone, V.; Mennucci, B.; Petersson, G. A.; Nakatsuji, H.; Caricato, M.; Li, X.; Hratchian, H. P.; Izmaylov, A. F.; Bloino, J.; Zheng, G.; Sonnenberg, J. L.; Hada, M.; Ehara, M.; Toyota, K.; Fukuda, R.; Hasegawa, J.; Ishida, M.; Nakajima, T.; Honda, Y.; Kitao, O.; Nakai, H.; Vreven, T.; Montgomery, J. A., Jr.; Peralta, J. E.; Ogliaro, F.; Bearpark, M.; Heyd, J. J.; Brothers, E.; Kudin, K. N.; Staroverov, V. N.; Kobayashi, R.; Normand, J.; Raghavachari, K.; Rendell, A.; Burant, J. C.; Iyengar, S. S.; Tomasi, J.; Cossi, M.; Rega, N.; Millam, J. M.; Klene, M.; Knox, J. E.; Cross, J. B.; Bakken, V.; Adamo, C.; Jaramillo, J.; Gomperts, R.; Stratmann, R. E.; Yazyev, O.; Austin, A. J.; Cammi, R.; Pomelli, C.; Ochterski, J. W.; Martin, R. L.; Morokuma, K.; Zakrzewski, V. G.; Voth, G. A.; Salvador, P.; Dannenberg, J. J.; Dapprich, S.; Daniels, A. D.; Farkas, Ö.; Foresman, J. B.; Ortiz, J. V.; Cioslowski, J.; Fox, D. J., *Gaussian 09, Revision E.01*. Gaussian, Inc. : Wallingford CT, 2009.
3. Bally, T.; Rablen, P. R., Quantum-Chemical Simulation of ^1H NMR Spectra. 2. Comparison of DFT-Based Procedures for Computing Proton–Proton Coupling Constants in Organic Molecules. *J. Org. Chem.* **2011**, *76* (12), 4818-4830.
4. Pierens, G. K.; Venkatachalam, T.; Reutens, D. C., NMR and DFT investigations of structure of colchicine in various solvents including density functional theory calculations. *Sci. Rep.* **2017**, *7* (1), 5605.
5. Lodewyk, M. W.; Siebert, M. R.; Tantillo, D. J., Computational Prediction of ^1H and ^{13}C Chemical Shifts: A Useful Tool for Natural Product, Mechanistic, and Synthetic Organic Chemistry. *Chem. Rev.* **2012**, *112* (3), 1839-1862.
6. Saiga, Y.; Iijima, I.; Ishida, A.; Miyagishima, T.; Takamura, N.; Oh-Ishi, T.; Matsumoto, M.; Matsuoka, Y., Synthesis of 1, 2, 3, 4-Tetrahydro- β -carboline Derivatives as Hepatoprotective Agents. IV. Positional Isomers of 1, 2, 3, 4-Tetrahydro-2-methylthiothiocarbonyl- β -carboline-3-carboxylic Acid and Its 1-Alkylated Derivatives. *Chem. Pharm. Bull.* **1987**, *35* (9), 3705-3712.
7. Nakagawa, M.; Fukushima, H.; Kawate, T.; Hongu, M.; Une, T.; Kodato, S.-i.; Taniguchi, M.; Hino, T., Synthetic Approaches to Fumitremorgins. III. : Synthesis of Optically Active Pentacyclic Ring Systems, and Their Oxidation at Ring C. *Chem. Pharm. Bull.* **1989**, *37* (1), 23-32.
8. Ishida, A.; Nakamura, T.; Irie, K.; Ohishi, T., A New Method for the Preparation of 3, 4-Dihydro- and 1, 2, 3, 4-Tetrahydro- β -carbolines. *Chem. Pharm. Bull.* **1985**, *33* (8), 3237-3249.
9. Liu, L. MMV008138 and analogs: potential novel antimalarial agents for *P. falciparum*. Virginia Polytechnic Institute and State University, Blacksburg, VA, 2018.
10. Yao, Z.-K.; Krai, P. M.; Merino, E. F.; Simpson, M. E.; Slebodnick, C.; Cassera, M. B.; Carlier, P. R., Determination of the active stereoisomer of the MEP pathway-targeting antimalarial agent MMV008138, and initial structure–activity studies. *Bioorg. Med. Chem. Lett.* **2015**, *25* (7), 1515-1519.

11. Viveros-Ceballos, J. L.; Sayago, F. J.; Cativiela, C.; Ordóñez, M., First Practical and Efficient Synthesis of 3-Phosphorylated β -Carboline Derivatives Using the Pictet–Spengler Reaction. *Eur. J. Org. Chem.* **2015**, *2015* (5), 1084-1091.

5 Supporting information for Chapter 2

5.1 Tabulated NMR data for analyzed compounds

Table 5.1 ¹³C NMR chemical shifts (CDCl₃) of C-1 and C-3 for **4a-ar** and **5a-ar**.

		δ C1 [ppm]			δ C3 [ppm]		
		<i>trans</i> (4)	<i>cis</i> (5)	Δ _{δ4-δ5}	<i>trans</i> (4)	<i>cis</i> (5)	Δ _{δ4-δ5}
a	2', 4'-Cl ₂	51.3 ^b	53.9 ^b	-2.6	52.34 ^c	56.7 ^b	-4.3
b	H	55.1 ^b	58.8 ^b	-3.8	52.7 ^b	57.0 ^b	-4.3
c^e	2'-Cl	51.8	54.4	-2.6	52.23	56.8	-4.58
d^e	4'-Cl	54.3	58.1	-3.8	52.5	56.9	-4.4
e^{e,g}	2'-Cl, 4'-CH ₃	51.4	53.9	-2.5	52.0	56.7	-4.7
f^e	2'-CH ₃ , 4'-Cl	51.4	53.5	-2.1	52.6	57.0	-4.4
g^e	2', 4'-F ₂	47.8 ^b	50.6 ^b	-2.8	52.4 ^b	56.8 ^b	-4.4
h^e	2'-F, 4'-Cl	47.9 ^a	50.6 ^a	-2.7	52.6	56.8	-4.3
i	2'-Cl, 4'-F	51.2 ^b	53.8 ^b	-2.6	52.30 ^c	56.7 ^b	-4.4
j^{e,g}	2'-Cl, 4'-Br	51.2	53.9	-2.7	52.2	56.6	-4.4
k	2'-Br, 4'-Cl	53.7 ^b	56.6 ^b	-2.9	52.36 ^c	56.7 ^b	-4.3
l	2', 4'-Br ₂	53.7 ^b	56.57 ^c	-2.8	52.1 ^c	56.57 ^c	-4.5
m	2'-Br	54.2 ^b	57.0 ^d	-2.8	52.2 ^c	56.7 ^d	-4.5
n	2'-F, 4'-Br	47.9 ^b	50.6 ^b	-2.7	52.2 ^b	56.7 ^b	-4.5
o	2'-Br, 4'-F	53.5 ^b	56.4 ^d	-2.9	52.3 ^c	56.7 ^d	-4.4
p	2'-I, 4'-F	58.0 ^b	61.6 ^b	-3.6	52.46 ^c	56.8 ^b	-4.3
q	2'-F, 4'-I	48.0 ^b	50.7 ^b	-2.7	52.5 ^c	56.8 ^b	-4.3
r	2'-Br, 4'-I	53.9 ^b	56.8 ^b	-2.9	52.36 ^c	56.7 ^b	-4.3
w	2'-Cl, 4'-OCH ₃	51.3 ^b	53.9 ^b	-2.6	52.2 ^c	56.9 ^b	-4.7
x	2'-OCH ₃ , 4'-Cl	48.8 ^b	51.3 ^b	-2.5	52.29 ^c	57.0 ^b	-4.7
y	2'-Cl, 4'-CO ₂ CH ₃	51.6 ^b	54.3 ^b	-2.7	52.30 ^c	56.7 ^b	-4.4
z^{e,g}	2', 4'-(CF ₃) ₂	49.8	53.4	-3.6	53.0	56.6	-3.6
aa^{e,g}	2', 4'-(CH ₃) ₂	51.4	53.5	-2.1	52.4	57.0	-4.6
ab^e	2', 4'-(OCH ₃) ₂	49.0	51.5	-2.5	51.9	57.0	-5.1
ac	3', 4'-Cl ₂	53.9 ^b	57.9 ^b	-4.0	52.5 ^c	56.8 ^b	-4.3
ad^e	3', 4'-(OCH ₃) ₂	54.8	58.7	-3.9	53.0	57.1	-4.1
ae	2', 6'-F ₂ , 4'-Cl	44.6 ^b	48.0 ^b	-3.4	53.9 ^b	57.3 ^b	-3.4
ag	2', 3', 4'-F ₃	47.9 ^b	50.5 ^b	-2.6	52.39 ^c	56.7 ^b	-4.3
ah^{e,g}	2'-Br, 4'-F, 5'-OCH ₃	53.5	56.4	-2.9	53.1	56.7	-3.6
an	cyclohexyl	55.4	57.8	-2.4	53.5	56.6	-3.1
ao	<i>n</i> -butyl	50.4	52.9	-2.5	52.7	56.6	-3.9
ap	<i>i</i> -butyl	48.2	50.7	-2.5	52.5	56.6	-4.1
aq	<i>t</i> -butyl	59.4	62.6	-3.2	54.4	56.5	-2.1
ar	CH(CH ₂ CH ₃) ₂	51.0	54.6	-3.6	54.1	56.6	-2.5
Average		51.7	54.6	-2.9	52.6	56.8	-4.2
St. deviation		3.2	3.4	0.5	0.6	0.2	0.6

Signals identified via: ^aJCF, ^bHSQC, ^c(C)DEPT and HSQC, ^dHMBC and HSQC. ^eSample is unavailable. ^gSample and NMR data unavailable. ^hIf the values are identical, only one of them is shown. ^{e,g}Shifts were assigned based on the pattern seen in proven compounds, unless stated otherwise.

Table 5.2 ¹³C NMR chemical shifts (CDCl₃) of C=O and C1' for **4a-ar** and **5a-ar**.

		δ C=O [ppm]			δ C1' [ppm]		
		<i>trans</i> (4)	<i>cis</i> (5)	Δ _{δ4-δ5}	<i>trans</i> (4)	<i>cis</i> (5)	Δ _{δ4-δ5}
a ^a	2', 4'-Cl ₂	173.8	173.1	0.8	137.9	137.4	0.5
b ^a	H	174.3	173.3	1.0	142.1	140.8	1.3
c ^d	2'-Cl	173.9	173.2	0.7	–	–	–
d ^d	4'-Cl	174.1	173.2	0.9	–	–	–
e ^{d, e}	2'-Cl, 4'-CH ₃	173.7	173.1	0.6	–	–	–
f ^d	2'-CH ₃ , 4'-Cl	174.3	173.3	1.0	–	–	–
g ^{b, d}	2', 4'-F ₂	173.9	173.2	0.7	125.2	124.0	1.2
h ^{c, d}	2'-F, 4'-Cl	173.9	173.1	0.8	128.0	126.7	1.3
i ^{a, b}	2'-Cl, 4'-F	173.4	173.1	0.3	135.3	134.7	0.6
j ^{d, e}	2'-Cl, 4'-Br	173.7	172.9	0.8	–	–	–
k ^a	2'-Br, 4'-Cl	173.8	173.1	0.8	139.5	139.2	0.3
l ^a	2', 4'-Br ₂	173.7	173.0	0.7	139.9	139.5	0.4
m ^a	2'-Br	173.9	173.1	0.8	140.7	140.4	0.3
n ^b	2'-F, 4'-Br	173.8	173.1	0.7	128.3	127.2	1.1
o ^b	2'-Br, 4'-F	173.9	173.1	0.8	136.8	136.4	0.4
p ^{a, b}	2'-I, 4'-F	173.9	173.1	0.8	139.8	139.5	0.3
q ^b	2'-F, 4'-I	173.9	173.1	0.8	129.2	128.0	1.2
r ^a	2'-Br, 4'-I	173.8	173.0	0.8	140.7	140.4	0.3
w ^a	2'-Cl, 4'-OCH ₃	173.9	173.2	0.7	131.2	130.5	0.7
x ^a	2'-OCH ₃ , 4'-Cl	174.1	173.4	0.7	128.8	127.9	0.9
y ^a	2'-Cl, 4'-CO ₂ CH ₃	173.8	173.1	0.7	144.1	143.7	0.4
z ^{d, e}	2', 4'-(CF ₃) ₂	173.8	172.8	1.0	–	–	–
aa ^{d, e}	2', 4'-(CH ₃) ₂	174.2	173.3	0.9	–	–	–
ab ^d	2', 4'-(OCH ₃) ₂	174.0	173.5	0.5	–	–	–
ac ^a	3', 4'-Cl ₂	174.1	173.1	1.0	142.4	141.2	1.2
ad ^d	3', 4'-(OCH ₃) ₂	174.4	173.3	1.1	–	–	–
ae ^b	2', 6'-F ₂ , 4'-Cl	174.1	173.2	1.0	116.7	114.8	1.9
ag ^b	2', 3', 4'-F ₃	173.8	173.1	0.7	126.7	125.6	1.1
ah ^{d, e}	2'-Br, 4'-F, 5'-OCH ₃	173.9	172.9	1.0	–	–	–
an ^b	cyclohexyl	174.7	174.0	0.7	43.3	42.5	0.8
ao ^a	<i>n</i> -butyl	174.4	173.9	0.5	35.5	34.7	0.8
ap ^b	<i>i</i> -butyl	174.4	173.9	0.5	44.5	44.5	0.0
aq ^a	<i>t</i> -butyl	175.1	174.0	1.1	36.8	35.7	1.1
ar ^b	CH(CH ₂ CH ₃) ₂	174.7	174.1	0.6	46.7	46.1	0.6
Average		174.0	173.3	0.8	–	–	–
St. deviation		0.3	0.3	0.2	–	–	–
Average (a-ah)		–	–	–	134.4	133.6	0.8
St. deviation (a-ah)		–	–	–	7.5	7.8	0.5
Average (an-ar)		–	–	–	41.4	40.7	0.7
St. deviation (an-ar)		–	–	–	4.9	5.2	0.4

Carbonyl shifts were assigned based on a characteristic δ [ppm] which are isolated in their area for both **4** and **5**. C1' signals were identified via: ^aHMBC, ^bHSQC and ^cJ_{CF}, ^dJ_{CF}. ^dArchival sample was unavailable. ^eSample and 2D NMR data unavailable.

Table 5.3 ¹H NMR chemical shifts (CDCl₃) of H-3, H-4 α , and H-4 β for **4a-ar** and **5a-ar**.

		δ H-3 [ppm]			δ H-4 α [ppm]			δ H-4 β [ppm]		
		4	5	Δ_{4-5}	4	5	Δ_{4-5}	4	5	Δ_{4-5}
a	2', 4'-Cl ₂	3.84	3.99	-0.15	3.26	3.25	0.01	3.10	3.02	0.08
b	H	3.98	3.99	-0.01	3.28	3.24	0.04	3.14	3.02	0.12
c	2'-Cl	3.86	4.00	-0.14	3.27	3.25	0.02	3.09	3.04	0.05
d	4'-Cl	3.91	3.95	-0.04	3.26	3.24	0.02	3.11	3.01	0.10
e	2'-Cl, 4'-CH ₃	3.81	3.96	-0.15	3.22	3.21	0.01	3.04	3.00	0.04
f	2'-CH ₃ , 4'-Cl	3.89	3.96	-0.07	3.25	3.24	0.01	3.11	2.99	0.12
g	2', 4'-F ₂	3.89	3.97	-0.08	3.24	3.24	0.00	3.07	3.01	0.06
h	2'-F, 4'-Cl	3.90	3.98	-0.08	3.25	3.23	0.02	3.08	3.00	0.08
i	2'-Cl, 4'-F	3.85	4.00	-0.15	3.26	3.24	0.02	3.09	3.02	0.07
j	2'-Cl, 4'-Br	3.84	3.99	-0.15	3.26	3.24	0.02	3.10	3.01	0.09
k	2'-Br, 4'-Cl	3.85	4.00	-0.15	3.26	3.24	0.02	3.10	3.02	0.08
l	2', 4'-Br ₂	3.82	3.98	-0.16	3.25	3.25	0.00	3.08	3.03	0.05
m	2'-Br	3.86	4.01	-0.15	3.27	3.24	0.03	3.09	3.03	0.06
n	2'-F, 4'-Br	3.90	3.97	-0.07	3.24	3.25	-0.01	3.08	3.00	0.08
o	2'-Br, 4'-F	3.85	4.00	-0.15	3.26	3.25	0.01	3.10	3.03	0.07
p	2'-I, 4'-F	3.88	4.01	-0.13	3.26	3.24	0.02	3.12	3.02	0.10
q	2'-F, 4'-I	3.89	3.97	-0.08	3.24	3.23	0.01	3.08	2.99	0.09
r	2'-Br, 4'-I	3.85	3.99	-0.14	3.25	3.24	0.01	3.10	3.01	0.09
w	2'-Cl, 4'-OCH ₃	3.85	4.00	-0.15	3.25	3.23	0.02	3.08	3.01	0.07
x	2'-OCH ₃ , 4'-Cl	3.82	3.97	-0.15	3.22	3.21	0.01	3.03	2.98	0.05
y	2'-Cl, 4'-CO ₂ CH ₃	3.85	4.01	-0.16	3.27	3.25	0.02	3.10	3.03	0.07
z	2', 4'-(CF ₃) ₂	4.00	4.02	-0.02	3.30	3.30	0.00	3.23	3.09	0.14
aa	2', 4'-(CH ₃) ₂	3.90	3.93	-0.03	3.22	3.20	0.02	3.08	2.97	0.11
ab	2', 4'-(OCH ₃) ₂	3.80	3.96	-0.16	3.21	3.21	0.00	3.14	3.00	0.14
ac	3', 4'-Cl ₂	3.94	3.95	-0.01	3.27	3.23	0.04	3.14	3.00	0.14
ad	3', 4'-(OCH ₃) ₂	4.00	3.96	0.04	3.27	3.23	0.04	3.15	3.02	0.13
ae	2', 6'-F ₂ , 4'-Cl	4.12	3.97	0.15	3.28	3.23	0.05	3.15	2.97	0.18
ag	2', 3', 4'-F ₃	3.89	3.97	-0.08	3.24	3.24	0.00	3.06	3.00	0.06
ah	2'-Br, 4'-F, 5'-OCH ₃	3.99	4.00	-0.01	3.29	3.24	0.05	3.20	3.03	0.17
an	cyclohexyl	4.02	3.74	0.28	3.10	3.11	-0.01	3.00	2.78	0.22
ao	<i>n</i> -butyl	3.99	3.80	0.19	3.12	3.13	-0.01	2.99	2.82	0.17
ap	<i>i</i> -butyl	3.99	3.80	0.19	3.13	3.14	-0.01	3.00	2.83	0.17
aq	<i>t</i> -butyl	4.09	3.68	0.41	3.11	3.14	-0.03	3.08	2.77	0.31
ar	CH(CH ₂ CH ₃) ₂	4.05	3.74	0.31	3.12	3.12	0.00	3.12	2.78	0.34
Average		3.91	3.95	-0.04	3.23	3.22	0.01	3.10	2.98	0.11
St. deviation		0.08	0.09	0.15	0.05	0.04	0.02	0.05	0.08	0.07
Average (a-ah)		3.89	3.98	-0.09	3.26	3.24	0.02	3.10	3.01	0.09
St. deviation (a-ah)		0.07	0.02	0.08	0.02	0.02	0.02	0.04	0.02	0.04
Average (an-ar)		4.03	3.75	0.28	3.12	3.13	-0.01	3.04	2.80	0.24
St. deviation (an-ar)		0.04	0.05	0.09	0.01	0.01	0.01	0.06	0.03	0.08

Table 5.4 J_{HH} [Hz] values (CDCl_3) for H-3, H-4 α , and H-4 β for **4a-ar** and **5a-ar**.

		4	5	4	5	4	5	4	5	4	5
		${}^2J_{4\alpha-4\beta}$	${}^2J_{4\alpha-4\beta}$	${}^3J_{4\alpha-3}$	${}^3J_{4\alpha-3}$	${}^3J_{4\beta-3}$	${}^3J_{4\beta-3}$	${}^5J_{4\alpha-1}$	${}^5J_{4\alpha-1}$	${}^5J_{4\beta-1}$	${}^5J_{4\beta-1}$
a	2', 4'-Cl ₂	15.4	15.1	5.0	4.1	7.8	11.0	1.2	1.9	1.5	2.5
b	H	15.4	15.2	5.4	4.3	6.8	11.2	1.4	1.9	1.6	2.6
c	2'-Cl	15.3	15.1	4.9	4.1	8.1	11.0	1.1	1.8	1.5	2.5
d	4'-Cl	15.5	15.2	5.4	4.2	7.0	11.2	1.3	1.9	1.6	2.6
e	2'-Cl, 4'-CH ₃	15.0	15.0	5.0	4.0	8.0	11.0	1.0	2.0	1.5	2.5
f	2'-CH ₃ , 4'-Cl	15.4	15.1	5.3	4.2	7.0	11.1	1.3	1.9	1.6	2.6
g	2', 4'-F ₂	15.4	15.1	5.0	4.2	7.9	11.1	1.1	1.8	1.5	2.5
h	2'-F, 4'-Cl	15.4	15.1	5.1	4.2	7.7	11.1	1.1	1.9	1.4	2.5
i	2'-Cl, 4'-F	15.4	15.1	5.0	4.1	7.8	11.0	1.2	1.8	1.5	2.5
j	2'-Cl, 4'-Br	15.4	15.1	5.0	4.1	7.7	11.0	1.2	1.9	1.6	2.5
k	2'-Br, 4'-Cl	15.4	15.1	5.0	4.1	7.6	11.0	1.2	1.8	1.5	2.5
l	2', 4'-Br ₂	15.4	15.1	4.9	4.1	8.0	11.0	1.1	1.9	1.5	2.5
m	2'-Br	15.3	15.0	5.0	4.1	8.0	11.0	1.1	1.8	1.5	2.5
n	2'-F, 4'-Br	15.4	15.1	5.1	4.2	7.7	11.1	1.2	1.9	1.5	2.5
o	2'-Br, 4'-F	15.4	15.0	5.1	4.1	7.6	11.1	1.2	1.8	1.5	2.5
p	2'-I, 4'-F	15.4	15.1	5.2	4.1	7.1	11.1	1.3	1.8	1.6	2.5
q	2'-F, 4'-I	15.4	15.1	5.1	4.2	7.8	11.1	1.1	1.9	1.6	2.5
r	2'-Br, 4'-I	15.3	15.1	5.1	4.1	7.6	11.0	1.2	1.8	1.5	2.5
w	2'-Cl, 4'-OCH ₃	15.3	15.1	4.9	4.2	8.1	11.0	1.1	1.9	1.5	2.6
x	2'-OCH ₃ , 4'-Cl	15.2	15.1	4.8	4.2	8.7	11.0	0.9	1.9	1.5	2.6
y	2'-Cl, 4'-CO ₂ CH ₃	15.4	15.1	5.0	4.1	7.8	11.0	1.2	1.8	1.5	2.5
z^a	2', 4'-(CF ₃) ₂	15.5	15.1	5.5	4.0	5.5	11.1	1.5	1.8	1.5	2.4
aa	2', 4'-(CH ₃) ₂	15.0	15.0	5.0	4.0	7.0	11.0	1.5	1.5	1.5	2.0
ab	2', 4'-(OCH ₃) ₂	15.2	15.0	4.7	4.2	9.4	11.0	0.8	1.9	1.3	2.6
ac^b	3', 4'-Cl ₂	15.5	15.1	5.5	4.1	6.4	11.2	1.4	1.8	1.6	2.5
ad^b	3', 4'-(OCH ₃) ₂	15.5	15.1	5.6	4.3	6.3	11.2	1.5	1.9	1.6	2.6
ae^b	2', 6'-F ₂ , 4'-Cl	15.4	15.3	5.4	4.4	6.0	11.2	1.6	1.9	1.8	2.6
ag	2', 3', 4'-F ₃	15.4	15.2	5.0	4.1	7.9	11.1	1.1	1.9	1.6	2.5
ah^b	2'-Br, 4'-F, 5'-OCH ₃	15.4	15.0	5.5	4.1	5.7	11.1	1.6	1.8	1.6	2.5
an	cyclohexyl	15.3	14.9	5.3	4.1	6.9	11.2	1.3	1.8	1.5	2.6
ao	<i>n</i> -butyl	15.3	15.1	5.3	4.2	7.3	11.2	1.2	1.9	1.5	2.6
ap	<i>i</i> -butyl	15.4	15.0	5.3	4.2	7.4	11.2	1.2	1.9	1.5	2.6
aq^b	<i>t</i> -butyl	15.0	14.6	5.1	3.6	5.3	11.2	1.5	1.5	1.6	2.4
ar^a	CH(CH ₂ CH ₃) ₂	–	15.0	5.4	4.1	5.4	11.2	1.7	1.9	1.7	2.6
Average		15.3	15.1	5.1	4.1	7.3	11.1	1.2	1.8	1.5	2.5
St. deviation		0.1	0.1	0.2	0.1	0.9	0.1	0.2	0.1	0.1	0.1
Average (a-ah)		15.4	15.1	5.1	4.1	7.4	11.1	1.2	1.8	1.5	2.5
St. deviation (a-ah)		0.1	0.1	0.2	0.1	0.9	0.1	0.2	0.1	0.1	0.1
Average (an-ar)		15.3	14.9	5.3	4.0	6.5	11.2	1.4	1.8	1.6	2.6
St. deviation (an-ar)		0.2	0.2	0.1	0.3	1.0	0.0	0.2	0.2	0.1	0.1

^aH-3 signal in the *trans* diastereomer is a triplet, ^bH-3 signal in the *trans* diastereomer is an apparent triplet.

Table 5.5 Selected 1D NOE correlations observed in **4a/5a** upon irradiation of H1, H3, H4 α , and H4 β .

Irradiated proton	Observed NOE in 4a [%]				Observed NOE in 5a [%]			
	H1	H3	H4 α	H4 β	H1	H3	H4 α	H4 β
H-1	–	–	–	–	–	4.3	–	–
H-3	–	–	3.5	–	3.4	–	3.0	–
H-4α	–	5.5	–	13.8	–	6.0	–	20.1
H-4β	–	1.2	10.0	–	–	–	18.3	–

5.1.1 Conformational distribution in compound **4a/4b** and **5a/5b**

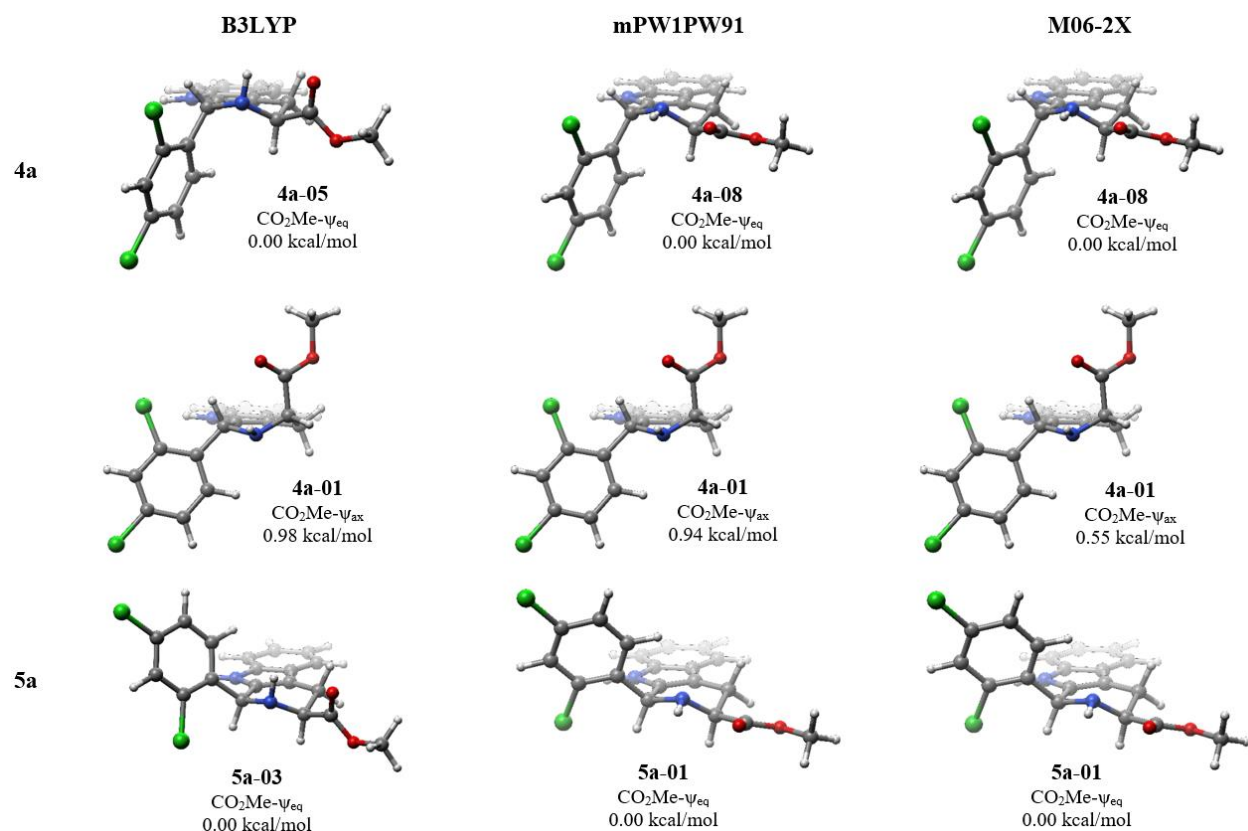


Figure 5.1 The lowest ΔG (298 K) ψ_{eq} - and ψ_{ax} - conformers of **4a** and the global minimum of **5a**. Geometries were obtained by B3LYP/6-31G(d) optimization; free energies were calculated from single point energies using either the B3LYP/6-311+G(2d,p), mPW1PW91/6-311+G(2d,p), or M06-2X/def2-TZVP (SCRF: PCM = CHCl₃). Free energy correction was obtained from the B3LYP/6-31G(d) frequencies.

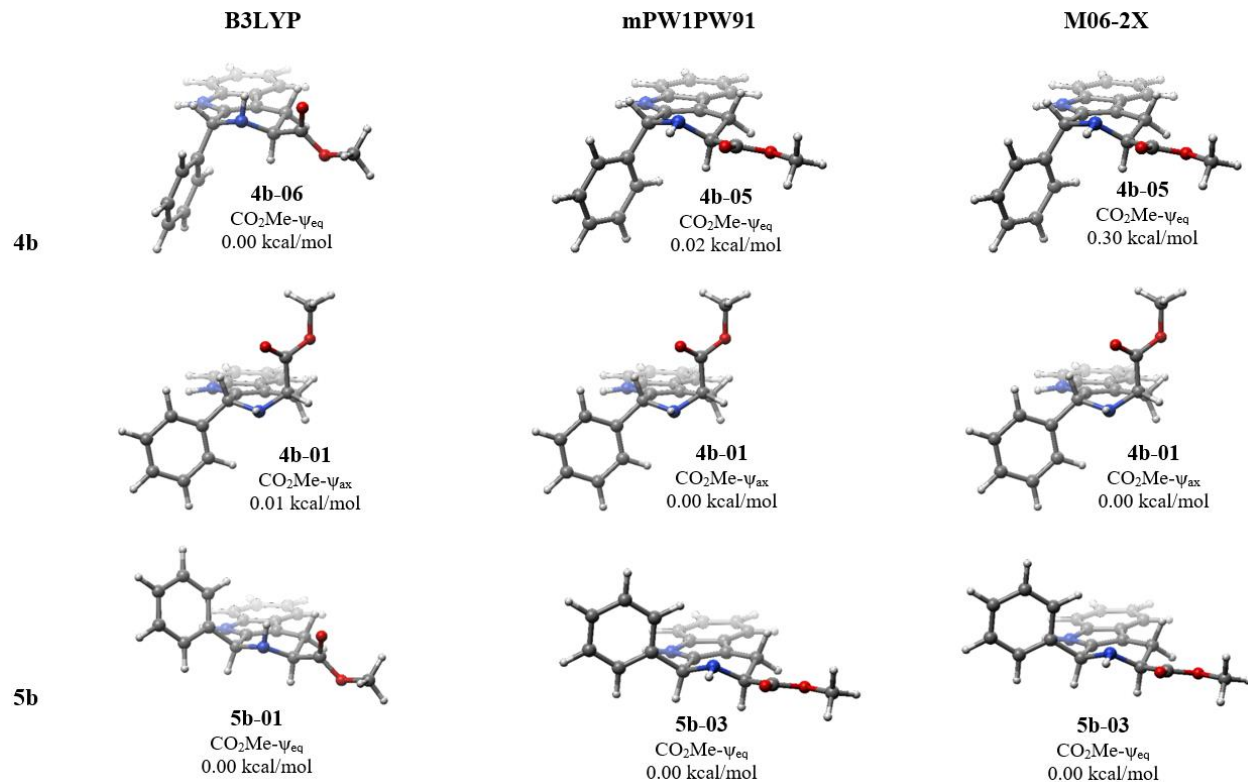


Figure 5.2 The lowest ΔG (298 K) ψ_{eq} - and ψ_{ax} - conformers of **4b** and the global minimum of **5b**. Geometries were obtained by B3LYP/6-31G(d) optimization; free energies were calculated from single point energies using either the B3LYP/6-311+G(2d,p), mPW1PW91/6-311+G(2d,p), or M06-2X/def2-TZVP (SCRF: PCM = CHCl₃). Free energy correction was obtained from the B3LYP/6-31G(d) frequencies.

Table 5.6 Calculated energies of **4a** at MMFF94 and B3LYP/6-31G(d) levels of theory.

Structural features				B3LYP/6-31G(d), vacuum					$\Delta G(298)$ [kcal/mol]	
CO ₂ Me	2'-Cl	H2	H-bond (H2 to X)	MMFF94 Energy [kJ/mol]	e_0 [Hartree]	ZPVE [Hartree]	G_{corr}^a [Hartree]	G(298) [Hartree]		
4a-1	ψ_{ax}	<i>exo</i>	<i>eq</i>	C=O	237.34	-1914.01436080	0.317204	0.264808	-1913.74955280	0.00
4a-2	ψ_{ax}	<i>exo</i>	<i>eq</i>	OCH ₃	243.65	-1914.01270533	0.317049	0.264372	-1913.74833333	0.77
4a-3	ψ_{ax}	<i>endo</i>	<i>eq</i>	C=O	252.89	-1914.00942053	0.316971	0.264333	-1913.74508753	2.80
4a-4	ψ_{ax}	<i>endo</i>	<i>ax</i>	none ^b	254.24	-1914.00669434	0.317024	0.264215	-1913.74247934	4.44
4a-5	ψ_{eq}	<i>exo</i>	<i>ax</i>	C=O	254.63	-1914.01118957	0.316725	0.263415	-1913.74777457	1.12
4a-6	ψ_{eq}	<i>exo</i>	<i>eq</i>	OCH ₃	255.98	-1914.01103429	0.316673	0.263891	-1913.74714329	1.51
4a-7	ψ_{ax}	<i>exo</i>	<i>ax</i>	none ^b	256.20	-1914.00796854	0.316920	0.263858	-1913.74411054	3.42
4a-8	ψ_{eq}	<i>exo</i>	<i>eq</i>	C=O	256.61	-1914.01209044	0.316635	0.263982	-1913.74810844	0.91
4a-9	ψ_{eq}	<i>exo</i>	<i>ax</i>	OCH ₃	257.95	-1914.00962662	0.316815	0.263635	-1913.74599162	2.23
4a-10	ψ_{ax}	<i>endo</i>	<i>ax</i>	none ^c	260.51	-1914.00459481	0.317006	0.264311	-1913.74028381	5.82
4a-11	ψ_{ax}	<i>endo</i>	<i>eq</i>	OCH ₃	262.72	-1914.00718234	0.316897	0.264267	-1913.74291534	4.17
4a-12	ψ_{ax}	<i>exo</i>	<i>ax</i>	none ^c	264.81	-1914.00688677	0.316952	0.263775	-1913.74311177	4.04
4a-13	ψ_{eq}	<i>endo</i>	<i>ax</i>	C=O	272.33	-1914.00582376	0.316682	0.264074	-1913.74174976	4.90
4a-14	ψ_{eq}	<i>endo</i>	<i>eq</i>	C=O	276.11	-1914.00427431	0.316387	0.263246	-1913.74102831	5.35
4a-15	ψ_{eq}	<i>endo</i>	<i>eq</i>	OCH ₃	277.22	-1914.00290824	0.316454	0.263129	-1913.73977924	6.13
4a-16	ψ_{eq}	<i>endo</i>	<i>ax</i>	OCH ₃	277.82	-1914.00227563	0.316509	0.263098	-1913.73917763	6.51

^aCalculated at 298 K. ^bC=O is oriented towards N2 but H-bond is not geometrically possible. ^cOCH₃ is oriented towards N2 but H-bond is not geometrically possible.

Table 5.7 Calculated energies of **4a** at B3LYP/6-311+G(2d,p)// B3LYP/6-31G(d) (**Method 1**), mPW1PW91/6-311+G(2d,p)// B3LYP/6-31G(d) (**Method 2**), and M06-2X/def2-TZVP//B3LYP/6-31G(d) (**Method 3**), all with SCRFF=(PCM, solvent=chloroform).

	Method 1		Method 2		Method 3	
	e_0 [Hartree]	$G_{298\text{ K}}$ [Hartree]	e_0 [Hartree]	$G_{298\text{ K}}$ [Hartree]	e_0 [Hartree]	$G_{298\text{ K}}$ [Hartree]
4a-1	-1914.37029604	-1914.10548804	-1914.14966185	-1913.88485385	-1914.01318382	-1913.74837582
4a-2	-1914.36936006	-1914.10498806	-1914.14866297	-1913.88429097	-1914.01189123	-1913.74751923
4a-3	-1914.36790766	-1914.10357466	-1914.14733659	-1913.88300359	-1914.01129940	-1913.74696640
4a-4	-1914.36562128	-1914.10140628	-1914.14491549	-1913.88070049	-1914.00864481	-1913.74442981
4a-5	-1914.37046055	-1914.10704555	-1914.14961148	-1913.88619648	-1914.01195294	-1913.74853794
4a-6	-1914.36976928	-1914.10587828	-1914.14909618	-1913.88520518	-1914.01219656	-1913.74830556
4a-7	-1914.36688658	-1914.10302858	-1914.14618278	-1913.88232478	-1914.00956577	-1913.74570777
4a-8	-1914.37078946	-1914.10680746	-1914.15033222	-1913.88635022	-1914.01323651	-1913.74925451
4a-9	-1914.36922485	-1914.10558985	-1914.14831487	-1913.88467987	-1914.01090188	-1913.74726688
4a-10	-1914.36455952	-1914.10024852	-1914.14396943	-1913.87965843	-1914.00741454	-1913.74310354
4a-11	-1914.36652171	-1914.10225471	-1914.14587465	-1913.88160765	-1914.00960845	-1913.74534145
4a-12	-1914.36639500	-1914.10262000	-1914.14583808	-1913.88206308	-1914.00894024	-1913.74516524
4a-13	-1914.36519480	-1914.10112080	-1914.14424588	-1913.88017188	-1914.00682103	-1913.74274703
4a-14	-1914.36401716	-1914.10077116	-1914.14315101	-1913.87990501	-1914.00574076	-1913.74249476
4a-15	-1914.36273918	-1914.09961018	-1914.14157422	-1913.87844522	-1914.00434922	-1913.74122022
4a-16	-1914.36263186	-1914.09953386	-1914.14138970	-1913.87829170	-1914.00397433	-1913.74087633
	$\Delta G_{298\text{ K}}$ [kcal/mol]	Boltzmann distribution	$\Delta G_{298\text{ K}}$ [kcal/mol]	Boltzmann distribution	$\Delta G_{298\text{ K}}$ [kcal/mol]	Boltzmann distribution
4a-1	0.98	7.2%	0.94	7.2%	0.55	14.8%
4a-2	1.29	4.2%	1.29	4.2%	1.09	6.0%
4a-3	2.18	0.9%	2.10	0.9%	1.44	3.3%
4a-4	3.54	0.1%	3.55	0.1%	3.03	0.2%
4a-5	0.00	37.9%	0.10	37.9%	0.45	17.6%
4a-6	0.73	10.9%	0.72	10.9%	0.60	13.7%
4a-7	2.52	0.5%	2.53	0.5%	2.23	0.9%
4a-8	0.15	29.4%	0.00	29.4%	0.00	37.7%
4a-9	0.91	8.0%	1.05	8.0%	1.25	4.6%
4a-10	4.27	0.0%	4.20	0.0%	3.86	0.1%
4a-11	3.01	0.2%	2.98	0.2%	2.46	0.6%
4a-12	2.78	0.3%	2.69	0.3%	2.57	0.5%
4a-13	3.72	0.1%	3.88	0.1%	4.08	0.0%
4a-14	3.94	0.0%	4.04	0.0%	4.24	0.0%
4a-15	4.67	0.0%	4.96	0.0%	5.04	0.0%
4a-16	4.71	0.0%	5.06	0.0%	5.26	0.0%

Table 5.8 Calculated energies of **4b** at MMFF94 and B3LYP/6-31G(d) levels of theory.

Structural features		MMFF94	B3LYP/6-31G(d), vacuum					$\Delta G_{298\text{ K}}$ [kcal/mol]
CO ₂ Me	H2	H-bond (H2 to X)	Energy [kJ/mol]	e_0 [Hartree]	ZPVE [Hartree]	G_{corr}^a [Hartree]	$G_{298\text{ K}}$ [Hartree]	
4b-1	ψ_{ax}	<i>eq</i>	282.54	-994.825578974	0.336524	0.287502	-994.538076974	0.00
4b-2	ψ_{ax}	<i>eq</i>	289.74	-994.823944440	0.336427	0.287525	-994.536419440	1.04
4b-3	ψ_{ax}	<i>ax</i>	292.86	-994.821156197	0.336384	0.287347	-994.533809197	2.68
4b-4	ψ_{eq}	<i>eq</i>	295.43	-994.821855495	0.336085	0.287207	-994.534648495	2.15
4b-5	ψ_{eq}	<i>eq</i>	295.65	-994.823088326	0.335979	0.287010	-994.536078326	1.25
4b-6	ψ_{eq}	<i>ax</i>	296.65	-994.822366886	0.336118	0.286375	-994.535991886	1.31
4b-7	ψ_{ax}	<i>ax</i>	297.48	-994.819721433	0.336393	0.287380	-994.532341433	3.60
4b-8	ψ_{eq}	<i>ax</i>	301.06	-994.820741727	0.336125	0.286397	-994.534344727	2.34

^aCalculated at 298 K. ^bC=O is oriented towards N2 but H-bond is not geometrically possible. ^cOCH₃ is oriented towards N2 but H-bond is not geometrically possible.

Table 5.9 Calculated energies of **4b** at B3LYP/6-311+G(2d,p)// B3LYP/6-31G(d) (**Method 1**), mPW1PW91/6-311+G(2d,p)// B3LYP/6-31G(d) (**Method 2**), and M06-2X/def2-TZVP//B3LYP/6-31G(d) (**Method 3**), all with SCRF=(PCM, solvent=chloroform).

	Method 1		Method 2		Method 3	
	e_0 [Hartree]	$G_{298\text{ K}}$ [Hartree]	e_0 [Hartree]	$G_{298\text{ K}}$ [Hartree]	e_0 [Hartree]	$G_{298\text{ K}}$ [Hartree]
4b-1	-995.124145275	-994.836643275	-994.885390029	-994.597888029	-994.808015506	-994.520513506
4b-2	-995.123143164	-994.835618164	-994.884347134	-994.596822134	-994.806852067	-994.519327067
4b-3	-995.121060656	-994.833713656	-994.882227215	-994.594880215	-994.804934854	-994.517587854
4b-4	-995.122386525	-994.835179525	-994.883436878	-994.596229878	-994.805716591	-994.518509591
4b-5	-995.123558562	-994.836548562	-994.884865213	-994.597855213	-994.807044518	-994.520034518
4b-6	-995.123039313	-994.836664313	-994.884166772	-994.597791772	-994.806319801	-994.519944801
4b-7	-995.120364677	-994.832984677	-994.881664652	-994.594284652	-994.804021854	-994.516641854
4b-8	-995.121743096	-994.835346096	-994.882813198	-994.596416198	-994.805156824	-994.518759824
	$\Delta G_{298\text{ K}}$ [kcal/mol]	Boltzmann distribution	$\Delta G_{298\text{ K}}$ [kcal/mol]	Boltzmann distribution	$\Delta G_{298\text{ K}}$ [kcal/mol]	Boltzmann distribution
4b-1	0.01	26.4%	0.00	27.5%	0.00	36.2%
4b-2	0.66	8.9%	0.67	8.9%	0.74	10.2%
4b-3	1.85	1.2%	1.89	1.1%	1.84	1.6%
4b-4	0.93	5.6%	1.04	4.7%	1.26	4.3%
4b-5	0.07	23.9%	0.02	26.6%	0.30	21.7%
4b-6	0.00	27.0%	0.06	24.8%	0.36	19.8%
4b-7	2.31	0.5%	2.26	0.6%	2.43	0.6%
4b-8	0.83	6.6%	0.92	5.8%	1.10	5.6%

Table 5.10 Calculated energies of **5a** at MMFF94 and B3LYP/6-31G(d) levels of theory.

Structural features				B3LYP/6-31G(d), vacuum					$\Delta G_{298\text{ K}}$ [kcal/mol]	
CO ₂ Me	2'-Cl	H2	H-bond (H2 to X)	MMFF94 Energy [kJ/mol]	e_0 [Hartree]	ZPVE [Hartree]	G_{corr}^a [Hartree]	$G_{298\text{ K}}$ [Hartree]		
5a-1	ψ_{eq}	<i>exo</i>	<i>eq</i>	C=O	245.12	-1914.01456172	0.316708	0.264065	-1913.75049672	0.00
5a-2	ψ_{eq}	<i>exo</i>	<i>eq</i>	OCH ₃	245.59	-1914.01294988	0.316692	0.263776	-1913.74917388	0.83
5a-3	ψ_{eq}	<i>exo</i>	<i>ax</i>	C=O	250.02	-1914.01130588	0.316766	0.263040	-1913.74826588	1.40
5a-4	ψ_{ax}	<i>exo</i>	<i>eq</i>	OCH ₃	253.85	-1914.00865712	0.316741	0.264333	-1913.74432412	3.87
5a-5	ψ_{eq}	<i>exo</i>	<i>ax</i>	OCH ₃	254.02	-1914.00985971	0.316841	0.263552	-1913.74630771	2.63
5a-6	ψ_{eq}	<i>endo</i>	<i>ax</i>	C=O	254.77	-1914.00844097	0.316665	0.263177	-1913.74526397	3.28
5a-7	ψ_{eq}	<i>endo</i>	<i>ax</i>	OCH ₃	256.56	-1914.00728927	0.316802	0.263695	-1913.74359427	4.33
5a-8	ψ_{ax}	<i>exo</i>	<i>eq</i>	C=O	258.34	-1914.00673342	0.316767	0.263866	-1913.74286742	4.79
5a-9	ψ_{ax}	<i>exo</i>	<i>ax</i>	none ^c	261.41	-1914.00511940	0.316734	0.264326	-1913.74079340	6.09
5a-10	ψ_{eq}	<i>endo</i>	<i>eq</i>	C=O	264.78	-1914.00857821	0.316494	0.263896	-1913.74468221	3.65
5a-11	ψ_{eq}	<i>endo</i>	<i>eq</i>	OCH ₃	265.29	-1914.00725406	0.316492	0.263649	-1913.74360506	4.32
5a-12	ψ_{ax}	<i>exo</i>	<i>ax</i>	none ^b	272.62	-1914.00141662	0.316749	0.264237	-1913.73717962	8.36
5a-13	ψ_{ax}	<i>endo</i>	<i>eq</i>	C=O	277.59	-1913.99970041	0.316840	0.264779	-1913.73492141	9.77
5a-14	ψ_{ax}	<i>endo</i>	<i>eq</i>	OCH ₃	282.12	-1913.99920233	0.316777	0.264989	-1913.73421333	10.22

^aCalculated at 298 K. ^bC=O is oriented towards N2 but H-bond is not geometrically possible. ^cOCH₃ is oriented towards N2 but H-bond is not geometrically possible.

Table 5.11 Calculated energies of **5a** at B3LYP/6-311+G(2d,p)// B3LYP/6-31G(d) (**Method 1**), mPW1PW91/6-311+G(2d,p)// B3LYP/6-31G(d) (**Method 2**), and M06-2X/def2-TZVP//B3LYP/6-31G(d) (**Method 3**), all with SCRF=(PCM, solvent=chloroform).

	Method 1		Method 2		Method 3	
	e_0 [Hartree]	$G_{298\text{ K}}$ [Hartree]	e_0 [Hartree]	$G_{298\text{ K}}$ [Hartree]	e_0 [Hartree]	$G_{298\text{ K}}$ [Hartree]
5a-1	-1914.37124126	-1914.10717626	-1914.15049755	-1913.88643255	-1914.01302460	-1913.74895960
5a-2	-1914.36989820	-1914.10612220	-1914.14888337	-1913.88510737	-1914.01156644	-1913.74779044
5a-3	-1914.37047890	-1914.10743890	-1914.14935969	-1913.88631969	-1914.01118126	-1913.74814126
5a-4	-1914.36621981	-1914.10188681	-1914.14589369	-1913.88156069	-1914.01210700	-1913.74777400
5a-5	-1914.36935580	-1914.10580380	-1914.14819240	-1913.88464040	-1914.01203058	-1913.74667858
5a-6	-1914.36846112	-1914.10528412	-1914.14743271	-1913.88255571	-1914.0101486	-1913.74697160
5a-7	-1914.36752967	-1914.10383467	-1914.14644047	-1913.88274547	-1914.00914825	-1913.74545325
5a-8	-1914.36485810	-1914.10099210	-1914.14449099	-1913.88062499	-1914.01007648	-1913.74621048
5a-9	-1914.36411026	-1914.09978426	-1914.14384254	-1913.87951654	-1914.00945487	-1913.74512887
5a-10	-1914.36825899	-1914.10436299	-1914.14759393	-1913.88369793	-1914.01051805	-1913.74662205
5a-11	-1914.36716693	-1914.10351793	-1914.14624157	-1913.88259257	-1914.00930004	-1913.74565104
5a-12	-1914.36165907	-1914.09742207	-1914.14116815	-1913.87693115	-1914.00664588	-1913.74240888
5a-13	-1914.35865601	-1914.09387701	-1914.13801560	-1913.87323660	-1914.00390664	-1913.73912764
5a-14	-1914.35871373	-1914.09372473	-1914.13805779	-1913.87306879	-1914.00421326	-1913.73922426
	$\Delta G_{298\text{ K}}$ [kcal/mol]	Boltzmann distribution	$\Delta G_{298\text{ K}}$ [kcal/mol]	Boltzmann distribution	$\Delta G_{298\text{ K}}$ [kcal/mol]	Boltzmann distribution
5a-1	0.16	32.1%	0.00	40.4%	0.00	41.5%
5a-2	0.83	10.5%	0.83	9.9%	0.73	12.0%
5a-3	0.00	42.4%	0.07	35.8%	0.51	17.4%
5a-4	3.48	0.1%	3.06	0.2%	0.74	11.8%
5a-5	1.03	7.4%	1.12	6.0%	1.43	3.7%
5a-6	1.35	4.3%	1.37	4.0%	1.25	5.0%
5a-7	2.26	0.9%	2.31	0.8%	2.20	1.0%
5a-8	4.05	0.0%	3.64	0.1%	1.73	2.2%
5a-9	4.80	0.0%	4.34	0.0%	2.40	0.7%
5a-10	1.93	1.6%	1.72	2.2%	1.47	3.5%
5a-11	2.46	0.7%	2.41	0.7%	2.08	1.2%
5a-12	6.29	0.0%	5.96	0.0%	4.11	0.0%
5a-13	8.51	0.0%	8.28	0.0%	6.17	0.0%
5a-14	8.61	0.0%	8.39	0.0%	6.11	0.0%

Table 5.12 Calculated energies of **5b** at MMFF94 and B3LYP/6-31G(d) levels of theory.

Structural features			B3LYP/6-31G(d), vacuum						
CO ₂ Me	H2	H-bond (H2 to X)	MMFF94		ZPVE		G _{298 K}		$\Delta G_{298 K}$ [kcal/mol]
			Energy [kJ/mol]	e ₀ [Hartree]	[Hartree]	G _{corr} ^a [Hartree]	[Hartree]	[Hartree]	
5b-1	ψ_{eq}	ax	291.03	-994.823809034	0.336080	0.286129	-994.537680034	0.73	
5b-2	ψ_{eq}	eq	291.46	-994.824456311	0.336034	0.286823	-994.537633311	0.76	
5b-3	ψ_{eq}	eq	291.87	-994.825784125	0.336026	0.286945	-994.538839125	0.00	
5b-4	ψ_{eq}	ax	293.71	-994.822507772	0.336175	0.286669	-994.535838772	1.88	
5b-5	ψ_{ax}	eq	295.00	-994.819243218	0.336164	0.287649	-994.531594218	4.55	
5b-6	ψ_{ax}	eq	301.90	-994.817316664	0.336256	0.287156	-994.530160664	5.45	
5b-7	ψ_{ax}	ax	304.78	-994.815792636	0.336267	0.288082	-994.527710636	6.42	
5b-8	ψ_{ax}	ax	315.26	-994.812854690	0.336270	0.287749	-994.525105690	8.27	

^aCalculated at 298 K. ^bC=O is oriented towards N2 but H-bond is not geometrically possible. ^cOCH₃ is oriented towards N2 but H-bond is not geometrically possible.

Table 5.13 Calculated energies of **5b** at B3LYP/6-311+G(2d,p)// B3LYP/6-31G(d) (**Method 1**), mPW1PW91/6-311+G(2d,p)// B3LYP/6-31G(d) (**Method 2**), and M06-2X/def2-TZVP//B3LYP/6-31G(d) (**Method 3**), all with SCRF=(PCM, solvent=chloroform).

	Method 1		Method 2		Method 3	
	e_0 [Hartree]	$G_{298\text{ K}}$ [Hartree]	e_0 [Hartree]	$G_{298\text{ K}}$ [Hartree]	e_0 [Hartree]	$G_{298\text{ K}}$ [Hartree]
5b-1	-995.124312659	-994.838183659	-994.885065648	-994.598936648	-994.806461995	-994.520332995
5b-2	-995.123982150	-994.837159150	-994.884864392	-994.598041392	-994.806701119	-994.51987819
5b-3	-995.125082968	-994.838137968	-994.886229910	-994.599284910	-994.807950115	-994.521005115
5b-4	-995.123213232	-994.836544232	-994.883953279	-994.597284279	-994.805695866	-994.519026866
5b-5	-995.118342782	-994.830693782	-994.879675706	-994.592026706	-994.804884848	-994.517235848
5b-6	-995.116968010	-994.829812010	-994.878223751	-994.591067751	-994.802598341	-994.515442341
5b-7	-995.116184082	-994.828102082	-994.877885019	-994.589803019	-994.803579255	-994.515497255
5b-8	-995.113689095	-994.825940095	-994.875248592	-994.587499592	-994.800781284	-994.513032284
	$\Delta G_{298\text{ K}}$ [kcal/mol]	Boltzmann distribution	$\Delta G_{298\text{ K}}$ [kcal/mol]	Boltzmann distribution	$\Delta G_{298\text{ K}}$ [kcal/mol]	Boltzmann distribution
5b-1	0.00	40.6%	0.22	33.2%	0.42	25.3%
5b-2	0.64	13.6%	0.78	12.8%	0.71	15.6%
5b-3	0.03	38.7%	0.00	48.2%	0.00	51.6%
5b-4	1.03	7.1%	1.26	5.7%	1.24	6.3%
5b-5	4.70	0.0%	4.55	0.0%	2.37	0.9%
5b-6	5.25	0.0%	5.16	0.0%	3.49	0.1%
5b-7	6.33	0.0%	5.95	0.0%	3.46	0.1%
5b-8	7.68	0.0%	7.40	0.0%	5.00	0.0%

Table 5.14 Boltzmann distribution of conformer ensembles of **4a**, **5a**, **4b**, **5b** [%].

Method	4a [%]			5a [%]			4b [%]			5b [%]		
	M1	M2	M3	M1	M2	M3	M1	M2	M3	M1	M2	M3
3-CO₂Me-ψ_{ax}	13.6	14.0	26.3	0.2	0.3	14.7	37.0	38.1	48.6	0.0	0.0	1.2
3-CO₂Me-ψ_{eq}	86.4	86.0	73.7	99.8	99.7	85.3	63.0	61.9	51.4	100	100	98.8
2'-Cl_{exo}	98.6	98.5	95.7	92.5	92.3	89.3	–	–	–	–	–	–
2'-Cl_{endo}	1.4	1.5	4.3	7.5	7.7	10.7	–	–	–	–	–	–
H-2_{ax}	47.0	38.9	23.8	55.1	46.6	27.8	35.3	32.3	27.6	47.7	39.0	31.7
H-2_{eq}	53.0	61.1	76.2	44.9	53.4	72.2	64.7	67.7	72.4	52.3	61.0	68.3
H-bonding^a	99.0	99.0	98.4	100	100	99.3	98.3	98.3	97.8	100	100	99.8
H-bond to C=O	75.5	77.3	73.5	80.4	82.4	69.6	77.2	78.9	77.7	79.2	81.4	77.0
H-bond to OMe	23.5	21.7	24.9	19.6	17.6	29.6	21.1	19.3	20.1	20.8	18.6	22.8
No H-bond^a	1.0	1.0	1.6	0.0	0.0	0.7	1.7	1.7	2.2	0.0	0.0	0.2

Methods used for determination of conformer energies:

M1 – B3LYP/6-311+G(2d,p)//B3LYP/6-31G(d), SCRF(PCM=chloroform),

M2 – mPW1PW91/6-311+G(2d,p)//B3LYP/6-31G(d), SCRF(PCM=chloroform),

M3 – M06-2X/def2-TZVP//B3LYP/6-31G(d), SCRF(PCM=chloroform).

^aH-bonding assumed for H-2 \cdots O distance ranging between 2.3 Å and 2.7 Å. For those conformers described as

“No H-bonding”, this distance was \geq 3.7 Å.

5.1.2 ^1H - ^1H coupling constants for conformers of 4a/4b and 5a/5b

Table 5.15 Calculated (B3LYP/6-31G(d,p)u+1s//B3LYP/6-31G(d)) ^1H - ^1H coupling constants for all conformers of 4a, 5a, 4b, 5b.^a

	4a-01	4a-02	4a-03	4a-04	4a-05	4a-06	4a-07	4a-08
$^3J_{4\beta-3}$ [Hz]	1.8	1.5	1.6	1.0	10.7	10.8	1.0	11.0
$^3J_{4\alpha-3}$ [Hz]	5.7	5.9	6.0	7.0	4.2	3.9	6.8	3.7
$^2J_{4\alpha-4\beta}$ [Hz]	-15.1	-15.0	-15.2	-16.0	-15.3	-15.9	-16.0	-15.0
$^5J_{4\beta-1}$ [Hz]	1.8	2.0	1.8	2.1	2.0	1.7	2.0	1.7
$^5J_{4\alpha-1}$ [Hz]	2.9	2.9	3.2	3.3	0.5	0.5	3.0	0.5
	4a-09	4a-10	4a-11	4a-12	4a-13	4a-14	4a-15	4a-16
$^3J_{4\beta-3}$ [Hz]	10.8	1.0	1.5	1.0	10.6	10.7	10.5	10.6
$^3J_{4\alpha-3}$ [Hz]	4.2	6.5	6.0	6.4	3.6	3.5	3.6	3.2
$^2J_{4\alpha-4\beta}$ [Hz]	-15.5	-15.7	-15.1	-15.7	-14.3	-14.8	-15.7	-14.4
$^5J_{4\beta-1}$ [Hz]	2.0	2.2	1.9	2.2	2.7	2.4	2.5	2.8
$^5J_{4\alpha-1}$ [Hz]	0.5	3.3	3.2	3.1	0.9	0.8	0.8	0.9
	5a-01	5a-02	5a-03	5a-04	5a-05	5a-06	5a-07	5a-08
$^3J_{4\beta-3}$ [Hz]	10.9	10.7	10.5	0.9	10.7	10.7	10.8	1.0
$^3J_{4\alpha-3}$ [Hz]	3.5	3.6	4.1	6.7	4.0	4.2	4.1	6.8
$^2J_{4\alpha-4\beta}$ [Hz]	-14.7	-15.6	-15.1	-15.4	-15.3	-15.1	-15.2	-15.8
$^5J_{4\beta-1}$ [Hz]	2.9	3.0	3.1	0.6	3.1	3.2	3.3	0.6
$^5J_{4\alpha-1}$ [Hz]	2.0	1.9	2.1	2.0	2.1	2.2	2.2	2.0
	5a-09	5a-10	5a-11	5a-12	5a-13	5a-14		
$^3J_{4\beta-3}$ [Hz]	0.6	10.8	10.7	0.6	1.2	1.1		
$^3J_{4\alpha-3}$ [Hz]	6.5	3.5	3.8	6.7	7.0	7.0		
$^2J_{4\alpha-4\beta}$ [Hz]	-16.0	-14.7	-15.6	-16.3	-15.8	-15.5		
$^5J_{4\beta-1}$ [Hz]	0.7	3.1	3.2	0.6	0.9	1.0		
$^5J_{4\alpha-1}$ [Hz]	2.3	1.9	1.9	2.2	2.8	2.8		
	4b-01	4b-02	4b-03	4b-04	4b-05	4b-06	4b-07	4b-08
$^3J_{4\beta-3}$ [Hz]	1.5	1.3	1.0	10.7	10.9	10.8	1.0	1.5
$^3J_{4\alpha-3}$ [Hz]	6.2	6.2	6.9	3.7	3.6	4.6	6.4	6.2
$^2J_{4\alpha-4\beta}$ [Hz]	-15.3	-15.1	-15.9	-15.7	-14.8	-15.5	-15.6	-15.3
$^5J_{4\beta-1}$ [Hz]	1.9	2.1	2.1	1.8	1.8	1.8	2.3	1.9
$^5J_{4\alpha-1}$ [Hz]	3.1	3.1	3.1	0.5	0.5	0.5	3.1	3.1
	5b-01	5b-02	5b-03	5b-04	5b-05	5b-06	5b-07	5b-08
$^3J_{4\beta-3}$ [Hz]	10.6	10.7	11.0	10.7	1.1	1.3	0.6	0.5
$^3J_{4\alpha-3}$ [Hz]	4.1	3.9	3.7	4.0	6.4	6.2	6.6	6.9
$^2J_{4\alpha-4\beta}$ [Hz]	-15.0	-15.6	-14.7	-15.2	-15.2	-15.5	-16.0	-16.5
$^5J_{4\beta-1}$ [Hz]	3.1	3.1	3.0	3.1	0.7	0.6	0.6	0.5
$^5J_{4\alpha-1}$ [Hz]	2.2	2.0	2.0	2.2	2.3	2.4	2.1	1.9

^aOnly Fermi contact terms (major contributor to J_{HH}) were included to calculate J_{HH} ; values have been scaled by 0.9117 as recommended. To perform these calculations in Gaussian09, the following route was used: #n B3LYP/6-31G(d,p) nmr=(fonly,readatoms) iop(3/10=1100000) specifying the desired H atoms at the end of the molecule specification (e.g. atom=16,25,40,41 for 4a, preceded by a blank line; route recommended by the CHESHIRE Chemical Shift Repository <http://cheshirenmr.info/Recommendations.htm>, last accessed on 11/16/2020).

Table 5.16 Observed and calculated Boltzmann weighted average ^1H - ^1H coupling constants for **4a**, **5a**, **4b**, **5b**, and RMSD values, based on Table 15.

4a	Observed	Boltzmann distribution based on					
		B3LYP		mPW1PW91		M06-2X	
		$ J_{\text{HH}} $	Error ^a	$ J_{\text{HH}} $	Error	$ J_{\text{HH}} $	Error
$^3J_{4\beta-3}$ [Hz]	7.8	9.6	1.8	9.6	1.8	8.4	0.6
$^3J_{4\alpha-3}$ [Hz]	5.0	4.2	0.8	4.2	0.8	4.4	0.6
$^2J_{4\alpha-4\beta}$ [Hz]	15.4	15.3	0.1	15.2	0.2	15.2	0.2
$^5J_{4\beta-1}$ [Hz]	1.5	1.9	0.4	1.8	0.3	1.8	0.0
$^5J_{4\alpha-1}$ [Hz]	1.2	0.9	0.3	0.9	0.3	1.2	0.3
5a							
$^3J_{4\beta-3}$ [Hz]	11.0	10.7	0.3	10.7	0.3	9.3	1.7
$^3J_{4\alpha-3}$ [Hz]	4.1	3.9	0.2	3.8	0.3	4.2	0.1
$^2J_{4\alpha-4\beta}$ [Hz]	15.1	15.0	0.1	15.0	0.1	15.1	0.0
$^5J_{4\beta-1}$ [Hz]	2.5	3.0	0.5	3.0	0.5	2.0	0.1
$^5J_{4\alpha-1}$ [Hz]	1.9	2.1	0.2	2.0	0.1	2.6	0.1
4b							
$^3J_{4\beta-3}$ [Hz]	6.8	6.7	0.1	6.7	0.1	5.7	1.1
$^3J_{4\alpha-3}$ [Hz]	5.4	5.0	0.4	5.0	0.4	5.2	0.2
$^2J_{4\alpha-4\beta}$ [Hz]	15.4	15.2	0.2	15.2	0.2	15.2	0.2
$^5J_{4\beta-1}$ [Hz]	1.6	1.9	0.3	1.9	0.3	1.9	0.3
$^5J_{4\alpha-1}$ [Hz]	1.4	1.6	0.2	1.6	0.2	1.9	0.5
5b							
$^3J_{4\beta-3}$ [Hz]	11.2	10.8	0.4	10.8	0.4	10.7	0.5
$^3J_{4\alpha-3}$ [Hz]	4.3	3.9	0.4	3.9	0.4	3.9	0.4
$^2J_{4\alpha-4\beta}$ [Hz]	15.2	15.0	0.2	15.0	0.2	15.0	0.2
$^5J_{4\beta-1}$ [Hz]	2.6	3.0	0.4	3.0	0.4	3.0	0.4
$^5J_{4\alpha-1}$ [Hz]	1.9	2.1	0.2	2.1	0.2	2.1	0.2
MAD [Hz]			0.4		0.4		0.4
RMSD [Hz]			0.5		0.5		0.5

^aError calculated as an absolute value of difference between observed and calculated coupling constant.

5.1.3 Calculated ^{13}C NMR chemical shifts and shielding tensors of 4a/4b and 5a/5b

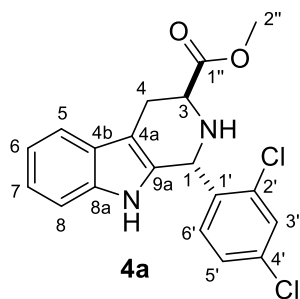


Table 5.17 Calculated Boltzmann weighted average ^{13}C NMR compared to experimentally obtained chemical shifts in compound **4a**. ^{13}C NMR shifts were calculated by B3LYP/6-311+G(2d,p)//B3LYP/6-31G(d), SCRF=(PCM, CHCl₃) (method **M1**) and mPW1PW91/6-311+G(2d,p)//B3LYP/6-31G(d), SCRF=(PCM, CHCl₃) (methods **M2**, and **M3**).

Carbon	^{13}C NMR Chemical shifts [ppm]						
	Exp.	M1	M2	M3	$\Delta_{\text{M1-Exp.}}$	$\Delta_{\text{M2-Exp.}}$	$\Delta_{\text{M3-Exp.}}$
1	51.3	53.3	52.7	52.9	2.1	1.4	1.7
3	52.3	53.6	52.5	53.2	1.3	0.2	0.8
4	25.0	27.8	27.0	26.6	2.8	2.1	1.7
4a	109.8	111.5	111.1	110.5	1.7	1.3	0.7
4b	126.9	127.0	126.2	126.1	0.1	-0.7	-0.8
5	118.5	116.7	117.4	117.4	-1.8	-1.1	-1.1
6	119.9	118.4	118.6	118.5	-1.5	-1.3	-1.4
7	122.5	120.7	121.2	121.0	-1.8	-1.3	-1.5
8	111.2	108.8	109.4	109.4	-2.4	-1.8	-1.8
8a	136.3	135.4	134.7	134.7	-0.9	-1.6	-1.6
9a	131.6	131.7	131.2	131.4	0.1	-0.4	-0.2
1'	137.9	140.1	139.2	139.2	2.2	1.3	1.3
2'	134.0	142.4	141.2	140.9	8.4	7.2	6.9
3'	129.9	129.7	129.7	129.7	-0.2	-0.2	-0.2
4'	134.0	141.3	140.3	140.3	7.3	6.3	6.3
5'	127.4	125.9	126.2	126.3	-1.5	-1.2	-1.1
6'	131.0	130.0	130.4	130.7	-1.0	-0.6	-0.3
1''	173.8	176.0	175.4	175.4	2.2	1.5	1.5
2''	52.4	51.5	51.5	51.6	-0.9	-0.8	-0.8
MAD					2.1	1.7	1.7
RMSD					3.0	2.5	2.4

Methods used to calculate Boltzmann distribution:

M1 – B3LYP/6-311+G(2d,p)//B3LYP/6-31G(d), SCRF(PCM=chloroform),

M2 – mPW1PW91/6-311+G(2d,p)//B3LYP/6-31G(d), SCRF(PCM=chloroform),

M3 – M06-2X/def2-TZVP//B3LYP/6-31G(d), SCRF(PCM=chloroform).

Table 5.18 **4a** Shielding tensors B3LYP/6-311+G(2d,p)//B3LYP/6-31G(d) SCRF = (PCM, CHCl₃)

	4a-01	4a-02	4a-03	4a-04	4a-05	4a-06	4a-07	4a-08
1	127.39	126.30	121.04	121.58	127.11	124.72	126.27	125.04
3	120.96	120.36	121.25	121.97	126.69	126.95	121.97	127.10
4	154.79	155.60	155.44	152.25	151.69	153.85	151.55	152.86
4a	70.56	69.55	69.04	69.11	64.90	64.79	67.04	64.25
4b	49.87	50.05	49.95	49.24	49.15	49.44	49.15	49.18
5	60.24	60.45	60.89	61.03	60.03	59.28	60.60	60.07
6	59.13	59.20	59.12	59.07	57.99	58.68	58.65	58.23
7	56.55	56.66	56.71	56.74	55.54	56.11	56.09	55.72
8	68.26	68.74	68.32	68.32	68.46	67.24	67.94	68.27
8a	40.98	40.12	40.59	41.02	40.69	40.33	40.50	40.25
9a	42.39	43.15	43.76	42.47	44.79	45.70	42.77	44.14
1'	33.62	33.90	36.06	37.29	35.21	36.34	34.98	36.20
2'	35.09	35.30	31.39	33.24	32.40	33.71	31.24	33.61
3'	47.51	47.28	44.68	45.56	46.38	46.35	46.50	46.37
4'	34.66	34.50	33.53	33.22	34.50	33.94	33.72	34.27
5'	49.33	48.95	50.27	49.23	50.58	50.34	49.47	50.62
6'	44.50	44.58	42.96	41.45	46.61	46.04	46.10	46.29
1''	-3.55	-2.20	-3.62	-2.17	-2.85	-0.02	-1.52	-1.32
2''	128.14	127.92	128.27	128.58	128.10	127.99	128.57	127.86
	4a-09	4a-10	4a-11	4a-12	4a-13	4a-14	4a-15	4a-16
1	126.45	120.37	119.81	126.37	121.96	119.28	118.85	121.51
3	123.59	120.11	120.45	120.43	124.00	124.55	123.40	121.04
4	152.21	153.92	156.68	152.98	150.37	152.77	154.40	149.85
4a	65.42	67.64	68.07	65.58	68.62	65.61	66.25	67.95
4b	48.99	49.01	49.46	48.63	48.76	48.57	49.02	49.00
5	59.36	60.44	60.34	59.88	60.45	58.48	59.51	60.41
6	57.80	58.81	58.83	58.27	58.08	58.95	58.52	58.34
7	55.53	56.51	56.58	55.72	55.93	56.51	56.52	55.99
8	68.21	68.47	68.52	67.98	67.89	67.87	67.89	68.14
8a	40.81	40.62	40.24	40.45	40.59	40.56	40.09	40.83
9a	44.39	42.97	44.06	43.22	42.65	43.91	44.70	42.86
1'	36.25	37.66	36.49	35.63	34.92	33.51	34.12	35.66
2'	32.29	33.48	31.49	31.99	32.74	33.78	32.67	33.21
3'	46.33	45.24	44.36	46.65	45.22	44.86	45.14	45.06
4'	34.14	33.15	33.43	33.80	34.03	33.65	33.31	33.77
5'	50.53	49.36	50.35	49.34	50.25	49.43	49.32	50.23
6'	46.04	41.82	43.14	46.03	44.49	42.20	42.14	44.34
1''	-0.06	-1.40	-2.49	-1.11	-3.64	-1.62	0.18	-0.39
2''	128.26	128.03	128.10	127.98	127.71	128.03	128.20	127.93

Table 5.19 **4a** Shielding tensors mPW1PW91/6-311+G(2d,p)//B3LYP/6-31G(d) SCRf = (PCM, CHCl₃)

	4a-01	4a-02	4a-03	4a-04	4a-05	4a-06	4a-07	4a-08
1	132.80	131.75	126.78	127.34	132.65	130.28	131.74	130.57
3	126.85	126.25	127.08	127.90	132.63	132.55	127.89	132.68
4	160.03	160.80	160.66	157.65	157.10	159.10	157.01	158.17
4a	75.86	74.80	74.25	74.46	70.14	69.93	72.23	69.50
4b	55.38	55.49	55.38	54.77	54.71	55.03	54.72	54.77
5	64.32	64.51	64.93	65.09	64.07	63.40	64.61	64.11
6	63.60	63.64	63.58	63.54	62.41	63.11	63.09	62.64
7	60.93	61.00	61.07	61.10	59.84	60.33	60.35	60.01
8	72.39	72.93	72.52	72.49	72.55	71.47	72.09	72.37
8a	46.44	45.65	46.17	46.61	46.26	45.79	46.09	45.76
9a	47.75	48.48	48.99	47.76	50.07	50.89	48.07	49.43
1'	39.48	39.73	42.00	43.19	41.03	41.95	40.88	41.89
2'	40.99	41.16	37.16	38.98	38.38	39.68	37.18	39.57
3'	52.17	51.92	49.40	50.27	51.09	51.09	51.15	51.10
4'	40.51	40.31	39.32	39.01	40.30	39.89	39.48	40.07
5'	53.83	53.49	54.81	53.79	55.06	54.80	54.00	55.06
6'	49.00	49.07	47.35	45.83	50.92	50.47	50.50	50.62
1''	1.91	3.24	1.80	3.33	2.61	5.39	3.96	4.13
2''	132.74	132.55	132.89	133.25	132.76	132.62	133.24	132.50
	4a-09	4a-10	4a-11	4a-12	4a-13	4a-14	4a-15	4a-16
1	132.00	126.19	125.64	131.83	127.64	125.16	124.75	127.25
3	129.79	126.10	126.33	126.36	129.91	130.27	129.19	127.15
4	157.65	159.26	161.82	158.42	155.77	158.06	159.66	155.23
4a	70.61	72.98	73.30	70.82	73.80	71.15	71.71	73.24
4b	54.52	54.55	54.92	54.25	54.41	54.20	54.60	54.58
5	63.45	64.48	64.41	63.91	64.52	62.84	63.64	64.50
6	62.26	63.30	63.31	62.76	62.58	63.41	62.97	62.88
7	59.81	60.85	60.92	60.01	60.31	60.85	60.83	60.38
8	72.35	72.61	72.64	72.04	72.02	71.91	71.96	72.21
8a	46.33	46.25	45.86	46.01	46.19	45.82	45.57	46.33
9a	49.73	48.28	49.33	48.52	48.08	49.03	49.83	48.23
1'	41.94	43.63	42.47	41.52	40.76	39.51	40.02	41.44
2'	38.28	39.25	37.31	37.81	38.57	39.52	38.48	38.92
3'	51.07	49.93	49.07	51.32	49.87	49.54	49.84	49.79
4'	40.02	38.97	39.23	39.49	39.75	39.38	39.12	39.49
5'	55.01	53.93	54.91	53.85	54.77	53.87	53.86	54.78
6'	50.41	46.27	47.58	50.45	48.89	46.67	46.68	48.74
1''	5.43	4.06	3.02	4.33	1.87	3.81	5.60	5.13
2''	132.89	132.65	132.70	132.61	132.36	132.65	132.83	132.58

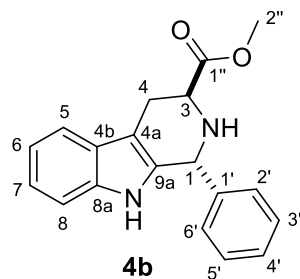


Table 5.20 Calculated Boltzmann weighted average ^{13}C NMR compared to experimentally obtained chemical shifts in compound **4b**. ^{13}C NMR shifts were calculated by B3LYP/6-311+G(2d,p)//B3LYP/6-31G(d), SCRF=(PCM, CHCl_3) (method **M1**) and mPW1PW91/6-311+G(2d,p)//B3LYP/6-31G(d), SCRF=(PCM, CHCl_3) (methods **M2**, and **M3**).

Carbon	^{13}C NMR Chemical shifts [ppm]						
	Exp.	M1	M2	M3	$\Delta_{\text{M1-Exp.}}$	$\Delta_{\text{M2-Exp.}}$	$\Delta_{\text{M3-Exp.}}$
1	55.1	57.5	56.54	56.5	2.5	1.5	1.4
3	52.7	54.8	53.78	54.3	2.1	1.1	1.6
4	24.8	27.0	26.37	26.1	2.3	1.6	1.3
4a	108.6	109.1	108.58	108.0	0.5	0.0	-0.5
4b	127.1	127.6	126.80	126.8	0.5	-0.3	-0.4
5	118.4	116.5	117.23	117.2	-1.9	-1.2	-1.2
6	119.7	118.2	118.50	118.4	-1.5	-1.2	-1.2
7	122.1	120.2	120.54	120.5	-1.9	-1.6	-1.6
8	111.0	109.0	109.57	109.5	-2.0	-1.5	-1.5
8a	136.3	135.7	134.84	134.8	-0.6	-1.5	-1.5
9a	133.3	134.3	133.70	133.9	0.9	0.4	0.6
1'	142.1	144.9	143.87	143.8	2.8	1.8	1.7
2'	128.6	129.1	129.26	129.1	0.6	0.7	0.6
3'	128.9	127.8	128.13	128.1	-1.1	-0.8	-0.8
4'	128.3	126.8	127.23	127.3	-1.5	-1.1	-1.0
5'	128.9	127.3	127.75	127.9	-1.6	-1.2	-1.0
6'	128.6	127.2	127.49	127.7	-1.4	-1.1	-0.9
1''	174.3	176.6	176.02	176.1	2.4	1.7	1.8
2''	52.3	51.3	51.35	51.3	-1.0	-0.9	-0.9
MAD					1.5	1.1	1.1
RMSD					1.7	1.2	1.2

Methods used to calculate Boltzmann distribution:

M1 – B3LYP/6-311+G(2d,p)//B3LYP/6-31G(d), SCRF(PCM=chloroform),

M2 – mPW1PW91/6-311+G(2d,p)//B3LYP/6-31G(d), SCRF(PCM=chloroform),

M3 – M06-2X/def2-TZVP//B3LYP/6-31G(d), SCRF(PCM=chloroform).

Table 5.21 **4b** Shielding tensors B3LYP/6-311+G(2d,p)//B3LYP/6-31G(d) SCRF = (PCM, CHCl₃)

	4b-01	4b-02	4b-03	4b-04	4b-05	4b-06	4b-07	4b-08
1	122.3475	121.5511	122.7069	119.6161	120.1419	122.755	122.5338	122.175
3	121.2533	120.4276	121.9359	126.7257	127.3429	126.6166	120.5222	123.7218
4	155.3685	156.0723	152.0397	154.1438	153.0938	151.5335	152.8969	152.1903
4a	71.8384	70.1304	68.6232	65.8282	65.3758	66.6313	65.8549	66.4389
4b	49.1992	48.328	48.7876	48.8445	48.6932	48.1878	48.5593	48.3412
5	60.5605	59.936	60.7871	60.0991	59.7792	60.4575	60.4009	60.2128
6	58.6485	59.0539	58.5199	58.4475	58.1558	58.1963	58.9981	58.5605
7	56.713	56.7449	56.3189	56.2739	56.6245	55.9383	56.1866	55.8271
8	68.3444	68.2327	68.0123	68.0532	67.514	68.0986	68.2646	68.0736
8a	40.4074	39.9568	41.0802	39.6633	40.1078	40.2491	40.1538	40.5912
9a	40.3515	40.5757	41.4741	43.3677	42.9563	41.8454	41.5906	41.9793
1'	30.6007	31.324	30.5434	30.973	31.1831	29.7556	32.9739	29.899
2'	48.1048	48.1138	44.5239	47.9987	47.8017	45.3906	45.7357	45.3525
3'	48.8392	49.3104	48.0471	47.6028	47.7613	48.5581	48.8678	48.2141
4'	49.063	49.0079	48.9444	49.1302	49.2594	50.1694	48.6853	50.103
5'	48.0278	48.1371	48.2187	48.832	49.0687	49.7995	48.747	49.5583
6'	47.8521	47.4484	50.5145	49.4939	49.6667	49.9	49.0562	49.6496
1''	-3.4409	-2.5902	-1.6735	-0.3724	-1.5255	-3.4342	-1.491	-0.6233
2''	128.3693	128.0755	128.7087	128.071	128.0803	128.2265	128.1948	128.2969

Table 5.22 **4b** Shielding tensors mPW1PW91/6-311+G(2d,p)//B3LYP/6-31G(d) SCRF = (PCM, CHCl₃)

	4b-01	4b-02	4b-03	4b-04	4b-05	4b-06	4b-07	4b-08
1	128.0079	127.2749	128.4267	128.5594	125.554	126.0445	128.177	127.9535
3	127.1486	126.2765	127.8764	132.4641	132.2988	132.8862	126.3669	129.8368
4	160.5948	161.2546	157.485	156.9403	159.4594	158.3741	158.2906	157.6138
4a	76.9614	75.4322	73.7343	71.9052	71.0478	70.5736	71.1759	71.714
4b	54.6608	53.9213	54.3041	53.7993	54.4664	54.3095	54.1132	53.9783
5	64.6167	63.985	64.7442	64.3298	63.9627	63.7572	64.4148	64.119
6	63.1199	63.5389	62.9865	62.6456	62.8783	62.5734	63.4854	63.0257
7	61.0757	61.1651	60.6586	60.3032	60.6063	60.8676	60.6253	60.2086
8	72.5197	72.2675	72.1514	72.2421	72.208	71.7386	72.3439	72.1897
8a	46.008	45.5638	46.6914	45.9564	45.3381	45.685	45.7572	46.2331
9a	45.6713	45.9098	46.7037	47.356	48.6639	48.198	46.9352	47.4105
1'	36.5372	37.2917	36.4822	35.5826	36.7399	36.9346	39.0455	35.7134
2'	52.5494	52.6179	49.0568	50.0225	52.5119	52.3365	50.2603	49.9208
3'	53.2421	53.7024	52.4797	52.9278	52.108	52.2578	53.2641	52.5803
4'	53.414	53.3373	53.2925	54.4485	53.5224	53.6572	52.9964	54.3427
5'	52.4362	52.4815	52.631	54.1058	53.1788	53.4293	53.0947	53.8657
6'	52.3442	51.8815	54.8084	54.3645	54.0421	54.1774	53.5245	54.102
1''	1.983	2.8499	3.7839	2.1064	5.0771	3.9087	3.9016	4.8793
2''	132.9791	132.7181	133.3643	132.8904	132.72	132.7085	132.8235	132.9491

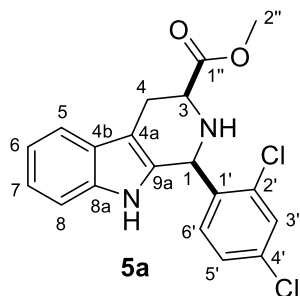


Table 5.23 Calculated Boltzmann weighted average ^{13}C NMR compared to experimentally obtained chemical shifts in compound **5a**. ^{13}C NMR shifts were calculated by B3LYP/6-311+G(2d,p)//B3LYP/6-31G(d), SCRF=(PCM, CHCl_3) (method **M1**) and mPW1PW91/6-311+G(2d,p)//B3LYP/6-31G(d), SCRF=(PCM, CHCl_3) (methods **M2**, and **M3**).

Carbon	^{13}C NMR Chemical shifts [ppm]						
	Exp.	M1	M2	M3	$\Delta_{\text{M1-Exp.}}$	$\Delta_{\text{M2-Exp.}}$	$\Delta_{\text{M3-Exp.}}$
1	53.9	55.9	55.2	55.2	2.0	1.3	1.3
3	56.7	58.7	57.4	56.9	2.0	0.7	0.2
4	25.5	27.9	27.1	26.3	2.3	1.6	0.7
4a	109.5	109.8	109.0	108.7	0.3	-0.5	-0.8
4b	127.0	127.2	126.4	126.3	0.2	-0.6	-0.7
5	118.4	116.8	117.6	117.6	-1.6	-0.8	-0.8
6	119.9	118.3	118.5	118.4	-1.6	-1.4	-1.5
7	122.3	120.5	120.9	120.8	-1.8	-1.4	-1.5
8	111.1	109.2	109.8	109.7	-1.9	-1.3	-1.4
8a	136.3	134.7	133.9	133.9	-1.6	-2.4	-2.4
9a	133.3	133.5	133.1	132.9	0.2	-0.2	-0.4
1'	137.4	139.7	138.8	139.1	2.3	1.4	1.7
2'	134.2	142.2	140.9	140.6	8.0	6.7	6.4
3'	129.5	129.3	129.3	129.3	-0.2	-0.2	-0.2
4'	134.7	141.7	140.7	140.7	7.0	6.0	6.0
5'	128.1	127.1	127.3	127.2	-1.0	-0.8	-0.9
6'	131.5	130.7	131.2	131.5	-0.8	-0.3	0.0
1''	173.1	175.8	175.1	175.1	2.7	2.0	2.0
2''	52.5	51.6	51.7	51.6	-0.8	-0.8	-0.9
MAD					2.0	1.6	1.6
RMSD					2.9	2.4	2.3

Methods used to calculate Boltzmann distribution:

M1 – B3LYP/6-311+G(2d,p)//B3LYP/6-31G(d), SCRF(PCM=chloroform),

M2 – mPW1PW91/6-311+G(2d,p)//B3LYP/6-31G(d), SCRF(PCM=chloroform),

M3 – M06-2X/def2-TZVP//B3LYP/6-31G(d), SCRF(PCM=chloroform).

Table 5.24 **5b** Shielding tensors B3LYP/6-311+G(2d,p)//B3LYP/6-31G(d) SCRF = (PCM, CHCl₃)

	5a-01	5a-02	5a-03	5a-04	5a-05	5a-06	5a-07
1	123.2424	123.0253	124.5188	125.7839	123.9887	118.3157	117.2873
3	120.6582	120.237	121.0327	125.0976	117.8691	120.3565	116.9153
4	153.1466	154.2828	151.9047	157.7095	152.3807	151.974	152.6891
4a	69.5784	68.8268	65.4008	66.6129	64.7392	67.7289	67.4782
4b	49.405	49.2185	48.7247	49.3867	49.1548	48.7507	48.6831
5	59.8227	60.0005	59.7493	59.2373	60.5246	59.6165	60.1879
6	58.5256	58.5199	58.0586	58.7455	58.4956	58.5133	58.3951
7	56.2813	55.9968	55.7327	56.1439	55.7451	56.4153	55.8429
8	67.8026	68.3478	67.736	68.6508	68.1495	67.66	68.5173
8a	42.05	41.278	40.7513	40.38	40.9227	41.3914	41.3588
9a	41.3211	42.2783	43.2326	45.7185	43.1065	42.3987	42.3536
1'	34.8139	34.4731	36.8291	35.783	36.8442	38.0048	38.8832
2'	35.4298	35.141	31.9276	33.2266	31.6184	33.2434	33.5821
3'	47.5548	47.5242	46.523	47.0119	46.4213	45.073	45.3006
4'	34.4679	34.2563	33.6288	33.7608	33.4503	32.8882	32.7891
5'	49.007	48.9461	49.2945	49.9355	49.3487	49.2919	49.261
6'	44.8868	44.9824	46.1672	44.7402	46.3908	41.8092	42.1607
1''	-1.2859	0.6689	-2.6908	-3.3525	0.1707	-2.761	0.0261
2''	127.7413	127.823	127.844	128.7967	128.3385	128.0147	128.167
	5a-08	5a-09	5a-10	5a-11	5a-12	5a-13	5a-14
1	125.8347	126.2946	116.1691	115.7368	126.4183	121.9585	121.2309
3	124.7949	124.4588	119.6681	119.6213	123.5796	122.9416	122.9609
4	157.4084	156.1761	153.5556	154.8891	155.7036	157.5584	157.6768
4a	65.6188	65.078	67.0027	67.2964	64.6966	67.5412	67.4042
4b	49.6801	49.3073	49.1604	48.6084	49.0644	49.0371	48.7703
5	59.9864	59.7294	59.8349	59.468	60.0928	60.3263	60.0828
6	58.8562	58.9164	58.4755	58.1453	58.9223	58.6435	58.7059
7	56.0503	56.0276	56.5384	56.2827	56.1133	55.9621	56.1509
8	67.7665	68.3405	67.8214	68.0891	68.0088	68.4069	68.1103
8a	40.1874	40.3228	41.077	41.0876	40.4593	39.9047	39.806
9a	43.7915	43.8511	42.2329	43.175	43.6012	45.6172	45.4898
1'	33.9853	36.3873	37.6313	37.2255	35.7879	34.6811	34.6238
2'	33.2687	31.8534	31.744	31.07	31.5746	33.1009	33.0535
3'	46.915	46.9431	44.5002	44.569	46.6023	45.1292	45.4992
4'	34.3185	34.3229	33.0949	32.9191	34.5116	34.0089	33.692
5'	50.3916	50.6691	50.2733	50.1607	50.9479	49.3091	49.0341
6'	46.3562	44.4465	43.2847	42.9983	45.9489	42.4235	41.9052
1''	-4.0772	-2.4	-0.9625	0.4737	-0.7391	-3.8693	-2.6819
2''	128.4821	128.5402	127.83	127.9628	128.7929	127.8722	128.2179

Table 5.25 **5b** Shielding tensors mPW1PW91/6-311+G(2d,p)//B3LYP/6-31G(d) SCRf = (PCM, CHCl₃)

	5a-01	5a-02	5a-03	5a-04	5a-05	5a-06	5a-07
1	128.8008	128.631	130.0945	131.4085	129.5127	124.2144	123.2759
3	126.6067	126.2065	127.1493	130.9445	124.2869	126.5478	123.41
4	158.4903	159.6111	157.2159	162.8718	157.7357	157.3493	157.9574
4a	74.749	74.1966	70.6775	71.6895	70.0198	73.0284	72.8509
4b	54.8682	54.6736	54.3068	54.9095	54.7157	54.2965	54.2521
5	63.7457	63.9174	63.769	63.3869	64.5419	63.7035	64.2581
6	63.0643	63.0679	62.4931	63.1564	62.9528	63.0558	62.9474
7	60.7119	60.4293	60.0323	60.4268	60.0813	60.7857	60.2752
8	71.8688	72.3443	71.8949	72.7729	72.3147	71.7859	72.5691
8a	47.4256	46.7802	46.2555	45.7969	46.3347	46.8406	46.7972
9a	46.7937	47.6779	48.525	50.9224	48.3821	47.7027	47.711
1'	40.6819	40.3588	42.6578	41.4363	42.66	43.9172	44.6316
2'	41.3231	41.0947	37.7828	39.2194	37.4953	39.0714	39.3459
3'	52.2075	52.2374	51.1903	51.6012	51.1011	49.7861	50.0359
4'	40.1882	40.0079	39.3795	39.6614	39.2647	38.6365	38.5294
5'	53.5334	53.4693	53.8359	54.3839	53.8799	53.8365	53.7751
6'	49.3746	49.4623	50.5383	49.2015	50.781	46.2711	46.5506
1''	4.1243	6.117	2.8214	2.3522	5.6521	2.769	5.527
2''	132.3265	132.4534	132.5321	133.4658	132.952	132.6561	132.8171
	5a-08	5a-09	5a-10	5a-11	5a-12	5a-13	5a-14
1	131.4335	131.8371	122.1166	121.7828	131.9493	127.7972	127.138
3	130.6591	130.3783	125.6938	125.5757	129.6685	128.8829	128.8637
4	162.5668	161.4826	158.9089	160.128	160.9532	162.6862	162.7855
4a	71.0357	70.3839	72.2884	72.616	70.0054	72.8536	72.7086
4b	55.182	54.8015	54.6713	54.2045	54.6503	54.5511	54.2972
5	64.043	63.7982	63.9191	63.5748	64.0966	64.4012	64.1092
6	63.2909	63.3454	63.0337	62.6548	63.3751	63.0846	63.1562
7	60.388	60.354	60.9324	60.6467	60.4437	60.3299	60.5165
8	71.8918	72.4522	71.9329	72.2064	72.1089	72.6017	72.3065
8a	45.6658	45.7925	46.4695	46.5098	45.9663	45.4627	45.4128
9a	49.2525	49.3793	47.5378	48.5063	49.0854	50.6146	50.6326
1'	39.7927	42.0795	43.4512	43.0267	41.4883	40.6651	40.5927
2'	39.2503	37.8459	37.4574	36.8496	37.5878	38.8794	38.8597
3'	51.5772	51.541	49.2051	49.3308	51.2872	49.8859	50.2765
4'	40.1055	40.1325	38.8594	38.7059	40.2671	39.863	39.4926
5'	54.8944	55.1234	54.7891	54.6583	55.4402	53.9269	53.6831
6'	50.7203	48.9345	47.6447	47.4259	50.4072	46.937	46.443
1''	1.6528	3.2853	4.4296	5.8893	4.9145	1.7209	2.934
2''	133.1355	133.232	132.4536	132.588	133.4543	132.554	132.8777

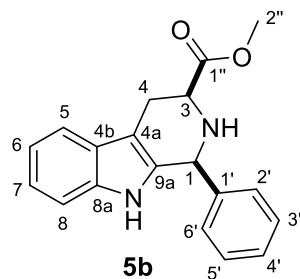


Table 5.26 Calculated Boltzmann weighted average ^{13}C NMR compared to experimentally obtained chemical shifts in compound **5b**. ^{13}C NMR shifts were calculated by B3LYP/6-311+G(2d,p)//B3LYP/6-31G(d), SCRF=(PCM, CHCl_3) (method **M1**) and mPW1PW91/6-311+G(2d,p)//B3LYP/6-31G(d), SCRF=(PCM, CHCl_3) (methods **M2**, and **M3**).

Carbon	^{13}C NMR Chemical shifts [ppm]						
	Exp.	M1	M2	M3	$\Delta_{\text{M1-Exp.}}$	$\Delta_{\text{M2-Exp.}}$	$\Delta_{\text{M3-Exp.}}$
1	58.8	60.8	59.81	59.96	2.0	1.0	1.1
3	57.0	59.0	57.70	57.74	2.0	0.7	0.7
4	25.8	27.9	27.10	26.91	2.1	1.3	1.1
4a	109.1	109.0	108.26	108.10	-0.1	-0.8	-1.0
4b	127.2	127.8	127.09	127.09	0.6	-0.1	-0.1
5	118.4	117.0	117.55	117.50	-1.3	-0.8	-0.9
6	119.8	118.3	118.60	118.61	-1.5	-1.2	-1.2
7	122.1	120.0	120.43	120.42	-2.1	-1.7	-1.7
8	111.1	108.9	109.47	109.41	-2.1	-1.6	-1.7
8a	136.3	135.3	134.63	134.69	-1.0	-1.6	-1.6
9a	134.8	135.9	135.48	135.57	1.1	0.7	0.8
1'	140.8	143.2	142.16	142.25	2.4	1.3	1.4
2'	128.8	128.7	128.65	128.41	-0.1	-0.1	-0.3
3'	129.1	127.4	127.63	127.61	-1.8	-1.5	-1.5
4'	128.8	127.7	128.05	128.04	-1.1	-0.7	-0.7
5'	129.1	128.2	128.58	128.60	-0.9	-0.5	-0.5
6'	128.8	127.8	128.28	128.34	-1.0	-0.5	-0.4
1''	173.3	175.9	175.26	175.13	2.6	1.9	1.8
2''	52.4	51.5	51.58	51.59	-0.9	-0.8	-0.8
MAD					1.4	1.0	1.0
RMSD					1.6	1.1	1.1

Methods used to calculate Boltzmann distribution:

M1 – B3LYP/6-311+G(2d,p)//B3LYP/6-31G(d), SCRF(PCM=chloroform),

M2 – mPW1PW91/6-311+G(2d,p)//B3LYP/6-31G(d), SCRF(PCM=chloroform),

M3 – M06-2X/def2-TZVP//B3LYP/6-31G(d), SCRF(PCM=chloroform).

Table 5.27 **5b** Shielding tensors B3LYP/6-311+G(2d,p)//B3LYP/6-31G(d) SCRF = (PCM, CHCl₃)

	5b-01	5b-02	5b-03	5b-04	5b-05	5b-06	5b-07	5b-08
1	119.7767	116.7167	117.2034	118.7587	120.9346	121.3299	122.8195	123.6806
3	120.8299	119.6897	120.1121	117.4989	124.9719	124.0013	123.9525	122.6274
4	151.5696	154.201	153.2238	152.3809	157.8562	157.8366	156.4641	155.7107
4a	66.6307	69.4623	69.3968	66.3085	66.5976	66.5505	66.3663	67.4106
4b	48.4866	47.7594	48.5007	48.4502	48.7576	49.3057	48.4298	48.2199
5	59.0301	58.6664	60.6549	60.0507	59.2215	59.5067	59.1388	59.3529
6	58.5358	58.7008	57.9704	58.191	58.9695	58.9859	59.0201	59.0033
7	56.4706	56.886	56.4583	56.2697	56.4208	56.4097	56.3884	56.4632
8	67.6033	68.2479	68.6529	67.8316	68.0768	68.264	67.637	67.8087
8a	41.3169	40.6981	39.8707	40.6168	40.204	40.0269	40.9205	41.5086
9a	41.1077	39.3535	38.7588	41.3257	44.3214	43.7245	44.6593	43.5052
1'	32.9148	32.0619	31.8827	32.4868	30.4629	30.0536	32.3461	33.0061
2'	45.6805	49.0096	49.3291	45.2079	48.1062	47.8496	45.151	44.9841
3'	48.7018	49.0245	49.3329	47.2503	47.7609	48.3507	48.6917	49.0691
4'	48.5437	48.6599	48.4589	48.8474	49.2601	49.2213	50.0174	50.2085
5'	48.2249	48.0041	47.6984	48.4579	48.5038	48.9875	49.9351	50.2461
6'	48.96	47.9456	47.6448	50.8589	48.3642	48.9686	48.0688	49.8045
1''	-2.9426	0.1264	-1.5574	-0.0947	-3.4803	-3.8975	-1.4941	0.1212
2''	128.1357	127.9082	127.8355	128.3818	129.0169	128.5566	128.9634	129.1278

Table 5.28 **5b** Shielding tensors mPW1PW91/6-311+G(2d,p)//B3LYP/6-31G(d) SCRF = (PCM, CHCl₃)

	5b-01	5b-02	5b-03	5b-04	5b-05	5b-06	5b-07	5b-08
1	125.6949	122.7393	123.1648	124.6905	126.9518	127.2819	128.6799	129.4753
3	127.0067	125.7269	126.1043	123.9514	130.8401	129.9767	129.9018	128.8085
4	157.002	159.5501	158.546	157.7749	162.9761	162.9768	161.6953	160.993
4a	71.8495	74.758	74.6291	71.5913	71.8769	71.8119	71.5675	72.6384
4b	53.9287	53.3765	54.0635	54.0342	54.3464	54.8247	54.0077	53.825
5	63.0851	62.8529	64.6558	64.0441	63.2725	63.7023	63.2178	63.3829
6	63.07	63.1802	62.4827	62.6236	63.4665	63.4372	63.4623	63.4426
7	60.8418	61.2229	60.8362	60.576	60.8067	60.7146	60.7504	60.812
8	71.7287	72.31	72.7105	71.9979	72.1076	72.4378	71.7854	71.9533
8a	46.7232	46.1947	45.5798	46.2294	45.6892	45.5327	46.3896	47.0443
9a	46.4416	44.8257	44.2283	46.6691	49.4593	48.7885	49.7149	48.7025
1'	38.9117	37.9654	37.8286	38.2353	36.3509	36.027	38.1549	38.7511
2'	50.1433	53.4788	53.8095	49.6321	52.6461	52.374	49.8421	49.7377
3'	53.0525	53.4715	53.7511	51.735	52.3231	52.8444	53.1414	53.5085
4'	52.9031	53.0358	52.8756	53.206	53.6335	53.611	54.3714	54.5791
5'	52.6639	52.3986	52.1223	52.8558	52.9005	53.3711	54.3068	54.6726
6'	53.2957	52.3842	52.0542	55.1676	52.9327	53.4384	52.6183	54.2846
1''	2.5772	5.5764	3.8428	5.4047	2.1842	1.7096	4.0984	5.7235
2''	132.7801	132.5492	132.4624	133.0071	133.6777	133.1967	133.6496	133.829

Table 5.29 Predicted ¹³C NMR shifts in C-1 and C-3 for conformers of compound **4a**, grouped according to conformer ensembles **B** and **C**.

		Ensemble B								Weighted average
		4a-5	4a-6	4a-8	4a-9	4a-13	4a-14	4a-15	4a-16	
Method 1	Boltzmann distribution [%]	37.9	10.9	29.4	8.0	0.1	0.0	0.0	0.0	–
	δ C1 [ppm]	52.4	54.6	54.3	53.0	57.3	59.9	60.3	57.7	53.4
	δ C3 [ppm]	52.8	52.5	52.4	55.7	55.3	54.8	55.9	58.2	52.9
Method 2	Boltzmann distribution [%]	31.5	11.0	37.1	6.3	0.1	0.0	0.0	0.0	–
	δ C1 [ppm]	51.5	53.8	53.5	52.2	56.3	58.7	59.1	56.7	52.7
	δ C3 [ppm]	51.6	51.6	51.5	54.3	54.2	53.8	54.9	56.8	51.8
Method 3	Boltzmann distribution [%]	17.6	13.7	37.7	4.6	0.0	0.0	0.0	0.0	–
	δ C1 [ppm]	51.5	53.8	53.5	52.2	56.3	58.7	59.1	56.7	53.0
	δ C3 [ppm]	51.6	51.6	51.5	54.3	54.2	53.8	54.9	56.8	51.7
		Ensemble C								Weighted average
		4a-1	4a-2	4a-3	4a-4	4a-7	4a-10	4a-11	4a-12	
Method 1	Boltzmann distribution [%]	7.2	4.2	0.9	0.1	0.5	0.0	0.2	0.3	–
	δ C1 [ppm]	52.1	53.1	58.2	57.7	53.2	58.8	59.4	53.1	53.1
	δ C3 [ppm]	58.3	58.8	58.0	57.3	57.3	59.1	58.7	58.8	58.4
Method 2	Boltzmann distribution [%]	7.6	4.2	1.1	0.1	0.5	0.0	0.2	0.4	–
	δ C1 [ppm]	51.4	52.4	57.2	56.6	52.4	57.7	58.3	52.3	52.4
	δ C3 [ppm]	57.1	57.7	56.9	56.1	56.1	57.8	57.6	57.6	57.2
Method 3	Boltzmann distribution [%]	14.8	6.0	3.3	0.2	0.9	0.1	0.6	0.5	–
	δ C1 [ppm]	51.4	52.4	57.2	56.6	52.4	57.7	58.3	52.3	52.6
	δ C3 [ppm]	57.1	57.7	56.9	56.1	56.1	57.8	57.6	57.6	57.2

Methods used for calculation of conformer energies:

M1 – B3LYP/6-311+G(2d,p)//B3LYP/6-31G(d), SCRF(PCM=chloroform),

M2 – mPW1PW91/6-311+G(2d,p)//B3LYP/6-31G(d), SCRF(PCM=chloroform),

M3 – M06-2X/def2-TZVP//B3LYP/6-31G(d), SCRF(PCM=chloroform).

Methods used for ¹³C NMR shift calculation:

M1 – B3LYP/6-311+G(2d,p)//B3LYP/6-31G(d), SCRF(PCM=chloroform),

M2 and M3 – mPW1PW91/6-311+G(2d,p)//B3LYP/6-31G(d), SCRF(PCM=chloroform).

Table 5.30 Predicted ^{13}C NMR shifts in C-1 and C-3 for calculated conformers of compound **4b**, grouped according to conformer ensemble **B** and **C**.

		Ensemble B				Weighted average
		4b-4	4b-5	4b-6	4b-8	
Method 1	Boltzmann distribution [%]	5.6%	23.9%	27.0%	6.6%	–
	δ C1 [ppm]	59.5	59.0	56.5	57.1	57.8
	δ C3 [ppm]	52.7	52.1	52.8	55.6	52.8
Method 2	Boltzmann distribution [%]	4.7%	26.6%	24.8%	5.8%	–
	δ C1 [ppm]	58.4	57.9	55.5	56.0	56.8
	δ C3 [ppm]	51.9	51.3	51.7	54.2	51.8
Method 3	Boltzmann distribution [%]	4.3%	21.7%	19.8%	5.6%	–
	δ C1 [ppm]	58.4	57.9	55.5	56.0	56.8
	δ C3 [ppm]	51.9	51.3	51.7	54.2	51.8
		Ensemble C				Weighted average
		4b-1	4b-2	4b-3	4b-7	
Method 1	Boltzmann distribution [%]	26.4%	8.9%	1.2%	0.5%	–
	δ C1 [ppm]	56.9	57.7	56.6	56.7	57.1
	δ C3 [ppm]	58.0	58.8	57.3	58.7	58.2
Method 2	Boltzmann distribution [%]	27.5%	8.9%	1.1%	0.6%	–
	δ C1 [ppm]	56.0	56.7	55.6	55.8	56.1
	δ C3 [ppm]	56.8	57.7	56.1	57.6	57.0
Method 3	Boltzmann distribution [%]	36.2%	10.2%	1.6%	0.6%	–
	δ C1 [ppm]	56.0	56.7	55.6	55.8	56.1
	δ C3 [ppm]	56.8	57.7	56.1	57.6	57.0

Methods used for calculation of conformer energies:

M1 – B3LYP/6-311+G(2d,p)//B3LYP/6-31G(d), SCRF(PCM=chloroform),

M2 – mPW1PW91/6-311+G(2d,p)//B3LYP/6-31G(d), SCRF(PCM=chloroform),

M3 – M06-2X/def2-TZVP//B3LYP/6-31G(d), SCRF(PCM=chloroform).

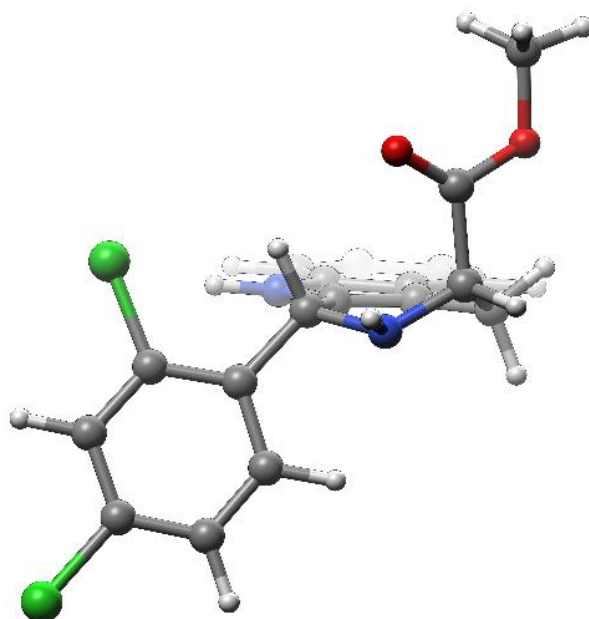
Methods used for ^{13}C NMR shift calculation:

M1 – B3LYP/6-311+G(2d,p)//B3LYP/6-31G(d), SCRF(PCM=chloroform),

M2 and M3 – mPW1PW91/6-311+G(2d,p)//B3LYP/6-31G(d), SCRF(PCM=chloroform).

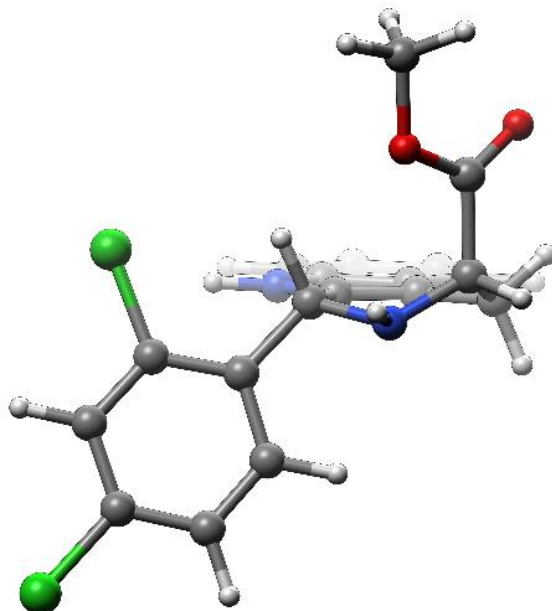
5.1.4 B3LYP/6-31G(d) Cartesian coordinates for all conformers of 4a, 4b, 5a, and 5b

4a-01



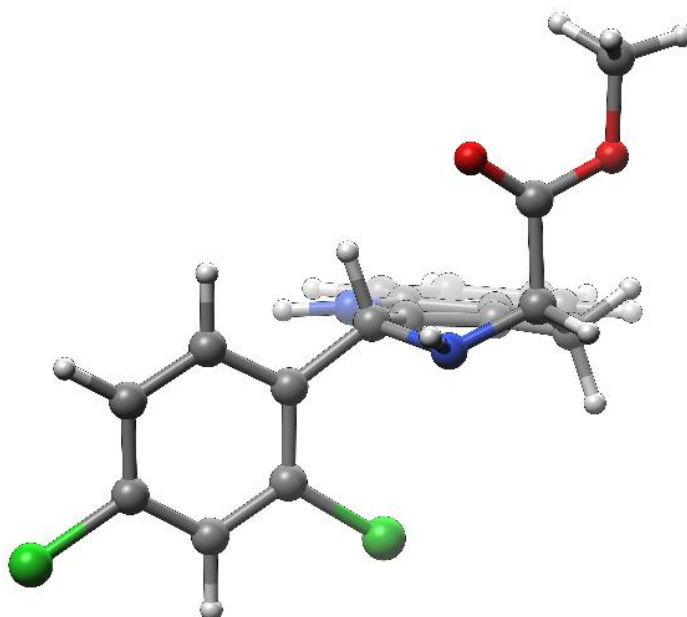
C	0.00000000	0.00000000	0.00000000	H	3.27071100	-2.36515300	2.36132700
C	-0.45182000	1.09447300	0.91818900	H	1.95676600	-3.51246300	2.79013100
C	0.10110700	2.39544600	1.18837800	H	-2.42477400	-2.10676700	0.94324700
C	1.20882500	3.11306400	0.70643100	H	-2.32128800	-0.72494300	2.77654300
H	1.85790200	2.68165500	-0.05157300	C	-3.92346300	0.09711500	1.61093800
C	1.46315000	4.38238700	1.21205200	C	-4.77698100	0.37922400	2.68466500
C	0.62933900	4.95500500	2.19366000	C	-6.12125400	0.71009600	2.50862000
C	-0.47539100	4.27067200	2.68983000	C	-6.62684000	0.76933500	1.21369300
C	-0.72813900	2.99430800	2.17932800	C	-5.81273600	0.50724100	0.11273500
N	-1.73409100	2.09484600	2.47762600	C	-4.47826800	0.17599900	0.32583700
H	-2.44514600	2.21809900	3.18275400	H	-3.82868900	-0.05107100	-0.51240200
C	-1.55813000	0.95422200	1.71629500	H	-6.21844000	0.56030000	-0.89163500
C	-2.44427100	-0.26107900	1.78778700	Cl	-8.31707000	1.18134100	0.97356100
N	-2.03854200	-1.19362300	0.71358500	H	-6.75391700	0.91525900	3.36362800
C	-0.59922400	-1.33411300	0.48744200	Cl	-4.18020300	0.34674500	4.35194800
H	-0.47732500	-2.07913400	-0.31113000	H	-1.11769100	4.71339000	3.44678400
C	0.13084900	-1.91871300	1.71048700	H	0.85269000	5.94944000	2.57033000
O	-0.43050000	-2.40647400	2.67000500	H	2.31730200	4.94573500	0.84615400
O	1.46994200	-1.88942300	1.56678800	H	1.09103700	-0.07817200	-0.02805200
C	2.22421400	-2.46183600	2.65092700	H	-0.33781800	0.17316400	-1.03080900
H	2.02955400	-1.91764200	3.57847500				

4a-02



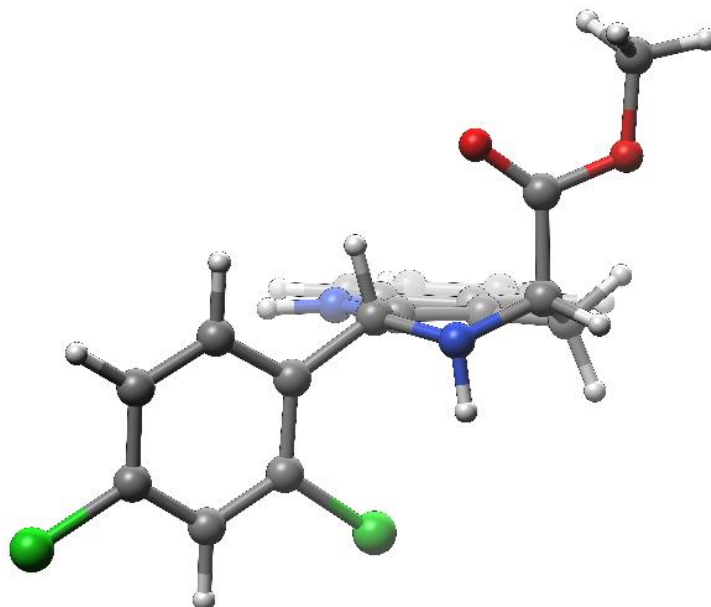
C	0.00000000	0.00000000	0.00000000	H	0.94616600	4.03219600	3.83645000
C	0.41697300	-1.04524700	0.98995100	H	-0.43777100	2.89376900	3.95653100
C	-0.19592600	-2.29422600	1.35930100	H	2.59898700	2.00406800	0.69019200
C	-1.34666100	-2.98483100	0.94313300	H	2.39822100	0.81377700	2.67799600
H	-1.98801600	-2.57098000	0.16917500	C	3.95068600	-0.18772900	1.59669000
C	-1.65438300	-4.20303300	1.53668000	C	4.79171700	-0.40430200	2.69509200
C	-0.83282800	-4.75038500	2.54283000	C	6.11769700	-0.81654800	2.55592500
C	0.31229700	-4.09090400	2.97691000	C	6.61711000	-1.02664900	1.27429600
C	0.61872500	-2.86586700	2.37757300	C	5.81401300	-0.83499500	0.15075000
N	1.67237000	-1.99981300	2.60099100	C	4.49759000	-0.42045300	0.32680800
H	2.39718700	-2.11987300	3.29212300	H	3.85711600	-0.24778000	-0.53130200
C	1.54209700	-0.90834800	1.76139700	H	6.21418700	-1.00670600	-0.84248600
C	2.49191800	0.25970800	1.73147600	Cl	8.28467400	-1.54077300	1.08021700
N	2.13399600	1.10682800	0.57805700	H	6.74134800	-0.96818600	3.42855900
C	0.70376500	1.32493500	0.34517900	Cl	4.20191200	-0.17744200	4.35038000
H	0.63458600	1.99169500	-0.52578400	H	0.94437100	-4.51373000	3.75364300
C	-0.05901700	2.06723800	1.46213000	H	-1.09869400	-5.70482200	2.98900600
O	-1.26370200	2.08839800	1.57990100	H	-2.54238500	-4.74485000	1.22266200
O	0.77905700	2.76566500	2.26429100	H	-1.08218800	0.16189900	0.02006200
C	0.13804900	3.54290000	3.29228900	H	0.27040000	-0.28659700	-1.02514400
H	-0.53313500	4.28263300	2.84842800				

4a-03



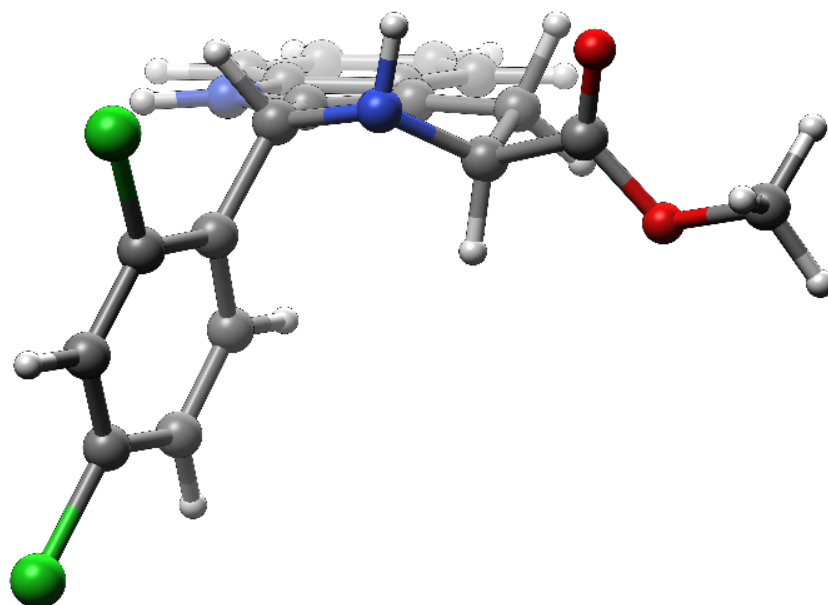
C	0.00000000	0.00000000	0.00000000	H	-3.04331400	-2.82422400	-2.15851100
C	0.40242700	1.07072900	-0.96777600	H	-1.63673400	-3.89374500	-2.48035100
C	-0.20810400	2.33018400	-1.30372000	H	2.59368400	-1.98697400	-0.76313300
C	-1.36917800	3.00301200	-0.88732800	H	2.30340500	-0.73747400	-2.69544900
H	-2.02706300	2.55859600	-0.14461700	C	3.95667800	0.13890900	-1.71429000
C	-1.66338600	4.24626200	-1.43475900	C	4.59694400	0.87185500	-0.69871100
C	-0.81806300	4.83672800	-2.39532300	C	5.96605300	1.13946500	-0.74113500
C	0.33700900	4.19475400	-2.83057300	C	6.71980900	0.66917700	-1.81415200
C	0.62881800	2.94443300	-2.27938000	C	6.12837900	-0.06030300	-2.84080900
N	1.68300200	2.08243200	-2.52241100	C	4.75933600	-0.31220400	-2.77149200
H	2.48508700	2.28453700	-3.09941700	H	4.29060200	-0.88840800	-3.56552600
C	1.54691100	0.96977200	-1.71247200	H	6.72229400	-0.42567200	-3.67118400
C	2.47069900	-0.21278200	-1.73981000	Cl	8.44202400	1.00841700	-1.86298900
N	2.13973300	-1.09124000	-0.59900900	H	6.43256300	1.70781200	0.05449500
C	0.71190600	-1.31874000	-0.37057900	Cl	3.71899600	1.50937100	0.67791800
H	0.63390000	-2.00047000	0.48777400	H	0.98732500	4.65075900	-3.57282100
C	0.04284100	-2.06141900	-1.54285500	H	-1.07239500	5.81053700	-2.80481400
O	0.64883700	-2.57685600	-2.46083100	H	-2.55820200	4.77503700	-1.11765800
O	-1.29529700	-2.13544900	-1.40388300	H	-1.08235000	-0.16058000	0.00334000
C	-1.98950800	-2.86011900	-2.43533400	H	0.29069500	0.26944200	1.02423000
H	-1.83040800	-2.38587000	-3.40704700				

4a-04



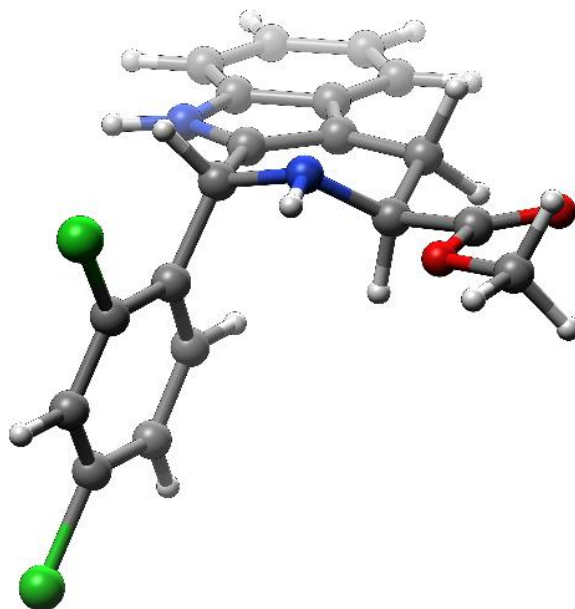
C	0.00000000	0.00000000	0.00000000	H	-2.86621000	-3.28837800	-1.84166300
C	0.47126700	1.09197600	-0.91349000	H	-1.37323600	-4.00932600	-2.53046600
C	-0.12023900	2.36185500	-1.24538300	H	2.59745600	-0.83277500	0.32044900
C	-1.29727600	3.02849000	-0.86501800	H	2.36651400	-0.73586000	-2.56821400
H	-1.98958900	2.56814000	-0.16439900	C	4.04439000	0.10746800	-1.60692600
C	-1.56372100	4.28591500	-1.39414500	C	4.70457800	0.85010400	-0.61390100
C	-0.67463000	4.89722400	-2.30059700	C	6.07548300	1.10409000	-0.66108100
C	0.49768900	4.26224500	-2.69854800	C	6.81730300	0.60421500	-1.72822200
C	0.76094200	2.99720500	-2.16682900	C	6.21011500	-0.14300400	-2.73399200
N	1.82376500	2.13840200	-2.38049100	C	4.83967800	-0.37856200	-2.65559600
H	2.64209700	2.34495400	-2.93244800	H	4.36168600	-0.96885000	-3.43247200
C	1.65213700	1.00530500	-1.60532200	H	6.79600800	-0.53441500	-3.55816600
C	2.55147500	-0.20451500	-1.62813300	Cl	8.54141200	0.92437300	-1.79557200
N	2.19439600	-1.16144700	-0.55480600	H	6.55125500	1.68040300	0.12318400
C	0.75170300	-1.32378500	-0.33331900	Cl	3.83531400	1.50349700	0.77367400
H	0.64168000	-2.00290000	0.52072700	H	1.18207400	4.73421800	-3.39905800
C	0.10854500	-2.04611000	-1.51910400	H	-0.90832900	5.88145900	-2.69727300
O	0.62523100	-2.28733700	-2.58806800	H	-2.47097400	4.80949700	-1.10490900
O	-1.15886000	-2.40295900	-1.21273500	H	-1.08169200	-0.15807800	-0.07619000
C	-1.87948800	-3.08012600	-2.25608100	H	0.20002900	0.25310800	1.05211300
H	-1.96020400	-2.44398500	-3.14138100				

4a-05



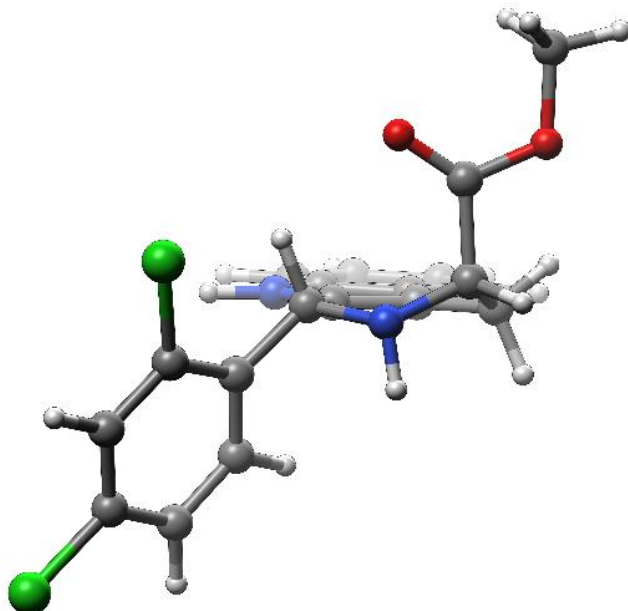
C	0.00000000	0.00000000	0.00000000	H	1.48408800	4.20903300	-2.27593900
C	-0.04335600	-1.45555900	0.35765400	H	2.29677700	4.42269700	-0.68933500
C	-1.07136500	-2.44301600	0.14938800	H	1.79446700	0.48047400	2.09791800
C	-2.34503600	-2.42386200	-0.44326300	H	2.42791100	-1.59575300	2.50465600
H	-2.74288700	-1.50429600	-0.86503200	C	3.50835300	-1.96127500	0.70572300
C	-3.08915600	-3.59687300	-0.48266300	C	4.79249800	-1.86804700	1.26517000
C	-2.58622400	-4.79567200	0.06169800	C	5.92880000	-2.32541200	0.60001500
C	-1.32997900	-4.84662100	0.65693600	C	5.78288100	-2.88740300	-0.66659400
C	-0.58413600	-3.66493400	0.69465300	C	4.53013500	-2.99845100	-1.26280200
N	0.67341800	-3.41362200	1.21262500	C	3.41289900	-2.53806500	-0.56714900
H	1.28103100	-4.09918800	1.63433200	H	2.43205800	-2.62962700	-1.02408500
C	0.99069100	-2.08058800	1.00621200	H	4.42867700	-3.43794000	-2.24899000
C	2.27201800	-1.41961000	1.43375400	Cl	7.20826800	-3.46709100	-1.51318000
N	2.19792800	0.04314300	1.27267200	H	6.90544300	-2.24318400	1.06155100
C	1.47259900	0.50211800	0.08827700	Cl	5.03089900	-1.16678600	2.86223100
H	2.01152500	0.15889400	-0.80086600	H	-0.94448000	-5.77204200	1.07717400
C	1.47544000	2.02283000	0.10920900	H	-3.19046300	-5.69756100	0.01644000
O	1.38999900	2.69035400	1.11786300	H	-4.07528600	-3.59319500	-0.93884800
O	1.51872000	2.53665300	-1.13527600	H	-0.62702700	0.59135200	0.68412600
C	1.44951000	3.97214700	-1.21241600	H	-0.38560200	0.17907700	-1.01208600
H	0.52068400	4.33594400	-0.76532300				

4a-06



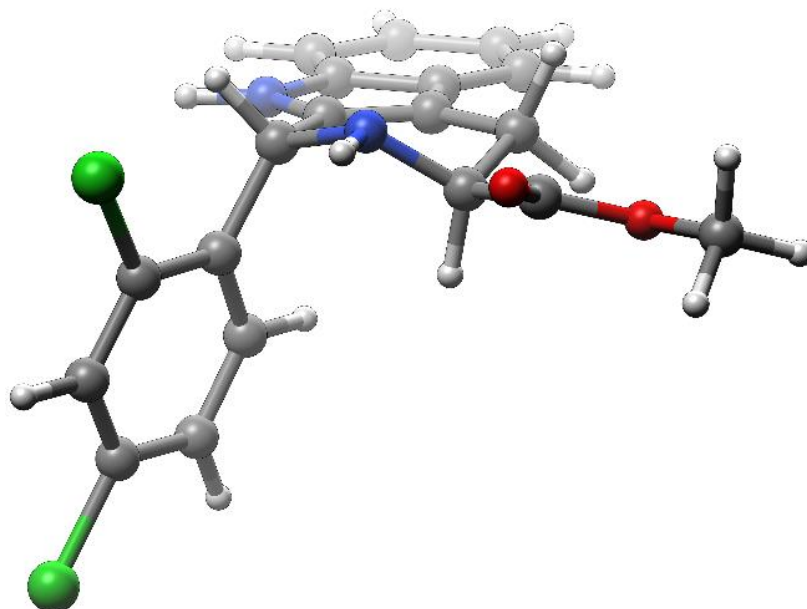
C	0.00000000	0.00000000	0.00000000	H	4.61253600	3.32456800	0.43057700
C	-0.32952400	-1.37562200	0.50096800	H	2.95198700	3.99914800	0.54187300
C	-1.52098700	-2.17243400	0.35859200	H	2.94884900	0.11993100	1.56661300
C	-2.75667300	-1.98345300	-0.28303100	H	2.04847800	-1.80336400	2.73754900
H	-2.96425400	-1.05943300	-0.81650400	C	3.04578000	-2.45828500	0.96015100
C	-3.70927400	-2.99347800	-0.22459000	C	4.34278700	-2.52719000	1.49348200
C	-3.45388700	-4.19552800	0.46576800	C	5.38276500	-3.20290200	0.85828100
C	-2.24112700	-4.41301000	1.11138000	C	5.12539000	-3.82836800	-0.35991700
C	-1.28520400	-3.39497700	1.05034700	C	3.85738200	-3.78550700	-0.93342300
N	-0.01132300	-3.32870900	1.58472000	C	2.83849000	-3.10720600	-0.26637400
H	0.43403000	-4.05025100	2.13038700	H	1.84470300	-3.08626500	-0.70290200
C	0.55186600	-2.10744800	1.25319900	H	3.66797800	-4.27767700	-1.88108800
C	1.92582800	-1.66491900	1.65625000	Cl	6.42490900	-4.68381300	-1.17232000
N	1.99845900	-0.20859100	1.41941800	H	6.36960100	-3.23852600	1.30389600
C	1.52077800	0.21083600	0.09603800	Cl	4.72495900	-1.73318100	3.02499800
H	2.00324400	-0.36401300	-0.72069500	H	-2.04644400	-5.34048900	1.64394600
C	1.89154600	1.66661400	-0.16521600	H	-4.21807400	-4.96738700	0.49504600
O	1.18521700	2.47434800	-0.72502300	H	-4.66825600	-2.85718300	-0.71692000
O	3.14585100	1.93933700	0.26067100	H	-0.50760500	0.77102500	0.59374000
C	3.60004000	3.28438300	0.02852300	H	-0.32162900	0.14387700	-1.03760600
H	3.59990200	3.50706800	-1.04150800				

4a-07



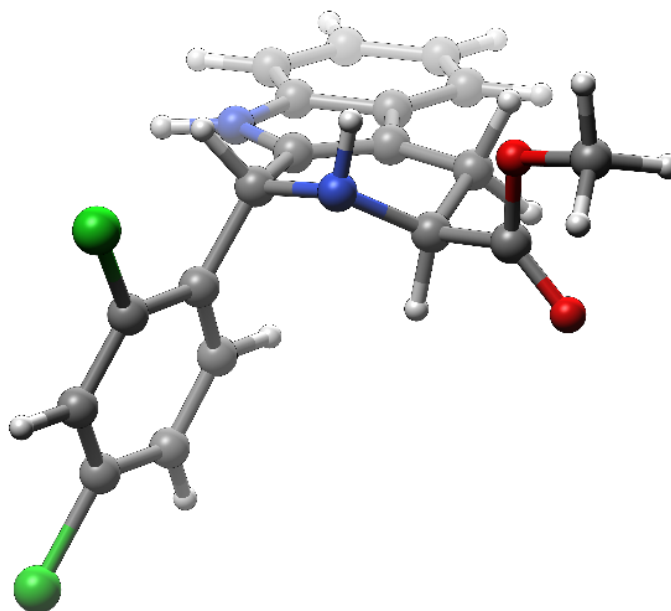
C	0.00000000	0.00000000	0.00000000	H	2.73491100	-3.54181800	1.57734200
C	-0.33536200	1.06288300	1.00470300	H	1.23791600	-4.15747300	2.35438200
C	0.39404700	2.23781200	1.40741300	H	-2.65840600	-0.66264000	-0.21274200
C	1.60388900	2.82898300	1.00645400	H	-2.38754100	-0.68173200	2.67012600
H	2.20341500	2.37816000	0.21949200	C	-3.92719300	0.38856800	1.63665100
C	2.02307200	3.99927800	1.62823100	C	-5.00489400	-0.27732000	2.24171300
C	1.25490400	4.59664100	2.64765200	C	-6.32155400	0.16152500	2.09200000
C	0.05376500	4.03483700	3.06833900	C	-6.57230300	1.28664800	1.31110300
C	-0.36248700	2.85574200	2.44381100	C	-5.53462300	1.97407500	0.68553500
N	-1.48826300	2.08022700	2.65097300	C	-4.23090500	1.51558800	0.85870300
H	-2.23155900	2.28576700	3.30083000	H	-3.41370000	2.05063200	0.38237600
C	-1.47250400	1.01062100	1.77164900	H	-5.74211600	2.84925300	0.07983300
C	-2.48861100	-0.10087000	1.74829000	Cl	-8.22642100	1.84342900	1.11982800
N	-2.22570200	-1.04008900	0.62867500	H	-7.13272700	-0.36943900	2.57528200
C	-0.81143200	-1.28815700	0.32699600	Cl	-4.74805100	-1.70646600	3.22959600
H	-0.78812100	-1.94339300	-0.55191400	H	-0.53619700	4.49518100	3.85682900
C	-0.15466300	-2.08100500	1.45827400	H	1.60716000	5.51182700	3.11559700
O	-0.62263400	-2.30147300	2.55250600	H	2.95715800	4.46440400	1.32514400
O	1.06334600	-2.52110100	1.06786700	H	1.07244200	-0.22525100	-0.00676400
C	1.79519600	-3.26559500	2.05631800	H	-0.25275500	0.31754300	-1.02293500
H	1.98004100	-2.64972100	2.94037600				

4a-08



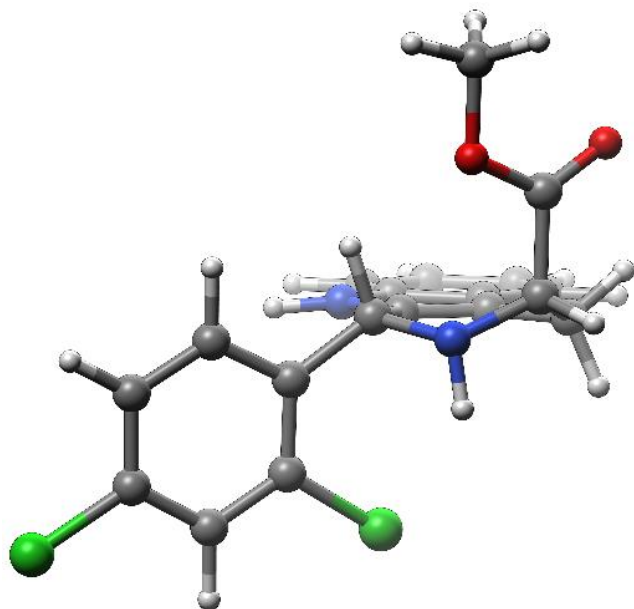
C	0.00000000	0.00000000	0.00000000	H	0.48506500	4.19197200	-1.88329600
C	-0.12280200	-1.45504600	0.35237600	H	2.21615900	4.07595100	-1.41917400
C	-1.19293300	-2.39262500	0.12853400	H	2.89847800	0.40006800	1.58817500
C	-2.45719200	-2.31250100	-0.47944600	H	2.33485800	-1.77542700	2.51672100
H	-2.80579800	-1.37431600	-0.90372200	C	3.38722400	-2.09824300	0.68056500
C	-3.25607300	-3.44845800	-0.52951100	C	4.68884400	-2.03487100	1.20317600
C	-2.81771700	-4.67093100	0.01823700	C	5.80330200	-2.49014100	0.50118500
C	-1.57193800	-4.78303200	0.62685700	C	5.61763000	-3.02184400	-0.77322100
C	-0.77117900	-3.63842300	0.67543300	C	4.34765500	-3.10225800	-1.33813800
N	0.49254200	-3.45055400	1.20490200	C	3.25408100	-2.64454100	-0.60460600
H	1.04783000	-4.15743400	1.66190300	H	2.26060900	-2.72113500	-1.03559300
C	0.87092700	-2.13288200	1.01094500	H	4.21485700	-3.51962500	-2.33029100
C	2.17767500	-1.54432500	1.45587200	Cl	7.01188800	-3.60046600	-1.66923400
N	2.03129900	-0.08337000	1.36873400	H	6.79225800	-2.42904800	0.93931600
C	1.48773400	0.39596700	0.10198100	Cl	4.97821700	-1.35307600	2.80584300
H	2.00782700	-0.03706400	-0.77726800	H	-1.23569700	-5.72660900	1.04910500
C	1.74387100	1.89462300	0.01463200	H	-3.46418900	-5.54259100	-0.03526400
O	2.58111700	2.48530300	0.66331500	H	-4.23565100	-3.39685100	-0.99687000
O	0.96448400	2.48106600	-0.91423700	H	-0.59062600	0.62152300	0.68691000
C	1.18590500	3.88987500	-1.10484600	H	-0.36702100	0.20396200	-1.01181600
H	0.99209200	4.43573500	-0.17807000				

4a-09



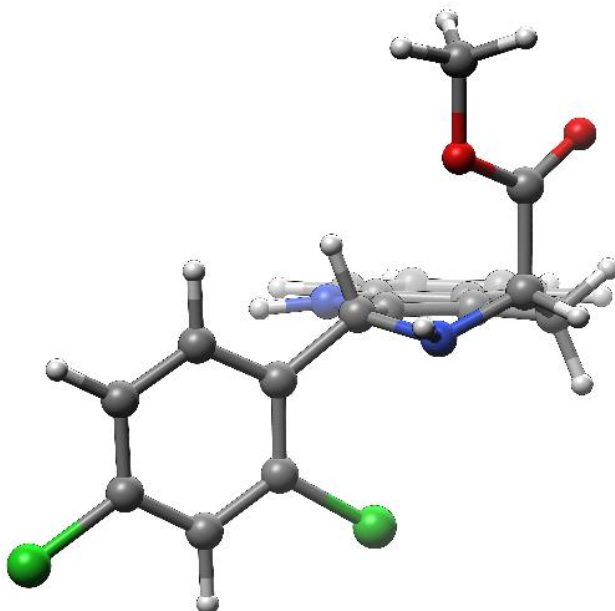
C	0.00000000	0.00000000	0.00000000	H	0.97813300	4.59873300	1.56631100
C	-0.06468400	-1.38434000	0.57536000	H	0.49449100	4.43411900	-0.15547300
C	-1.09863400	-2.38486400	0.50159200	H	1.66945300	0.74043400	2.06999100
C	-2.36384200	-2.44638700	-0.10644200	H	2.36652300	-1.22920400	2.77007800
H	-2.74629900	-1.59903200	-0.66977800	C	3.48010500	-1.82307200	1.05574100
C	-3.11907500	-3.60577800	0.02205700	C	4.75552400	-1.62724300	1.60905600
C	-2.63570400	-4.71186500	0.74970300	C	5.90614900	-2.16316500	1.03372900
C	-1.38794700	-4.68181000	1.36373700	C	5.78403600	-2.91378500	-0.13393400
C	-0.63109400	-3.51390900	1.23266500	C	4.54060600	-3.13360900	-0.71923000
N	0.62120700	-3.19686500	1.72674600	C	3.40840100	-2.58916900	-0.11443300
H	1.21542300	-3.81565500	2.25686300	H	2.43467900	-2.76465400	-0.56186600
C	0.95419400	-1.91250600	1.32695400	H	4.45754500	-3.71938300	-1.62799800
C	2.22939600	-1.19890300	1.68237100	Cl	7.22755100	-3.59396600	-0.86641000
N	2.14893300	0.23372200	1.32930100	H	6.87559100	-1.99704400	1.48776300
C	1.47260300	0.49933900	0.05337600	Cl	4.96313400	-0.69208500	3.08634500
H	2.03989700	-0.00176500	-0.73666700	H	-1.01724900	-5.53570500	1.92505600
C	1.52904700	1.98549200	-0.27105900	H	-3.24824800	-5.60538300	0.83304100
O	1.75616600	2.44800200	-1.36605400	H	-4.09861400	-3.66379900	-0.44449100
O	1.22906000	2.73599400	0.81366800	H	-0.64366000	0.69241700	0.56258500
C	1.23274600	4.15830800	0.60200000	H	-0.35265100	0.02098800	-1.03946800
H	2.22072400	4.49217200	0.27507900				

4a-10



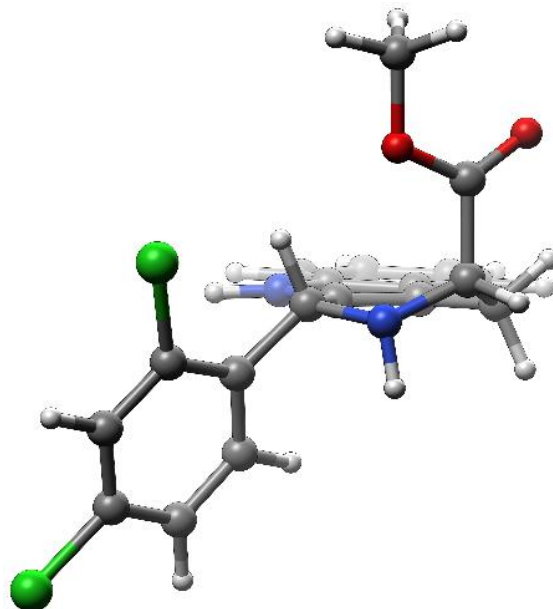
C	0.00000000	0.00000000	0.00000000	H	-1.21676500	3.96030800	-3.77061700
C	-0.38188100	-1.04655600	-1.00443300	H	0.32584500	3.03814600	-3.75823100
C	0.30335500	-2.24023800	-1.42786900	H	-2.65919400	0.63643300	0.33360200
C	1.52143300	-2.84864900	-1.08104800	H	-2.40798000	0.76071700	-2.55248800
H	2.17049300	-2.39584500	-0.33588300	C	-4.00797200	-0.27917800	-1.66411200
C	1.88467900	-4.03694000	-1.70365000	C	-4.60942400	-1.13751500	-0.72821000
C	1.05307900	-4.63512100	-2.67148800	C	-5.95516800	-1.49701000	-0.80532100
C	-0.15654400	-4.05494700	-3.03999900	C	-6.73151100	-0.98941400	-1.84388100
C	-0.51681100	-2.85848600	-2.41431100	C	-6.18275600	-0.13097600	-2.79277000
N	-1.63347900	-2.05929700	-2.58366900	C	-4.83635700	0.20861900	-2.68571800
H	-2.43903200	-2.29254600	-3.14380700	H	-4.40594800	0.88539300	-3.41878400
C	-1.55478000	-0.98648700	-1.71156300	H	-6.79495600	0.26532700	-3.59519000
C	-2.54312500	0.15038300	-1.65012500	Cl	-8.42310600	-1.44230900	-1.94825000
N	-2.26316200	1.04836400	-0.50861700	H	-6.38542000	-2.16079600	-0.06514600
C	-0.83616800	1.28446800	-0.24698600	Cl	-3.69704500	-1.81057100	0.62065200
H	-0.79704000	1.90006700	0.66195600	H	-0.79544500	-4.51586800	-3.78918000
C	-0.15252300	2.15411700	-1.31100400	H	1.36237100	-5.56503000	-3.14089400
O	1.04501700	2.34233300	-1.33753600	H	2.82451100	-4.51541600	-1.44186400
O	-1.00935600	2.72652900	-2.18010800	H	1.06406500	0.25162400	-0.05756200
C	-0.39729500	3.59123300	-3.15322600	H	-0.18737300	-0.35195600	1.02534900
H	0.11523500	4.42027800	-2.65863200				

4a-11



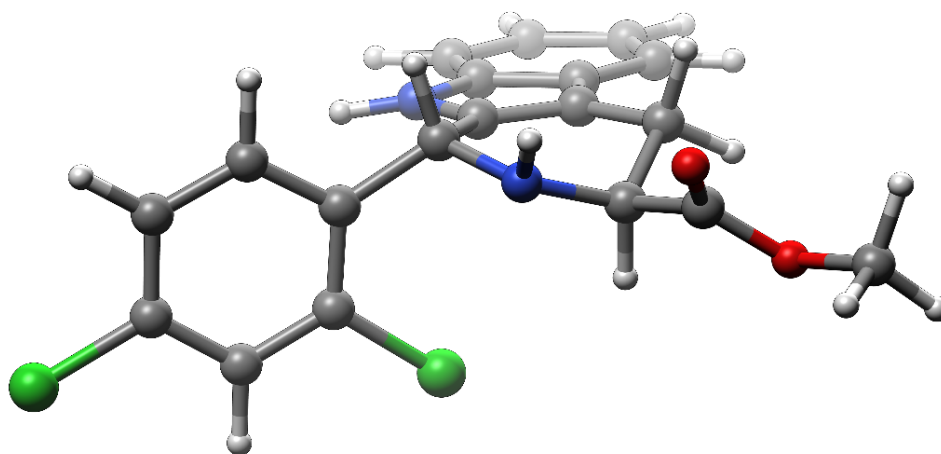
C	0.00000000	0.00000000	0.00000000	H	-1.26422100	4.21026200	-3.56061800
C	-0.34708400	-1.03665300	-1.02546200	H	0.19207400	3.17969100	-3.77024600
C	0.34079000	-2.23237400	-1.43752100	H	-2.75442900	1.83194200	-0.59577500
C	1.54588000	-2.85061000	-1.06416500	H	-2.37582800	0.74439200	-2.64028500
H	2.18000500	-2.40538300	-0.30180400	C	-3.95900400	-0.29974300	-1.71395600
C	1.91505900	-4.03954000	-1.68199300	C	-4.54460900	-1.13592100	-0.74579100
C	1.10238200	-4.62832100	-2.67140800	C	-5.89290000	-1.49180000	-0.80619600
C	-0.09367600	-4.03797500	-3.06693300	C	-6.68082700	-1.00866800	-1.84850000
C	-0.46046500	-2.84156400	-2.44517000	C	-6.14321100	-0.17968500	-2.82819500
N	-1.56719500	-2.03411000	-2.63932800	C	-4.79414500	0.15924600	-2.74201200
H	-2.36739700	-2.26539100	-3.20796000	H	-4.36841300	0.81210600	-3.50029700
C	-1.49883900	-0.96644800	-1.76159200	H	-6.76297100	0.19423600	-3.63555800
C	-2.49927000	0.15185200	-1.71495300	Cl	-8.37600800	-1.45917400	-1.91922700
N	-2.22158400	0.96948400	-0.52206400	H	-6.31706100	-2.13839200	-0.04744600
C	-0.81221500	1.28170700	-0.27146200	Cl	-3.62181900	-1.79711400	0.58868200
H	-0.79281200	1.90008400	0.63700300	H	-0.71804700	-4.49178100	-3.83248500
C	-0.11133900	2.14743500	-1.33999200	H	1.41567100	-5.55924600	-3.13610900
O	1.08740900	2.26185500	-1.46410600	H	2.84465100	-4.52604000	-1.39930300
O	-1.00283300	2.84035900	-2.09076000	H	1.06518600	0.25023200	-0.02153900
C	-0.42206400	3.73488100	-3.05679900	H	-0.23457500	-0.35564600	1.01192400
H	0.20135000	4.48211400	-2.55912100				

4a-12



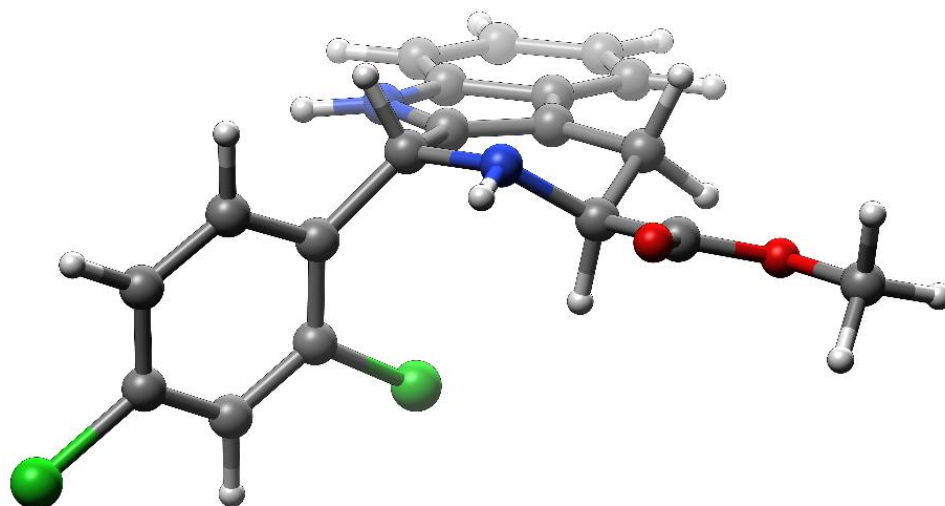
C	0.00000000	0.00000000	0.00000000	H	1.36868200	3.95748500	3.70225200
C	0.25034900	-1.01412700	1.07773200	H	-0.24190400	3.16176700	3.64823100
C	-0.56840400	-2.10015900	1.55289500	H	2.71190100	0.41905400	-0.24019200
C	-1.81929600	-2.62064300	1.18132500	H	2.44018300	0.67662200	2.63151000
H	-2.38044300	-2.17474400	0.36416300	C	3.88245800	-0.59015900	1.69867300
C	-2.32884000	-3.71245500	1.87385400	C	5.00450100	0.01109800	2.28941200
C	-1.61198700	-4.29928100	2.93603000	C	6.28002900	-0.54722000	2.19151700
C	-0.37319700	-3.80435100	3.33057700	C	6.44366500	-1.73138100	1.47766500
C	0.13421700	-2.70379400	2.63410500	C	5.35943200	-2.35939900	0.86826000
N	1.31422700	-2.00223800	2.80269600	C	4.09852800	-1.78079300	0.98912000
H	2.04784800	-2.23741300	3.45348500	H	3.24476600	-2.26800500	0.52574300
C	1.38462800	-0.99800100	1.85016000	H	5.49872400	-3.28175300	0.31534700
C	2.48807800	0.02287800	1.75367000	Cl	8.04445100	-2.44002100	1.35277300
N	2.30772400	0.89173500	0.56648800	H	7.12678500	-0.06263400	2.66238900
C	0.91730200	1.22904000	0.23535100	Cl	4.86110200	1.51026800	3.19720100
H	0.96223400	1.81174200	-0.69463400	H	0.17646000	-4.25557600	4.15276300
C	0.25950500	2.18159200	1.24292100	H	-2.03513100	-5.15252200	3.45909300
O	-0.92055300	2.45999200	1.20966500	H	-3.29549500	-4.12274400	1.59484200
O	1.12180100	2.70796200	2.13110600	H	-1.04431400	0.32901400	-0.00874400
C	0.54543600	3.64177200	3.06129300	H	0.20927200	-0.41422000	-0.99755800
H	0.12037500	4.49673600	2.52926700				

4a-13



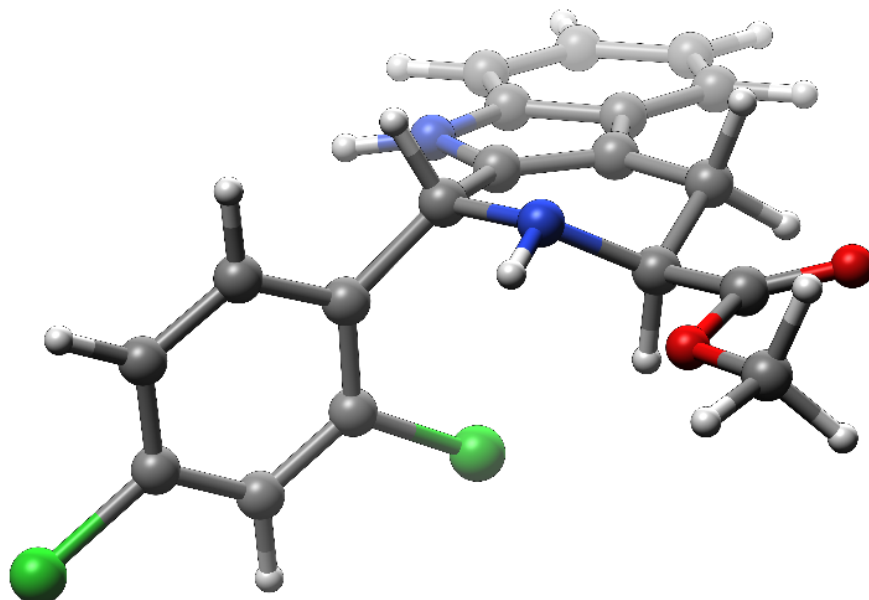
C	0.00000000	0.00000000	0.00000000	H	-1.80034900	4.10388200	-1.84726700
C	0.72080900	-1.31143400	0.02461100	H	-0.43403400	4.85511700	-0.95707400
C	0.28433900	-2.65394000	-0.25552700	H	2.20340600	1.68159500	1.19502200
C	-0.94191300	-3.23376300	-0.62233700	H	2.95046200	-0.25955500	1.86030400
H	-1.82962900	-2.61728800	-0.73978100	C	4.37005400	-0.31679200	0.31456900
C	-1.00439200	-4.60597100	-0.83242700	C	4.81411600	-0.26779700	-1.01649100
C	0.13797400	-5.41795100	-0.68281100	C	6.16598200	-0.35340600	-1.34897600
C	1.36555500	-4.87488400	-0.31800600	C	7.10685400	-0.49597600	-0.33122100
C	1.42477000	-3.49480200	-0.10537400	C	6.71475600	-0.55512000	1.00236600
N	2.48729100	-2.69075100	0.26568500	C	5.35577000	-0.46428700	1.29966300
H	3.44808300	-2.98699900	0.34625600	H	5.04519100	-0.50050300	2.34149100
C	2.05604100	-1.37740100	0.32150100	H	7.45262600	-0.66363100	1.78951100
C	2.90258000	-0.21747800	0.76024800	Cl	8.80874800	-0.60337000	-0.74851800
N	2.28469600	1.06480800	0.39324700	H	6.47580300	-0.31042500	-2.38629000
C	1.03923300	1.10111700	-0.36807600	Cl	3.68672300	-0.10580100	-2.35302100
H	1.25658800	0.99233500	-1.43555700	H	2.24557700	-5.50247000	-0.20242900
C	0.41920200	2.47363900	-0.15082900	H	0.05918500	-6.48795400	-0.85455300
O	0.64205100	3.19250900	0.80211500	H	-1.94801200	-5.06381400	-1.11651000
O	-0.45500900	2.77386600	-1.12851600	H	-0.45746800	0.23254200	0.97371600
C	-1.14652700	4.02666500	-0.97844800	H	-0.80718500	0.00514000	-0.74183000
H	-1.73048000	4.03440800	-0.05433000				

4a-14



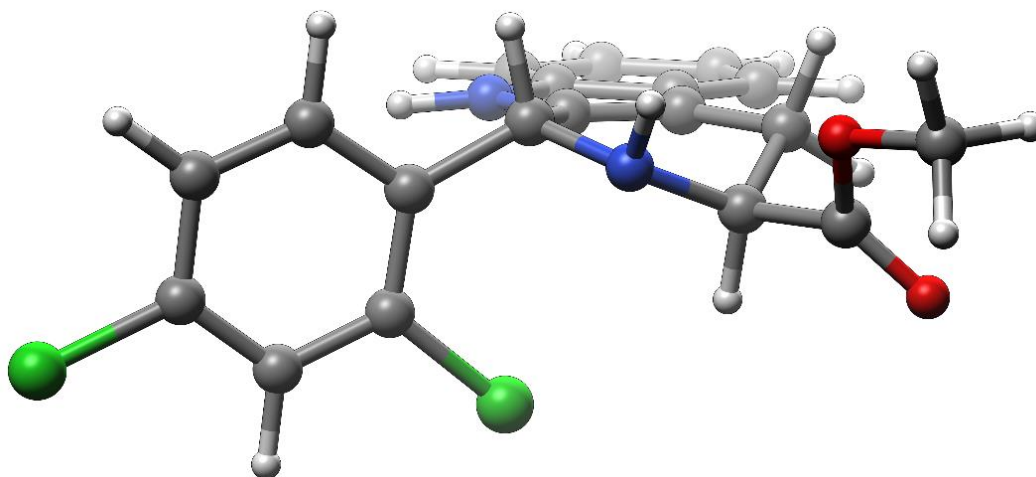
C	0.00000000	0.00000000	0.00000000	H	0.85286300	4.28981400	1.49027700
C	-0.29369800	-1.46005500	-0.18651500	H	-0.91494500	4.56889200	1.34214600
C	0.50835500	-2.62571800	0.07754800	H	-2.96216600	1.01441100	-1.14865500
C	1.81083600	-2.83186200	0.56274000	H	-2.74216200	-1.23781600	-2.21152500
H	2.44334500	-1.98559200	0.81876000	C	-4.02888200	-1.34477800	-0.55947300
C	2.27897800	-4.13194400	0.71100300	C	-4.37909600	-1.58328500	0.78155400
C	1.46981800	-5.23826600	0.38287100	C	-5.69990500	-1.80989100	1.17444800
C	0.17725200	-5.06745800	-0.10241800	C	-6.71016300	-1.79287100	0.21705800
C	-0.28914100	-3.75874100	-0.25262700	C	-6.41638300	-1.56018000	-1.12322200
N	-1.50490700	-3.28844300	-0.71466700	C	-5.08861900	-1.34650300	-1.48257900
H	-2.30877900	-3.85928800	-0.92676500	H	-4.85640900	-1.16985100	-2.53029200
C	-1.50312300	-1.90563300	-0.65052300	H	-7.20493000	-1.55065600	-1.86757000
C	-2.62721100	-1.03888900	-1.13409800	Cl	-8.36857700	-2.07507800	0.71513100
N	-2.19535800	0.35896100	-1.03557100	H	-5.93065600	-1.99685700	2.21635400
C	-1.34629100	0.74578900	0.08781300	Cl	-3.18561000	-1.63525700	2.07511800
H	-1.78849600	0.50814700	1.07231300	H	-0.44503200	-5.92195600	-0.35612700
C	-1.22674300	2.26414900	0.06358600	H	1.86199900	-6.24359200	0.51018700
O	-2.01192600	3.00496700	-0.49067200	H	3.28460100	-4.30194500	1.08598500
O	-0.17566900	2.69541100	0.78667500	H	0.58815700	0.40261900	-0.83632800
C	-0.03213200	4.12394100	0.87567700	H	0.57703400	0.17762100	0.91380100
H	0.10186600	4.55737100	-0.11866500				

4a-15



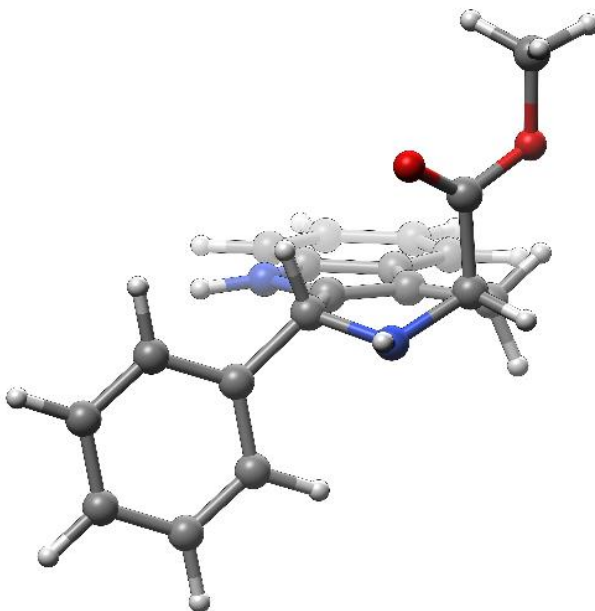
C	0.00000000	0.00000000	0.00000000	H	-3.80423600	4.25675600	-0.05486100
C	-0.10050500	-1.47569200	-0.24341300	H	-2.13614100	4.48992300	-0.67724300
C	0.84599600	-2.53886500	-0.02955800	H	-3.15191500	0.61583100	-0.95658900
C	2.16412600	-2.59649400	0.45350200	H	-2.53575100	-1.45099600	-2.27431700
H	2.68157900	-1.68806800	0.75123300	C	-3.81414500	-1.87035800	-0.66828000
C	2.79627100	-3.83064500	0.54614600	C	-4.15431400	-2.20106500	0.65604000
C	2.13709600	-5.01619600	0.16363200	C	-5.42572200	-2.66291100	1.00152600
C	0.83348800	-4.99207200	-0.32157600	C	-6.39629300	-2.79636700	0.01220300
C	0.20179500	-3.74901500	-0.41572900	C	-6.11034700	-2.48171000	-1.31281100
N	-1.06536500	-3.41940200	-0.86153600	C	-4.83053300	-2.03087700	-1.62521000
H	-1.78869100	-4.07899700	-1.10393300	H	-4.60299300	-1.78871700	-2.66071000
C	-1.24211500	-2.05185000	-0.73204700	H	-6.86757900	-2.58979300	-2.08149100
C	-2.46847200	-1.31853200	-1.18254300	Cl	-7.99380100	-3.37340300	0.45112900
N	-2.26286600	0.12723500	-0.97488300	H	-5.64980100	-2.91396100	2.03135900
C	-1.42110300	0.56279000	0.14917300	Cl	-3.00451200	-2.07445600	1.98147200
H	-1.81584000	0.23728300	1.12755400	H	0.32711200	-5.90739800	-0.61750400
C	-1.40739300	2.08730400	0.20177100	H	2.65603800	-5.96716500	0.24772900
O	-0.43361000	2.77225200	0.41859600	H	3.81532400	-3.88597700	0.91924000
O	-2.65152700	2.59435200	0.03153100	H	0.51043100	0.51637000	-0.82341500
C	-2.74963300	4.02736800	0.10010700	H	0.57037300	0.22049200	0.90897700
H	-2.41655500	4.38622500	1.07730400				

4a-16



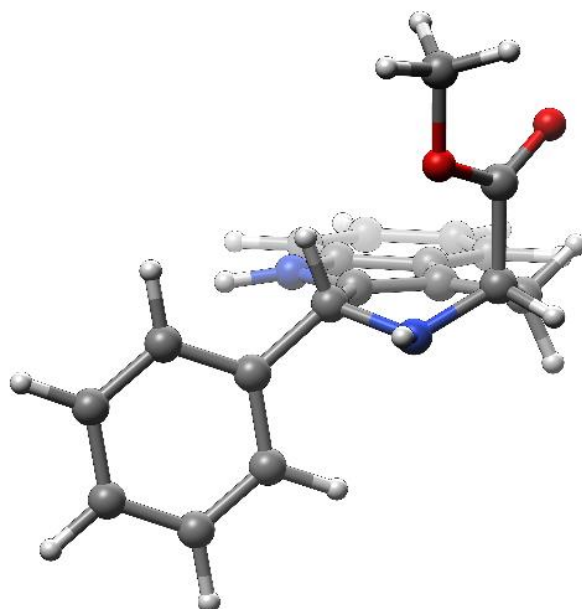
C	0.00000000	0.00000000	0.00000000	H	-0.41805000	4.82470800	-1.60405100
C	-0.62033000	-1.35118400	-0.17522000	H	0.89239100	4.37768800	-0.45997700
C	-0.09773700	-2.68039700	0.00218900	H	-2.20623700	1.57851500	-1.18967600
C	1.15654000	-3.20493900	0.35749100	H	-2.86679900	-0.30102300	-1.98655900
H	1.99457300	-2.54190500	0.55699300	C	-4.32533400	-0.57794800	-0.50719000
C	1.31032500	-4.58274500	0.45095900	C	-4.82038800	-0.68104300	0.80282600
C	0.23252900	-5.45449600	0.19557300	C	-6.17542000	-0.88045300	1.06843600
C	-1.02051600	-4.96669700	-0.16034300	C	-7.06753200	-0.98563200	0.00367700
C	-1.17155700	-3.58049500	-0.25567600	C	-6.62368000	-0.89632800	-1.31201100
N	-2.27877100	-2.82149200	-0.58931700	C	-5.26391100	-0.69438900	-1.54190200
H	-3.21353900	-3.17485300	-0.72603400	H	-4.91493600	-0.61636700	-2.56910300
C	-1.94035700	-1.48172200	-0.51792200	H	-7.32334100	-0.97756300	-2.13640100
C	-2.85431300	-0.34891300	-0.88641600	Cl	-8.77270500	-1.23575400	0.33679500
N	-2.33202300	0.94725600	-0.40719000	H	-6.52445500	-0.95279700	2.09153100
C	-1.13278600	0.97397900	0.43775700	Cl	-3.75788000	-0.57404300	2.19572700
H	-1.41128900	0.70227000	1.45861800	H	-1.85066000	-5.64034700	-0.35712400
C	-0.57092300	2.38552200	0.52846800	H	0.38241100	-6.52755300	0.27742800
O	0.02034100	2.82015600	1.49076100	H	2.27599400	-4.99834100	0.72562400
O	-0.73791500	3.08325800	-0.62094800	H	0.46569000	0.36480000	-0.92796100
C	-0.18801700	4.41234700	-0.62130500	H	0.78180500	-0.00931500	0.76897700
H	-0.64688700	5.01433500	0.16691400				

4b-01



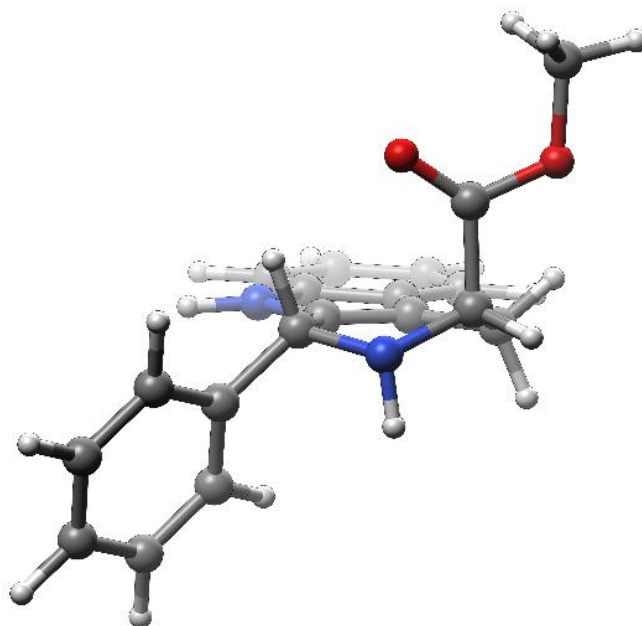
C	0.00000000	0.00000000	0.00000000	H	2.73647700	2.91870800	-2.40701100
C	-0.35177300	-1.15697200	-0.88553800	H	1.25330100	3.89357400	-2.68224500
C	0.33330000	-2.39644100	-1.14633500	H	-2.78659200	1.70844600	-0.74917300
C	1.53770500	-2.96670900	-0.70219900	H	-2.42955400	0.42595500	-2.67088500
H	2.17396600	-2.43285000	-0.00061600	C	-3.95334000	-0.59902800	-1.58490200
C	1.90365400	-4.22399600	-1.16923900	C	-4.76717100	-0.65732900	-2.72136400
C	1.08749500	-4.92837800	-2.07649100	C	-6.06206400	-1.17902400	-2.64560300
C	-0.10861500	-4.38830700	-2.53927100	C	-6.55574700	-1.64168000	-1.42644700
C	-0.47263800	-3.12363400	-2.06956800	C	-5.75049100	-1.57987600	-0.28461400
N	-1.57793100	-2.34368300	-2.35797900	C	-4.45831600	-1.06457100	-0.36306200
H	-2.39035000	-2.64124500	-2.87718700	H	-3.82969400	-1.00359700	0.51981500
C	-1.50549300	-1.17418600	-1.62408500	H	-6.13270900	-1.93521700	0.66896900
C	-2.52566100	-0.07226500	-1.69143100	H	-7.56363300	-2.04332700	-1.36243800
N	-2.24086600	0.86548700	-0.58457200	H	-6.68416600	-1.21333200	-3.53626400
C	-0.83456800	1.23235500	-0.41124600	H	-4.38988100	-0.27963700	-3.66984700
H	-0.79518200	1.95836100	0.41299000	H	-0.73565500	-4.93152700	-3.24178000
C	-0.26461200	1.98060300	-1.63154500	H	1.39752600	-5.91046000	-2.42322200
O	-0.94041300	2.43156300	-2.53376000	H	2.83285000	-4.67418400	-0.83027400
O	1.07169000	2.14416100	-1.55395600	H	1.06494400	0.24611900	-0.05406100
C	1.67041100	2.88431800	-2.63265500	H	-0.22302000	-0.22871600	1.05107500
H	1.49475400	2.37883100	-3.58559000				

4b-02



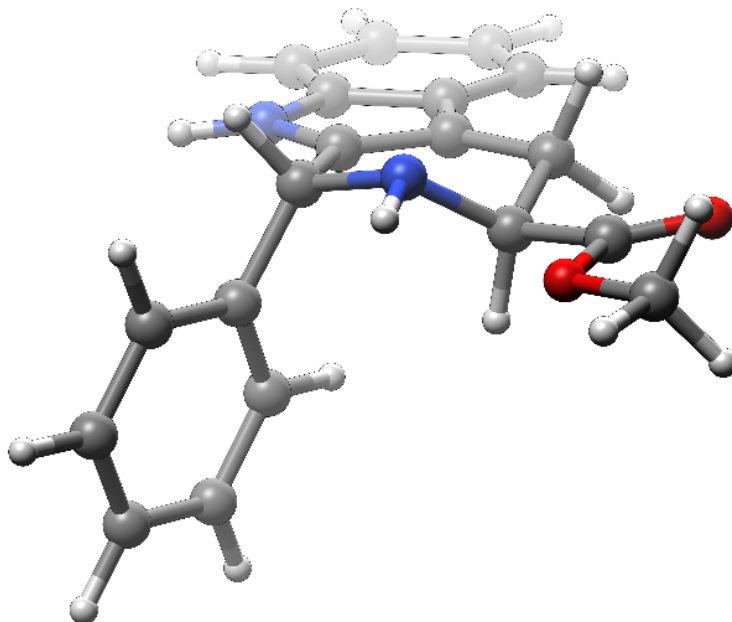
C	0.00000000	0.00000000	0.00000000	H	-3.12795700	3.01318500	-3.64956700
C	0.13120700	-1.17181800	-0.92644500	H	-1.38789900	2.67395600	-3.93765700
C	1.26635400	-1.99371600	-1.25868600	H	-3.29428900	0.34121100	-0.55646200
C	2.61471700	-2.01227700	-0.86522700	H	-2.48940800	-0.55724500	-2.58964700
H	2.99164100	-1.27878700	-0.15694100	C	-3.39322200	-2.17661800	-1.54054600
C	3.45974000	-2.98175700	-1.39290100	C	-4.14880400	-2.52136400	-2.66621300
C	2.98449100	-3.93848600	-2.31179300	C	-5.10167500	-3.54236800	-2.60084600
C	1.65633700	-3.94185300	-2.72674500	C	-5.30993700	-4.22392000	-1.40238900
C	0.81024000	-2.96452600	-2.19622000	C	-4.56204900	-3.88104600	-0.27142900
N	-0.53078400	-2.71775000	-2.42976700	C	-3.60876300	-2.86700200	-0.33992700
H	-1.16104100	-3.32514900	-2.93175400	H	-3.02964900	-2.58774200	0.53467900
C	-0.93271900	-1.65410400	-1.64161500	H	-4.72327000	-4.40729800	0.66591600
C	-2.32643000	-1.08996300	-1.63437700	H	-6.05314400	-5.01488900	-1.34610200
N	-2.42271100	-0.17673800	-0.48142800	H	-5.68407400	-3.79595500	-3.48285100
C	-1.30631400	0.75693200	-0.31034700	H	-3.99940400	-1.97927200	-3.59826000
H	-1.55765800	1.38082400	0.55906800	H	1.29207400	-4.67829100	-3.43868400
C	-1.09031600	1.76806200	-1.45638200	H	3.66732800	-4.68611900	-2.70631300
O	-0.05985200	2.36505100	-1.67523700	H	4.50419400	-3.00511500	-1.09379300
O	-2.23059500	1.97734300	-2.15815100	H	0.84050500	0.69361000	-0.10326500
C	-2.13672200	2.96728900	-3.19753800	H	-0.02560800	-0.32895500	1.04754000
H	-1.85852500	3.93744800	-2.77764400				

4b-03



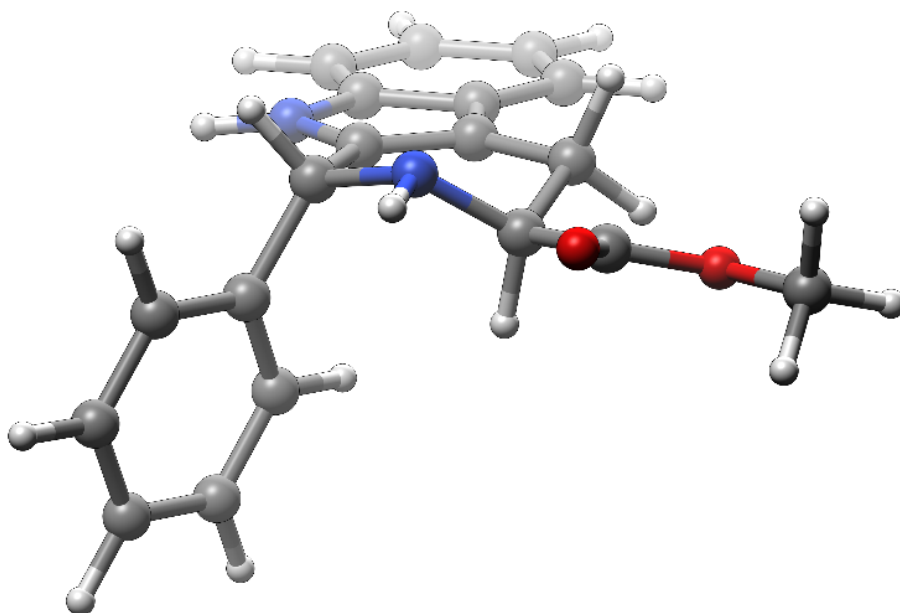
C	0.00000000	0.00000000	0.00000000	H	2.35120900	3.60810100	-1.93559000
C	-0.22307800	-1.18748800	-0.88906400	H	0.78189300	4.05713400	-2.68356400
C	0.61418000	-2.32744000	-1.16093100	H	-2.72915700	0.37617100	0.17469200
C	1.87246200	-2.75488500	-0.70495100	H	-2.42716900	0.17320400	-2.69861400
H	2.42702800	-2.16199200	0.01829900	C	-3.87380600	-0.94957000	-1.60437200
C	2.39772500	-3.94783100	-1.18819400	C	-4.94103700	-0.40570000	-2.33008900
C	1.68913800	-4.72855900	-2.12308100	C	-6.22892700	-0.92562700	-2.20046400
C	0.44290900	-4.33039200	-2.59707900	C	-6.46734500	-1.99833500	-1.33843500
C	-0.08062000	-3.12894400	-2.11192900	C	-5.41187200	-2.54533900	-0.60694400
N	-1.27097700	-2.48775700	-2.40036800	C	-4.12354200	-2.02360300	-0.73931500
H	-2.01374700	-2.85739500	-2.97396400	H	-3.30245200	-2.45760700	-0.17381200
C	-1.36008000	-1.33109100	-1.64445100	H	-5.58926800	-3.38089100	0.06524900
C	-2.48581200	-0.33422000	-1.72829000	H	-7.46965100	-2.40659800	-1.23909800
N	-2.33269600	0.72333500	-0.69713100	H	-7.04603600	-0.49416200	-2.77269400
C	-0.95652600	1.15213400	-0.42856200	H	-4.75604500	0.43415700	-2.99522300
H	-1.00629500	1.87853400	0.39198100	H	-0.10123200	-4.93218400	-3.32067100
C	-0.39897100	1.92264100	-1.62768800	H	2.12371700	-5.65747800	-2.48231000
O	-0.91740100	2.04243100	-2.71528600	H	3.36980300	-4.28723500	-0.84056000
O	0.78911300	2.48573800	-1.30756800	H	1.03958200	0.34469100	-0.03551300
C	1.42105100	3.23077400	-2.36146300	H	-0.20536800	-0.24503100	1.05312300
H	1.62489900	2.58430600	-3.21909800				

4b-04



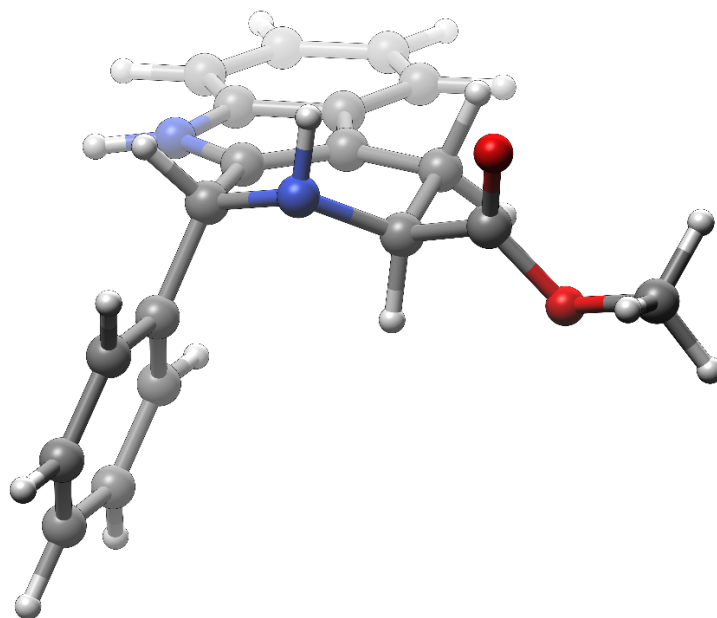
C	0.0000000	0.0000000	0.0000000	H	5.66775200	-0.47233400	-0.45678900
C	-0.97204100	1.10240200	-0.29897100	H	4.57806900	-1.84783000	-0.83777800
C	-2.39391400	1.19386100	-0.08783900	H	2.61454400	1.63512300	-1.28132600
C	-3.36389500	0.33268200	0.45181700	H	0.82530100	2.93136900	-2.33941000
H	-3.08413700	-0.65316900	0.81448400	C	1.42134800	3.80090500	-0.48599400
C	-4.68560200	0.75827600	0.51511600	C	2.36662800	4.63044000	-1.10645000
C	-5.06263800	2.03295900	0.04704500	C	2.99166300	5.65965600	-0.40240700
C	-4.12657000	2.90763100	-0.49548600	C	2.67613300	5.87809600	0.94025900
C	-2.79876500	2.47599600	-0.55859200	C	1.73006600	5.06560600	1.56721400
N	-1.67131500	3.11324100	-1.04329200	C	1.10446000	4.03730200	0.85948300
H	-1.63263700	4.06502400	-1.37408400	H	0.35283800	3.42383200	1.34831200
C	-0.57725500	2.28053800	-0.87698200	H	1.47181700	5.23557300	2.60928600
C	0.82180800	2.63362800	-1.28005700	H	3.15827700	6.68111900	1.49128600
N	1.62953300	1.39159300	-1.21331400	H	3.71881400	6.29409000	-0.90263800
C	1.42029700	0.58765300	-0.00063900	H	2.61241900	4.46786700	-2.15465100
H	1.54922300	1.18701400	0.92331900	H	-4.41929200	3.88983400	-0.85807700
C	2.47143200	-0.51355900	0.08438200	H	-6.10343800	2.33891700	0.10958900
O	2.26451200	-1.65024300	0.44530400	H	-5.44317200	0.09945000	0.93087800
O	3.69944800	-0.04900800	-0.24466600	H	-0.05765100	-0.80195300	-0.74727000
C	4.76596700	-1.00959400	-0.16198600	H	-0.19926100	-0.46460600	0.97218800
H	4.85949700	-1.38932900	0.85870800				

4b-05



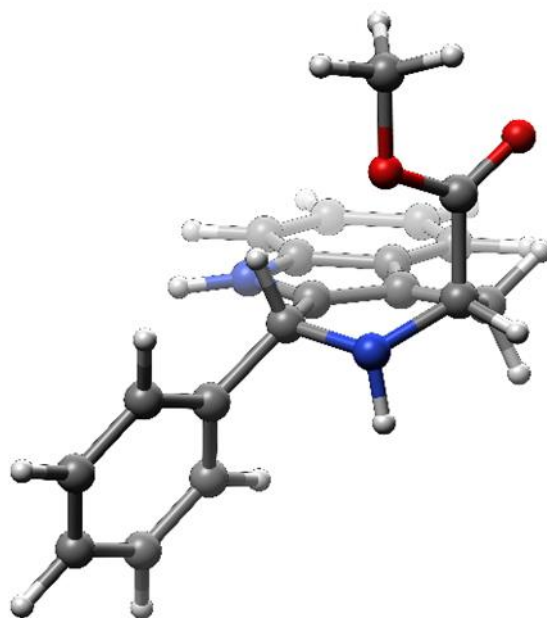
C	0.00000000	0.00000000	0.00000000	H	-2.93546500	3.25129400	1.45498300
C	0.98786000	-1.11538500	-0.18732600	H	-4.23118100	2.03343700	1.20344200
C	2.40179300	-1.17936200	0.07912500	H	-2.54720200	-1.69361000	-1.31130900
C	3.34856600	-0.27238700	0.58391900	H	-0.72913800	-3.10924300	-2.14214100
H	3.05207200	0.73659700	0.85951500	C	-1.39303800	-3.83418400	-0.24934200
C	4.66913000	-0.68211600	0.72628000	C	-2.33136000	-4.69825800	-0.83182900
C	5.06802700	-1.98656300	0.37225000	C	-2.98040800	-5.67145500	-0.07236400
C	4.15537200	-2.90723800	-0.13282200	C	-2.69650200	-5.79829800	1.28913000
C	2.82871100	-2.49150500	-0.27559000	C	-1.75820200	-4.95042500	1.87944300
N	1.72145200	-3.17283800	-0.74632200	C	-1.10853000	-3.97810900	1.11608300
H	1.70011900	-4.14589800	-1.01017500	H	-0.36333200	-3.33652000	1.57813800
C	0.61843500	-2.33867700	-0.68483000	H	-1.52495500	-5.04870800	2.93658000
C	-0.76586500	-2.72932700	-1.11009600	H	-3.19792300	-6.55737300	1.88353600
N	-1.56163500	-1.48677100	-1.16712400	H	-3.70262000	-6.33313800	-0.54353900
C	-1.41557300	-0.61123400	-0.00654400	H	-2.55442800	-4.60610400	-1.89353400
H	-1.55046800	-1.14844400	0.95464600	H	4.46496500	-3.91261400	-0.40710400
C	-2.54235500	0.41230200	-0.04604600	H	6.10724600	-2.27947900	0.49461500
O	-3.58223600	0.26499300	-0.65298800	H	5.40858700	0.01225400	1.11603300
O	-2.27299600	1.48390400	0.72537300	H	0.07993100	0.74222200	-0.80616600
C	-3.31633900	2.47120700	0.79542600	H	0.16759200	0.53192200	0.94285700
H	-3.52776500	2.87541100	-0.19781900				

4b-06



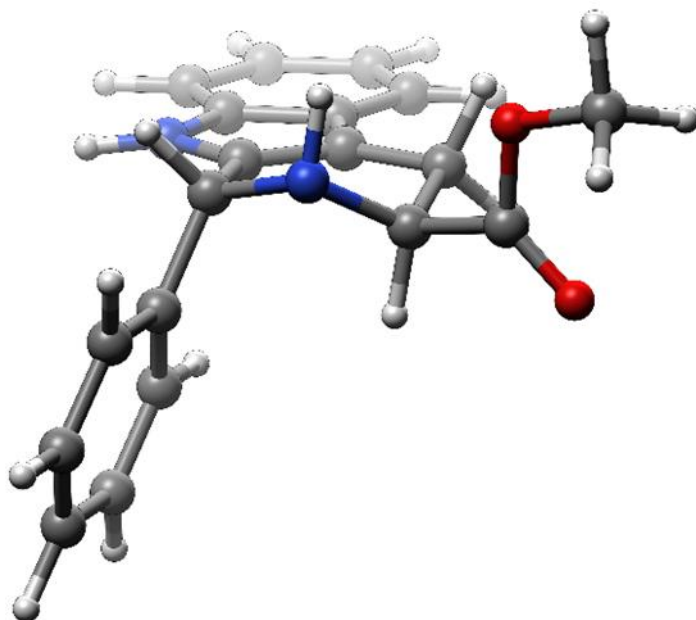
C	0.00000000	0.00000000	0.00000000	H	4.03957200	-2.24092800	1.89686300
C	-1.03706400	1.04966500	-0.27049600	H	4.69118400	-1.77657700	0.28978600
C	-2.45681700	1.04695600	-0.02761900	H	1.40355300	0.94986100	-2.17191500
C	-3.35527900	0.12586400	0.53651700	H	0.59461800	3.01647700	-2.34710800
H	-3.00236800	-0.83583800	0.90040300	C	1.26230400	3.80249500	-0.48182600
C	-4.70123400	0.46137200	0.62426700	C	2.46808900	4.36492900	-0.92559100
C	-5.17286200	1.70431900	0.15670800	C	3.07482000	5.39994500	-0.21904200
C	-4.30901900	2.63659800	-0.40927700	C	2.48609700	5.88912200	0.95140900
C	-2.95641300	2.29562700	-0.49635900	C	1.29252700	5.33156300	1.40548100
N	-1.88333600	3.00377500	-1.00644800	C	0.68359100	4.29354800	0.69228400
H	-1.91898600	3.94838000	-1.35777700	H	-0.24366600	3.86303600	1.05851700
C	-0.73065800	2.24769100	-0.86337000	H	0.83053200	5.69908000	2.31819400
C	0.64528100	2.66384000	-1.30652000	H	2.95816200	6.69709700	1.50418600
N	1.55704400	1.50266800	-1.33030600	H	4.00818200	5.82569600	-0.57847400
C	1.42024500	0.62146900	-0.16860300	H	2.93470800	3.97032000	-1.82436800
H	1.65596400	1.20487900	0.72695500	H	-4.67487700	3.59418500	-0.77120400
C	2.43422500	-0.50209600	-0.31083800	H	-6.23045600	1.93979500	0.23881500
O	2.75556000	-1.00509600	-1.36635000	H	-5.40399700	-0.24389400	1.05957500
O	2.88476600	-0.91783900	0.89012200	H	-0.11247400	-0.84704100	-0.69389900
C	3.79195000	-2.03347500	0.85556100	H	-0.09650600	-0.41250400	1.01283000
H	3.31597700	-2.90143000	0.39157700				

4b-07



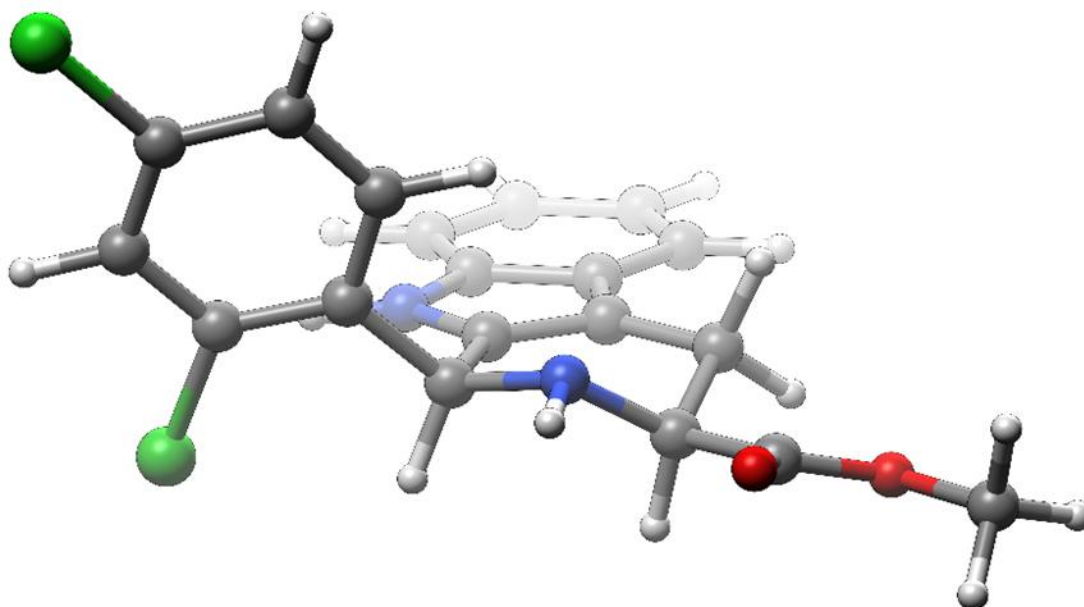
C	0.00000000	0.00000000	0.00000000	H	-2.55066100	2.99367200	-3.99485500
C	0.14282400	-1.13167400	-0.97504200	H	-0.77090400	2.76213000	-3.90892100
C	1.29021800	-1.92817200	-1.32793800	H	-2.71070200	-0.51669600	0.18950700
C	2.62689700	-1.96863200	-0.89778800	H	-2.42664400	-0.41944600	-2.69073500
H	2.97963100	-1.28224200	-0.13221200	C	-3.40887000	-2.01122600	-1.67574700
C	3.49130000	-2.89838500	-1.46389100	C	-4.61929200	-1.77360300	-2.33880400
C	3.04692900	-3.79366000	-2.45734800	C	-5.67411900	-2.68116400	-2.24389400
C	1.73102500	-3.77421100	-2.90901200	C	-5.53223900	-3.84154300	-1.47959800
C	0.86569300	-2.83569500	-2.34006600	C	-4.33201100	-4.08593200	-0.81041600
N	-0.47001600	-2.57931600	-2.59100000	C	-3.27725700	-3.17609700	-0.90796900
H	-1.07295000	-3.13558200	-3.17787200	H	-2.34185100	-3.37366500	-0.39020700
C	-0.90377000	-1.56898000	-1.74739800	H	-4.21371800	-4.98643800	-0.21341400
C	-2.28952700	-0.97967300	-1.75547200	H	-6.35207200	-4.55124400	-1.40728000
N	-2.45553900	-0.00336500	-0.65237200	H	-6.60628300	-2.48323800	-2.76654200
C	-1.27552400	0.81315700	-0.34533300	H	-4.73242200	-0.86620500	-2.92704600
H	-1.54616000	1.41965300	0.52993200	H	1.39090200	-4.46287900	-3.67839700
C	-0.95233400	1.84990900	-1.43031700	H	3.74456400	-4.51097700	-2.88117000
O	0.06922700	2.50371800	-1.43522000	H	4.52700500	-2.93821300	-1.13748500
O	-1.92997500	2.00030900	-2.34514400	H	0.86766300	0.66763300	-0.02389100
C	-1.67559100	3.00275400	-3.34439200	H	-0.08503400	-0.37128100	1.03224300
H	-1.55179600	3.98399000	-2.87895300				

4b-08



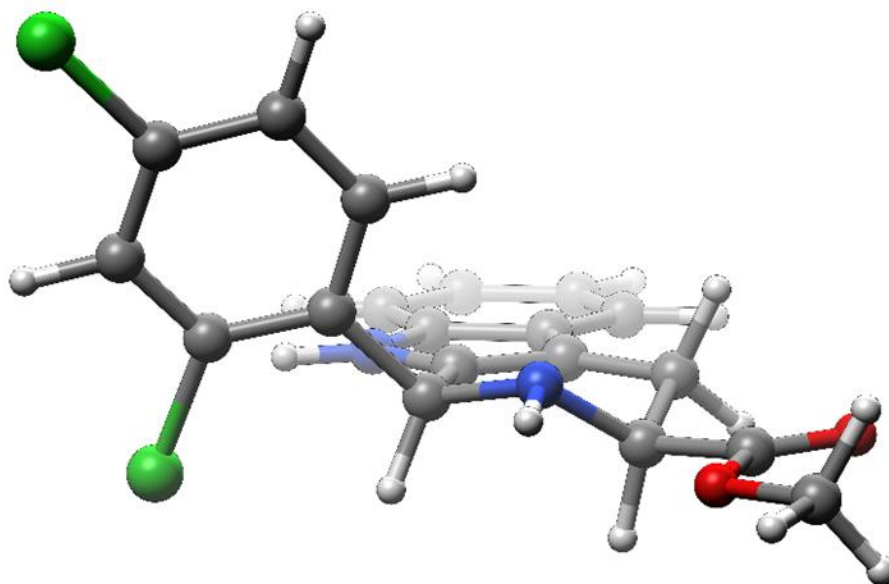
C	0.00000000	0.00000000	0.00000000	H	3.64273500	-2.70779800	-1.99060500
C	-1.00694500	1.00880100	-0.47067000	H	3.29646400	-2.99600800	-0.25233800
C	-2.43969900	1.04015900	-0.32644500	H	1.49964700	0.66498100	-2.16591400
C	-3.38429900	0.19492100	0.27958300	H	0.78174700	2.71081800	-2.64891200
H	-3.06717100	-0.71799800	0.77737600	C	1.33633600	3.70865200	-0.85017900
C	-4.72914500	0.54308000	0.23589700	C	2.55216500	4.23845800	-1.30608000
C	-5.15404800	1.72407700	-0.40500000	C	3.12496900	5.34561500	-0.68578200
C	-4.24369200	2.58054700	-1.01602400	C	2.49073400	5.94152400	0.40881700
C	-2.89218500	2.22719700	-0.97047400	C	1.28604000	5.41845900	0.87442100
N	-1.77915400	2.86702200	-1.48539200	C	0.71135100	4.30790600	0.24777400
H	-1.77940900	3.76666100	-1.94107300	H	-0.22567100	3.90589800	0.62188100
C	-0.64757000	2.12894400	-1.17635700	H	0.78891400	5.86974800	1.72918100
C	0.75928900	2.48527000	-1.57264500	H	2.93645200	6.80545300	0.89471500
N	1.65372800	1.31837500	-1.39953800	H	4.06717400	5.74430300	-1.05294100
C	1.42723900	0.60649200	-0.13308900	H	3.05389700	3.76345200	-2.14527000
H	1.58181800	1.32250200	0.67928800	H	-4.57366000	3.49061500	-1.51071200
C	2.47295800	-0.48231500	0.05625300	H	-6.21196500	1.97145800	-0.42269600
O	3.03559000	-0.73302500	1.09820500	H	-5.46745000	-0.10331600	0.70258100
O	2.65834900	-1.18911500	-1.08343600	H	-0.06283800	-0.92542300	-0.59202500
C	3.61250500	-2.26033700	-0.99668300	H	-0.17526600	-0.28676900	1.04527200
H	4.59627400	-1.87364400	-0.71855300				

5a-01



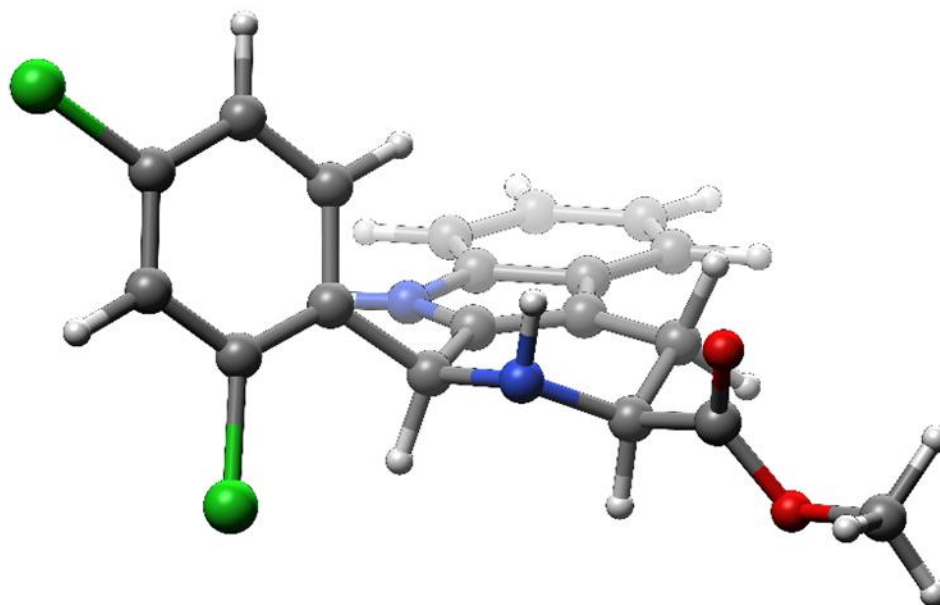
C	0.00000000	0.00000000	0.00000000	H	-1.75776200	-4.40005800	1.06024600
C	0.80104600	1.24462800	0.24993500	H	-1.51805800	-4.24305400	-0.69672200
C	0.47780800	2.63160800	0.04233700	H	-2.98212000	-3.53863800	0.06790700
C	-0.63483600	3.31409800	-0.47821400	H	2.41700900	-2.06506700	0.98355800
H	-1.49971100	2.76342200	-0.83963800	C	4.23441600	-0.06299700	0.67641200
C	-0.61362400	4.70269800	-0.52624300	C	5.32512500	0.41596800	1.41266700
C	0.50169300	5.42985400	-0.06326000	C	6.62903800	0.40233000	0.91596500
C	1.61802900	4.78384800	0.45740700	C	6.84780500	-0.10153300	-0.36267400
C	1.59326800	3.38702900	0.50451100	C	5.79158400	-0.58121800	-1.13587400
N	2.54059000	2.49026100	0.96094000	C	4.50426700	-0.55493300	-0.60858700
H	3.42847700	2.73116800	1.37455100	H	3.66674400	-0.93493700	-1.18356500
C	2.05614000	1.20517900	0.80308800	H	5.97557400	-0.96912500	-2.13173100
C	2.79624200	-0.04942900	1.19941600	Cl	8.48242600	-0.12870000	-1.00276900
H	2.83955500	-0.09752600	2.30231900	H	7.45021800	0.77559000	1.51574400
N	2.05463400	-1.18102300	0.63346300	Cl	5.10075500	1.09078200	3.03495800
C	0.61128900	-1.12470000	0.85634700	H	2.47747500	5.34579800	0.81395400
H	0.35928800	-0.90520600	1.91473100	H	0.49018500	6.51519900	-0.11376400
C	0.04069500	-2.51096800	0.58337100	H	-1.46867200	5.23996900	-0.92751100
O	0.69629500	-3.53194800	0.58700400	H	0.02371900	-0.29308000	-1.05879700
O	-1.29077000	-2.47576700	0.39349400	H	-1.05222500	0.13803400	0.27113100
C	-1.92103500	-3.75416300	0.19375000				

5a-02



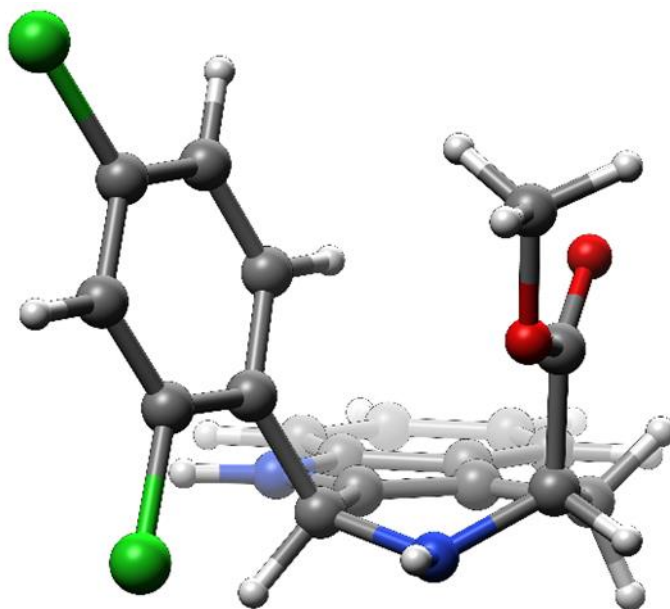
C	0.00000000	0.00000000	0.00000000	H	-0.77276600	4.92819900	-0.45647100
C	-0.61671300	-1.33675500	0.28488000	H	0.10906200	5.01609200	1.08727300
C	-0.10249300	-2.66988900	0.11262800	H	-1.65303000	5.36099200	1.04778800
C	1.09800100	-3.20188500	-0.38773400	H	-2.67955400	1.71897100	1.00821000
H	1.87945300	-2.54392500	-0.75947900	C	-4.20123200	-0.50896000	0.69892700
C	1.27130400	-4.58053300	-0.40100800	C	-5.21398900	-1.10512200	1.46046000
C	0.26547800	-5.44513000	0.07649600	C	-6.51140400	-1.27938900	0.97664000
C	-0.93369000	-4.94954900	0.57750800	C	-6.80311900	-0.85021200	-0.31454800
C	-1.10441900	-3.56219100	0.59036700	C	-5.82398100	-0.26126700	-1.11357600
N	-2.17038000	-2.79568600	1.02224600	C	-4.54158000	-0.10007700	-0.59854700
H	-3.01804900	-3.14836200	1.43991100	H	-3.76549300	0.36816200	-1.19425700
C	-1.86751700	-1.45946500	0.83344600	H	-6.06320500	0.06507100	-2.11975800
C	-2.77140600	-0.31284200	1.20806900	Cl	-8.43114500	-1.05851500	-0.93728100
H	-2.81363400	-0.24587400	2.30964600	H	-7.27204300	-1.73911000	1.59595800
N	-2.20390300	0.90983800	0.61675900	Cl	-4.89236500	-1.69358400	3.09936100
C	-0.75510900	1.05738900	0.81819900	H	-1.70843600	-5.61752900	0.94518100
H	-0.47745300	0.92917200	1.88454600	H	0.42910100	-6.51907900	0.05310400
C	-0.31434200	2.46956400	0.44527100	H	2.19564000	-5.00256400	-0.78603200
O	0.70910500	2.74872300	-0.13632600	H	-0.05541900	0.26004300	-1.06511200
O	-1.19286700	3.39452300	0.89707600	H	1.06117100	0.02256400	0.27178600
C	-0.84682500	4.76377600	0.62141300				

5a-03



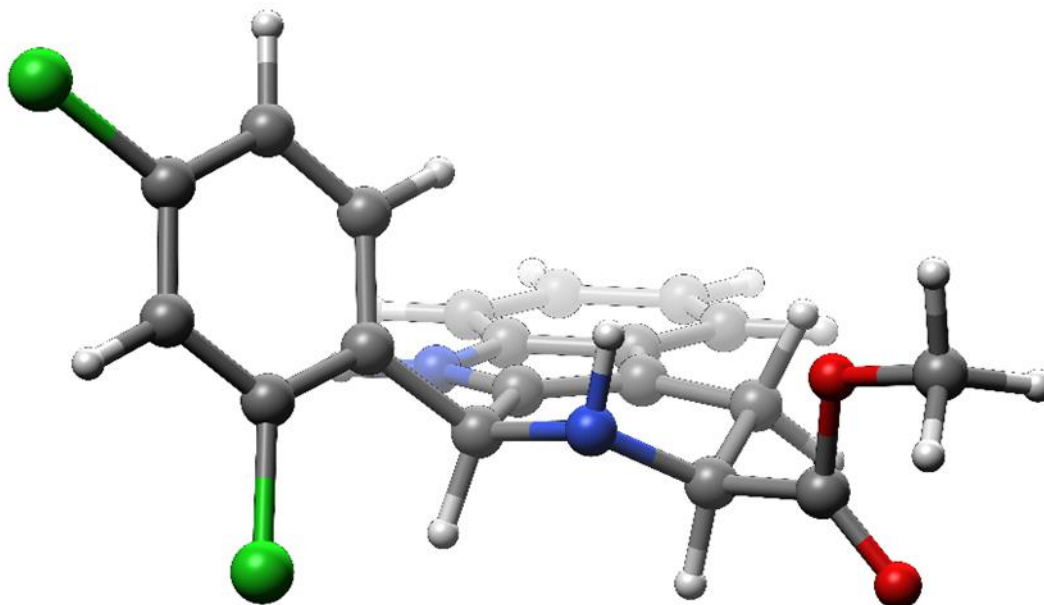
C	0.00000000	0.00000000	0.00000000	H	0.18882300	-5.04209600	-0.02966600
C	0.49984200	1.35792900	0.39659400	H	-1.04357600	-4.21032700	-1.00813300
C	-0.15820600	2.63923500	0.38662200	H	-1.45935400	-4.79500200	0.63840400
C	-1.42783600	3.08817100	-0.01423800	H	2.61182500	-0.84559800	-0.41305100
H	-2.15459000	2.39148700	-0.42443200	C	4.17062700	0.78891200	0.71587300
C	-1.74073900	4.43566500	0.11866300	C	5.31763400	0.38011800	1.41303400
C	-0.80701800	5.35069200	0.64523400	C	6.60359600	0.65942500	0.94845100
C	0.45689500	4.93697600	1.05335200	C	6.74963400	1.35515600	-0.24882000
C	0.76644300	3.58020500	0.92280100	C	5.63867200	1.77170300	-0.97929800
N	1.91934200	2.88824800	1.24654700	C	4.36861500	1.48355400	-0.48620000
H	2.77540700	3.30090900	1.58417500	H	3.49560900	1.80990800	-1.04482200
C	1.75699100	1.55428400	0.90908300	H	5.76526600	2.31088300	-1.91150500
C	2.75765800	0.46001200	1.18177500	Cl	8.36356100	1.71215600	-0.83842000
H	2.79483500	0.29406300	2.26713400	H	7.47106400	0.33593100	1.51086300
N	2.33818200	-0.81325100	0.56792800	Cl	5.19381700	-0.50987000	2.92525800
C	0.90191400	-1.08410300	0.66277100	H	1.17460100	5.64373100	1.46209300
H	0.63712800	-1.15895400	1.72277800	H	-1.07899200	6.39872000	0.73606400
C	0.64343100	-2.42348100	-0.01071100	H	-2.71964400	4.79322500	-0.18880900
O	1.19467800	-2.79055100	-1.02652100	H	0.02155700	-0.13218200	-1.09199400
O	-0.31678300	-3.12367600	0.62316400	H	-1.04162400	-0.14940300	0.31322200
C	-0.67562800	-4.37445200	0.00809100				

5a-04



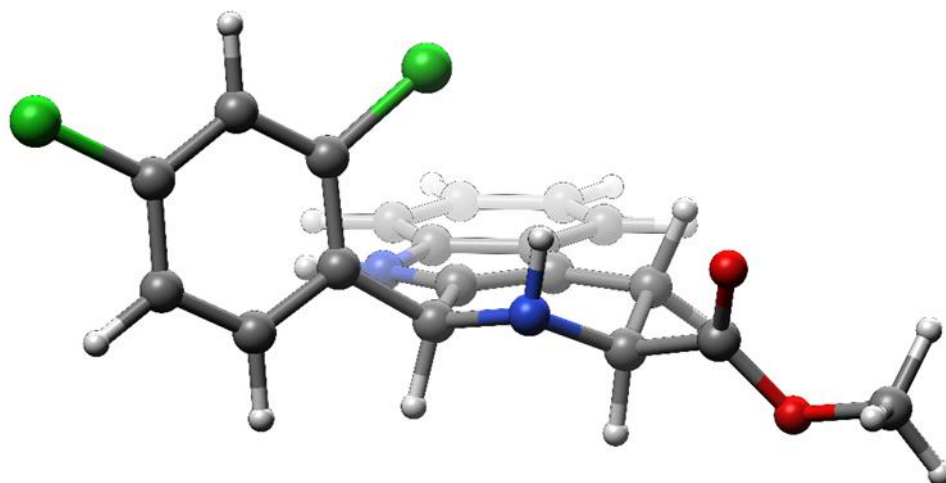
C	0.00000000	0.00000000	0.00000000	H	-4.52999100	-0.58219500	-2.34400700
C	0.25022300	-1.46920500	0.15752800	H	-4.14662600	1.11046800	-2.74594800
C	1.39231300	-2.27059100	-0.20008200	H	-5.46575500	0.74585600	-1.58278500
C	2.62185000	-2.00257600	-0.82439500	H	-2.95994600	-0.11566000	1.59289300
H	2.86706000	-0.99408200	-1.14732700	C	-3.16256900	-2.54931900	0.52740500
C	3.51837700	-3.04504600	-1.02623600	C	-4.42935400	-2.70107800	1.11220800
C	3.21185500	-4.35770000	-0.61468500	C	-5.50508900	-3.27865100	0.44001700
C	2.00351600	-4.65533100	0.00689700	C	-5.31352400	-3.71836100	-0.86781400
C	1.10478600	-3.60400500	0.20877200	C	-4.07731000	-3.58358700	-1.49576000
N	-0.14998200	-3.59654100	0.78982500	C	-3.02185200	-3.00601500	-0.79141300
H	-0.63080200	-4.40269700	1.15794100	H	-2.05917400	-2.89817300	-1.28075100
C	-0.65315800	-2.30555900	0.75480800	H	-3.93911800	-3.92804900	-2.51482900
C	-1.99091400	-1.90614800	1.29467000	Cl	-6.65699800	-4.45141500	-1.72842000
H	-2.07062300	-2.25239300	2.33354200	H	-6.46731900	-3.38280400	0.92685800
N	-2.01967100	-0.43031500	1.37163300	Cl	-4.72597600	-2.14483200	2.76307900
C	-1.48719600	0.32482900	0.22872500	H	1.76922100	-5.66839600	0.32397700
H	-1.57577300	1.38091000	0.51500700	H	3.93199700	-5.15312500	-0.78604300
C	-2.31031700	0.19965000	-1.06909700	H	4.47158500	-2.84870500	-1.50940800
O	-1.89045500	-0.09139100	-2.16777200	H	0.29109400	0.34479200	-0.99756600
O	-3.60516800	0.50520300	-0.82199000	H	0.59437200	0.56823200	0.72797400
C	-4.48816700	0.43806300	-1.95469400				

5a-05



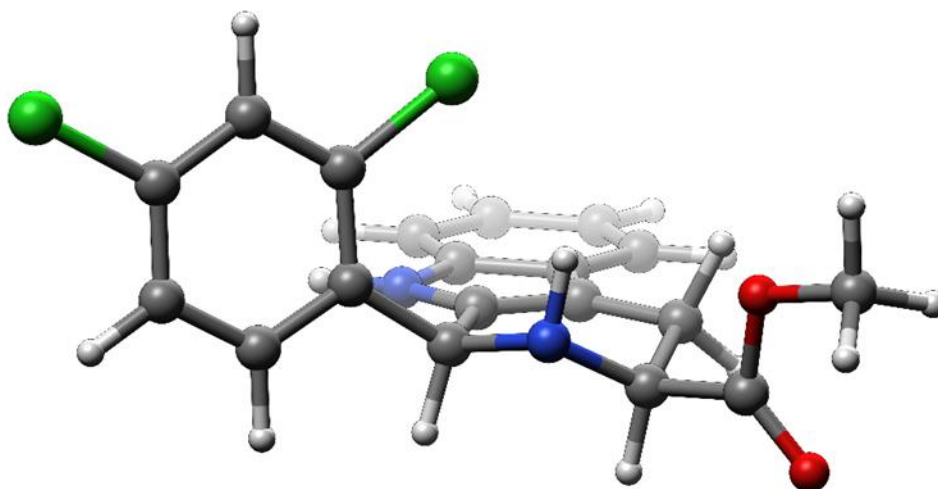
C	0.00000000	0.00000000	0.00000000	H	-0.39284800	4.16328500	-1.57863200
C	-0.31339200	-1.44290800	0.27126900	H	-1.89982600	4.58178700	-0.72877600
C	0.51594700	-2.61633700	0.17264200	H	-1.97567100	3.86227100	-2.37184200
C	1.83817800	-2.85194700	-0.24010100	H	-2.66301800	0.44750300	-0.44926100
H	2.46436900	-2.03051600	-0.57896900	C	-4.03372000	-1.41751100	0.56809800
C	2.33337400	-4.15002800	-0.21050200	C	-5.23164000	-1.20001800	1.26603900
C	1.53197100	-5.22467500	0.22486700	C	-6.46540900	-1.61571000	0.76375500
C	0.22073900	-5.02346500	0.64319500	C	-6.50777800	-2.25534800	-0.47250000
C	-0.27271800	-3.71588700	0.61599300	C	-5.34446600	-2.48405400	-1.20418500
N	-1.51316700	-3.21811100	0.97151100	C	-4.12750800	-2.06349500	-0.67322900
H	-2.30421100	-3.77072600	1.26467400	H	-3.21410800	-2.24397100	-1.23349700
C	-1.53541900	-1.85153500	0.74367100	H	-5.39012900	-2.98217500	-2.16625300
C	-2.68234600	-0.92988600	1.07462400	Cl	-8.05583300	-2.78098500	-1.11022100
H	-2.74755500	-0.83579800	2.16678800	H	-7.37330900	-1.43886500	1.32759000
N	-2.43952400	0.42756200	0.54479600	Cl	-5.23979400	-0.38794900	2.82577700
C	-1.05383600	0.88326400	0.72710700	H	-0.39472200	-5.85306200	0.98173900
H	-0.83863700	0.87111700	1.80025200	H	1.94600300	-6.22917200	0.23642900
C	-0.92071900	2.33410900	0.28529000	H	3.35439800	-4.34340900	-0.52782800
O	-0.31691300	3.19199200	0.88845600	H	-0.01772500	0.22178300	-1.07721200
O	-1.52068700	2.53723300	-0.91011500	H	1.00466600	0.26268900	0.35646900
C	-1.43660500	3.87740400	-1.42425200				

5a-06



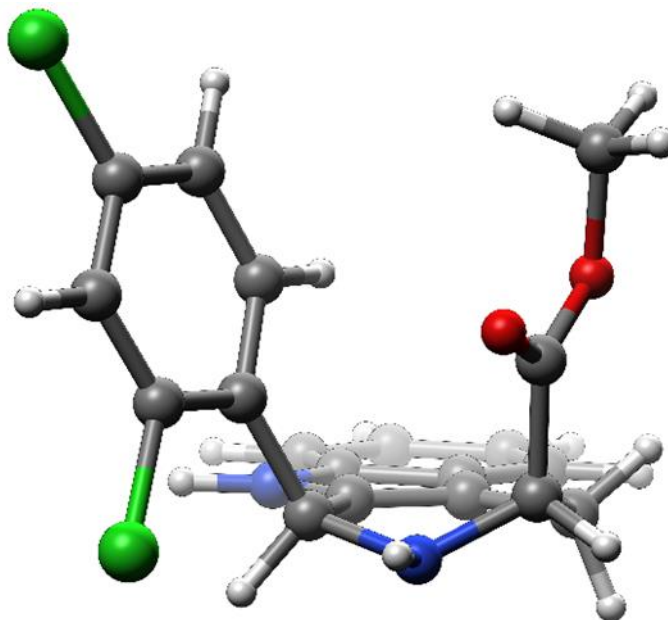
C	0.00000000	0.00000000	0.00000000	H	0.66481800	-4.96787800	-0.29959700
C	-0.69905200	1.29360300	-0.29430700	H	1.66330900	-4.00808500	0.81789700
C	-0.24971500	2.65579500	-0.16955100	H	2.26415700	-4.35547000	-0.83861200
C	0.94341400	3.26195400	0.25846800	H	-2.46032900	-1.24104200	0.37982900
H	1.78136600	2.65462300	0.59146100	C	-4.28643800	0.22612400	-0.78739000
C	1.03631600	4.64866200	0.25419300	C	-4.79648200	0.45151300	0.50244800
C	-0.04331300	5.44888700	-0.17022100	C	-6.16630200	0.53958500	0.75305100
C	-1.23608400	4.87880900	-0.60369600	C	-7.05817700	0.40072900	-0.30717700
C	-1.32454900	3.48420500	-0.60216900	C	-6.60029700	0.17237200	-1.60203400
N	-2.36097000	2.65114800	-0.98459300	C	-5.22716300	0.08820500	-1.81836200
H	-3.29109700	2.95238000	-1.23243700	H	-4.86552300	-0.09816500	-2.82601500
C	-1.98388600	1.33680600	-0.76852700	H	-7.30122100	0.05977200	-2.42154900
C	-2.80374300	0.12378300	-1.13543200	Cl	-8.78108200	0.51562500	0.00322800
H	-2.76820500	0.02763700	-2.23226500	H	-6.52553800	0.71151300	1.76049800
N	-2.21205000	-1.11278700	-0.59939600	Cl	-3.73238700	0.62766400	1.89271400
C	-0.75257700	-1.16145500	-0.71850900	H	-2.06727000	5.49729100	-0.93296400
H	-0.49660800	-1.13059100	-1.78366000	H	0.05712100	6.53077200	-0.16053900
C	-0.28398200	-2.48702200	-0.13842500	H	1.95423400	5.12699200	0.58496300
O	-0.79966700	-3.04068900	0.80839600	H	0.02293400	-0.19878800	1.08205000
O	0.82009800	-2.93838200	-0.76760200	H	1.04426200	0.01857700	-0.33795100
C	1.38399400	-4.14775400	-0.22970900				

5a-07



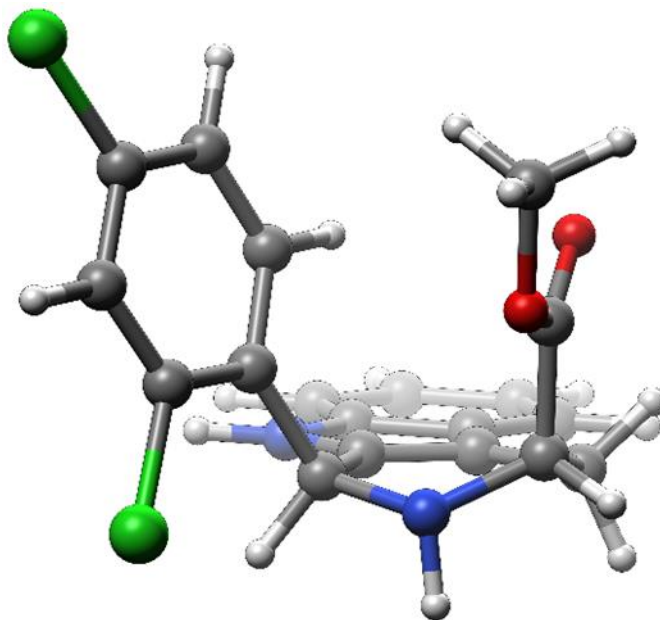
C	0.0000000	0.0000000	0.0000000	H	-0.3555420	4.2702150	1.2796190
C	0.5585600	-1.3834040	-0.1640250	H	1.0939680	4.8763290	0.4432720
C	-0.0443060	-2.6734170	0.0481770	H	1.2248890	4.2828960	2.1326050
C	-1.3081530	-3.1081020	0.4821220	H	2.5393530	0.9114890	0.4361990
H	-2.0804230	-2.3876360	0.7395390	C	4.2592100	-0.7731570	-0.6233260
C	-1.5562790	-4.4718760	0.5812200	C	4.7203410	-0.9697130	0.6893510
C	-0.5639580	-5.4177940	0.2543720	C	6.0659180	-1.2000480	0.9772640
C	0.6951960	-5.0194220	-0.1827920	C	6.9842340	-1.2375140	-0.0688420
C	0.9400660	-3.6473550	-0.2848950	C	6.5759290	-1.0445340	-1.3858940
N	2.0731700	-2.9672120	-0.6944990	C	5.2257700	-0.8153610	-1.6389190
H	2.9679290	-3.3890090	-0.8913680	H	4.9045660	-0.6563960	-2.6647750
C	1.8418370	-1.6063560	-0.5917300	H	7.2974870	-1.0699450	-2.1948030
C	2.8046270	-0.5223750	-1.0120930	Cl	8.6763490	-1.5310900	0.2882470
H	2.7982720	-0.4825360	-2.1122320	H	6.3868100	-1.3455310	2.0017030
N	2.3464950	0.8041400	-0.5581500	Cl	3.6215670	-0.9264610	2.0647340
C	0.9039420	1.0016940	-0.7750780	H	1.4588740	-5.7501670	-0.4369260
H	0.7114580	0.8853330	-1.8466920	H	-0.7860310	-6.4777100	0.3432070
C	0.5204760	2.4350490	-0.4350740	H	-2.5299670	-4.8179860	0.9172110
O	-0.1977570	3.1400770	-1.1076820	H	-0.0412890	0.2899240	1.0601770
O	1.0445620	2.8127800	0.7527280	H	-1.0267290	0.0674480	-0.3834660
C	0.7256660	4.1502060	1.1724900				

5a-08



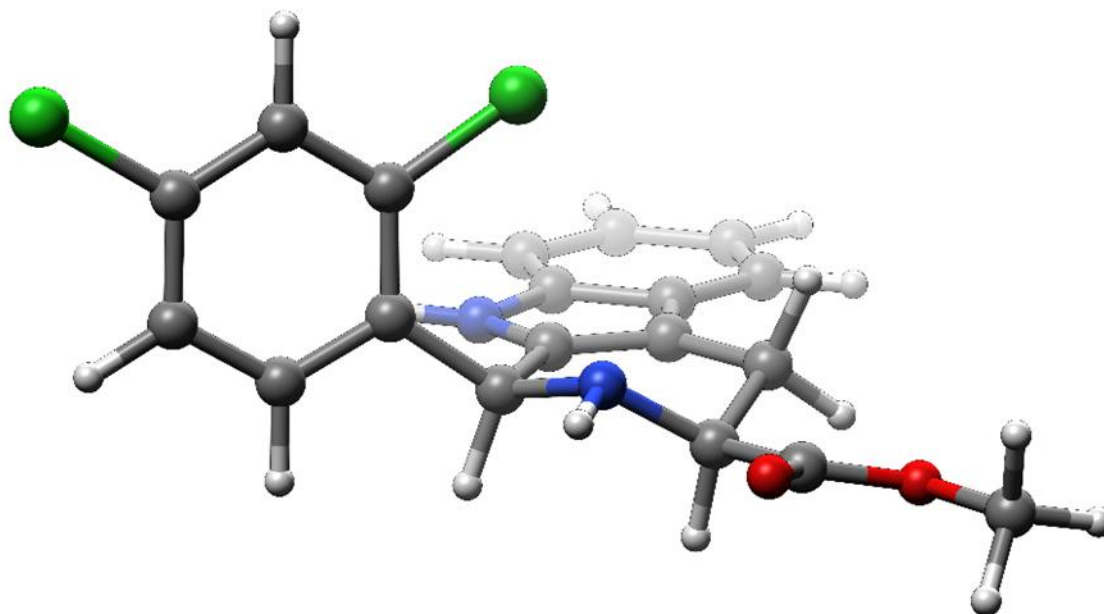
C	0.00000000	0.00000000	0.00000000	H	-3.01894600	1.55942800	-3.33861400
C	0.18621700	-1.48547800	-0.05486000	H	-3.29288500	-0.19766400	-3.39227200
C	1.29975100	-2.27937700	-0.50674600	H	-1.84322700	0.50253300	-4.19186800
C	2.54799400	-1.98341800	-1.07938800	H	-3.00342500	-0.20192800	1.48629500
H	2.84044200	-0.95220200	-1.26044400	C	-3.26528400	-2.46073600	0.11868400
C	3.40331400	-3.02710700	-1.41210200	C	-4.55742600	-2.60876200	0.64430500
C	3.03743200	-4.36854400	-1.18198500	C	-5.63753100	-3.03836800	-0.12436400
C	1.80971400	-4.69440500	-0.61471200	C	-5.42277400	-3.33251700	-1.46844200
C	0.95245800	-3.64205400	-0.28091900	C	-4.15840600	-3.20207400	-2.03778900
N	-0.30810300	-3.65821500	0.28718200	C	-3.10115700	-2.77115200	-1.23884700
H	-0.82832300	-4.48476300	0.53816100	H	-2.11416500	-2.66821100	-1.67923300
C	-0.75864300	-2.35451700	0.41992400	H	-4.00260100	-3.43964500	-3.08461100
C	-2.08997400	-1.97484600	0.98932400	Cl	-6.77066600	-3.88202000	-2.45007500
H	-2.20699800	-2.45659800	1.96917100	H	-6.62164500	-3.14007400	0.31689100
N	-2.06214300	-0.52133600	1.27108700	Cl	-4.88027600	-2.24192300	2.34141900
C	-1.47847200	0.35581300	0.24810800	H	1.52999400	-5.72967700	-0.43681500
H	-1.51378200	1.36482800	0.68080800	H	3.72650900	-5.16404900	-1.45209200
C	-2.37647200	0.47807000	-1.00024400	H	4.37082600	-2.80900400	-1.85594400
O	-3.57369000	0.65626200	-0.91605700	H	0.34567000	0.48308100	-0.91899800
O	-1.71413000	0.41758100	-2.17246600	H	0.59133500	0.42274200	0.82380100
C	-2.52886900	0.58247400	-3.34799400				

5a-09



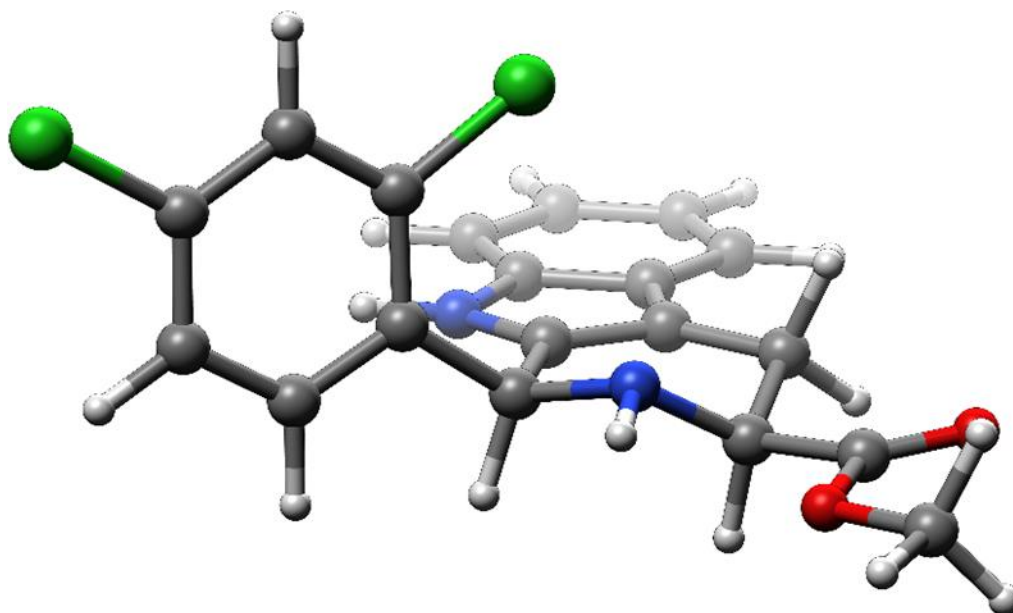
C	0.00000000	0.00000000	0.00000000	H	-4.47827100	-0.31249700	-2.49238600
C	0.23132700	-1.47977800	0.05986000	H	-3.94098100	1.34791900	-2.84895300
C	1.37240500	-2.26467500	-0.33561600	H	-5.34486200	1.07718800	-1.76084100
C	2.62018900	-1.96201300	-0.90550000	H	-1.78784600	-0.21930900	2.16777000
H	2.88432800	-0.93366300	-1.13845800	C	-3.22290700	-2.54640300	0.35304500
C	3.50990100	-2.99593900	-1.17138700	C	-4.47490500	-2.73342700	0.95972300
C	3.17828300	-4.33390800	-0.87782300	C	-5.56603800	-3.25964500	0.27033600
C	1.95151700	-4.66582500	-0.31207400	C	-5.40586900	-3.60669400	-1.06949900
C	1.05981600	-3.62296300	-0.04504400	C	-4.18385500	-3.43637100	-1.71458900
N	-0.20691500	-3.64568600	0.50938200	C	-3.11011900	-2.91333800	-0.99429300
H	-0.71901100	-4.47569000	0.76566400	H	-2.15868800	-2.76991000	-1.49639600
C	-0.69858800	-2.34974000	0.56494400	H	-4.07025100	-3.70916500	-2.75803400
C	-2.03575700	-1.96276900	1.12834400	Cl	-6.77347900	-4.27204900	-1.94863600
H	-2.11479700	-2.35118400	2.15123500	H	-6.51779500	-3.39587300	0.76953900
N	-2.15677700	-0.49298000	1.26142100	Cl	-4.72770800	-2.31768100	2.65261400
C	-1.49551700	0.32176300	0.22785900	H	1.69804800	-5.69846000	-0.08592800
H	-1.59015700	1.35688400	0.57892800	H	3.89332700	-5.12198900	-1.09765500
C	-2.28447500	0.28416700	-1.09216100	H	4.47703900	-2.77296800	-1.61359700
O	-1.82297000	-0.01299200	-2.17421700	H	0.31621400	0.40766800	-0.96618100
O	-3.55576200	0.68004500	-0.90623700	H	0.59231200	0.51582400	0.77073300
C	-4.37614900	0.69699300	-2.08588900				

5a-10



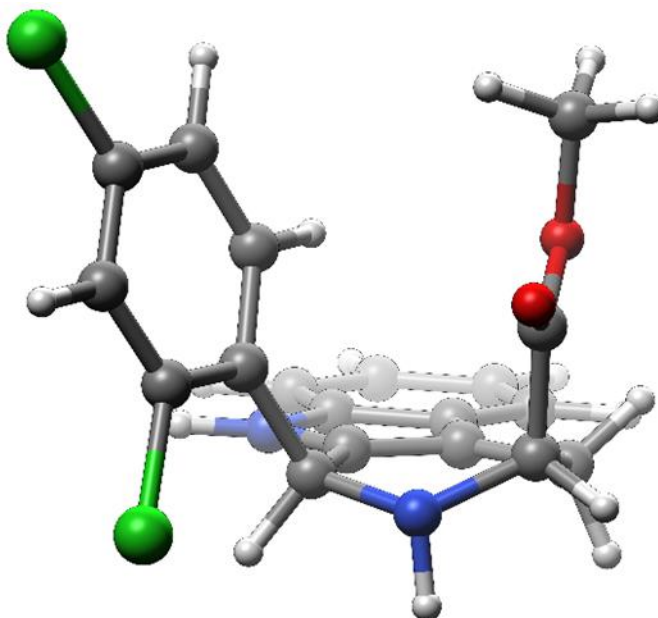
C	0.00000000	0.00000000	0.00000000	H	1.27088300	-4.61994400	-0.69996400
C	-0.66151000	1.30718900	-0.32748300	H	0.98728800	-4.34156100	1.03525000
C	-0.19262400	2.66297100	-0.20946000	H	2.54406600	-3.83712100	0.29608500
C	0.99874200	3.25492200	0.24280400	H	-2.64967500	-1.84804300	-0.82750300
H	1.81627500	2.63805500	0.60747700	C	-4.25637400	0.31428800	-0.81010800
C	1.11579400	4.63963700	0.22213300	C	-4.73605100	0.53986500	0.49330000
C	0.06259300	5.45215300	-0.24346800	C	-6.10265400	0.63671300	0.76162800
C	-1.12742200	4.89648500	-0.70243500	C	-7.01495100	0.50834900	-0.28303100
C	-1.24054700	3.50389900	-0.68301100	C	-6.58423600	0.28664600	-1.58750200
N	-2.28053600	2.68408800	-1.08408200	C	-5.21464100	0.19304400	-1.82603800
H	-3.20101100	2.99691500	-1.35286100	H	-4.87094300	0.01304400	-2.84178700
C	-1.92987200	1.36837200	-0.84144200	H	-7.30024300	0.18559300	-2.39540700
C	-2.78301500	0.17786600	-1.18823100	Cl	-8.73193700	0.63176400	0.06062100
H	-2.76959000	0.07738600	-2.29418300	H	-6.44443500	0.81021700	1.77491600
N	-2.18570100	-0.99024000	-0.53861800	Cl	-3.65730300	0.72935800	1.86018300
C	-0.74677900	-1.11128800	-0.76336500	H	-1.93823000	5.52423400	-1.06342800
H	-0.48289900	-1.00271300	-1.83761400	H	0.18152900	6.53220500	-0.24558200
C	-0.33262300	-2.53048700	-0.39409600	H	2.03233200	5.10696100	0.57199200
O	-1.09108700	-3.47728300	-0.37465100	H	-0.04002800	-0.20786500	1.07786400
O	0.98781500	-2.62353500	-0.15241500	H	1.05644400	-0.00262600	-0.28953600
C	1.47112200	-3.94738700	0.13812100				

5a-11



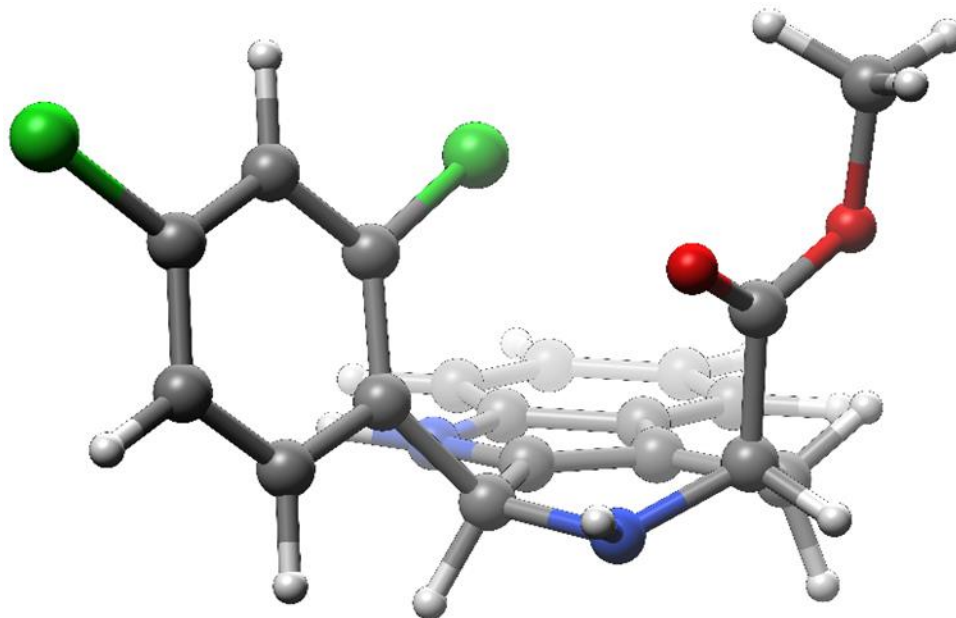
C	0.00000000	0.00000000	0.00000000	H	1.45417700	4.72076100	0.83780500
C	0.43926200	-1.39039000	-0.35090600	H	0.60639100	5.05032300	-0.69247300
C	-0.24300200	-2.65418300	-0.25512600	H	2.39889000	5.14277000	-0.62961900
C	-1.51772800	-3.05095900	0.18291500	H	2.92259500	1.39570800	-0.84391300
H	-2.22737000	-2.31443700	0.55120500	C	4.15122900	-0.99035500	-0.82348300
C	-1.85659200	-4.39817400	0.14341400	C	4.59393600	-1.31556300	0.47209700
C	-0.94474300	-5.36438100	-0.32693800	C	5.92731200	-1.64096000	0.72756200
C	0.32277800	-5.00286000	-0.77219000	C	6.84320300	-1.64471200	-0.32190800
C	0.65916500	-3.64710900	-0.73386400	C	6.44845100	-1.33050500	-1.61875700
N	1.82109200	-3.00110100	-1.11800200	C	5.11158500	-1.00882400	-1.84465700
H	2.68264800	-3.45550400	-1.37970600	H	4.79693200	-0.75700100	-2.85459400
C	1.68471700	-1.64893100	-0.85718300	H	7.16712700	-1.33441400	-2.43062700
C	2.71825700	-0.60862800	-1.18689100	Cl	8.51799800	-2.05528500	0.00570100
H	2.71650200	-0.48364700	-2.28976500	H	6.24090500	-1.88816400	1.73467500
N	2.32990500	0.63858700	-0.51382500	Cl	3.50518700	-1.34894100	1.84330200
C	0.91984200	0.99865800	-0.72107400	H	1.02413500	-5.74911600	-1.13692900
H	0.65407500	0.99076900	-1.79933900	H	-1.23639500	-6.41097300	-0.34389500
C	0.66902100	2.42684400	-0.24706300	H	-2.83915200	-4.71539200	0.48213800
O	-0.31216700	2.80114400	0.35347800	H	0.05321000	0.17779000	1.08170300
O	1.66909800	3.25374600	-0.63236800	H	-1.03759500	0.18837600	-0.29767900
C	1.51385600	4.63183700	-0.24977900				

5a-12



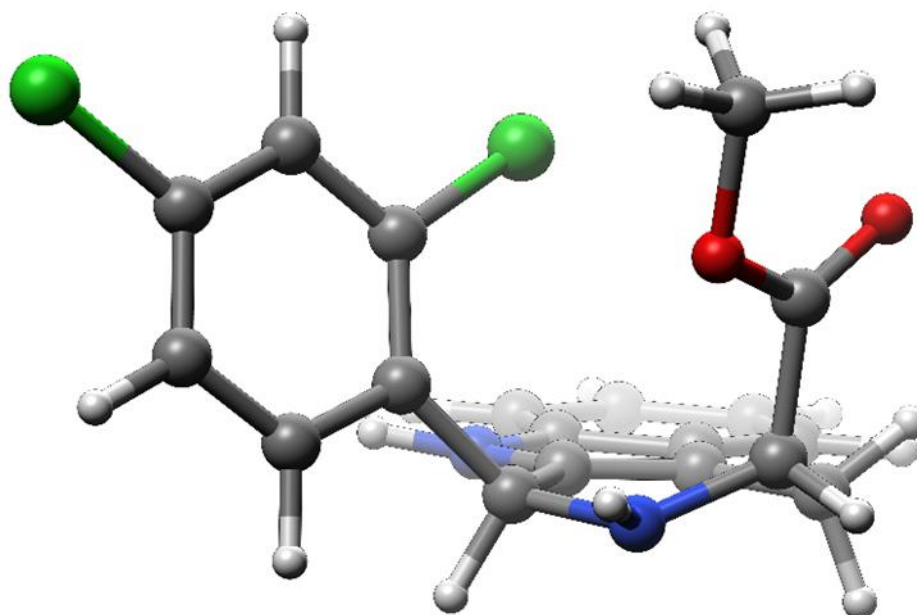
C	0.00000000	0.00000000	0.00000000	H	-2.71955500	1.21046400	-3.57437100
C	0.17935400	-1.48823100	0.00347400	H	-3.33918600	-0.44243600	-3.35442300
C	1.29936600	-2.29778100	-0.40217900	H	-1.76562500	-0.18453600	-4.18439900
C	2.56521400	-2.01963900	-0.94440800	H	-1.83572400	-0.23002400	2.12776000
H	2.86851800	-0.99368200	-1.13718900	C	-3.31121800	-2.43428800	0.19682200
C	3.42346700	-3.07407800	-1.23255400	C	-4.59578600	-2.53489200	0.75381700
C	3.04283400	-4.40886500	-0.98799900	C	-5.69179900	-2.98468900	0.01992500
C	1.79742400	-4.71696900	-0.45009000	C	-5.50238000	-3.34748200	-1.31166600
C	0.93728800	-3.65371900	-0.16081400	C	-4.24572600	-3.26916600	-1.90527600
N	-0.33790700	-3.65125700	0.37415300	C	-3.16938700	-2.81647200	-1.14294900
H	-0.87748800	-4.47091700	0.60642900	H	-2.18822200	-2.74794000	-1.60184100
C	-0.78642700	-2.34207300	0.46784100	H	-4.10970600	-3.56051800	-2.94112600
C	-2.12070800	-1.92634900	1.01878000	Cl	-6.87489100	-3.92075200	-2.24526400
H	-2.23687200	-2.34884400	2.02495100	H	-6.67047700	-3.05090800	0.47957800
N	-2.18995100	-0.46038400	1.20403700	Cl	-4.88298000	-2.11058000	2.43747200
C	-1.48874400	0.37245600	0.21277100	H	1.50637000	-5.74715500	-0.26113700
H	-1.53959400	1.39043500	0.61643900	H	3.73429900	-5.21323500	-1.22356300
C	-2.34225900	0.46948600	-1.06720000	H	4.40449000	-2.86981700	-1.65269100
O	-3.46603100	0.91406700	-1.08543400	H	0.36986800	0.44325800	-0.93074100
O	-1.68994500	0.05061400	-2.17562800	H	0.58636200	0.45639100	0.81234400
C	-2.43474400	0.16972800	-3.39964700				

5a-13



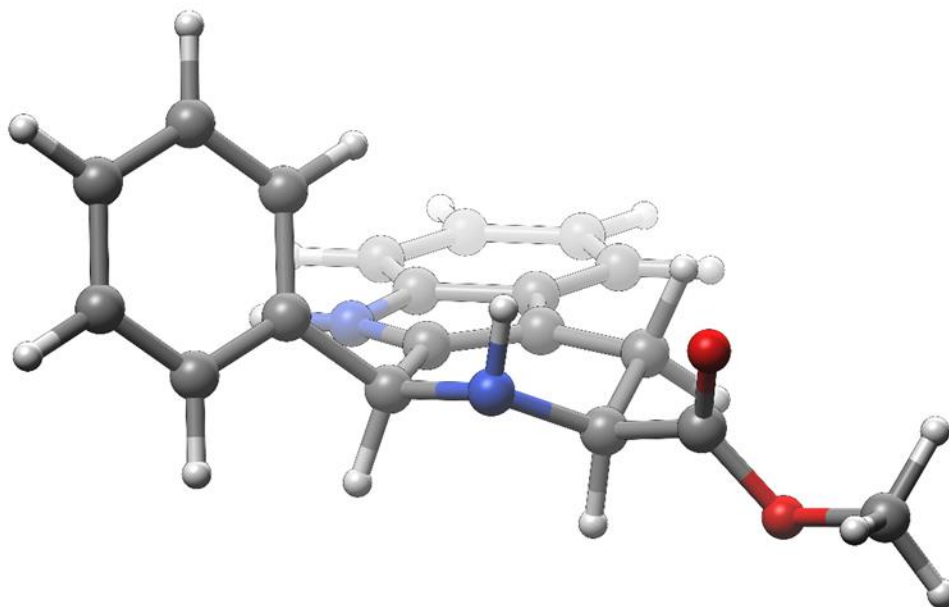
C	0.00000000	0.00000000	0.00000000	H	-2.54420500	2.89601700	-2.93735600
C	-0.00830200	-1.44578300	-0.38523900	H	-2.46751600	1.30410800	-3.73272500
C	1.01183000	-2.27033100	-0.97840000	H	-1.05864500	2.41440400	-3.82527600
C	2.32215500	-2.04022600	-1.42947100	H	-3.20442400	-0.03237000	1.00770300
H	2.76768200	-1.05195400	-1.34797600	C	-3.68219800	-2.17146400	-0.26036200
C	3.03938100	-3.09253900	-1.98652700	C	-3.92468100	-2.17806800	-1.64522800
C	2.47397700	-4.37831400	-2.09999500	C	-5.18663700	-2.46222800	-2.17250800
C	1.18186700	-4.63956700	-1.65501400	C	-6.24226800	-2.74256900	-1.31138700
C	0.46476200	-3.57977800	-1.09366900	C	-6.05215300	-2.75486900	0.06738800
N	-0.81135700	-3.54543100	-0.56015100	C	-4.78140800	-2.47763100	0.56098300
H	-1.49505700	-4.28142500	-0.65301100	H	-4.62684600	-2.49662300	1.63751400
C	-1.09581900	-2.24651600	-0.17116700	H	-6.87431300	-2.98347000	0.73642400
C	-2.37382100	-1.83402500	0.48560900	Cl	-7.82572200	-3.09662700	-1.98068400
H	-2.45164800	-2.41614600	1.41760400	H	-5.33624900	-2.46035500	-3.24538100
N	-2.26820000	-0.42057600	0.92782200	Cl	-2.66661100	-1.86439600	-2.83528200
C	-1.44069000	0.51862300	0.16812600	H	0.74802200	-5.63259700	-1.74092000
H	-1.38844700	1.42767200	0.78683500	H	3.05727200	-5.18144800	-2.54209900
C	-2.13405100	1.01161800	-1.11599700	H	4.05251800	-2.92432900	-2.34159800
O	-3.34121400	1.04378300	-1.23920900	H	0.51942900	0.61116800	-0.74358900
O	-1.27791900	1.50325700	-2.03025800	H	0.52710700	0.14192800	0.95365400
C	-1.88651300	2.06565600	-3.20745000				

5a-14



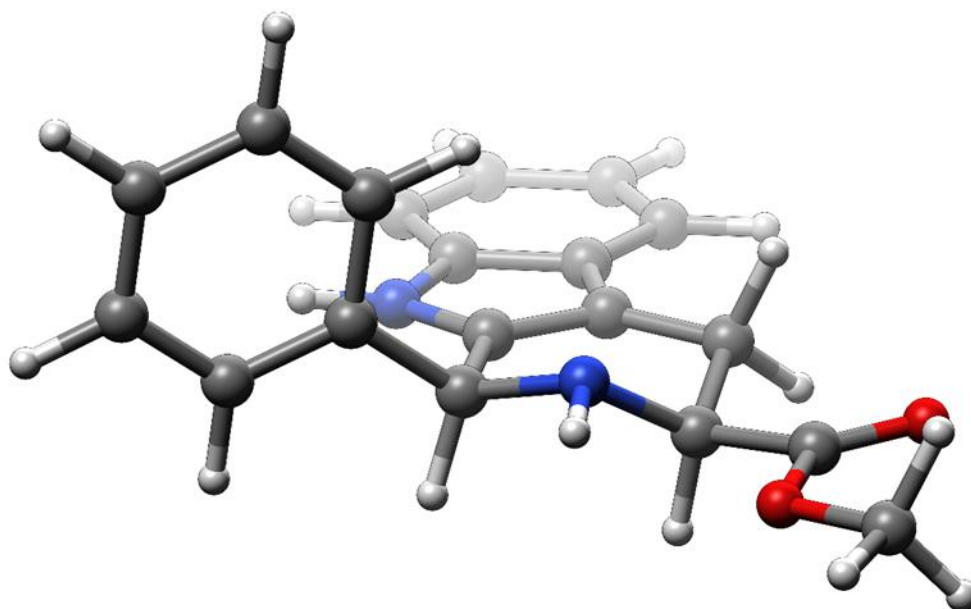
C	0.00000000	0.00000000	0.00000000	H	-3.82401400	0.72568600	-3.21205000
C	0.04126400	-1.47178700	-0.26932500	H	-3.77656300	2.38259800	-2.56051000
C	1.08832000	-2.29972500	-0.80869600	H	-5.14095100	1.29490400	-2.13312800
C	2.38623500	-2.05309700	-1.28585800	H	-3.19313000	-0.08015000	1.07245200
H	2.79087200	-1.04424700	-1.28538200	C	-3.60048200	-2.35797200	-0.01413000
C	3.14263100	-3.11610500	-1.76493400	C	-3.87981400	-2.46363500	-1.38824400
C	2.62828800	-4.42807500	-1.77562100	C	-5.12970700	-2.87591200	-1.85807800
C	1.34884100	-4.70501600	-1.30445300	C	-6.13672400	-3.18338100	-0.94852500
C	0.59247900	-3.63404600	-0.82104500	C	-5.90917000	-3.09590900	0.42196100
N	-0.68223800	-3.60833200	-0.28328900	C	-4.65019600	-2.69457300	0.85822800
H	-1.33515500	-4.37683600	-0.30759900	H	-4.46493900	-2.63819200	1.92853000
C	-1.01303400	-2.29554000	0.01285800	H	-6.69298700	-3.34453700	1.12888500
C	-2.29592800	-1.88623600	0.66254400	Cl	-7.70554400	-3.69572700	-1.54533900
H	-2.32488300	-2.38468700	1.64503700	H	-5.30707700	-2.95501300	-2.92402700
N	-2.24976600	-0.43837100	0.96610300	Cl	-2.68446200	-2.10758400	-2.62698700
C	-1.45694500	0.47630300	0.14178700	H	0.95450300	-5.71803000	-1.31134800
H	-1.44224300	1.42471900	0.70027600	H	3.24168000	-5.23935600	-2.15812500
C	-2.05852400	0.88580000	-1.21746700	H	4.14660600	-2.93584000	-2.13945600
O	-1.42809900	1.28426700	-2.17124900	H	0.47190700	0.56757500	-0.80782800
O	-3.41095500	0.86602000	-1.17245300	H	0.53908000	0.24103100	0.92619200
C	-4.07425700	1.35148800	-2.35242400				

5b-01



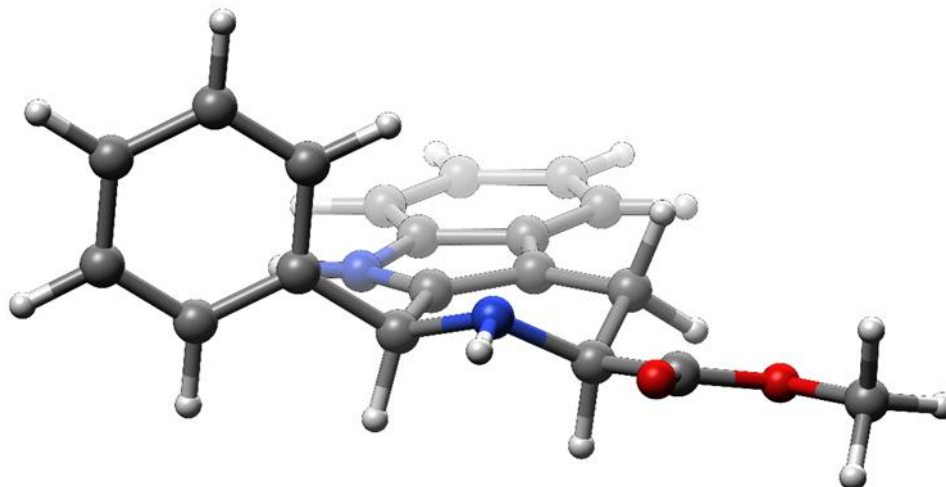
C	0.00000000	0.00000000	0.00000000	H	-4.92521000	-0.98405400	-0.32092900
C	1.23656700	0.79633800	-0.29391500	H	-3.89805200	-1.96894600	0.74752500
C	2.62904800	0.44138500	-0.19374600	H	-4.22996900	-2.52399500	-0.92801900
C	3.32355900	-0.70667700	0.22261200	H	-1.44451500	2.36198700	0.38711100
H	2.78164300	-1.58516400	0.56397900	C	-0.09362100	4.27001400	-0.57373500
C	4.71330900	-0.70298500	0.19627800	C	-0.65170800	5.29351200	-1.34819600
C	5.42930800	0.42976000	-0.23966400	C	-0.70405600	6.60260300	-0.86797800
C	4.77052900	1.57984500	-0.66304800	C	-0.19948500	6.90336700	0.39854400
C	3.37318600	1.57135600	-0.63934800	C	0.35598500	5.88900700	1.18075900
N	2.46399100	2.54720600	-1.00511600	C	0.40944600	4.58105200	0.69691200
H	2.69218800	3.50050600	-1.24345300	H	0.84941300	3.79495100	1.30579700
C	1.18084500	2.08111000	-0.77004300	H	0.75043600	6.11537300	2.16784700
C	-0.08290800	2.83668500	-1.09207200	H	-0.23788800	7.92262600	0.77352400
H	-0.18205400	2.88618300	-2.18880000	H	-1.13894700	7.38652700	-1.48235000
N	-1.27207100	2.12354100	-0.58816800	H	-1.05228200	5.05885500	-2.33158300
C	-1.21175500	0.66716000	-0.71903200	H	5.32425000	2.45165600	-1.00238900
H	-1.15748400	0.42128100	-1.78537000	H	6.51561700	0.40491600	-0.24758800
C	-2.49995000	0.09693900	-0.14600700	H	5.25955700	-1.58564300	0.51779000
O	-3.07101000	0.54163900	0.82673000	H	-0.20030500	-0.04260200	1.08117400
O	-2.89567700	-1.00586100	-0.81354200	H	0.09972000	-1.03888500	-0.34109600
C	-4.06503500	-1.65763700	-0.28704100				

5b-02



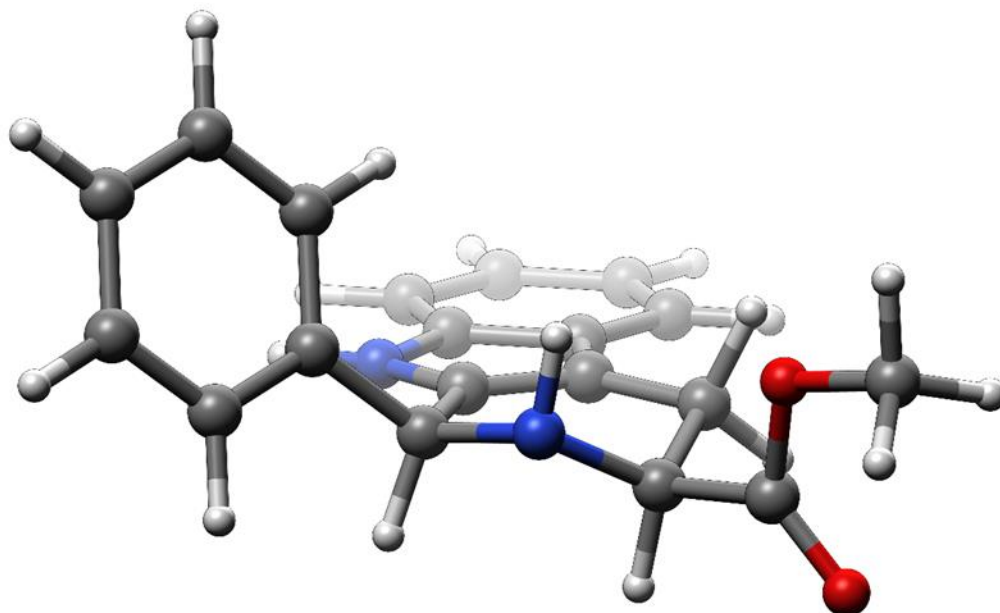
C	0.00000000	0.00000000	0.00000000	H	-4.92804800	-0.39824700	0.82554400
C	1.13722600	0.94167000	-0.26548400	H	-4.93226400	-1.17943700	-0.77372800
C	2.56191700	0.76242600	-0.15657400	H	-5.66255800	0.44947100	-0.57663100
C	3.39107100	-0.30455600	0.22791100	H	-2.34940200	2.29523400	-0.63142500
H	2.95989500	-1.25626800	0.52821800	C	-0.51869000	4.27433300	-0.46596800
C	4.76946200	-0.12515800	0.22324000	C	-0.44956500	5.35374900	-1.35326000
C	5.34170000	1.10431900	-0.15997200	C	-0.50673400	6.66868200	-0.88220200
C	4.54790200	2.17781500	-0.55180200	C	-0.64001600	6.91343000	0.48411100
C	3.16271500	1.99339800	-0.54905200	C	-0.71490700	5.83919200	1.37626400
N	2.14247100	2.86060600	-0.89714300	C	-0.65137600	4.52886900	0.90608500
H	2.24611000	3.84869300	-1.07366300	H	-0.71552600	3.68820200	1.58967000
C	0.93017000	2.22473900	-0.69871500	H	-0.82194200	6.02483400	2.44188000
C	-0.41197200	2.84437200	-0.98304200	H	-0.68958400	7.93430800	0.85352700
H	-0.54457100	2.88292000	-2.08425400	H	-0.45591900	7.49703400	-1.58406200
N	-1.42325500	1.98522900	-0.34854400	H	-0.36221000	5.16526100	-2.42171400
C	-1.26390800	0.56050300	-0.67306200	H	4.99095700	3.12454300	-0.85060600
H	-1.16771600	0.40388800	-1.76797800	H	6.42251700	1.21654000	-0.15162700
C	-2.50598500	-0.22009100	-0.25571300	H	5.41919600	-0.94385600	0.52072100
O	-2.50332800	-1.31582300	0.25773100	H	-0.18599600	-0.11655900	1.07551600
O	-3.63773700	0.44761600	-0.58150500	H	0.20098400	-1.00399700	-0.39093700
C	-4.86727400	-0.22159300	-0.25130000				

5b-03



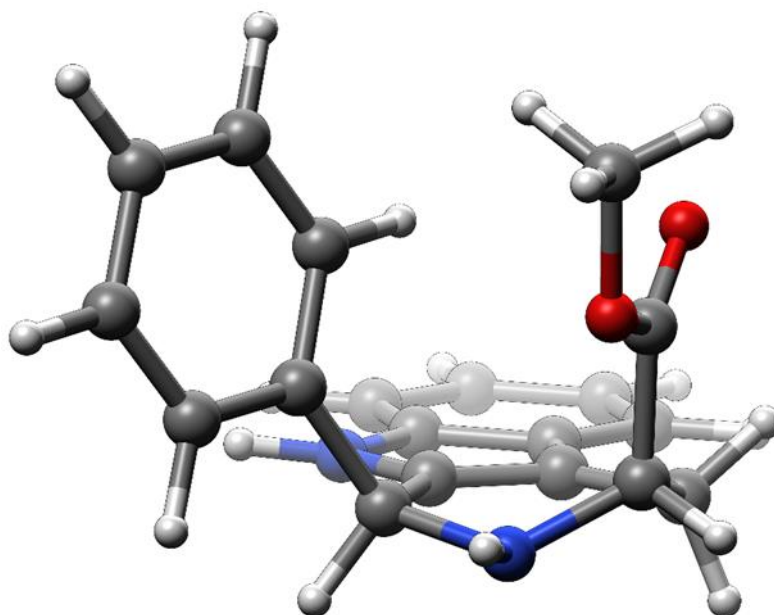
C	0.0000000	0.0000000	0.0000000	H	4.67017500	-1.02758100	-0.80031800
C	-1.48004000	-0.03249700	-0.25225900	H	4.35153400	-0.97320200	0.94993500
C	-2.48466500	0.99169700	-0.12848700	H	4.58451200	0.55727400	0.04020000
C	-2.47149200	2.33890800	0.26996700	H	0.42340400	-3.25123500	-0.59857400
H	-1.54168900	2.81514100	0.57119500	C	-2.25261400	-3.66915400	-0.46631900
C	-3.66372000	3.05362100	0.27832900	C	-2.99796900	-4.46111200	-1.34645000
C	-4.87707400	2.44886000	-0.10610400	C	-3.76897200	-5.52495800	-0.86921900
C	-4.92221100	1.11863900	-0.51177500	C	-3.79459100	-5.80850800	0.49587700
C	-3.72173300	0.40358400	-0.52158200	C	-3.04756700	-5.02449000	1.38047600
N	-3.46174100	-0.90615700	-0.88360200	C	-2.28447700	-3.95997700	0.90438800
H	-4.15682700	-1.61509000	-1.06428300	H	-1.69470400	-3.35033700	1.58157100
C	-2.11651300	-1.16319800	-0.69469200	H	-3.06087900	-5.24444400	2.44484700
C	-1.45077300	-2.48290800	-0.98954600	H	-4.38841100	-6.63831700	0.86995200
H	-1.38264300	-2.59301400	-2.09226500	H	-4.33907400	-6.13451800	-1.56548700
N	-0.12612000	-2.42756300	-0.36502200	H	-2.96499100	-4.25319500	-2.41439500
C	0.62716400	-1.22177500	-0.70171500	H	-5.85833900	0.65419600	-0.81139700
H	0.61400500	-1.01444900	-1.79309200	H	-5.79418800	3.03138500	-0.08767800
C	2.09126200	-1.46450200	-0.35787100	H	-3.66367400	4.09557400	0.58705900
O	2.59186200	-2.56301500	-0.23680000	H	0.22353700	-0.04169300	1.07505700
O	2.78243700	-0.31305200	-0.26041200	H	0.45681000	0.91829600	-0.38526600
C	4.18987100	-0.45812000	-0.00034400				

5b-04



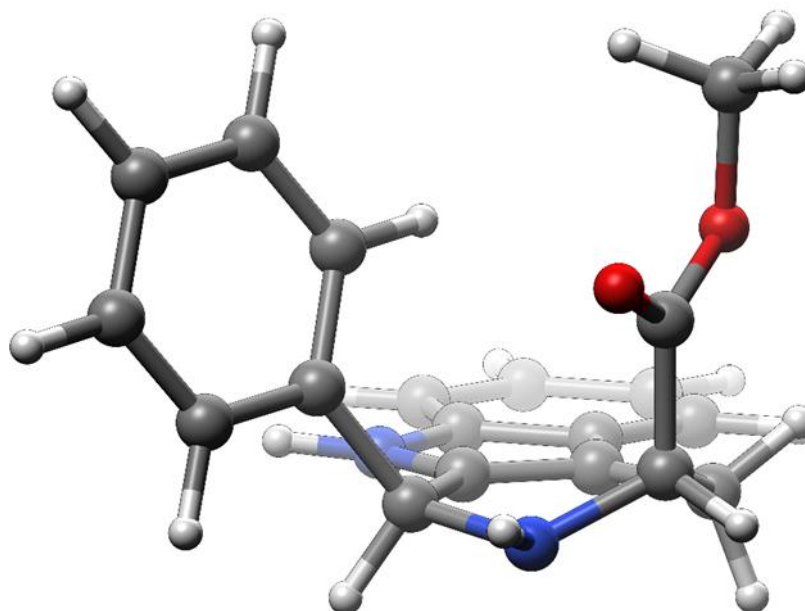
C	0.00000000	0.00000000	0.00000000	H	-3.58647600	-2.35299400	1.26145000
C	0.95479800	1.14645000	-0.16267700	H	-4.80819900	-1.34162400	0.45424900
C	2.38276200	1.21128400	0.01347800	H	-4.33317800	-0.98092500	2.14755300
C	3.36554800	0.29261400	0.41861900	H	-2.01938200	1.80474200	0.47021900
H	3.09308600	-0.72742700	0.67788300	C	-1.33436300	4.09481100	-0.38173200
C	4.69066300	0.70649900	0.48630300	C	-2.18682100	4.91143400	-1.13444700
C	5.05820700	2.02631900	0.15599200	C	-2.65292700	6.12122000	-0.61970800
C	4.10940600	2.95765700	-0.25400800	C	-2.27291300	6.52915900	0.66063300
C	2.77839100	2.53707000	-0.32517400	C	-1.42730900	5.72032800	1.42167700
N	1.63936900	3.22478100	-0.70245700	C	-0.96059900	4.51095100	0.90332200
H	1.58652900	4.21511900	-0.88671700	H	-0.29649500	3.88739300	1.49684500
C	0.54278200	2.38740200	-0.57849600	H	-1.12737300	6.03094400	2.41908700
C	-0.87316800	2.75534100	-0.94322400	H	-2.63257600	7.47276000	1.06220700
H	-0.94351300	2.81896800	-2.04089900	H	-3.31171400	6.74512100	-1.21790300
N	-1.81582000	1.69688200	-0.52246200	H	-2.48930000	4.59100900	-2.12853800
C	-1.31291300	0.33668500	-0.76314700	H	4.39501400	3.97423200	-0.51242000
H	-1.12386300	0.23896100	-1.83711400	H	6.10180400	2.32221600	0.21978200
C	-2.39470600	-0.68197300	-0.43334500	H	5.45808500	0.00377300	0.79941000
O	-2.69070000	-1.63226000	-1.12226300	H	-0.22991200	-0.18610900	1.05939300
O	-2.96071000	-0.42244200	0.76818500	H	0.42313400	-0.93274500	-0.39622200
C	-3.98858000	-1.33992800	1.17738500				

5b-05



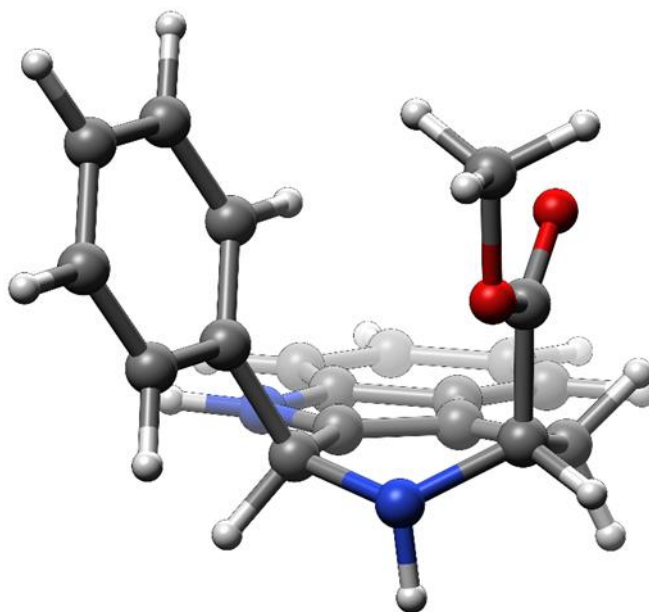
C	0.00000000	0.00000000	0.00000000	H	-4.24960100	-0.94088700	-2.75127900
C	0.55710200	-1.37024100	-0.23665700	H	-4.17700800	0.84097200	-2.76744500
C	1.83462700	-1.79169400	-0.75137300	H	-5.44454700	0.00497500	-1.80679300
C	2.97403700	-1.11863000	-1.22216300	H	-2.92136800	-1.15749300	1.19127400
H	3.00360200	-0.03214400	-1.24005000	C	-2.53636600	-3.28461600	-0.27002000
C	4.06109700	-1.86060900	-1.66938900	C	-3.60279900	-3.97668000	0.32061000
C	4.03503900	-3.26940900	-1.65501100	C	-4.56188700	-4.62231500	-0.46076600
C	2.92284600	-3.96532100	-1.19173800	C	-4.46106300	-4.59363700	-1.85276900
C	1.83254000	-3.21586600	-0.74158500	C	-3.39684000	-3.91687400	-2.45310600
N	0.61603900	-3.62415000	-0.22654300	C	-2.44048600	-3.26845600	-1.66896400
H	0.28337100	-4.57561900	-0.19516500	H	-1.61552700	-2.74684800	-2.14519100
C	-0.14743600	-2.50423100	0.06275900	H	-3.30350200	-3.89999400	-3.53606800
C	-1.52869400	-2.56046900	0.63539100	H	-5.20094600	-5.10238900	-2.46502300
H	-1.49488500	-3.13391100	1.57502000	H	-5.38024000	-5.15489100	0.01694000
N	-1.91631500	-1.18588700	1.04066700	H	-3.67904400	-4.01406700	1.40614300
C	-1.52701200	-0.06437000	0.17169900	H	2.90501400	-5.05226400	-1.17980200
H	-1.85837700	0.83820100	0.70256900	H	4.89892600	-3.82366100	-2.01188900
C	-2.26257400	-0.01396700	-1.18169700	H	4.94643100	-1.34921700	-2.03745100
O	-1.75958300	0.09335700	-2.27866700	H	0.23652100	0.67041200	-0.83271200
O	-3.59994100	-0.06486100	-0.97619200	H	0.43180000	0.44227200	0.90800700
C	-4.41371700	-0.03636800	-2.16019100				

5b-06



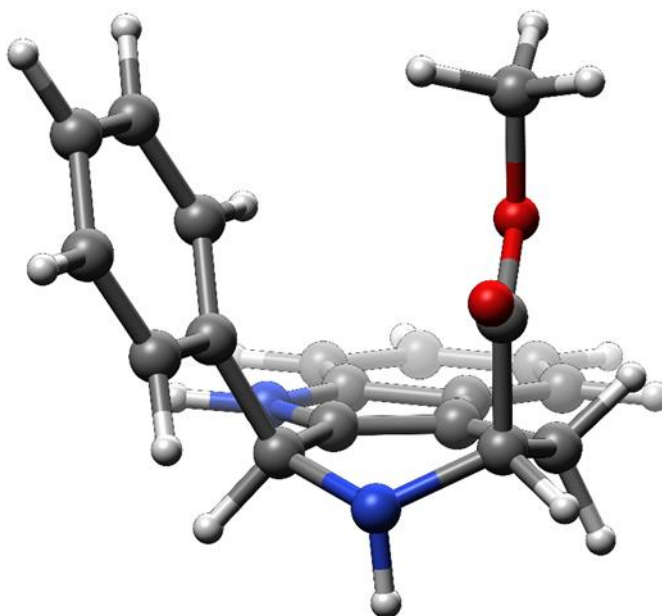
C	0.00000000	0.00000000	0.00000000	H	2.88599300	1.87409800	3.28591500
C	-0.45519400	-1.35441300	0.44692600	H	2.82538200	0.16780900	3.78511100
C	-1.70290800	-1.79591000	1.01514500	H	1.45317800	1.25948700	4.17853000
C	-2.89957200	-1.15556700	1.37699200	H	3.05892800	-1.06337000	-0.87471600
H	-3.01842300	-0.08526300	1.22802000	C	2.76270600	-3.04764300	0.75679800
C	-3.92923000	-1.90844500	1.92977200	C	3.85880100	-3.76789000	0.26427000
C	-3.78921500	-3.29645000	2.12840700	C	4.83663200	-4.26643300	1.12617900
C	-2.61846000	-3.96069700	1.77596300	C	4.72427400	-4.05957400	2.50167400
C	-1.58642000	-3.20101500	1.21854500	C	3.63007400	-3.35340000	3.00586100
N	-0.33479500	-3.58161000	0.77081300	C	2.65701500	-2.85243000	2.14089100
H	0.07799800	-4.49396000	0.89104700	H	1.80427900	-2.30978300	2.54047200
C	0.34186100	-2.45948000	0.32054000	H	3.53133000	-3.19637100	4.07704200
C	1.73124900	-2.49148800	-0.23479500	H	5.48031800	-4.45114800	3.17696700
H	1.74325900	-3.17293600	-1.09997700	H	5.68001300	-4.82200000	0.72440300
N	2.04783800	-1.15191800	-0.79867800	H	3.94517200	-3.94199000	-0.80691500
C	1.53438500	0.03945000	-0.10783600	H	-2.51304200	-5.03206500	1.92722600
H	1.80599200	0.88506600	-0.75523100	H	-4.61037800	-3.85968600	2.56344100
C	2.30349600	0.33516200	1.19580400	H	-4.85858700	-1.42207500	2.21367300
O	3.51490200	0.29446000	1.25176800	H	-0.33957900	0.78283800	0.68497100
O	1.52320800	0.68694300	2.23770400	H	-0.41436400	0.23880400	-0.98923400
C	2.22630800	1.01770500	3.44878600				

5b-07



C	0.0000000	0.0000000	0.0000000	H	-4.3254820	-1.2462470	-2.4400590
C	0.6071900	-1.3669720	-0.1075770	H	-4.2955970	0.5277060	-2.6167750
C	1.9065330	-1.7778580	-0.5742850	H	-5.5145940	-0.2442060	-1.5460800
C	3.0245800	-1.0994070	-1.0870280	H	-1.4846650	-0.9425970	2.1247290
H	3.0102300	-0.0178500	-1.1952880	C	-2.4781170	-3.2568810	-0.0222550
C	4.1467380	-1.8301400	-1.4597740	C	-3.6982640	-3.6377820	0.5541130
C	4.1770120	-3.2329420	-1.3295910	C	-4.6657490	-4.3016450	-0.1958040
C	3.0871610	-3.9335930	-0.8224010	C	-4.4277690	-4.5956560	-1.5423520
C	1.9612440	-3.1952540	-0.4475560	C	-3.2209570	-4.2144680	-2.1272100
N	0.7546830	-3.6087140	0.0873780	C	-2.2501440	-3.5491930	-1.3707690
H	0.4626540	-4.5674700	0.1991580	H	-1.3192780	-3.2444140	-1.8387200
C	-0.0574980	-2.5007140	0.2794390	H	-3.0279790	-4.4329940	-3.1743280
C	-1.4443590	-2.5390270	0.8554780	H	-5.1794360	-5.1179750	-2.1285460
H	-1.4173170	-3.0889820	1.8077390	H	-5.6049410	-4.5924980	0.2678260
N	-1.8978790	-1.1741090	1.2235120	H	-3.8885630	-3.3975630	1.5972970
C	-1.5178640	-0.1012930	0.2839290	H	3.1125510	-5.0158010	-0.7218890
H	-1.8555420	0.8288380	0.7587630	H	5.0670300	-3.7786270	-1.6311480
C	-2.3278830	-0.1923700	-1.0195970	H	5.0156630	-1.3147200	-1.8599310
O	-1.8539140	-0.1942720	-2.1359350	H	0.1578570	0.5729360	-0.9200900
O	-3.6487970	-0.2029220	-0.7683340	H	0.4736080	0.5709050	0.8132190
C	-4.4939580	-0.2965250	-1.9262780				

5b-08



C	0.00000000	0.00000000	0.00000000	H	3.18612000	0.52352300	3.32691300
C	-0.58084800	-1.37589600	0.13555600	H	3.42556500	-1.22578800	3.08338000
C	-1.87758300	-1.79818900	0.59760600	H	2.01262400	-0.64404700	4.02627400
C	-3.00741200	-1.12909400	1.09736500	H	1.42897000	-0.97038400	-2.15098100
H	-3.00679000	-0.04656800	1.19766600	C	2.56584700	-3.15365800	0.06449400
C	-4.12481200	-1.86965700	1.46499700	C	3.88084900	-3.20080000	-0.42007000
C	-4.13911100	-3.27346100	1.34272100	C	4.89471400	-3.79485400	0.32687800
C	-3.03727400	-3.96524300	0.84932900	C	4.61123800	-4.35227300	1.57731400
C	-1.91627700	-3.21698000	0.47955500	C	3.30886100	-4.30281100	2.07187800
N	-0.69943800	-3.61990600	-0.03977800	C	2.29154200	-3.70543300	1.31996800
H	-0.41320400	-4.57524300	-0.18886700	H	1.28479200	-3.66052900	1.72347100
C	0.10068500	-2.50386200	-0.23896600	H	3.07810200	-4.72649700	3.04616600
C	1.48479600	-2.52063000	-0.82471400	H	5.40164300	-4.81657300	2.16125400
H	1.46482200	-3.11358600	-1.75209100	H	5.90901200	-3.81852800	-0.06282100
N	1.88101900	-1.16021000	-1.25869600	H	4.10383300	-2.74379000	-1.37966000
C	1.51217800	-0.06315000	-0.33953900	H	-3.05047700	-5.04819700	0.75465400
H	1.79457100	0.85466500	-0.86652300	H	-5.02609700	-3.82682800	1.63903300
C	2.45942000	-0.07952600	0.87321100	H	-5.00295800	-1.36119500	1.85378400
O	3.63646500	0.19039500	0.80098000	H	-0.15281300	0.58736600	0.91255700
O	1.83391500	-0.39443500	2.02666100	H	-0.51136600	0.54943200	-0.80570800
C	2.67890900	-0.43479000	3.18876300				